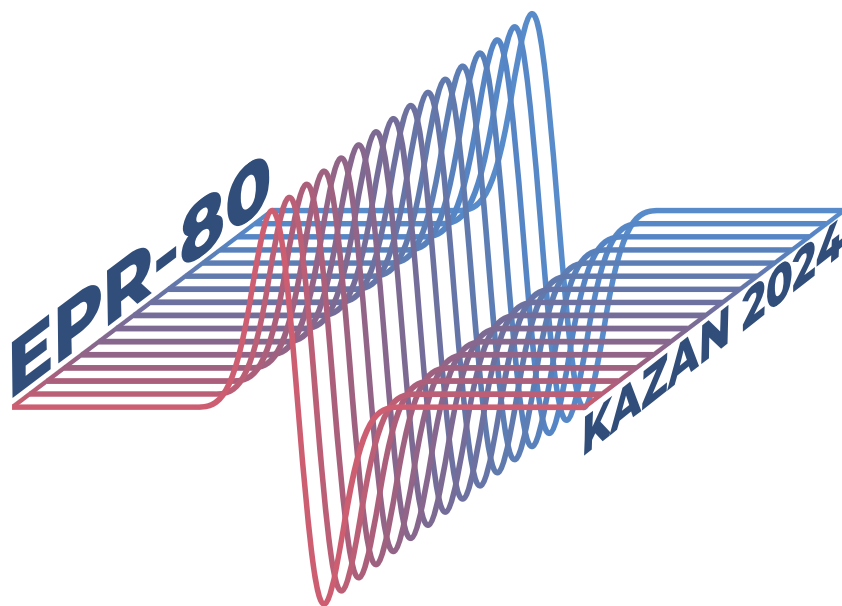


The International Conference

# MAGNETIC RESONANCE – CURRENT STATE AND FUTURE PERSPECTIVES (EPR-80)

Kazan, Russia, September 23–27, 2024



**BOOK OF ABSTRACTS**





**Казанский  
федеральный**  
УНИВЕРСИТЕТ



# MAGNETIC RESONANCE – CURRENT STATE AND FUTURE PERSPECTIVES (EPR-80)

BOOK OF ABSTRACTS  
OF THE INTERNATIONAL CONFERENCES

Editors:  
KEV M. SALIKHOV  
DMITRY A. TAYURSKII

KAZAN, SEPTEMBER 23–27, 2024

Conferences are supported by:



This work is subject to copyright.

All rights are reserved, whether the whole or part of the material is concerned, specifically those of translation, reprinting, re-use of illustrations, broadcasting, reproduction by photocopying machines or similar means, and storage in data banks.

© 2024 Zavoisky Physical-Technical Institute, FRC Kazan Scientific Center of RAS, Kazan

© 2024 Kazan Federal University, Kazan

Printed in Russian Federation

#### CHAIRMEN

Tayurskii D.A. (Kazan)  
Kalachev A.A. (Kazan)

#### PROGRAM COMMITTEE CHAIRMEN

Salikhov K.M. (Kazan)  
Tayurskii D.A. (Kazan)

#### PROGRAM COMMITTEE

Aganov A.V. (Kazan)  
Fedin M.V. (Novosibirsk)  
Kalachev A.A. (Kazan)  
Kamnev A.A. (Saratov)  
Krumkacheva O.A. (Novosibirsk)  
Malkin B.Z. (Kazan)  
Salikhov K.M. (Kazan)  
Smirnov A.I. (Moscow)  
Tagirov L.R. (Kazan)  
Usachev K.S. (Kazan)  
Vavilova E.L. (Kazan)  
Voronina E.V. (Kazan)  
Voronkova V.K. (Kazan)

#### LOCAL ORGANIZING COMMITTEE CHAIRMEN

Gafurov M.R.  
Khantimerov S.M.

#### SCIENTIFIC SECRETARIAT

Gavrilova T.P.  
Yusupov R.V.

# CONTENTS

<b>ZAVOISKY AWARD LECTURES</b>	<b>14</b>
<b>Anatoly F. Vanin.</b> FUNDAMENTAL ROLE OF EPR METHOD IN DISCOVERY, IDENTIFICATION AND STUDY OF DINITROSYL IRON COMPLEXES IN LIVING ORGANISMS	15
<b>Robert G. Griffin.</b> DNP and EPR at Millimeter Wavelengths	16
<b>PLENARY LECTURES</b>	<b>17</b>
<b>A.V. Dooglav.</b> HOW THE EPR HAS BEEN DISCOVERED? THE ANALYSIS OF ZAVOISKY'S LOGBOOKS	18
<b>E.L. Ivchenko.</b> ELECTRON AND HOLE $g$ FACTORS IN SEMICONDUCTORS AND SEMICONDUCTOR NANOSYSTEMS	19
<b>A.A. Kamnev.</b> MICROBIOLOGICAL APPLICATIONS of MÖSSBAUER SPECTROSCOPY	20
<b>S.V. Demishev.</b> EPR as a TOOL for STUDYING MAGNETIC FLUCTUATIONS in STRONGLY CORRELATED ELECTRONIC SYSTEMS	21
<b>K.S. Usachev.</b> MAGNETIC RESONANCE APPLICATIONS IN STRUCTURAL STUDIES OF LARGE MACROMOLECULAR COMPLEXES	23
<b>K.M. Salikhov.</b> CURRENT STATE OF SPIN EXCHANGE THEORY. NEW SPIN EXCHANGE PARADIGM	24
<b>M. Zhitomirskii.</b> Longitudinal Magnons: New Collective Quantum Excitations in Large-S Magnets	26
<b>Yu.M. Bunkov.</b> 40 YEARS of MAGNON BOSE EINSTEIN CONDENSATION	27
<b>INVITED TALKS</b>	<b>29</b>
<b>Yu. G. Kusrayev.</b> MULTIPLE-SPIN RAMAN PARAMAGNETIC RESONANCE INDUCED BY THE HOLE EXCHANGE FIELD IN CdSe/ZnMnSe QUANTUM DOTS	30
<b>M.V. Fedin.</b> EPR of Radical-Functionalized Materials	32
<b>A.I. Smirnov.</b> PSEUDOSPIN PARAMAGNET AND SPIN LIQUID IN A CHAIN ANTIFERROMAGNET $\text{Cs}_2\text{CoCl}_4$	33
<b>Jianzhang Zhao.</b> Study of the Electron Spin Polarization of the Triplet Excited States of BODIPY Compounds with Time-Resolved Electron Paramagnetic Resonance Spectroscopy	35
<b>A. A. Sukhanov.</b> Features of Photo-Excited Charge Separation States in TADF molecules	36
<b>K.V. Frolov.</b> MÖSSBAUER SPECTROSCOPY of the RARE EARTH FERROBORATES $\text{RFe}_3(\text{BO}_3)_4$ (R = Pr, Eu, Tb, Dy)	37
<b>E.A. Konstantinova.</b> On the question of the role of spin centers in radiative recombination processes in nanomaterials	38
<b>M.K. Bowman.</b> Impact of Random Processes on Coherences	40

<b>Yu. M. Shukrinov.</b> RESONANCE FEATURES OF ANOMALOUS JOSEPHSON JUNCTIONS	41
<b>I.V. Yanilkin.</b> GRADED THIN FERROMAGNETIC EPITAXIAL Pd-Fe FILMS: FMR MEASUREMENTS	42
<b>Sandra S. Eaton.</b> SPIN-LATTICE RELAXATION of Cr(V) NITRIDO COMPLEXES: EXPERIMENTS and CALCULATIONS	44
<b>Gareth R. Eaton.</b> ELECTRON SPIN RELAXATION of MANGANESE in the +2, +3, and +4 OXIDATION STATES	46
<b>A.I. Kokorin.</b> EPR of Copper(II) Complexes with Polymer Ligands	47
<b>A.A. Bukharaev.</b> INFLUENCE OF THE THERMALLY INDUCED MAGNETOELASTIC EFFECT ON MAGNETIZATION SWITCHING IN Ni MICROPARTICLES WITH CONFIGURATION ANISOTROPY	49
<b>L.A. Siurakshina.</b> ANISOTROPIC SPIN HAMILTONIANS FOR IRIDIUM OXIDES: JUSTIFICATION FROM THE EMBEDDED CLUSTER APPROACH	51
<b>V.R. Shaginyan.</b> STRONGLY CORRELATED QUANTUM SPIN LIQUIDS VERSUS HEAVY FERMION METALS	53
<b>V.I. Volkov.</b> COPPER (II) EPR in AMINO PHOSPHONIC POLYAMPHOLYTES	54
<b>ORAL TALKS</b>	<b>56</b>
<b>S.O. Nazarov.</b> The documentary legacy of academician E. K. Zavoisky in the Archives of RAS (in Russian)	57
<b>L.A. Nurtdinova.</b> VISUALISATION of the SURFACE of ISOLATED NERVOUS SYSTEM of a GRAPE SNAIL with FLUORESCENT NANOPROBES	59
<b>A.R. Safin.</b> ELECTRICALLY TUNABLE SUB-TERAHERTZ RESONANCE IN ANTIFERROMAGNET-BASED HETEROSTRUCTURE	60
<b>A.V. Leontyev.</b> CORE-SHELL NaYF <sub>4</sub> :Yb <sup>3+</sup> /Tm <sup>3+</sup> @NaGdF <sub>4</sub> :Ce <sup>3+</sup> /Tb <sup>3+</sup> NANOPARTICLES for DUAL-MODE FLUORESCENCE-BASED TEMPERATURE SENSING and ANTI-COUNTERFEITING	61
<b>I.N. Gracheva.</b> Electron-nuclear interactions in optically active NV <sup>-</sup> centers in 6H-SiC – a promising material platform for quantum technologies	62
<b>E.L. Vavilova.</b> STATIC and RESONANT PROPERTIES and MAGNETIC PHASE DIAGRAM of LiMn <sub>2</sub> TeO <sub>6</sub>	63
<b>F. Mikailzade.</b> MAGNETIC RESONANCE STUDY OF Fe DOPED TlInTe <sub>2</sub> CRYSTAL	64
<b>R.M. Eremina.</b> STUDY OF PECULIARITIES Co <sup>2+</sup> and Co <sup>3+</sup> EPR SPECTRA IN DIFFERENT SPIN STATES	65
<b>Yu.E. Kandrashkin.</b> On some properties of the ion spin system in pulsed EPR experiments	66
<b>A.A. Gol'dberg.</b> Features of modeling the NMR signal shape recorded using the modulation technique from liquid media	67
<b>A.G. Matveeva.</b> Analytical prediction of mean interspin distance and its uncertainties in PDS measurements by EPR	69
<b>S.A. Klimova.</b> Analysis of the trajectory of a symmetrical spinning top in the Earth's magnetic field	70

<b>R.P. Mironov.</b> Influence of the «frequency effect» on the Condon form of the electron oscillatory absorption spectrum of the impurity center in the case of a single-oscillator model	72
<b>K.B. Tsiberkin.</b> NUMERICAL SIMULATION OF LONG-TIME DYNAMICS OF FINITE DIPOLE ENSEMBLES	73
<b>N.A. Chumakova.</b> PHASE STATE OF POLAR LIQUIDS INSIDE GRAPHENE OXIDE MATERIALS ACCORDING TO SPIN PROBE TECHNIQUE	75
<b>A.V. Ilyasov.</b> DEVELOPMENT of FREE RADICAL EPR in KAZAN	76
<b>S.Y. Trakhinina.</b> Study of 3,3-bis-hydroxymethyl sterically shielded nitroxyl radicals of the pyrrolidine series by EPR spectroscopy	77
<b>G.A. Simenido.</b> PNIPAM Chains Collapse in Aqueous Solutions in Presence of Proteins: Spin Probe and Spin Label Study	78
<b>S.N. Arellano-Ahumada.</b> Paramagnetic markers in polycystic ovarian syndrome as a possible infertility cause: an EPR study	79
<b>D. Ramírez-Rosales.</b> Electrochemical test cell for in situ and in operando EPR characterization of Li-ion insertion battery electrodes	80
<b>N. Isaev.</b> Potential pharmaceutical pulse EPR applications for detection protein folding and environment upon lyophilization	81
<b>E.I. Boltenkova.</b> The different types of treatment effect on the DyF <sub>3</sub> nanoparticles agglomeration	82
<b>M.Ya. Fattakhova.</b> RECOVERY OF TEACHER'S VOICE FUNCTION AFTER CHRONIC DISEASES USING SPECTRAL VOICE ANALYSIS AND MRI	83
<b>Kh. L. Gainutdinov.</b> Investigation of NO and Copper Content in Injured and Non-Injured Areas of the Rats Brain by EPR Spectroscopy 24 Hours and 7 Days after Combined Brain and Spinal Cord Injury	84
<b>A. F. Shaidullina.</b> Structure determination and study of the internal dynamics of a $\beta$ -enaminone by NMR, UV spectroscopy and DFT	86
<b>S.A. Andreeva.</b> Pseudospin Quantum Phase Transition Probed by ESR	87
<b>V.N. Glazkov.</b> LOW-TEMPERATURE SPIN DYNAMICS AND MICROWAVE DIELECTRIC RESPONSE of 2D SQUARE KAGOMÉ LATTICE NABOKOITE FAMILY COMPOUNDS	88
<b>E.M. Alakshin.</b> Magnetic Properties of Rare-earth Trifluoride Nanoparticles	90
<b>R.A. Podarov.</b> Dipolar EPR Spectroscopy of Fullerene and Porphyrin Symmetric Pairs	91
<b>S.V. Sviyazov.</b> <sup>15</sup> N Hyperpolarization of Metronidazole Antibiotic in Aqueous Media Using Phase-Separated Signal Amplification by Reversible Exchange with Parahydrogen	93
<b>K.A. Baryshnikov.</b> RESTORATION of OPTICAL ORIENTATION of MANGANESE IONS SPINS in CUBIC ZnSe CRYSTAL in MAGNETIC FIELD	95
<b>G.Iu. Andreev.</b> MAGNETIC PROPERTIES OF LiErF <sub>4</sub> DIPOLAR MAGNET	96
<b>M. Gracheva.</b> IRON CITRATE COMPLEXES at BIOLOGICALLY RELEVANT CONDITIONS	97
<b>S.K. Dedushenko.</b> THE EFFECT OF THE SECOND COORDINATION SPHERE OF IRON ON THE <sup>57</sup> Fe-MÖSSBAUER ISOMER SHIFTS IN OXIDES	98

<b>F.G. Vagizov.</b> TRANSMISSION OF INFORMATION USING MÖSSBAUER PHOTONS	100
<b>E.V. Voronina.</b> ON THE MAGNETIC STRUCTURE OF TERNARY ORDERED Fe-Al-B ALLOYS	101
<b>A.A. Zalutskii.</b> SEPARATION OF CONTRIBUTIONS FROM EXCHANGEABLE AND STRUCTURAL FORMS OF IRON IN NATURAL CLAYS	103
<b>K.V. Frolov.</b> MOSSBAUER SPECTROSCOPY of the RARE EARTH FERROBORATES $\text{SmFe}_{3-x}\text{M}_x(\text{BO}_3)_4$ ( $\text{M} = \text{Al}, \text{Sc}$ )	105
<b>V.F. Musin.</b> HIGH-ENTROPY SYSTEM $\text{Mg}_{0.2}\text{Co}_{0.2}\text{Fe}_{0.2}\text{Ni}_{0.2}\text{Zn}_{0.2}\text{O}$ : SYNTHESIS, X-RAY DIFFRACTION and MÖSSBAUER STUDIES	106
<b>A.A. Samsonenko.</b> Microgravity-like Crystallization of Paramagnetic Species in Strong Magnetic Fields	108
<b>Z.I. Minnegulova.</b> AB INITIO RESEARCH of IMPURITY FERROMAGNETISM of PARAMAGNETIC PALLADIUM IONS	109
<b>R.V. Yusupov.</b> ULTRAFAST LIGHT-INDUCED MAGNETIZATION PRECESSION – A COMPLEMENTARY TOOL TO FMR FOR STUDIES OF THIN FERROMAGNETIC FILMS	110
<b>B.F. Gabbasov.</b> Surface induced anisotropy in MgO single crystals observed by EPR spectroscopy	111
<b>V.F. Tarasov.</b> UNUSUAL EPR SPECTRA of $\text{Cu}^{2+}$ DIMER ASSOCIATES in $\text{BaF}_2$ SINGLE CRYSTAL	112
<b>E.K. Abdrakhimova.</b> First-principles investigation of the Rashba–Dresselhaus giant spin splitting in the structure of $\text{OsH}_2(\text{bipyridine\_CN})$	113
<b>D.S. Rybin.</b> FREE RADICAL MECHANISMS of AMORPHIZATION of BIOINORGANIC COMPOUNDS	114
<b>S.V. Yurtaeva.</b> VARIATION OF THE EPR SPECTRA OF NON-MORPHOGENIC BUCKWHEAT CELL CULTURE DURING GROWTH AND CELL DIVISION	115
<b>N.E. Litovskikh.</b> STRUCTURE of ZINC FINGER of the <i>E. COLI</i> FPG in the SOLUTION	116
<b>V.A. Ulanov.</b> MUTUAL DEPENDENCES OF DINAMICAL PROPERTIES OF $\text{Mn}^{2+}$ AND $\text{Gd}^{3+}$ IMPURITY CENTERS IN $\text{Pb}_{1-x-y-z}\text{Cu}_x\text{Mn}_y\text{Gd}_z\text{S}$ NARROW-BAND SEMICONDUCTOR: RESULTS OF EPR STUDY	118
<b>A.M. Ziatdinov.</b> NEW PROPERTIES OF TITANIUM DIOXIDE HEAT-TREATED IN VARIOUS ENVIRONMENTS ACCORDING TO ELECTRON MAGNETIC RESONANCE DATA	120
<b>K.V. Evseev.</b> DFT INVESTIGATION of MAGNETOELECTRIC COUPLING in Fe/ $\text{BaTiO}_3$ HETEROSTRUCTURE	123
<b>D.A. Saritsky.</b> Electron Paramagnetic Resonance in Nanocrystalline Potassium Tetratitanate Doped with Copper Ions	125
<b>V.D. Zhaketov.</b> POLARIZED NEUTRON REFLECTOMETRY FOR INVESTIGATION OF LOW-DIMENSIONAL 2D MAGNETIC & SUPERCONDUCTING HETEROSTRUCTURES	127
<b>S.A. Dementev.</b> Effective Spin Traps for Singlet Oxygen Detection in Physiological Conditions	128



<b>T.A. Khlynova.</b> Investigation of the HTel-22 G-quadruplex Complex with Cationic Porphyrin by EPR and Optical Spectroscopy Methods	130
<b>M.V. Matveev.</b> JOINT USE OF SPIN PROBE TECHNIQUE AND SCANNING ELECTRON MICROSCOPY TO STUDY THE INTERNAL STRUCTURE OF GRAPHENE OXIDE MEMBRANES	131
<b>A.A. Timralieva.</b> LIGHT-INDUCED TWO-CYCLE RADICAL FORMATION in SUPRAMOLECULAR CRYSTALLINE MATRIX	132

## POSTERS

[134](#)

<b>M.M. Bakirov.</b> The Dipole–Dipole Interaction Contribution to EPR Spectra of Nitroxyl Free Radical Solution	135
<b>E.E. Batueva.</b> New Fe(III) complexes of NNO tridentate $\beta$ -enaminone in solutions: EPR research and molecular docking	136
<b>E.E. Batueva.</b> Heptanuclear Fe(II)–Fe(III) complex as a multifunctional magnetic material	137
<b>A.A. Evseev.</b> <i>AB INITIO</i> INVESTIGATION OF RASHBA SPLITTING HETEROSTRUCTURES FOR SPINTRON APPLICATIONS	138
<b>I.I. Gimazov.</b> Impact of spin correlations on resistivity and microwave absorption of iron pnictides doped with cobalt	139
<b>A.A. Karpeev.</b> EPR in polymer composites with carbon black	140
<b>Zh.K. Pulotov.</b> Magneto-resonant properties and spin-Hall effects in epitaxial Pd <sub>1-x</sub> Fe <sub>x</sub> and Pd <sub>1-x</sub> Fe <sub>x</sub> /Pt thin film structures	142
<b>V.O. Sakhin.</b> Magnetotransport Investigation of Pb/Bi <sub>1.08</sub> Sn <sub>0.02</sub> Sb <sub>0.9</sub> Te <sub>2</sub> S Heterostructures	144
<b>A.I. Shamsieva.</b> COMPUTER DESIGN OF NEW ORGANIC MATERIALS FOR METAL-ION BATTERIES	145
<b>A.V. Shestakov.</b> OBSERVATION OF A GRIFFITHS PHASE AND ANALYSIS OF THE CRITICAL EXPONENTS IN THE MAGNETIC BEHAVIOR OF La <sub>0.7</sub> Sr <sub>0.3</sub> Mn <sub>0.9</sub> Fe <sub>0.1-x</sub> Zn <sub>x</sub> O <sub>3</sub> ( $x = 0.05, 0.075, 0.1$ )	146
<b>A.V. Shestakov.</b> HIGH TEMPERATURE ESR ABSORPTION of Fe <sub>45</sub> Co <sub>30</sub> Si <sub>10</sub> B <sub>15</sub> MICROWIRE	147
<b>A.V. Shestakov.</b> STUDY of LOW-TEMPERATURE SPIN FLUCTUATION TRANSITION in the CONICAL PHASE of MnSi and ANISOTROPY FEATURES	148
<b>D.V. Starichenko.</b> Comprehensive study of magneto-resonance properties of dendrimer metal complexes of polydentate N,O-ligands using the example of a new Fe <sup>3+</sup> $\beta$ -diketonate	150
<b>A. A. Sukhanov.</b> Ferromagnetic resonance in Co-ions implanted SnO <sub>2</sub> films: Effects of oxygen vacancies	152
<b>N.Kh. Useinov.</b> RESONANCE CONDUCTANCE of ELECTRONS on INTERFACES of MAGNETIC TUNNEL JUNCTION	154
<b>V. Voronkova.</b> Electron Spin Polarization Dynamics of the Photoexcited Triplet States of the organic chromophores and donor-acceptor Dyads: Analysis of the TREPR spectra Evolution	156
<b>N.V. Yantsen.</b> Effect of carbon black content on the EPR linewidth in a composite based on an ethylene vinyl acetate matrix EPR	158

<b>R.B. Zaripov.</b> ESEEM study of Y3N@C80 under photoexcitation	161
<b>R.B. Zaripov.</b> EPR study of iron impurities in BaF <sub>2</sub> single crystal under X-ray irradiation	162
<b>A.V. Bogaychuk.</b> Cylindrical and sphere Halbach magnet arrays	163
<b>D.S. Ivanov.</b> PECULIARITIES OF PORE SPACE INVESTIGATION BY NMR RELAXOMETRY AND CRYOPOROMETRY METHODS	164
<b>I.T. Khairutdinov.</b> Simulation of CPMG Sequence Echo Signals with Gaussian Pulse Shape	166
<b>D. Ramírez-Rosales.</b> Electrochemical test cell for in situ and in operando EPR characterization of Li-ion insertion battery electrodes	168
<b>K.O. Sannikov.</b> LOW TEMPERATURE NMR PROBE with VARIABLE FREQUENCY	169
<b>A.V. Tuckachev.</b> THE PROMISES OF LOW-FIELD MAGNETIC RESONANCE IMAGING	170
<b>A.L. Valiullin.</b> Development of a software product for design gradient systems in nuclear magnetic resonance equipment	172
<b>A.M. Garaeva.</b> SURFACE AND VOLUME CENTERS IN LaF <sub>3</sub> PARTICLES	174
<b>T.P. Gavrilova.</b> Sorption-Oxidation Mechanism for the Removal of Arsenic (III) Using Cu-Doped ZnO in an Alkaline Medium	175
<b>A.Yu. Germov.</b> NMR and MOSSBAUER SPECTROSCOPY STUDY of the POSSIBILITY of OBTAINING HOMOGENEOUS NANOPARTICLES BASED on FeCu ALLOYS	177
<b>Yu. Goryunov.</b> The Mn <sup>2+</sup> EPR study of Cd <sub>3</sub> P <sub>2</sub> for topological tuning with 3D Dirac semimetal Cd <sub>3</sub> As <sub>2</sub>	178
<b>A.S. Gurin.</b> Electron paramagnetic resonance investigations of β -Ga <sub>2</sub> O <sub>3</sub> single crystals doped with chromium	179
<b>R.I. Khaibullin.</b> Magnetic anisotropy in rutile (TiO <sub>2</sub> ) heavily implanted with cobalt ions: FMR, VSM and TEM studies	181
<b>E.I. Kovvycheva.</b> MODELING THE MAGNETIC RESPONSE OF FUNCTIONALIZED CARBON STRUCTURES	182
<b>V.A. Latypov.</b> ESR of Yb <sup>3+</sup> ION at CUBIC SITES in Cs <sub>2</sub> NaScF <sub>6</sub> CRYSTALS	184
<b>R. F. Likerov.</b> <sup>59</sup> Co CENTERS IN MONOCLINIC Sc <sub>2</sub> <sup>28</sup> SiO <sub>5</sub> SINGLE CRYSTAL: CW EPR STUDY	186
<b>G.V. Mamin.</b> Electron nuclear double resonance of <sup>14</sup> N nuclei coupled to the V <sub>B</sub> <sup>-</sup> defect in hBN crystals	187
<b>F.F. Murzakhonov.</b> Optical Spin Initialization of Nitrogen Vacancy Centers in a <sup>28</sup> Si-Enriched 6H-SiC Crystal for Quantum Technologies	188
<b>A.V. Nikitina.</b> STUDIES OF STATIONARY SATURATION OF INHOMOGENEOUSLY BROADENED EPR LINES OF N-V CENTERS IN HPHT DIAMOND	189
<b>G.S. Patrín.</b> INFLUENCE OF THE INTERFACE ON MAGNETIC RESONANCE IN FILMS OF THE Fe-Bi SYSTEM	190
<b>G.S. Patrín.</b> LONG-RANGE INTERLAYER COUPLING IN [(CoP) <sub>hard</sub> /(NiP) <sub>am</sub> /(CoP) <sub>soft</sub> ] <sub>n</sub> STRUCTURES	191

<b>G.S. Patrin.</b> MAGNETIC RESONANCE STUDIES OF BIQUADRATIC INTERLAYER COUPLING IN CoNi/Si/FeNi FILMS	193
<b>A.P. Podshivalov.</b> THE INFLUENCE OF CENTRIFUGATION ON DOSIMETRIC PROPERTIES OF SYNTHETIZED HYDROXYAPATITE	194
<b>A.V. Popov.</b> Combined equation of semiclassical spin dynamics and electron paramagnetic resonance	195
<b>D.V. Popov.</b> ADDITIONAL EPR LINE IN Mn-CONTAINING DOUBLE PEROVSKITES	197
<b>I.V. Romanova.</b> SYNTHESIS AND STUDY OF MAGNETIC PROPERTIES OF [La <sub>0.5</sub> Dy <sub>0.5</sub> ]ES AND [La <sub>0.99</sub> Dy <sup>0.01</sup> ]ES COMPOUNDS	198
<b>N.S. Saenko.</b> Modeling of Magnetic Resonance Spectra of La <sub>1-x</sub> K <sub>x</sub> MnO <sub>3</sub>	199
<b>G.S. Shakurov.</b> ANTI-SITE DEFECTS and TRIGONAL CENTER of HOLMIUM in Y <sub>3</sub> Al <sub>5</sub> O <sub>12</sub> :Ho <sup>3+</sup> CRYSTAL ACCORDING to the RESULTS of WIDEBAND EPR SPECTROSCOPY	201
<b>A.A. Shavelev.</b> DISTRIBUTION OF Ce <sup>3+</sup> IMPURITY CENTERS IN HIGHLY DOPED LiCaAlF <sub>6</sub> CRYSTALS	202
<b>D.E. Zhelezniakova.</b> ESR IN EuSn <sub>2</sub> As <sub>2</sub> CRYSTALS CLOSE TO MAGNETIC ORDERING TEMPERATURE	203
<b>A.N. Afanaseva.</b> STUDYING PORE SPACE of a CORE by NUCLEAR MAGNETIC RESONANCE METHOD	204
<b>M.M. Akhmetov.</b> W-BAND EPR OF RADICALS IN CALCIUM GLUCONATE	206
<b>V. V. Andrianov.</b> STUDY by EPR SPECTROSCOPY of BRAIN TISSUE SAMPLES in MODELS with BRAIN DISORDERS	208
<b>M.A. Demekhin.</b> DFT CALCULATION as a TOOL to FIND C-CENTERED RADICALS LOCALIZATION in SUPRAMOLECULAR ASSEMBLIES	210
<b>A.R. Gafarova.</b> CALCIUM FREE RADICAL FORMATION at IRRADIATION and MECHANOACTIVATION of CALCIUM GLUCONATE	212
<b>R.T. Galeev.</b> STUDY OF BIRADICALS BY THE TRANSIENT NUTATION METHOD	213
<b>M.I. Ibragimova.</b> Identification of the signal with $g \sim 6.0$ in the X-band EPR spectra of human blood serum at 5-40 K	214
<b>D.L. Melnikova.</b> TRANSLATIONAL DIFFUSION FEATURES OF AN INTRINSICALLY DISORDERED PROTEIN	216
<b>A.A. Petrova.</b> EPR INVESTIGATIONS OF COMPOSITE MATERIALS BASED ON BIOCOMPATIBLE POLYMERS WITH CALCIUM PHOSPHATES	217
<b>M.A. Sadovnikova.</b> Study of hydroxyapatite doped with rare earth ions by various EPR spectroscopy techniques	219
<b>E.I. Shamsiyarova.</b> Determination of water content in crude oil by nuclear magnetic resonance: problems and possible solutions	220
<b>A.R. Sharipova.</b> EFFECT of COUNTERION on MAGNETIC PROPERTIES of the NEW Fe(III) COMPLEXES WITH a N <sub>2</sub> O TRIDENTATE LIGAND	221
<b>A.R. Sharipova.</b> Study of trans/cis isomerization of molecules of two 2-hydroxy-5-phenylazobenzaldehyde derivatives by NMR and UV spectroscopy	222

<b>Yu. Slesareva.</b> $^1\text{H}$ NMR ANALYSIS of ACETONITRILE INTERCALATED into the INTERPLANE SPACE of GRAPHITE OXIDE	223
<b>A.S. Tarasov.</b> Studying of paramagnetic effect of $\text{Dy}^{3+}$ ion on the complex of cyclosporin C (CsC) and DPC micelle in aqueous solution determined by NMR spectroscopy	224
<b>A.A. Troshkina.</b> Structure of the amyloidogenic peptide SEM2(49-107) by NMR spectroscopy	226
<b>D.A. Tsukhlova.</b> Features of nuclear magnetic relaxation in aqueous solutions of saccharides	228
<b>A.M. Uporova.</b> INVESTIGATION of Mn VALENCE STATE in $\text{Sr}_2\text{Ti}_{1-x}\text{Mn}_x\text{O}_4$ COMPOSITION COMPOUNDS by EPR METHOD	229
<b>V.E. Vorobeva.</b> Magnetic and EPR properties of the second generation dendrimeric $\text{Fe}^{3+}$ complexes with fluorescent environment	231
<b>I.V. Yatsyk.</b> MAGNETIC PROPERTIES OF PEROVSKITE TYPE HIGH ENTROPY OXIDES	233
<b>R.I. Zaripova.</b> Effect of motor activity restriction on copper content in rat liver	234
<b>M.R. Arifullin.</b> IMPLEMENTATION OF QUANTUM LOGIC BY PHASE SHIFT PULSES AND HIGH-SPIN IONS	236
<b>B.F. Farrakhov.</b> The SILICON SURFACE MICROSTRUCTURES INITIATED by a POWERFUL LIGHT PULSE for INCREASE The EFFECTIENCY OF a SOLAR CELLS	237
<b>A.A. Bayazitov.</b> DEVELOPMENT OF A PHASE-ADJUSTED RADIO-FREQUENCY SOLENOID SENSOR FOR MEDIUM-FIELD MAGNETIC RESONANCE IMAGING SYSTEM	238
<b>T.R. Islamov.</b> Study of the interaction of lovastatin with a transition group metal - gadolinium in solution using NMR spectroscopy	239
<b>V.V. Kuzmin.</b> HOME-BUILT SET-UP FOR NMR/DNP IN STRAY FIELD OF SUPERCONDUCTING MAGNET	241
<b>V. Odivanov.</b> Targeting interface for MR imaging	242
<b>D.I. Silantyeva.</b> Investigation of NO and copper content in different segments of spinal cord 24 hours and 7 days after combined brain and spinal cord injury in rat with using the method EPR Spectroscopy	244
<b>S.V. Yurtaeva.</b> EMR signals in rat spinal cord 7 days after its traumatic injury	246
<b>A.F. Abdullin.</b> FIRST PRINCIPLES CALCULATIONS of MAGNETIC ORDER of Fe-Al BASED TERNARY ALLOYS	247
<b>N.I. Chistyakova.</b> MÖSSBAUER STUDY OF THE MINERALS FORMED DURING SYNTHESIZED FERRIHYDRITE REDUCTION BY REPRESENTATIVES OF THE <i>MELIORIBACTERACEAE</i> FAMILY	248
<b>E.N. Dulov.</b> MÖSSBAUER SPECTROSCOPY BASED ON FAST STREAMING ANALOG TO DIGITAL CONVERTORS	249
<b>K.V. Frolov.</b> MÖSSBAUER SPECTROSCOPY of Fe ORGANIC-DERIVED COMPOSITE FISCHER-TROPSCH CATALYSTS OBTAINED by the HYDROTHERMAL SYNTHESIS	250

**A.V. Pyataev.** The WEATHERING RATE of ATACAMA METEORITES  
STUDIED by MÖSSBAUER SPECTROSCOPY 251

**SPONSORS** 253

# ZAVOISKY AWARD LECTURES

## FUNDAMENTAL ROLE OF EPR METHOD IN DISCOVERY, IDENTIFICATION AND STUDY OF DINITROSYL IRON COMPLEXES IN LIVING ORGANISMS

Anatoly F. Vanin

N.N. Semenov Federal Research Center for Chemical Physics of RAS, Moscow, Russia

In my lecture I plan to focus on the fact that

1. Using only the EPR method, based on the EPR signal characteristic of dinitrosyl iron complexes (the EPR signal with an average g-factor value of 2.03 – the "2.03 signal"), we were able not only to discover, but then identify first in yeast cells and then in animal tissues, the said complexes, which include thiol-containing ligands,
2. Analyzing the parameters of the 2.03 signal – the g-factor value and the hyperfine splitting of this signal, we came to the conclusion about the d<sup>7</sup> electron configuration of iron in the DNIC we discovered – [Fe(NO)<sub>2</sub>]<sup>7</sup> structure of the iron-dinitrosyl DNIC fragments in the Enemark-Feltham representation, corresponding to the resonance structure of the EPR-active mononuclear form of DNIC (M-DNIC): [(RS)<sub>2</sub>Fe<sup>2+</sup>(NO)(NO<sup>+</sup>)]. A similar resonance structure is also characteristic of the EPR-inactive binuclear form of DNIC (B-DNIC): [(RS)<sub>2</sub>Fe<sup>2+</sup><sub>2</sub>(NO)(NO<sup>+</sup>)]
3. These resonance structures of DNIC also follow from the analysis of the mechanism of formation of these complexes proposed by us, which is based on the reaction of disproportionation of NO molecules, which bind in pairs with the Fe<sup>2+</sup> ion. The nitroxide anion (NO<sup>-</sup>) that appears as a result of this reaction is protonated and leaves the ligand environment of iron, and its place is taken by another NO molecule. As for the nitrosonium cation that appears in the disproportionation reaction, its hydrolysis is suppressed as a result of the displacement of the electron density from the sulfur atom of one of the thiol-containing ligands to the nitrosonium cation.
4. The specified resonance structure ensures the functioning of DNIC with thiol-containing ligands in living organisms as donors of neutral NO molecules, now recognized as universal regulators of various biological processes, and as donors of nitrosonium cations, the cytotoxic components of DNIC. These properties of DNIC have been demonstrated by us and other researchers in experiments on cell cultures and animals, as well as in tests on volunteers.
5. DNIC with thiol-containing ligands act in living organisms as a "working form" of the endogenous nitric oxide system. This conclusion follows from the fact of the high biological activity of these complexes, comparable to the activity of the endogenous NO system, as well as from the results of a quantitative comparison of the level of endogenous NO and DNIC in animal tissues, carried out using the EPR method.
6. Chemical synthesis of DNIC with thiol-containing ligands can become the basis for creating virtually "natural" drugs with a variety of therapeutic effects.

*Research conducted in 2023-2024 under items 4-5 was carried out with the financial support of the Russian Science Foundation grant No. 23-74-00009*

## DNP and EPR at Millimeter Wavelengths

Robert G. Griffin

Francis Bitter Magnet Laboratory and Department of Chemistry  
Massachusetts Institute of Technology, Cambridge, Massachusetts 02139, USA  
rgg@mit.edu

In the 1950's DNP was demonstrated to enhance sensitivity of NMR spectra by Overhauser and Slichter. Nevertheless, it remained a latent technique, because there were not suitable high frequency microwave sources available to perform DNP or EPR at high fields ( $>5$  T). This stimulated us to introduce gyrotron oscillators as scalable frequency sources that would enable DNP at arbitrarily high fields/frequencies. Concurrently, we built a 140 GHz EPR which today operates in pulse mode. Currently, there are about 60 gyrotron oscillators operating in DNP spectrometers around the globe at frequencies up to 593 GHz and there are plans to operate them at 790 GHz (28.2 T). EPR is now also performed in the subterahertz regime

The primary continuous wave (CW) DNP mechanisms are the solid effect (SE), the Overhauser effect (OE) and cross effect (CE) and we discuss how each of these mechanism scales with  $\omega_0$ , and the polarizing agents appropriate for each.

One of the main thrusts of DNP was to provide increased sensitivity for magic angle spinning (MAS) spectroscopy of membrane and amyloid protein experiments. A problem frequently encountered in these experiments is the broadened resonances that occur at low temperatures when motion is quenched. In some cases it is clear that protein spectra are homogeneously broadened, and therefore that higher Zeeman fields and faster spinning is required to recall the resolution. We show this is the case for MAS DNP spectra of A $\beta$ <sub>1-42</sub> amyloid fibrils where the resolution at 100 K is identical to that at room temperature. Furthermore, we compare the sensitivity of DNP and <sup>1</sup>H detected experiments and find that DNP, even with a modest  $\epsilon=22$ , is  $\sim x6.5$  times more sensitive. Bacteriorhodopsin is the archetypical membrane protein and studies of its photocycle intermediates have been possible because of the signal enhancements provided by DNP.

Recently, we have also investigated time domain DNP/EPR experiments, such as time optimized pulsed (TOP) DNP, the frequency swept-integrated solid effect (FS-ISE) and two recently discovered variants – the stretched solid effect (SSE) and the adiabatic solid effect (ASE). We find that the latter two experiments can give up to a factor of  $\sim 2$  larger enhancement than the FS-ISE. The SSE and ASE experiments should function well at high fields.

Finally, we discuss two new instrumental advances. First, a frequency swept microwave source that permits facile investigation of field profiles. It circumvents the need for a  $B_0$  sweep coil and the compromise of field homogeneity and loss of helium associated with such studies. This instrumentation has permitted us to elucidate the polarization transfer mechanism of the Overhauser effect, and also revealed interesting additional couplings (ripples) in field profiles of cross effect polarizing agents. Second, to improve the spinning frequency in DNP experiments, we have developed MAS rotors laser machined from single crystal diamonds. Diamond rotors should permit higher spinning frequencies, improved microwave penetration, and sample cooling.



# PLENARY LECTURES

## HOW THE EPR HAS BEEN DISCOVERED? THE ANALYSIS OF ZAVOISKY'S LOGBOOKS

**A.V. Dooglav<sup>1,2</sup>, A.L. Larionov<sup>1</sup>, F.R. Vagapova<sup>2</sup>**

<sup>1</sup> Kazan Federal University, Institute of Physics, Kazan, Russia

<sup>2</sup> Kazan Federal University, Memorial Laboratory-Museum of E.K. Zavoisky

The analysis of E.K. Zavoisky's logbooks allowed us to come to the conclusion that the discovery of the EPR phenomenon took place due to four circumstances:

1. Zavoisky, long before the rest of the scientific community, realized that radio engineering methods allow indirect methods to study the interaction of matter with electromagnetic fields. The reason is that Zavoisky became interested in amateur radio from a young age. One of the discoverers of the NMR phenomenon, Nobel laureate Robert V. Pound, in his article "From radar to nuclear magnetic resonance" [1] concludes that in his scientific group such realization came only as a result of the fact that they spent all the years of World War II at the Massachusetts Institute of Technology developing a Radar. The Zavoisky generator, although it operated at very low frequencies, not typical of modern EPR spectrometers, had excellent sensitivity to additional losses in the coil of the oscillatory circuit of the generator arising from EPR absorption. The sensitivity of the generator was so high that if Zavoisky had an electromagnet with a highly uniform magnetic field, he could have discovered the NMR phenomenon [2].

2. Zavoisky realized that at a frequency of the order of 10 MHz, the ESR phenomenon should be observed in a magnetic field of several Oerstedes. To get rid of the residual magnetization of the electromagnet used, Zavoisky switched from an electromagnet to a solenoid, which, as is known, does not have a residual field.

3. The use of low-frequency (50 Hz) magnetic field modulation made it possible to easily observe the EPR phenomenon on the screen of the oscilloscope he had, the horizontal sweep of which was synchronized with the modulation voltage.

4. And finally, Zavoisky was very lucky that the width of the EPR line in the concentrated paramagnets he studied was not the typical several hundred Oerstedes, but due to exchange narrowing it was much lower. This, by the way, was noted by C.J. Gorter in his speech at the ceremony of awarding him the Fritz London Prize in 1966 [3].

1. R. Pound. "From Radar to nuclear magnetic resonance". Review of Modern Physics, Vol. 71, No. 2, S54-S58 (1999)

2. I.I. Silkin, F.R. Vagapova, A.V. Dooglav. "E.K. Zavoisky i YaMR: analiz laboratornyh zapisej i povtorenie eksperimentov." Low Temperature Physics, т. 41, № 1, 7-13 (2015) (In Russian)

3. C.J. Gorter. "Bad luck in attempts". Physics today, Vol. 76, 76-81 (1967)

## **ELECTRON AND HOLE $g$ FACTORS IN SEMICONDUCTORS AND SEMICONDUCTOR NANOSYSTEMS**

**E.L. Ivchenko**

Ioffe Institute, 194021, St.-Petersburg, Russia

In this talk, I will give an overview of experimental and theoretical studies of the Zeeman effect in semiconducting materials. The Landé factor, or  $g$  factor, is an important band parameter which describes spin splitting of electron and hole states as well as of Wannier—Mott exciton levels in an external magnetic field.

The first part of the talk presents different methods to measure the  $g$  factors, namely, (i) electron paramagnetic resonance (EPR), (ii) optically detected magnetic resonance (ODMR), (iii) spin-flip Raman scattering, (iv) spectral resolution of exciton sublevels, (v) magnetic circular polarization of luminescence (MCPL), (vi) the Hanle effect, (vii) quantum spin beats, (viii) magnetic-field induced anticrossing of exciton sublevels, (ix) measurements of spin noise in the magnetic field.

The second part is focused on the theory of Zeeman effect. I will start with the bulk semiconductors  $A_3B_5$  and  $A_2B_6$  of cubic symmetry, where the electron  $g$  factor is well described by the Roth—Lax—Zwerdling formula and where  $g$  factor values vary from  $\sim 2$  in the wide-gap semiconductors to  $-51$  in the narrow-gap InSb compound. Another example will be lead halide perovskite crystals  $APbX_3$  ( $A$  – Cs, MA, FA;  $X$  – Cl, Br, I). Then I will consider quantum well structures where the electron  $g$  factor becomes anisotropic with the longitudinal and transverse components strongly dependent on the well thickness. The theoretical part is concluded by an analysis of  $g$  factors in quantum dots and specifics of the Zeeman effect on holes in the valence band of a semiconductor.

## MICROBIOLOGICAL APPLICATIONS of MÖSSBAUER SPECTROSCOPY

A.A. Kamnev

Institute of Biochemistry and Physiology of Plants and Microorganisms, Saratov Federal Scientific Centre of the Russian Academy of Sciences, Saratov, Russia

Soon after the discovery of the Mössbauer effect, since early 1960s it has been used as a physical basis of the unique and highly informative technique, Mössbauer spectroscopy. While the latter is generally referred to the scientific field of nuclear chemistry, all the parameters that can be calculated from experimentally measured Mössbauer spectra provide information on the molecular-level properties of the Mössbauer-active nuclide and its microenvironment. Hence, Mössbauer spectroscopy may also be considered as a worthy representative of molecular spectroscopy techniques (for recent reviews on its diverse applications see, e.g., [1–5]).

Within the extremely sophisticated field of life sciences, whenever a Mössbauer-active nuclide is contained in (or can be inserted as a probe into) any tested biomaterials (biocomplexes, supramolecular structures, cells, tissues, organisms), Mössbauer spectroscopy as a nondestructive technique can be indispensable. It has indeed been increasingly used, providing unique data of highest resolution on the *in-situ* chemical state of Mössbauer-active nuclides. Since iron is among the most important biological microelements, the stable  $^{57}\text{Fe}$  isotope has largely been used in the transmission variant of Mössbauer spectroscopy (while radioactive  $^{57}\text{Co}$  can also be utilised as a probe in the highly sensitive emission variant) [4–6].

Microbiological *in-situ* and *in-vivo* applications (e.g., involving live cell biomass samples either rapidly frozen or in the dried state) of Mössbauer spectroscopy are of significant importance from the viewpoint of basic research, e.g., for investigating the chemical state of cellular iron, a vitally important component of many enzymes, metalloproteins and ferritins (iron storage-and-reserve compounds in all organisms), its uptake and redox transformations in microbial cells under different conditions [4, 5, 7]. These data are useful also for such applied fields as microbial and agricultural biotechnology, where microbial preparations are stored in deeply frozen or dried states, as well as for clarifying and optimising the conditions for their stability and long-term survival. Examples from such collaborative studies of the author's research team and from the recent literature will be illustrated and discussed in this talk.

The author's recent studies in this field have been supported by the Russian Science Foundation (grant # 24-26-00209).

1. Alenkina I.V., Oshtrakh M.I.: J. Pharmaceut. Sci. **113**, 1426–1454 (2024)
2. Dedushenko S.K., Perfiliev Yu.D.: J. Radioanal. Nucl. Chem. **332**, 2613–2632 (2023)
3. Wareppam B., Kuzmann E., Garg V.K., Herojit Singh L.: J. Mater. Res. **38**, 937–957 (2023)
4. Kamnev A.A., Tugarova A.V. Russ. Chem. Rev. **90**, 1415–1453 (2021)
5. Kamnev A.A., Tugarova A.V.: Talanta **174**, 819–837 (2017)
6. Kamnev A.A., Perfiliev Yu.D., Kulikov L.A., Tugarova A.V., Kovács K., Homonnay Z., Kuzmann E.: Spectrochim. Acta Part A: Mol. Biomol. Spectrosc. **172**, 77–82 (2017)
7. Kamnev A.A., Tugarova A.V., Shchelochkov A.G., Kovács K., Kuzmann E.: Spectrochim. Acta Part A: Mol. Biomol. Spectrosc. **229**, 117970 (2020)

## **EPR as a TOOL for STUDYING MAGNETIC FLUCTUATIONS in STRONGLY CORRELATED ELECTRONIC SYSTEMS**

**S.V. Demishev**

Vereshchagin Institute for High Pressure Physics of the Russian Academy of Sciences, Troitsk, Moscow,  
Russia

Semiclassical magnetization dynamics in presence of magnetic fluctuations (including the quantum ones) is of crucial importance for correct analysis of electron paramagnetic resonance (EPR) in various strongly correlated systems. This is due to essential difficulties arising in rigorous treatment of dynamic susceptibility in a magnetic field for this class of materials. In the present talk, we discuss semiclassical magnetization dynamics quantitatively accounting magnetic fluctuations in the region of the linear magnetic response [1]. Landau-Lifshitz (LL) and Gilbert (G) type equations are obtained with the effective parameters depending on the type of magnetic fluctuations and their magnitude and applied to evaluation of EPR problem in Faraday geometry. It is shown that in the studied systems LL and G equations are dramatically different except the case of weak relaxation, where new consistent Landau-Lifshitz-Gilbert (LLG) equation is proposed. Whereas G equation is affected by quantum fluctuations solely, the LL and LLG equations may be renormalized by magnetic fluctuations of any nature. In contrast to G equation, the LL and LLG magnetization dynamics may be characterized by the anisotropic relaxation term caused by anisotropic magnetic fluctuations. A consequence of anisotropic relaxation is the unusual polarization effect consisting in strong dependence of the EPR line magnitude on orientation of vector  $\mathbf{h}$  of the oscillating magnetic field with respect to the crystal structure (Fig. 1), so that EPR may be suppressed for some directions of  $\mathbf{h}$  [1,2]. In the case of dominating quantum fluctuations, the LL and LLG equations may lead to a universal relation between fluctuation induced contributions to the EPR line width  $\Delta W$  and g-factor  $\Delta g$  in the form  $\Delta W / \Delta g = a_0 k_B T / \mu_B$ , where  $a_0$  is a numerical coefficient of the order of unity and independent of the quantum fluctuation magnitude. It is shown that the proposed semiclassical magnetization dynamics models may be applied for the identification in spin nematic phases by EPR. Another promising area of this theory is detection by EPR method of a new group of magnetic phenomena – spin fluctuation transitions (SFTs) [3,4]. A SFT is a change in the characteristics of spin fluctuations in a magnet under the influence of control parameters (for example, temperature or material composition) that is not directly related to the formation of phases with long-range magnetic order. Therefore, SFT in most cases go beyond the standard theory of phase transitions, which is characterized by the consideration of fluctuations as some phenomenon accompanying the magnetic transition. At present SFTs are discovered in helical magnets MnSi and Mn<sub>1-x</sub>Fe<sub>x</sub>Si, magnetic semiconductors Hg<sub>1-x</sub>Mn<sub>x</sub>Te, doped compensated semiconductors Ge:As(Ga), strongly correlated metal with hidden order CeB<sub>6</sub> and in Ising disordered systems [3-5]. We argue that EPR analyzed on

the basis of semiclassical magnetization dynamics constitutes a powerful tool for investigation of SFTs, and further research in this direction may turn out to be one of the points of growth in modern physics of magnetic phenomena.

1. Demishev S.V.: Appl. Magn. Reson. (2024). <https://doi.org/10.1007/s00723-023-01638-4>
2. Demishev S.V., Semeno A.V.: Appl. Magn. Reson. **53**, 1505-1516 (2022)
3. Demishev S.V.: Appl. Magn. Reson. **51**, 473–522 (2020)
4. Demishev S.V.: Physics – Uspekhi, **67**, 22-43 (2024)
5. Demishev S.V., Shestakov A.V., Yatsyk I.V., Semeno A.V., Grigoriev S.V., Eremina R.M.: Sol. State Commun. **385**, 115501 (2024)

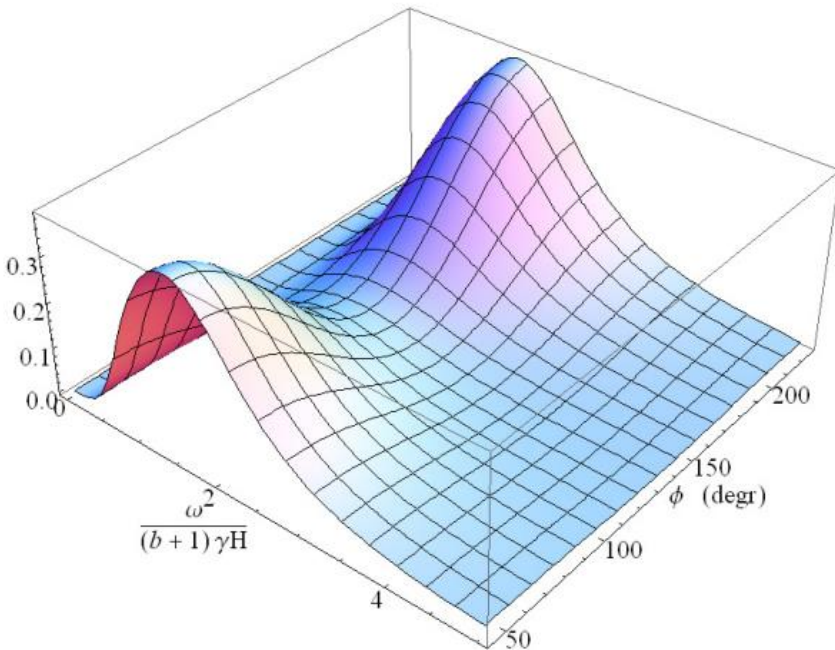


**Fig. 1.** Polarization effect in EPR line shape following from Landau-Lifshitz equation and consistent Landau-Lifshitz-Gilbert equation with anisotropic relaxation caused by anisotropic magnetic fluctuations. The case of broad EPR line and moderate anisotropy magnetic fluctuation anisotropy is shown. The 3D plot is presented in coordinates given by reduced microwave frequency  $\omega/(1+b)\gamma H$  and angle  $\phi$  between vector  $\mathbf{h}$  and crystallographic axis in the plane perpendicular to the direction of external magnetic field  $H$ . Here  $\gamma$  is gyromagnetic ratio and  $b$  describes the effect of quantum fluctuations. From [1].

## MAGNETIC RESONANCE APPLICATIONS IN STRUCTURAL STUDIES OF LARGE MACROMOLECULAR COMPLEXES

**K.S. Usachev<sup>1,2,3</sup>, V.V. Klochkov<sup>2</sup>, M.R. Gafurov<sup>4</sup>, A.V. Aganov<sup>2</sup>,  
M.M. Yusupov<sup>1,3</sup>**

<sup>1</sup>Laboratory of Structural Biology, Institute of Fundamental Medicine and Biology, Kazan Federal University, Kazan, Russia

<sup>2</sup>NMR laboratory, Institute of Physics, Kazan Federal University, Kazan, Russia

<sup>3</sup>Laboratory for Structural Studies of Biomacromolecules, FRC Kazan Scientific Center of RAS, Kazan, Russia

<sup>4</sup>Institute of Physics, Kazan Federal University, Kazan, Russia

Magnetic resonance is one of the key techniques in structural biology, along with X-ray crystallography and cryo-electron microscopy. The high-resolution structure of large macromolecular complexes is often difficult to analyze by magnetic resonance because of their large size and slow rotation in solution, leading to longer correlation times and signal broadening in spectra. NMR analysis of the structure and dynamics of individual components of the complex allows us to obtain information that is inaccessible by other methods, such as the structure of highly mobile regions that are not visible due to image averaging in cryo-electron microscopy, or intermolecular contacts using saturation transfer methods between molecules with natural isotopic abundance and enriched in <sup>13</sup>C/<sup>15</sup>N nuclei [1-3]. The possibility of increasing the molecular mass of the object by introducing membrane-mimetic media, such as micelles and bicelles, is another way of using NMR spectroscopy to analyze small molecules for which the NOE value falls in the range of values close to zero [4]. The introduction of paramagnetic tags into the structure of nucleic acid or protein molecules makes it possible to analyze inter-nuclear distances and the dynamics of large macromolecular ensembles, such as ribosomes, by EPR spectroscopy [5, 6]. As a result, the combination of structural biology techniques can reveal the details of biochemical reactions at atomic resolution and interpret intracellular molecular mechanisms.

This work was funded by the Russian Science Foundation [grant number 21-74-20034].

1. Usachev K.S., Validov S.Z., Khusainov I.Sh., Klochkov V.V., Aganov A.V., Yusupov M.M.: *J. Biomol. NMR* **73**, 223–227 (2019).
2. Khusainov I., Vicens Q., Ayupov R., Usachev K., Myasnikov A., Simonetti A., Validov Sh., Kieffer B., Yusupova G., Yusupov M., Hashem Y.: *EMBO J.* **36**, 2073–2087 (2017).
3. Bikmullin A.G., Fatkhullin B., Stetsenko A., Gabdulkhakov A., Garaeva N., Nurullina N., Klochkova E., Golubev A., Khusainov I., Trachtmann N., Blokhin D., Guskov A., Validov Sh., Usachev K., Yusupov M.: *IJMS* **24**, 2118 (2023).
4. Usachev K.S., Efimov S.V., Kolosova O.V., Filippov A.V., Klochkov V.V.: *J. Biomol. NMR* **61**, 227–234 (2015).
5. Usachev K.S., Klochkova E.A., Golubev A.A., Validov S.Z., Murzakhanov F.F., Gafurov M.R., Klochkov V.V., Aganov A.V., Khusainov I.Sh., Yusupov M.M.: *SN Applied Science*. **1**, 442 (2019).
6. Garaeva N., Fatkhullin B., Murzakhanov F., Gafurov M., Golubev A., Bikmullin A., Glazyrin M., Kieffer B., Jenner L., Klochkov V., Aganov A., Rogachev A., Ivankov O., Validov Sh., Yusupov M., Usachev K.: *Structure*. **32**, 74–82 (2023).

## CURRENT STATE OF SPIN EXCHANGE THEORY. NEW SPIN EXCHANGE PARADIGM

**K.M. Salikhov**

Zavoisky Physical-Technical Institute, FRC Kazan Scientific Center of RAS, Kazan, Russia

Many processes are determined by bimolecular collisions of particles. As a current example, we can note the collisions of spin-labeled substrate molecules (drug molecules) with the active catalytic centers of enzymes in biological systems. Collisions of paramagnetic particles cause very characteristic changes in the shape of the EPR spectrum, which open up the possibility of determining the frequency of bimolecular collisions of paramagnetic particles.

The change in the state of the electron spins of two paramagnetic particles caused by the Heisenberg exchange interaction between them during random collisions is usually called spin exchange [1, 2].

The new paradigm of spin exchange is given by the following provisions [2-5]:

Spin coherence transfer (spin coherence “recoil” effect) forms collective modes of spin motion. In the presence of spin coherence transfer, the EPR resonance lines correspond to different collective modes.

Due to the spin coherence recoil effect, the magnetizations of spin subensembles belonging to different components of the EPR spectrum of single spin probes do not develop independently; they turn out to be connected!

Both the exchange interaction in random particle collisions and the dipole-dipole interaction both lead to the transfer of spin coherence. These contributions “interfere” destructively: exchange and dipole-dipole interactions make contributions with opposite signs to the rate of coherence transfer from interaction partners.

In the case of slow spin coherence transfer, each EPR line has a mixed shape: each resonance line represents the sum of a Lorentz symmetric absorption line and a Lorentz antisymmetric dispersion line.

The mixed shape of each resonance line made it necessary to revise the protocol for finding the spin exchange rate from the analysis of experimentally measured EPR spectra.

The new paradigm gives a completely different interpretation of the effect of exchange narrowing of the EPR spectrum in the limit of fast spin exchange. In the case of fast transfer of spin coherence, the microwave field excites only one symmetric collective mode. The EPR frequency of this mode is equal to the frequency of the center of gravity of the spectrum. Other collective modes with different frequencies produce “forbidden” lines.

In dilute solutions, due to spin coherence transfer, the electron spins of paramagnetic particles (macroscopic magnetization of the spin system) and a strong microwave field create some combined states that can be called magnetic polaritons.

The main provisions of the new paradigm of spin exchange in dilute solutions and their manifestations in EPR spectroscopy [1-5] are confirmed by experimental data [6-10].



1. Zamaraev K.I., МИ. Molin Yu.N., Salikhov K.M.: Spin exchange. Novosibirsk: Nauka (1977), 230 (in Russian); Molin Yu.N., Salikhov K.M., Zamaraev K.I.: Spin exchange. Application in chemistry and biology. Springer Verlag: Heidelberg Berlin, 419 (1980).
2. Salikhov K.M.: Current state of the theory of spin exchange in dilute solutions of paramagnetic particles: New paradigm of spin exchange. *Physics Uspechi*, 1017-1043 (2019).
3. Salikhov K.M.: Fundamentals of spin exchange. Story of paradigm shift. Springer Verlag (2019)
4. Salikhov K.M.: New paradigm of spin exchange and its manifestations in EPR spectroscopy. *Applied Magnetic Resonance*, **51**, 297-325 (2020).
5. Salikhov K.M.: Interpretation of the Nature of the Mixed Form of Resonance Lines of the Electron Paramagnetic Resonance Spectrum in a New Paradigm of Spin Exchange: Abnormal “Resonance” of Non-Resonant Spins. *J. Phys. Chem. B*, **124**, 30, 6628-6641 (2020).
6. Bakirov, M. M.; Khairutdinov, I. T.; Salikhov, K. M.; Schwartz, R. N.; Bales, B. L.: The Effect of Power Saturation on the Line Shapes of Nitroxide Spin Probes Under the Influence of Spin-Exchange and Dipole-Dipole Interactions Studied by CW EPR. *Appl. Magn. Reson.* **53**, 1275-1315 (2022).
7. Bales B. L., Peric M., Dragutan I., Bowman M. K., Bakirov M. M. and Schwartz R. N.: Experimental Observation of a Peculiar Effect in Saturated Electron Paramagnetic Resonance Spectra Undergoing Spin Exchange. Magnetic Polariton?, *J. Phys. Chem. Lett.*, **13**, 10952–10957 (2022).
8. Salikhov K.M., Bakirov M.M., Zaripov R.B., Khairutdinov I.T.: Experimental confirmation of the formation of a spin polariton in dilute solutions of paramagnetic particles. *Phys.Chem. Chem. Phys.* **25**, 17966–17977 (2023)
9. Bales Barney L., Peric Miroslav, and Schwartz Robert N.: Experimental Observation of a Peculiar Effect in Electron Paramagnetic Resonance Spectra for Nitroxides Undergoing Fast Spin Exchange: Emission. *J. Phys. Chem. Lett.* **15**, 2082-2088 (2024).
10. Salikhov K.M., Bakirov M.M., Khairutdinov I.T., Zaripov R.B.: Experimental confirmation of the formation of collective modes of the magnetization motion of paramagnetic particles in dilute solutions due to spin exchange. *JMR*, **363**, 107703 (2024)

## Longitudinal Magnons: New Collective Quantum Excitations in Large- $S$ Magnets

M. Zhitomirskii

ILL, Grenoble, France

Coherently propagating spin waves or magnons are the lowest energy excitations in ordered magnetic solids. They obey bosonic statistics and have integer spin-quantum numbers  $\Delta S^z = \pm 1$ . For an easy-axis antiferromagnet, these are seen in the form of two ascending and descending AFMR branches. The standard picture of magnons needs to be updated for magnetic materials with a substantial single-ion anisotropy comparable to the magnetic exchange. Specifically, the infrared absorption experiments on Van der Waals spin-2 antiferromagnets  $\text{FePS}_3$  and  $\text{FePSe}_3$  [1,2] have demonstrated presence of unusual magnetic excitations that exhibit four times larger splitting in magnetic field in comparison to the normal AFMR modes. We identify these new excitations with longitudinal magnons, which correspond to full reversal of single iron spins ( $S = 2$ ) and have a total angular momentum  $\Delta S^z = \pm 4$ . We develop a theoretical description of the longitudinal magnons and demonstrated that they acquire a small finite dispersion thus providing an example of new type of coherently propagating modes in ordered magnetic systems. We also argue that condensation of longitudinal magnons in a magnetic field in strongly anisotropic materials can produced various exotic multipolar states.

1. J. Wyzula *et al.*, *High angular momentum excitations in collinear antiferromagnet  $\text{FePS}_3$* , Nano Lett. **22**, 9741 (2022).
2. F. Le Mardelé *et al.*, *Transverse and longitudinal magnons in strongly anisotropic antiferromagnet  $\text{FePSe}_3$* , Phys. Rev. B **109**, 134410 (2024).

## 40 YEARS of MAGNON BOSE EINSTEIN CONDENSATION

**Yu.M. Bunkov**

Laboratory of Quantum Magnonics, Russian Quantum Center, Skolkovo, Moscow, Russia

This year marks 40 years since the discovery of magnon Bose-Einstein condensation in antiferromagnetic superfluid  $^3\text{He-B}$  [1]. Under the conditions of BEC, a macroscopic number of quasiparticles occupied a single quantum state. Its formation is determined by the well-known BEC formation relation, which includes the density, temperature and mass of quasiparticles. In experiments with superfluid  $^3\text{He-B}$ , the nuclear magnetic induction signal, as usual, decayed with time  $T_2^*$ , determined by the inhomogeneity of the external magnetic field. However, the induction signal was restored with some time delay, which means the spontaneous formation of a coherent state of magnons. In this case, there is no spin-spin relaxation process and the signal lifetime is determined by spin-lattice relaxation (the lifetime of the magnons themselves). This behavior of the signal was explained by the redistribution of the magnon density due to “spin” superfluidity - the spatial countercurrent of superfluid currents of  $^3\text{He-B}$  quantum states with opposite magnetic moments [2]. In general, this process belongs to one of the mechanisms providing magnon BEC [3]. Further studies showed that the deflected magnetization breaks up into two domains. In one region it is stationary, and in the second it precesses spatially coherently and exhibits the quantum properties of a Bose condensate (mBEC). In a magnetic field gradient, the mBEC “swims” towards an area of lower magnetic field. Thus, from the behavior of the BEC signal and its frequency, it is possible to determine the number of magnons that arose after various quantum manipulations.

Magnon BEC was also discovered in Yttrium Iron Garnet (YIG) films magnetized perpendicular to the film plane. In [4], it was shown theoretically that this quantum state can be formed even at room temperature. In a number of studies, the formation of magnon BEC in YIG was demonstrated experimentally [5-8]. An overview of these works will be presented in the lecture.

Last year, we were able to directly observe a magnon BEC optically using the Faraday rotation effect [9]. In these experiments, the amplitude and phase of magnetization precession in the YIG film were measured outside the region of magnons excitation. According to the semiclassical Landau-Lifshitz-Hilbert (LLG) theory, the deflected magnetization should propagate from the excitation region in the form of spin waves. This is precisely the distribution we observed in our setup at a low amplitude of magnon excitation. The situation changed dramatically with increasing magnon density. The magnetization deflection increased sharply outside the excitation region, and it became spatially homogeneous [10]. At a low pump power of 0.05 mW, precession magnetization is observed mainly in the pump region. As the power increases to 6 mW, the precession deflection angle increases sharply even outside the pumping region. The dependence of the precession phase also strongly depends on the magnon concentration. Thus, at low power, excitation of spin waves beyond the pump region is observed. The length of the spin waves is determined by the shift of the magnetic field from the resonant one, in good agreement with the LLG theory. However, at high pump powers, the spin waves disappear and regions of uniform

precession are formed on both sides of the exciting band. Figure 1 shows the change in the spatial distribution of the precession phase with increasing pump power and, accordingly, the magnon density.

We compared the experimental results with the LLG theory. To do this, we simulated the spatial distribution of precession at different magnon pump energies. The model showed good agreement with experimental results at low pump values. However, it was not possible to obtain a state of spatially uniform precession outside the excitation region at any pump value [10]. In other words, the results of our experiments are not described within the framework of the semiclassical LLG theory. The transition from spin waves to the magnon Bose condensate occurs at magnetization deviation angles of about  $4^\circ$ , as shown in [11], which is consistent with the critical value of the magnon density predicted in [4].

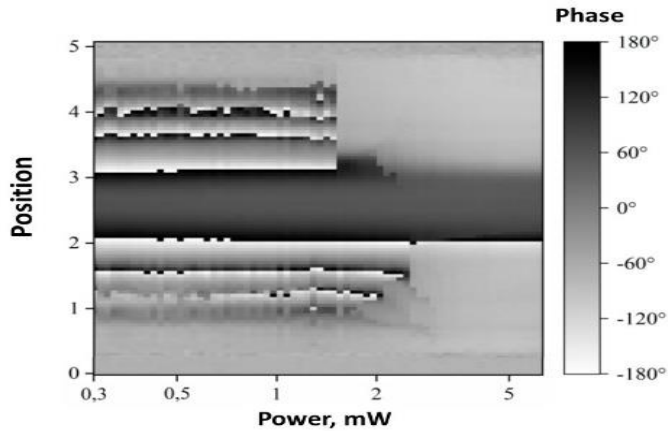


Fig. 1. Spatial distribution of the precession phase with increasing pump power. A transition from spin waves to coherent precession outside the excitation region is visible, corresponding to Bose condensation of magnons.

*This work was supported by RNF (#22-12-00322).*

### Bibliography

1. A. S. Borovik-Romanov, Yu. M. Bunkov, V. V. Dmitriev, Yu. M. Mukharsky, JETP Letters, 40, 256 (1984).
2. I. A. Fomin, JETP Letters, 40, 260 (1984).
3. G. E. Volovik, J. Low Temp. Phys., 153, 256 (2008).
4. Yu. M. Bunkov, V. L. Safonov, JMMM, 452 30 (2018).
5. Yu. M. Bunkov, et al., JETP Letters, 111, 52 (2020).
6. P. M. Vetoshko, et al., JETP Letters, 112, 313 (2020).
7. A. N. Kuzmichev, et al., JETP Letters, 112, 749 (2020).
8. Yu. M. Bunkov, et al., Scientific Reports, 11, 7673 (2021).
9. P. E. Petrov, et al., Optics Express 31, 8335 (2023).
10. G. A. Knyazev, et al., Optics Express, 32, 13761 (2024).
11. P. E. Petrov et al., JETP Letters, 119, 129 (2024).

# INVITED TALKS

## MULTIPLE-SPIN RAMAN PARAMAGNETIC RESONANCE INDUCED BY THE HOLE EXCHANGE FIELD IN CdSe/ZnMnSe QUANTUM DOTS

N. V. Kozyrev, B. R. Namozov, Yu. G. Kusrayev, N.S. Averkiev

Ioffe Institute, St. Petersburg 194021, Russia

The structures based on II-VI semiconductors that incorporate magnetic ions (usually  $\text{Mn}^{2+}$ ), known as diluted magnetic semiconductors (DMSs), are of great interest due to their unusual magnetic and optical properties induced by the strong exchange interaction of carriers with localized spins of magnetic ions and the interaction of the latter with each other. These include giant spin splitting, magnetic polaron formation, paramagnetic – spin glass phase transition, etc. The physics of DMSs, which have been intensively studied for several decades, is now well established. The background knowledge of the physics of DMSs has made DMS-based nanostructures a convenient model for investigation of spin-spin interactions in reduced dimensionalities.

Here we discuss the effects consisting in the coherent evolution of a large number of  $\text{Mn}^{2+}$  spins due to their exchange interaction with the spins of localized two-dimensional heavy holes. An interesting manifestation of such an interaction, namely, the observation of the *multi-spin Raman paramagnetic resonance* was first observed in quantum well CdMnTe/CdMgTe by Stühler et al. [1]. An interpretation of the phenomenon based on the model of coherent rotation of the ensemble of  $\text{Mn}^{2+}$  spins was proposed. The decrease in magnetization projection  $\Delta M = N\mu_B$  is proportional to the number of spin flips  $N$  that are observed in the Stokes spin-flip Raman (SFR) spectrum. Pronounced spin anisotropy of holes, resulting in non-conservation of the total angular momentum in the spin system, plays the key role in this effect.

Recently multiple  $\text{Mn}^{2+}$  spin-flip Raman scattering (SFRS) in Voigt geometry was observed in self-organized quantum dots (QDs) of CdSe/Zn<sub>0.99</sub>Mn<sub>0.01</sub>Se [2]. We have observed up to 11 lines in the SFRS spectrum (see Fig. 1). The magnetic ions and QD carriers are spatially separated by nonmagnetic barriers, so the exchange interaction between them is expected to be weak. Magneto-optical experiments showed that Zeeman splitting is undetectable against the photoluminescence line width which confirms the weakness of the exchange interaction energy. It means that effectively localized hole interacts with small number of manganese spins. At the same time, the more sensitive circular polarization measurements allowed us to estimate the effective  $g$ -factor, which turned out to be as small as  $g_{\text{eff}}=3$ . Despite the weak overlap of the localized hole with the spins of magnetic ions, up to 11 lines were observed in the SFRS spectrum. According to the model [1], for the short hole spin lifetime, the change in the magnitude of manganese spin (which is proportional to number of peaks) in the considered process is small compared to the total magnetic moment of  $\text{Mn}^{2+}$  spins with which the hole interacts, i.e.  $\Delta M \ll M$ . Thus, the presence of 11 lines in

the SFRS spectrum is difficult to explain in the model of coherent spin precession of  $Mn^{2+}$  spins in the exchange field of the hole.

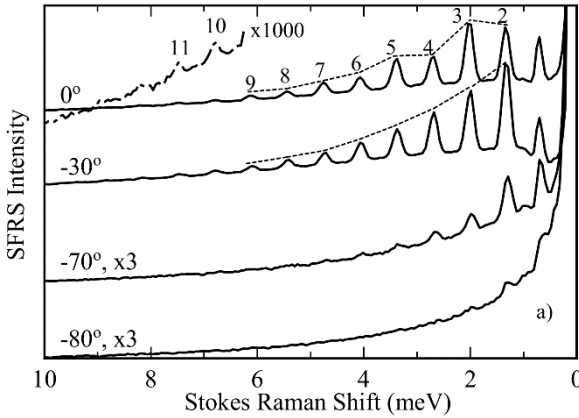


**Fig. 1.** SFRS spectra measured in different angles between normal to the external magnetic field and growth axis of the sample.  $B = 6$  T,  $T = 1.6$  K.

We propose an alternative explanation for the presence of a large number of peaks in the SFRS spectrum, taking into account the finite lifetime of the hole spin. The action of the hole exchange field which influences on the  $Mn^{2+}$  spins could be considered as a short pulse ( $\sim 1$  ps duration and  $\sim 1$  T amplitude) of magnetic field. Fourier component of this pulse at the Zeeman frequency (177 GHz) induces paramagnetic resonance. The amplitude of the component at Zeeman splitting (corresponding to the Larmor frequency in  $B = 6$  T), can be estimated as 5 G ( $5 \times 10^{-4}$  T). This value corresponds to the value of the amplitude of the magnetic component of the microwave field used in the EPR technique. In such a model, all magnetic ions within the sphere of influence of the localized carrier participate in the formation of the SFRS spectrum. On the contrary, in model [1], only a small part of magnetic ions in the localization region participates in the formation of the SFRS spectrum.

Работа поддержана грантом Российского научного фонда (проект № 22-12-00125)).

1. J. Stuhler, G. Schaack, M. Dahl, A. Waag, G. Landwehr, K. V. Kavokin, and I. A. Merkulov, Phys. Rev. Lett. **74**, 2567 (1995)
2. N. V. Kozyrev, R. R. Akhmadullin, B. R. Namozov, Yu. G. Kusrayev, I. V. Sedova, S. V. Sorokin, and S. V. Ivanov. Phys. Rev. B **99**, 035301 (2019).

## EPR of Radical-Functionalized Materials

**M.V. Fedin**

International Tomography Center SB RAS, Novosibirsk, Russia

Materials functionalized with stable organic radicals find various applications in chemistry and materials sciences, and they have been widely studied using EPR spectroscopy. In a recent series of works we employed radicals as spin probes, spin qubits, exchange interaction mediators and even traps for highly reactive species. This report briefly reviews this activity with the emphasis on new approaches, allowing one to obtain crucial information on studied materials by EPR.

In particular, encapsulation of radicals in metal-organic frameworks (MOFs) allows obtaining plethora of information on structure and properties of MOF cavities, guest-host interactions and responsiveness of MOFs to external stimuli [1,2]. Spin-probing nanostructures in ionic liquids provides new insights into peculiarities of molecular self-organization in these media on the nanoscale [3]. Triazinyl radicals grafted onto mesoporous silica materials can act as spin qubits operating at room temperature [4], having long enough phase memory times reaching  $T_m \sim 2.3 \mu\text{s}$ ; they can also act as selective traps of NO from air by reversible complexation with this toxic gas molecules [5]. Finally, stable mono- and polyradicals are important building blocks in spintronics and design of molecular magnets. Recently, a number of di-, tri- and tetradicals based on verdazyl-nitroxide units have been synthesized and studied using EPR, demonstrating their high-spin states and obtaining key spectroscopic parameters [6,7]. These few examples show great perspective of EPR applications to a variety of radical-containing materials, where new approaches often provide key structural or functional information inaccessible otherwise.

Russian Science Foundation (24-13-00119) is greatly acknowledged for support.

1. Poryvaev A. S., Efremov A. A., Alimov D. V., Smirnova K. A., Polyukhov D. M., Sagdeev R. Z., Jacoutot S., Marque S. R. A., Fedin M. V.: *Chem. Sci.* **15**, 5268-5276 (2024)
2. Poryvaev A. S., Larionov K. P., Albrekht Y. N., Efremov A. A., Kiryutin A. S., Smirnova K. A., Evtushok V. Yu., Fedin M. V.: *Phys. Chem. Chem. Phys.* **25**, 13846-13853 (2023)
3. Ivanov M. Yu., Bakulina O. D., Polienko Y. F., Kirilyuk I. A., Prikhod'ko S. A., Adonin N. Yu., Fedin M. V.: *J. Mol. Liquids* **381**, 121830 (2023)
4. Poryvaev A. S., Gjuzi E., Polyukhov D. M., Hoffmann F., Fröba M., Fedin M. V.: *Angew. Chem. Int. Ed.* **60**, 8683-8688 (2021)
5. Poryvaev A. S., Gjuzi E., Yazikova A. A., Polyukhov D. M., Albrekht Y. N., Efremov A. A., Kudriavkykh N. A., Yanshole V. V., Hoffmann F., Fröba M., Fedin M. V.: *ACS Appl. Mater. Interf.* **15**, 5191-5197 (2023)
6. Tretyakov E. V., Petunin P. V., Zhivetyeva S. I., Gorbunov D. E., Gritsan N. P., Fedin M. V., et al.: *J. Am. Chem. Soc.* **143**, 8164-8176 (2021)
7. Zayakin I. A., Petunin P. V., Postnikov P. S., Dmitriev A. A., Gritsan N. P., Dorovatovskii P., et al.: *J. Am. Chem. Soc.* **146**, 13666-13675 (2024)



## PSEUDOSPIN PARAMAGNET AND SPIN LIQUID IN A CHAIN ANTIFERROMAGNET $\text{Cs}_2\text{CoCl}_4$

A.I. Smirnov<sup>1</sup>, T.A. Soldatov<sup>1</sup>

<sup>1</sup> P.L. Kapitza Institute for Physical Problems RAS, Moscow, Russia

The spin system of  $\text{Cs}_2\text{CoCl}_4$  may be considered as an ensemble of weakly interacting strongly anisotropic chains of pseudospins  $S=1/2$  (the so-called XXZ chains). This is a result of a strong single-ion anisotropy with a characteristic energy of 7 K which separates the upper spin doublet of  $\text{Co}^{2+}$  ( $S=3/2$ ) from the lower one, and enables the use of a pseudospin  $S=1/2$  representation at low temperatures. A strong anisotropy of exchange and renormalization of  $g$ -factor naturally arise in this representation [1]. The frustration of lateral exchanges on the isosceles triangular lattice results in the effective exchange network which may be viewed as a system of spin chains along the bases of triangles. Due to the non-commuting action of the transverse magnetic field and anisotropy, these chains have a number of remarkable properties because of quantum entanglement of states, see, for example, [1-3]. In particular, in a zero field, the ground state is a quantum-critical spin liquid, and in moderate fields the chains have a long-range antiferromagnetic order with strongly reduced ordered spin component. And finally, in the field before saturation, a spin-liquid phase appears again. Thus,  $\text{Cs}_2\text{CoCl}_4$  represents a convenient model object for studying the quantum phases of XXZ chains and phase transitions between them. It may be compared with a well known Heisenberg  $S=1/2$  chain system  $\text{Cs}_2\text{CuCl}_4$  with the same crystal structure, which also demonstrates 1D behavior [4].

We study uniform spin oscillations of  $\text{Cs}_2\text{CoCl}_4$  at temperatures from 0.1 to 7 K by electron spin resonance (ESR) in the range of 25-120 GHz in the magnetic field  $\mathbf{H}$  oriented along the crystallographic axis  $b$ . This orientation corresponds to non-commuting action of magnetic field and anisotropy. Above the Néel temperature  $T_N=0.22$  K [1] but below the characteristic exchange temperature we expect the magnetic properties will correspond to an uncorrelated ensemble of XXZ chains. At the same time, there should be strong spin correlations within a chain due to the intrachain exchange of pseudospins  $J=3$  K. Our results show that at a temperature of 4-5 K, ESR with a  $g$ -factor of 3.3 is observed for the whole frequency range. This value of  $g$ -factor corresponds well to the pseudospin  $g$ -factor calculated in [1] for the anisotropy and exchange of  $\text{Cs}_2\text{CoCl}_4$ . We denote the values of resonant fields of this type as  $H_1$ . As the temperature decreases, a second resonant mode appears in the field  $H_2 > H_1$ , and this  $H_2$ -resonance dominates below 1 K down to 0.3 K. The majority of the spectral weight of ESR signal is placed near  $H_2$ -resonance in this temperature range. The spectrum is shifted down from the paramagnetic position recorded at  $T=4$  K. The temperature evolution of 41 GHz ESR is illustrated in Fig.1, and the frequency-field diagram of the observed resonances is shown in Fig.2.

The resonance frequencies in  $H_2$ -fields observed in the temperature range 0.3-1 K correspond well to the theoretical dependence of the most intense (lower)

maximum of the spectral density of the excitation continuum of  $S=1/2$  XXZ chain obtained numerically by the DMRG method [3] (solid line in Fig. 2). This theoretical dependence is calculated with the use of exchange and anisotropy parameters determined experimentally in [1] and the value of the  $g$ -factor 3.3 obtained in our experiment at a  $T=4$  K. Thus, the theoretical dependence in Fig.2 does not contain any fitting parameters. The transition of the resonance field from  $H_1$  to  $H_2$  occurs by the continuous spectral density flow from  $H_1$  to  $H_2$ , in the form of a temperature crossover, without critical behavior, while antiferromagnetic correlations appear within the chains.

Hence, we can conclude [5] that ground states of the XXZ chains are realized within the spin system of  $\text{Cs}_2\text{CoCl}_4$  in this temperature range, while mutual correlations of neighboring chains are destroyed by temperature.

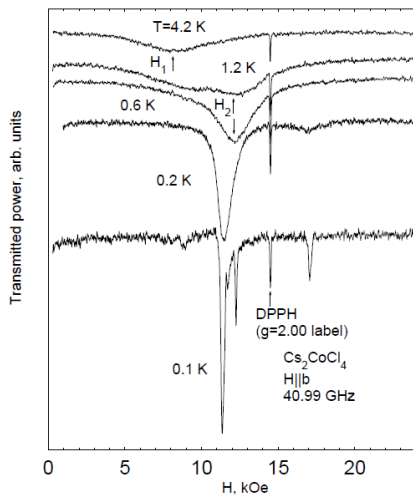


Fig 1. 40.99 GHz ESR records at different temperatures.

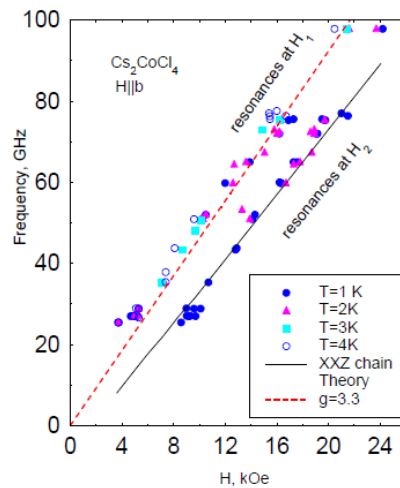


Fig2. frequency-field diagram for  $H_1$  and  $H_2$  resonances.

Below  $T_N=0.25$  K and down to the lowest temperature of the experiment 0.1 K, we observe another drastic change in the spectrum at the transition to the antiferromagnetic long-range order, which is due to inter-chain interaction. This spectrum change with the formation of new lines occurs via phase transition at the Néel point. We will report about the ESR spectrum of this phase later.

The work is supported by Russian Science Foundation Grant N 22-12-00259.

[1] O. Breunig et al, Phys. Rev. Lett. **111**, 187202 (2013).

[2] M Kenzelmann et al, Phys Rev.B **65**, 144432 (2002).

[3] P. Laurell, et al, Phys. Rev. Lett. **127**, 037201 (2021) and Supplement.

[4] R. Coldea, D. A. Tennant, and Z. Tylczynski, Phys. Rev. B **68**, 134424 (2003).

[5] T.A. Soldatov, V.S. Edelman, A.I. Smirnov *Appl Magn Reson* (2024). <https://doi.org/10.1007/s00723-024-01669-5>.

## Study of the Electron Spin Polarization of the Triplet Excited States of BODIPY Compounds with Time-Resolved Electron Paramagnetic Resonance Spectroscopy

**Jianzhang Zhao, Xue Zhang and Xi Chen**

State Key Laboratory of Fine Chemicals, Frontiers Science Center for Smart Materials, School of Chemical Engineering, Dalian University of Technology, Dalian 116024 (P.R. China)  
E-mail: zhaojzh@dlut.edu.cn

Electron spin changes upon photoexcitation of the organic molecules, especially in the process of intersystem crossing (ISC) and charge separated, are not characterized by the usually used optical spectra.[1,2] Moreover, due to the zero field splitting (ZFS) effect and anisotropic ISC, the population of the three sublevels is usually severely deviated from the Boltzmann distribution, this so-called electron spin polarization (ESP) is informative to reveal the ISC mechanisms.[3] This ESP cannot be studied with ordinary optical spectroscopy, however, the time-resolved electron paramagnetic resonance (TREPR) spectroscopy can be used to characterize this ESP and to determine the population rates of the three sublevels of the  $T_1$  state. Moreover, the spatial confinement of the  $T_1$  state is critical for organic materials used in photovoltaics or electronics. This  $T_1$  state wave function confinement can be also characterized by using TREPR spectra. Recently we studied the ESP and  $T_1$  state wave function confinements of some novel BODIPY compounds, and some insight into the photophysical property of the compounds were obtained with TREPR spectra.[4,5]

1. Verhoeven J. W. J. Photochem. Photobio. C: Photochem.Rev. **7**, 40–60 (2006).
2. Richert S., Tait C. E., Timmel C. R., J. Magn. Reson. **280**, 103–116 (2017).
3. Levanon H., Norris J. R. Chem. Rev., **78**, 185–198 (1978).
4. Imran M., Zhao J., Voronkova V. K. et al., Phys. Chem. Chem. Phys., **23**, 15835–15868 (2021)
5. Wang Z., Toffoletti A., Zhao, J., Barbon A., Dick B. et al., Chem. Sci., **12**, 2829–2840 (2021).

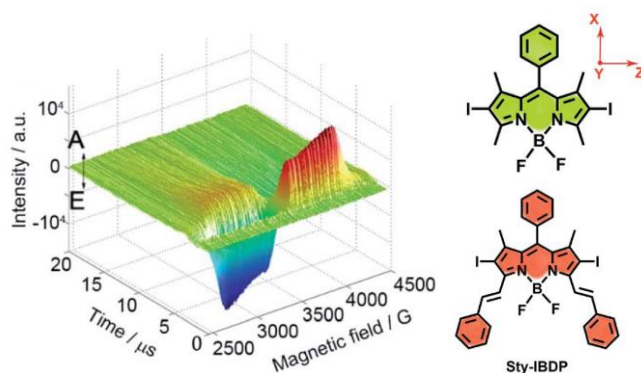


**Fig. 1.** Molecular structures of the BODIPY derivatives showing drastically different triplet state lifetimes (Right). Time-resolved EPR of Sty-IBDP, full surface of the TREPR spectrum of Sty-IBDP in toluene/2MeTHF (3 : 1, v/v) at 80 K (excited at 630 nm with a nanosecond pulsed laser) (Left).

## Features of Photo-Excited Charge Separation States in TADF molecules

**A. A. Sukhanov<sup>1</sup>, J. Zhao<sup>2</sup>, V. K. Voronkova<sup>1</sup>**

<sup>1</sup> Zavoisky Physical-Technical Institute, FRC Kazan Scientific Center of RAS, Kazan, Russia

<sup>2</sup> State Key Laboratory of Fine Chemicals, School of Chemical Engineering, Dalian University of Technology, Dalian 116024, P. R. China

Thermally activated delayed fluorescence (TADF) molecular materials has attracted much attention for application in organic light emitting diodes (OLEDs) [1], upconversion [2], photocatalysis [3] and etc. Initially in the TADF molecule is designed so that the energy difference between the excited singlet charge separation (<sup>1</sup>CS) state and the excited triplet charge separation (<sup>3</sup>CS) state is much small to occur enables reverse intersystem crossing (RISC). Recently the three-state model is proposed to be responsible for the TADF process, considering <sup>1</sup>CS, <sup>3</sup>CS and triplet locally excited state [4]. In both models import role play to formation of triplet states. EPR techniques can study triplet states and can provide to understanding of TADF mechanism.

Compact dyads with TADF properties were studied using CW and pulse time-resolved (TR) EPR. For such systems, two types of spectra are observed. One of the observed spectra is related to a localized triplet. The other spectrum is related to the delocalized triplet state (<sup>3</sup>CS) and has less value of ZFS. It was found inversion of polarization pattern of TR EPR signal of <sup>3</sup>CS state. The observed inversion may be associated with spin-vibronic interaction [5].

The study was supported by the government assignment for FRC Kazan Scientific Centre of RAS.

1. X. Wu, B.-K. Su, D.-G. Chen, D. Liu, C.-C. Wu, Z.-X. Huang, T.-C. Lin, C.-H. Wu, M. Zhu, E. Y. Li, W.-Y. Hung, W. Zhu, P.-T. Chou: *Nature Photonics* **15**, 780 (2021).

2. T. Huang, W. Jiang, L. Duan : *J. Mater. Chem. C*, **6**, 5577 (2018).

3. J. Lu, B. Pattengale, Q. Liu, S. Yang, W. Shi, S. Li, J. Huang, J. Zhang : *J. Am. Chem. Soc.*, **140**, 13719 (2018)

4. P. K. Samanta, D. Kim, V. Coropceanu, J.-L. Brédas : *J. Am. Chem. Soc.*, **139**, 4042 (2017).

5. Inkoo K., Soon O. J., Daun J., Hyeonho C., Won-Joon Son, Dongwook K., Young Min R., Hyo Sug L.: *J. Chem. Theory Comput.* **16**, 621–632 (2020).

## MÖSSBAUER SPECTROSCOPY of the RARE EARTH FERROBORATES $R\text{Fe}_3(\text{BO}_3)_4$ ( $R = \text{Pr}, \text{Eu}, \text{Tb}, \text{Dy}$ )

**K.V. Frolov<sup>1</sup>, E.S. Smirnova<sup>1</sup>, O.A. Alekseeva<sup>1</sup>, E.V. Sidorova<sup>1</sup>, I.A. Gudim<sup>2</sup>**

<sup>1</sup> Shubnikov Institute of Crystallography, KCC&Ph NRC Kurchatov Institute, Moscow, Russia

<sup>2</sup>Kirensky Institute of Physic, FRC KSC SB RAS, Krasnoyarsk, Russia

Rare-earth ferrobates  $R\text{Fe}_3(\text{BO}_3)_4$  ( $R = \text{Y}, \text{La}, \text{Ce} - \text{Lu}$ ) have been actively studied for the last 15 years due to their multiferroic properties arising from the peculiarities of the crystal structure and complex exchange interactions between the magnetic subsystems of  $R$  ions and Fe ions [1-6]. Depending on the radius of the  $R$  ion, a structural phase transition can occur in some of these compounds in the temperature range 80 – 500 K. Below the temperature of 40 K, magnetic ordering of iron ions occurs, and upon further cooling, magnetic ordering of  $R$  ions also occurs, while different types and dimensions of magnetic order are formed, spin reorientation may occur, and magnetoelectric effects are observed.

In this work, single crystals of compounds  $R\text{Fe}_3(\text{BO}_3)_4$  ( $R = \text{Pr}, \text{Eu}, \text{Tb}, \text{Dy}$ ) have been studied in the temperature range 4 – 295 K by Mössbauer spectroscopy on <sup>57</sup>Fe nuclei in combination with single crystal X-ray diffraction analysis. The dynamics of structural and magnetic phase transitions has been studied, taking into account the peculiarities of the nearest oxygen environment of rare-earth ions and iron ions, the values of the Neel temperature, types and dimensions of the magnetic order have been determined, and the values of the Debye temperature have been calculated.

This work was financially supported by the Russian Science Foundation (Agreement No. 23-22-00286).

1. Kadomtseva A.M., Popov Y.F., Vorob'ev G.P. et al.: Low Temp. Phys. **36**, 511 (2010)
2. Kuz'menko A.M., Mukhin A.A., Ivanov V.Y. et al.: JETP Lett. **94**, 294 (2011)
3. Kuzmenko A.M., Mukhin A.A., Ivanov V.Y. et al.: Solid State Phenom. **190**, 269 (2012)
4. Kurumaji T., Ohgushi K., Tokura Y.: Phys. Rev. B **89**, 195126 (2014)
5. Popova M.T.: Low Temp. Phys. **45**, 1000 (2019)
6. Zhang H., Liu S., Nelson C.S. et al.: J. Phys.: Condens. Matter **31**, 505704 (2019)

## On the question of the role of spin centers in radiative recombination processes in nanomaterials

**E.A. Konstantinova<sup>1</sup>, E.V. Kytina<sup>1,2</sup>, Yu.V. Nazarkina<sup>1,3</sup>, V.B. Zaitsev<sup>1</sup>**

<sup>1</sup>Physics Department, M.V. Lomonosov Moscow State University, Moscow, Russia

<sup>2</sup>N.N. Semenov Federal Research Center for Chemical Physics, RAS, Moscow, Russia

<sup>3</sup>National Research University of Electronic Technology – MIET, Zelenograd, Moscow, Russia

Nanomaterials have been actively attracting the attention of scientists in the last few decades [1-4]. This is due to the presence of unique properties in nanoparticles, which can be controlled by varying the synthesis conditions [1-4]. Such unusual properties primarily include a large specific surface area of nanomaterials and the manifestation of the quantum-size effect, when the de Broglie wavelength of an electron becomes comparable to the size of the nanoparticles. The presence of a huge specific surface area leads to an increase in the influence of molecules of the environment adsorbed on the surface of nanoparticles on the physicochemical properties of nanomaterials [1,4]. In addition, the quantum-size effect has a significant impact on the optoelectronic properties of nanoobjects, for example, it leads to an increase in the probability of radiative recombination of photoexcited charge carriers in nanoparticles with dimensions of several nanometers. Also, defects with unpaired electrons (spin centers), which have high chemical activity, have a significant impact on the luminescent characteristics of nanomaterials. The purpose of this work is to study the influence of the type and concentration of spin centers on the processes of radiative recombination of photoexcited charge carriers in nanomaterials of various chemical compositions obtained by the electrochemical method.

The formation of nanotube arrays of anodic titania and anodic aluminium oxide occurred by electrochemical oxidation of Al- and Ti-foil. Various electrolytes based on ammonium fluoride, sulfuric, oxalic and selenic acid were used for preparation. During the synthesis process, the current density, anodization time, and annealing temperature were varied.

Spin centers were studied on a Bruker ELEXSYS-E500 EPR spectrometer (X-band). Photoluminescence spectra were studied using an LS-55 Perkin Elmer luminescence spectrograph.

In the EPR spectra of a series of titania nanotubes annealed in air in the temperature range 250-500 °C, a signal from dangling carbon bonds ( $g=2.0027\pm 0.0003$ ) is recorded. The concentration of these spin centers decreased with increasing annealing temperature. For this series of samples, we also measured the photoluminescence spectra. It was found that there is a correlation between the concentration of defects and the intensity of photoluminescence, which indicates that in titania nanotubes the radiative recombination of photoexcited electrons and holes occurs at the dangling carbon bonds. It has been established that by annealing titania nanotubes in air at different temperatures (250-500 °C), it is possible to control the concentration of spin centers and the intensity of photoluminescence.

A series of aluminium oxide nanotubes prepared in electrolytes based on various acids - sulfuric (A1), oxalic (A2) and selenic (A3) - were studied by EPR and photoluminescence methods. It was found that all samples contain oxygen vacancies with an unpaired electron ( $g=2.0022\pm 0.0003$ ); their concentration is maximum in the samples A2. In addition,  $O_2^-$  radicals ( $g_1=2.023\pm 0.0003$ ,  $g_2=2.008\pm 0.0003$ ,  $g_3=2.0035\pm 0.0003$ ) were detected in samples A1 and A3. It was found that the photoluminescence intensity correlates with the concentration of oxygen vacancies. Therefore, it can be assumed that photoluminescence in aluminium oxide nanotubes is due to radiative recombination of electrons and holes at oxygen vacancies.

By controlling the photoluminescence intensity by varying the concentration of spin centers during the synthesis process, it is possible to obtain nanoporous aluminium oxide with low photoluminescence intensity for subsequent use as an optical sensing platform for detecting various biological analytes with high sensitivity and selectivity using various optical methods. Thus, the results obtained have important implications for practice.

The experiments were performed using the facilities of the Collective Use Center at the Moscow State University. The study was supported by a grant from Russian Science Foundation № 24-19-00402.

1. Chiesa M.; Livraghi, S., Paganini M. C., Salvadori E., Giamello E.: *Chem. Sci.* **11**(26), 6623–6631 (2020).
2. Gavrilin I., Dronov A., Volkov R., Savchuk T., Dronova D., Borgardt N., Pavlikov A., Gavrilov S., Gromov D.: *Appl. Surf. Sci.* **516**, 146120 (2020).
3. Savchuk T., Gavrilin I., Konstantinova E., Dronov A., Volkov R., Borgardt N., Maniecki T., Gavrilov S., Zaitsev V.: *Nanotechnology* **33**, 55706 (2022).
4. Feng Silu, Ji Weiwei: *Frontiers in Nanotechnology* **3** (2021).

## Impact of Random Processes on Coherences

**M.K. Bowman**

Department of Chemistry and Biochemistry, The University of Alabama, Tuscaloosa, Alabama, USA

Spin is a property of matter in the very interesting range extending from the sub-nanometer world of electrons, through atoms and molecular free radicals, and even into the macroscopic world of polymers, crystals, and conductors.

We can prepare, manipulate, and measure spin states in a highly reproducible manner for a wide range of purposes. Spins provide one approach to quantum computation and informatics based on their precise manipulation. But the broad range of responses that spins make to even a simple stimulus like an excitation pulse, makes magnetic resonance an excellent method for studying structure and dynamics of all phases of matter.

Polarized or coherent states involving spins are the basis for utilizing spins: polarizations or populations like  $M_z$ , coherences like  $M_x$ , and entangled states involving several spins. We usually think of these states as the result of careful manipulation of spins. But it is possible for random processes to transform a coherence or polarization into new, and quite different, polarizations or coherences. Well-documented examples include the phonon avalanche (super radiance) and chemically induced dynamic electron polarization (CIDEP).

Examples where random processes such as diffusion or stochastic motion result in new, unexpected coherences or mixed states will be discussed. Often, their presence can be detected in magnetic resonance experiments. When they are recognized, they supply new information and knowledge about the spin system, but when they are not recognized or understood, they could seem to be unexpected routes of relaxation.



## RESONANCE FEATURES OF ANOMALOUS JOSEPHSON JUNCTIONS

**Yu. M. Shukrinov<sup>1,2</sup>, M. Nashaat<sup>1,3</sup>, E. Kovalenko<sup>4</sup>**

<sup>1</sup> *JINR, Dubna, Moscow region, 141980, Russia, [shukrinv@theor.jinr.ru](mailto:shukrinv@theor.jinr.ru)*

<sup>2</sup> *Dubna State University, Dubna, Russia*

<sup>3</sup> *Cairo University, Cairo, Egypt*

<sup>4</sup> *Center for the Development of Digital Technologies, Krasnogorsk, 143407, Russia*

The  $\varphi_0$  junction with direct coupling of Josephson phase and magnetization leads to the interesting perspectives in superconducting spintronics based, in particular, on magnetization reversal and Kapitza pendulum features [1].

We discuss results of our recent studies of the dynamics and IV-characteristics of the  $\varphi_0$  junction under external electromagnetic radiation in the ferromagnetic resonance region [2]. The novel mechanisms of synchronization and corresponding manifestation in IV-characteristics and magnetization dynamics are demonstrated. The implementation of two types of dynamical states of magnetization, transitions between these states with increasing and decreasing bias current and related hysteresis are discussed [3,4].

The combination of Buzdin and Kittel ferromagnetic resonances with various types of synchronization creates an extremely interesting physics of this system and opens up a number of new applications.

1. Yu. M. Shukrinov // *Physics-Uspokhi*. – 2022. - V. 65. - N.4. - P.317.
2. Abdelmoneim S. A., Shukrinov Yu. M., Kulikov K. V., ElSamman H., and Nashaat M. // *Phys. Rev. B*. – 2022. – V.106. – C. 014505.
3. Shukrinov Yu. M., Kovalenko E., Tekic J., Kulikov K., and Nashaat M. // *Phys. Rev. B*. – 2024. – V.109. – C. 024511.
4. Nashaat M., Kovalenko E., and Shukrinov Yu. M. // *Cond-mat arXiv*: 2403.03621.

## GRADED THIN FERROMAGNETIC EPITAXIAL Pd-Fe FILMS: FMR MEASUREMENTS

**I.V. Yanilkin<sup>1</sup>, I.A. Golovchanskiy<sup>2,3</sup>, A.I. Gumarov<sup>1</sup>, B.F. Gabbasov<sup>1</sup>,  
R.V. Yusupov<sup>1</sup>, L.R. Tagirov<sup>4</sup>**

<sup>1</sup>Institute of Physics, Kazan Federal University, Kazan, Russia

<sup>2</sup>Moscow Institute of Physics and Technology, National Research University, Dolgoprudny, Russia

<sup>3</sup>University of Science and Technology MISIS, Moscow, Russia

<sup>4</sup>Zavoisky Physical-Technical Institute, FRC Kazan Scientific Center of RAS, Kazan, Russia

Nowadays, spin waves are studied intensely in thin ferromagnetic films and heterostructures. In the majority of the reports, homogeneous films or magnonic crystals with a homogeneous periodic structure are investigated. However, the studies of the spin waves in films with artificially created inhomogeneity of magnetic properties across the thickness, known in the literature as graded magnetic materials, have been performed mostly in theory. This work aimed at the experimental investigation of the possibility to engineer the spin wave spectra by means of controlling a magnetic property profile in graded films of Pd-Fe alloy

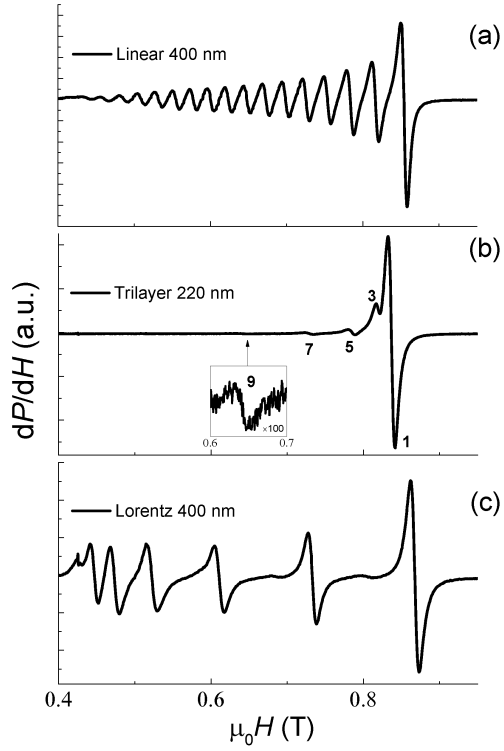
The synthesized collection of epitaxial Pd-Fe alloy films with variable distribution profiles of a composition across the thickness included films with linear, step-like, Lorentzian, Sine, and Cosine film profiles with thicknesses in the range of 50-400 nm [1,2]. The high-purity (99.95 %) Pd and Fe metals were evaporated from the effusion cells and deposited to a rotating (001) MgO single-crystal substrate. The entire synthesis process was carried out under ultrahigh vacuum (5·10<sup>-10</sup> mbar) in the molecular beam epitaxy (MBE) chamber manufactured by SPECS GmbH. The iron concentration profile in the palladium matrix was realized by a controllable variation of the iron evaporation cell temperature with a fixed palladium cell temperature.

Figure 1 clearly demonstrates the possibility of manipulating the standing spin wave spectrum in thin film structures by varying the magnetization profile.

Analysis of the standing spin wave spectra provided the following common parameters for the ferromagnetic Pd-Fe films: the normalized exchange stiffness constant  $D=16 \text{ T}\cdot\text{nm}^2$ , the surface pinning coefficient  $\alpha_s=-0.05$ , the skin layer depth  $\sigma_f=170 \text{ nm}$  and the ratio of the effective magnetization to saturation magnetization  $M_{\text{eff}}/M_s=1.35$ . The obtained results indicate that the approach suggested and realized in this work can be applied to engineer the spin waves dispersion in graded ferromagnetic films.

This work was supported by the Russian Science Foundation (Project № 22-22-00629).

1. I.V. Yanilkin et. al. – Phys. Rev. Mat., 6(6), 064406(8) (2022).
2. I.V. Yanilkin et. al. – Nanomaterials, 12(24), 4361(12) (2022).



**Fig. 1.** Experimental standing spin-waves resonance spectra of the samples with linear (a), step-like (b) and Lorentz (c) profiles.

## SPIN-LATTICE RELAXATION of Cr(V) NITRIDO COMPLEXES: EXPERIMENTS and CALCULATIONS

**Sandra S. Eaton**,<sup>1</sup> **Gareth R. Eaton**,<sup>1</sup> **Lorenzo A. Mariano**,<sup>2</sup> **Vu Ha Anh Nguyen**,<sup>2</sup> and **Alessandro Lunghi**<sup>2</sup>

<sup>1</sup>Department of Chemistry and Biochemistry, University of Denver, Denver, Colorado USA

<sup>2</sup>School of Physics and AMBER Research Centre, Trinity College, Dublin 2, Ireland

Recent interest in electron spins as qubits has invigorated studies of electron spin relaxation and the molecular properties that drive relaxation. Historically, trends in  $T_1$  have been widely explored and interpreted in terms of the direct, Raman, and local mode processes, which are conceptual models [1,2]. Although it has been recognized that spin-lattice relaxation rates depend strongly on spin orbit coupling [3], computational models based on  $g$  and nuclear hyperfine Hamiltonian parameters have not been able to predict the frequency, temperature, or orientation dependence of  $T_1$ . A new approach for calculating  $T_1$  for  $S = 1/2$  systems based on ab initio quantum theory, including the first electronic excited state, show that Raman relaxation is driven by phonons with energies less than about  $100 \text{ cm}^{-1}$ . Results are compared with data obtained by three-pulse electron spin echo experiments for two  $S = 1/2$  Cr(V) nitrido complexes at temperatures between 20 and 250 K. The Cr(V) complexes have the advantage that  $^{53}\text{Cr}$  (9.5% abundance) has  $I = 3/2$  and  $^{52}\text{Cr}$  (90.5% abundance) has  $I = 0$  so in the same sample it can be shown experimentally that nuclear hyperfine interaction does not impact  $T_1$ . For these complexes  $T_1$  is the same, within experimental uncertainty, at X-band and Q-band. These observations were predicted correctly by the calculations [4]. The results show the importance of ab initio models of magnetic resonance and suggest new chemical strategies to control electron spin relaxation.

[1] S. S. Eaton and G. R. Eaton, *eMagRes*, **5**, 1543-1556 (2016).

[2] S. S. Eaton and G. R. Eaton, *Biol. Magn. Reson.* **19**, 29-154 (2000).

[3] A. Lunghi, *Science Advances* **8**, eabn7880 (2022)

[4] L. A. Mariano, V. H. A. Nguyen, J. B. Petersen, M. Bjornsson, J. Bendix, G. R. Eaton, S. S. Eaton and A. Lunghi, <http://arxiv.org/abs/2407.01380>

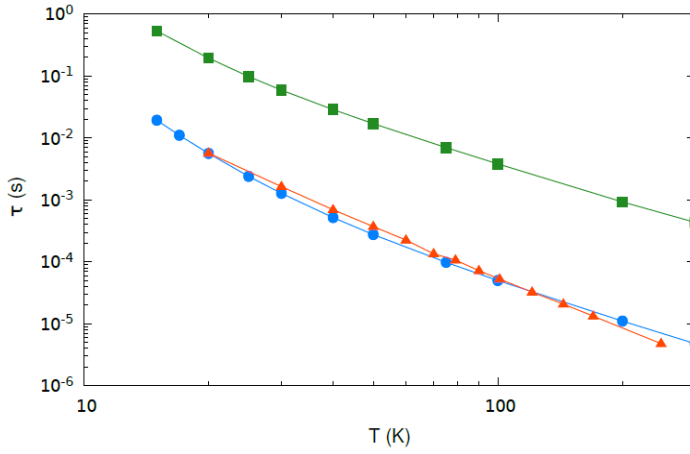


**Fig. 1.** Temperature dependence of  $T_1$  at X-band for Cr(V) nitrido complex doped in Re analog.  $\blacktriangle$   $T_1$  at  $g_{\text{perp}}$ ,  $\bullet$  Raman process calculated from electronic structure, and  $\blacksquare$  Raman process calculated from  $g$  and  $A$ .

## ELECTRON SPIN RELAXATION of MANGANESE in the +2, +3, and +4 OXIDATION STATES

**Gareth R. Eaton,<sup>1</sup> Sandra S. Eaton,<sup>1</sup> and Surendra Mahapatro<sup>2</sup>**

<sup>1</sup>Department of Chemistry and Biochemistry, University of Denver, Denver, Colorado 80210 USA

<sup>2</sup>Department of Chemistry, Regis University, Denver, Colorado 80221, USA

EPR spectra of  $\text{Mn}^{2+}$  were first reported in aqueous solution at 25 meter wavelength by Zavoisky in 1945 and in solid  $\text{MnSO}_4 \cdot 4\text{H}_2\text{O}$  and  $\text{MnCl}_2 \cdot 4\text{H}_2\text{O}$  at 2.93 GHz by Cummerow [1] and Halliday in 1946 [2]. Since then many CW studies of Mn(II) and a few studies of Mn(III) and Mn(IV) have been reported. Relatively few relaxation times have been reported. We recently reported the temperature dependence of electron spin relaxation rates for  $3d^1 \text{MnO}_4^{2-}$  ion in glassy solution and doped solid [3].

We now report pulsed EPR spin echo and inversion recovery measurements of  $T_m$  and  $T_1$  for  $3d^5 \text{Mn(II)}$ ,  $3d^4 \text{Mn(III)}$ , and  $3d^3 \text{Mn(IV)}$  in several ligand environments. Experiments were performed on a Bruker E580 with a dielectric resonator and  $B_1$  perpendicular to  $B_0$ . In each case the maximum temperature at which measurements were made was limited by the decrease in  $T_m$  with increasing temperature. The spin lattice relaxation of  $\text{Mn}(\text{H}_2\text{O})_6^{2+}$  in aqueous solution is surprisingly similar to that in an unusual solid tetrahedral lattice [4]. The relaxation rates for  $\text{Mn}(\text{acac})_3$  are so fast that data were acquired only up to 5 K, but for the Mn(III) citrate complex relaxation could be measured up to about 80 K. Relaxation of Mn(IV) complexes of sorbitol and metformin could be measured up to about 25 K. Further studies are planned to decipher the factors that control the relaxation rates.

[1] E. Zavoisky, *J. Phys. (USSR)* **9**, 211 – 216 (1945).

[2] R. L. Cummerow and D. Halliday, *Phys. Rev.* **70**, 433 (1946).

[3] S. N. Mahapatro, T. A. Hovey, T. Ngendahimana, S. S. Eaton, and G. R. Eaton, *J. Inorg. Biochem.* **229**, 111732 (2022).

[4] M. J. Henrichsen, J. Bendix, H. Weihe, *Compte Rendus Chimie*, doi.org/10.5802/crchim.266

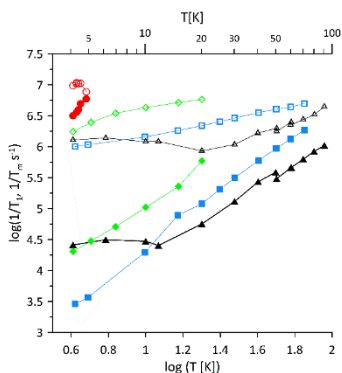


**Fig. 1.** Temperature dependence of  $1/T_1$  and  $1/T_m$  for Mn complexes. Open symbols are for  $T_m$  and closed symbols are for  $T_1$ : aquo Mn(II) (blue squares), aquo Mn(II) in solid tetrahedral lattice (black diamonds),  $\text{Mn}(\text{acac})_3$  (red circles), and Mn(IV) sorbitol (green diamonds).

## EPR of Copper(II) Complexes with Polymer Ligands

A.I. Kokorin

N.N. Semenov FRC of Chemical Physics of RAS, Moscow, Russia

Interest to systematic investigating structures, physical-chemical behavior and transformations of functional polymer materials with transition, radioactive and toxic metal ions was started more than 80 years [1-4]. A lot of ion-exchange resins (ionites) have been synthesized, specialized to different metals due to an interest to metal complexes with macromolecular ligands, stable in liquid solutions [5-7].

The main goal of this work was to analyze structural regulations and peculiarities of Copper(II) complexes with polymer ligands studied by EPR technique, which included the following: (1) organization of the coordination sphere, distinguishing polymers with monodentate or chelating functional groups and with cross-linked polymers (ion exchangers). (2) Spatial organization of the polymer-metal coils and local concentrations of paramagnetic centers in the macromolecular coil. (3) Transformations of Cu(II) complexes with macromolecules under oxidation processes.

In our report we will present the most interesting results revealed upon investigation of Cu(II) complexes with water-soluble linear and branched macromolecules such as poly-4-vinylpyridine (P4VP), poly-2-methyl-5-vinylpyridine (P2M5VP), poly-2-vinylpyridine (P2VP), their partially quaternized analogues (PVP-Q), linear (PEI) and branched (BPEI) poly-ethyleneimine, poly-trimethyleneimin (PTMI).

Evidently, such factors as protonation, quaternization of functional groups, substitution, and cross-linking of polymer chains will be analyzed since they influence on the composition and structure of the coordination sphere (Fig. 1).

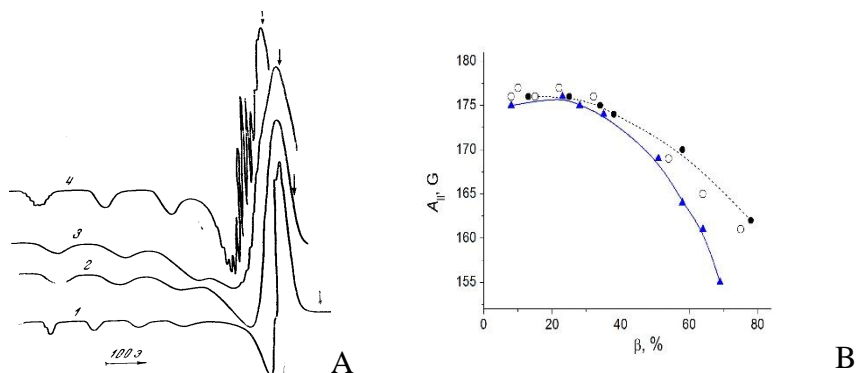


**Fig. 1.** **A** - EPR spectra of Cu(NO<sub>3</sub>)<sub>2</sub> (1) and complexes P4VP partially quaternized with *iso*-valeric acid (2), ethylene chloride (3), and Cu(Py)<sub>4</sub><sup>2+</sup> (4) dissolved in D<sub>2</sub>O-CD<sub>3</sub>OD (1:1 by volume). Arrows ↓ correspond to  $g = 2.0036$ .  $T = 77^\circ \text{K}$  [8]. **B** - Experimental dependences of the hfs constant  $A_{||}$  on the degree of quaternization  $\beta$  for P4VP-Q with methyl (●), ethyl (○), and benzyl (▲) residues [9].

Another important structural aspect of such supramolecular systems is their spatial organization including characterization of clustering metal complexes in the polymer

coils and measuring local concentrations of paramagnetic centers in them (Fig. 2A). The last topic of the paper concerns to functional behavior of polymer-metal materials and their structural changes in the presence of different oxidizing agents (Fig. 2B).

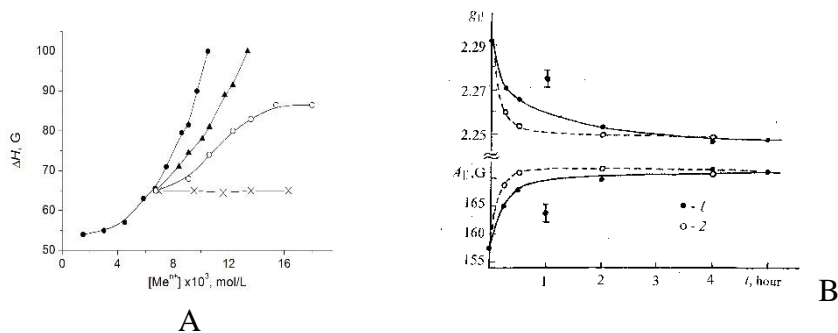


**Fig. 2. A** – Experimental dependences of the low-field line of parallel hfs orientation  $\Delta H_{1/2}$  on concentration of the added metal ions:  $\text{Cu}^{2+}$  ( $\bullet$ ),  $\text{Ni}^{2+}$  ( $\blacktriangle$ ),  $\text{Ca}^{2+}$  ( $\circ$ ), and  $\text{Na}^+$  ( $\times$ ) to 0.1 mol/L linear PEI solutions in  $\text{D}_2\text{O}-\text{CH}_3\text{OH}$  (1:1 by volume).  $T = 77^\circ \text{K}$  [10]. **B** – Experimental changes of  $A_{||}$  and  $g_{||}$  values on time for Cu(II) complexes with AN-25 anionite under reaction of catalytic oxidation of cyclohexanol at two  $\text{Cu}^{2+}$  concentrations ( $\bullet$ ,  $\circ$ ) [11].

1. Ion Exchange. Theory and Application. F.C. Nachod(ed.). New York: Acad. Press (1940), 320 p.
2. Saldadze K.M., Kopylova-Valova V.D. Complex-Forming Ionites (Complexites). M.: Khimiya (1980), 236 p. (In Russian)
3. Kopylova V.D., Astanina A.N. Ionite Complexes in Catalysis. M.: Khimiya (1987), 216 p. (In Russian)
4. Wawrzekiewicz M., Hubicki Z. Anion Exchange Resins as Effective Sorbents for Removal of Acid, Reactive, and Direct Dyes from Textile Wastewaters. DOI: 10.5772/60952, 2015.
5. Gembitskii P.A., Zhuk D.S., Kargin V.A. Polyethyleneimines. M.: Nauka (1971), 196 p. (In Russian)
6. Zezin A.B., Kabanov V.A. Russ. Chem. Reviews **51**, 833–855 (1982)
7. Kabanov V.A. Russ. Chem. Reviews **74**, 3–20 (2005)
8. Kokorin A.I., Vengerova N.A., Kirsh Yu.E., Zamaraev K.I. Doklady AN SSSR **202**, 597–600 (1972)
9. Our own results.
10. Kokorin A.I., Shubin A.A. Zh. Strukt. Khimii **30**, 106–112 (1989)
11. Kokorin A.I. Oxidation Comm. **22**, 68–74 (1999)

**Acknowledgement:** This work was performed within the framework of the Program of Fundamental Research of the Russian Federation (Reg. No. 122040500068-0).



## INFLUENCE OF THE THERMALLY INDUCED MAGNETOELASTIC EFFECT ON MAGNETIZATION SWITCHING IN Ni MICROPARTICLES WITH CONFIGURATION ANISOTROPY

**A.A. Bukharaev, D.A. Bizyaev, N.I. Nurgazizov, A.P. Chuklanov**

Zavoisky Physical-Technical Institute, FRC Kazan Scientific Center of RAS, Kazan, Russia

Planar magnetic particles are widely used in logic and memory devices. The operation of such elements is based on the fact of magnetization switching (rotation) in isolated particles (usually by  $180^\circ$ ). Typically, this rotation is induced by an external magnetic field. The configuration anisotropy of shape is often used to create a specific magnetization direction in planar particles (e.g., highly elongated ellipse, triangle, or square with different degrees of concavity of the sides) [1, 2].

In the field of straintronics (from “strain”, by analogy with “spintronic”) it is proposed to use the mechanical deformation and the resulting magnetoelastic effect for significant reduction of particles switching field [1]. In an ideal case, magnetization in the particles rotates without the application of any magnetic field. Recently, it has been demonstrated [3] that the magnetoelastic effect can be induced in particles by using single-crystal substrates with different thermal expansion coefficients along different axes. It has been shown that by slightly heating a crystal of lithium triborate  $\text{LiB}_3\text{O}_5$  (hereinafter LBO), the switching field of submicron Ni particles with rectangular shape can be significantly reduced. In this work, thermally induced magnetoelastic effect was used to modify the switching field of Ni square particles with concave sides (hereinafter CS-particles) and cross-shaped (X-particles) particles formed on LBO. The particles had a side size of  $1.1 \mu\text{m}$  and a height of  $30 \text{ nm}$  in which they could be inscribed.

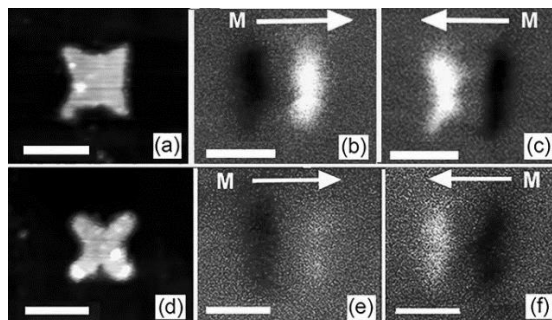


**Fig. 1.** (a) AFM image of a CS-particle, (b) MFM image corresponding to this particle obtained after applying field of 20 mT, (c) same particle after applying switching field. (d) AFM image of X-particle and MFM images corresponding to this particle obtained after applying 20 mT magnetic field (e) and after applying switching field (f). Color gradient for AFM images is equal to 40 nm. Color gradient for MFM images is equal  $0.5^\circ$  of phase shift. Lateral scale bar –  $1 \mu\text{m}$ , **M** –magnetization.

Ensembles of 35 individually positioned CS- (fig. 1a) and X- (fig. 1d) particles were prepared by scanning probe lithography. Ni deposition for particle preparation was performed at 50 °C. Measurement of the switching field of the particles was performed at three different temperatures (30, 50, and 70 °C). Due to the difference in thermal expansion coefficients along different axes, the compression of particles occurred at 30 °C, there was no deformation at 50 °C, and the particles were stretched at 70 °C. The number of particles that switched their magnetization direction at a given temperature and external magnetic field was determined by magnetic force microscopy (MFM) (fig. 1), and the graphs with normalized to the total number of particles was plotted by using this data (fig. 2a, c). MFM images were obtained using a single-pass technique. To determine the switching field value of the particles, the experimental data were fitted with a curve of the form:  $Y = a/(1+b \cdot \exp(-k \cdot X))$ . Then, the switching field values were found as the extremum of the derivative of these curves with respect to the field (fig. 2b, d).

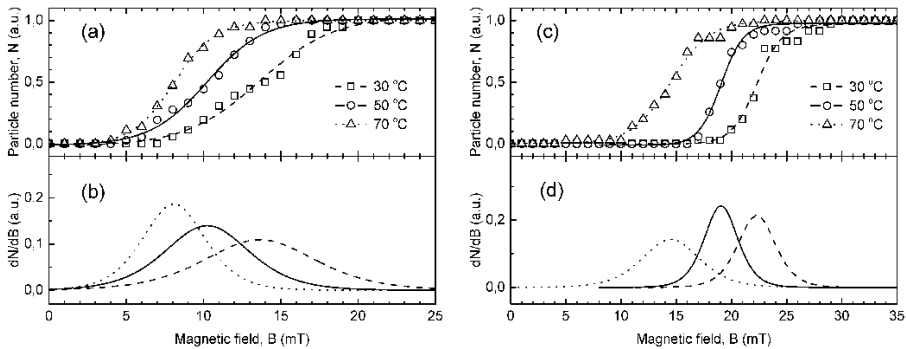


**Fig. 2.** The normalized dependence of CS-particles number that switch its magnetization direction on external field at different temperatures (a) and the corresponding derivative graphs (b). The normalized number of X-particles that switched its magnetization direction depending on the external magnetic field and temperature (c), and a corresponding derivative graphs (d). The figures (triangle, circle, square) show the experimental data, the lines (solid, dotted and dots) show the fitting results for the corresponding temperatures.

It was shown that changing the temperature of lithium triborate crystal by 40 °C (from 30 to 70 °C) allows reducing the magnetization switching field of square Ni particles with concave walls by 6 mT (by 1.75 times), and in X-shaped particles by 8 mT (by 1.53 times).

The work supported by RSF (grant № 23-29-00085).

1. Bukharaev A.A., Zvezdin A.K., Pyatakov A.P. et al.: *Physics – Uspekhi*. **61**, 1175-1212 (2018).
2. Gorev R.V. and Udalov O.U.: *Phys. Solid State*. **61**, 1563-1571 (2019).
3. Bizyaev D.A., Chuklanov A.P., Nurgazizov N.I, Bukharaev A.A.: *Jetp Lett.* **118**, 591–596 (2023).

## ANISOTROPIC SPIN HAMILTONIANS FOR IRIDIUM OXIDES: JUSTIFICATION FROM THE EMBEDDED CLUSTER APPROACH

L.A. Siurakshina<sup>1</sup>, V.Yu. Yushankhai<sup>2</sup>

<sup>1</sup>Meshcheryakov Laboratory of Information Technologies, JINR, Dubna, Russian Federation

<sup>2</sup>Bogoliubov Laboratory of Theoretical Physics, JINR, Dubna, Russian Federation

e-mail: siuraksh@jinr.ru

Our approach to the quantum magnetism of complex materials is based on computational quantum chemistry methods. The overall procedure starts with the basic all-electron Hamiltonian and allows us to (a) treat rigorously effects of electron correlations and (b) calculate exchange coupling between magnetic moments formed by partially filled electronic subshells of the constituent atoms.

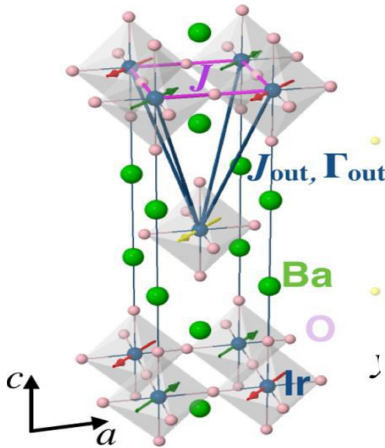


Fig.1. Lattice fragment and the ground-state magnetic structure of  $\text{Ba}_2\text{IrO}_4$  with indication of intra- and interlayer spin coupling between Ir ions in the octahedral oxygen surrounding.

obtained along this way. A typical result of calculations is the effective spin Hamiltonian  $H_S$  of general form including both the isotropic and strongly anisotropic couplings of neighboring spins-1/2:

$$H_S = \sum_{i,j} J_{ij} \vec{S}_i \vec{S}_j + \sum_{i,j} \Gamma_{ij}^{\alpha\beta} S_i^\alpha S_j^\beta$$

With this aim, for a properly chosen lattice fragment/cluster the wave functions of the lowest many-electron states and their energies are calculated and their symmetries are determined. The next step is to develop and apply a rigorous procedure for mapping these data onto the low-energy effective spin Hamiltonian  $H_S$  together with accurate estimate of the underlying spin-spin coupling parameters. In case of iridium oxides under consideration,  $\text{BaIrO}_3$ ,  $\text{Ba}_2\text{IrO}_4$ ,  $\text{Na}_2\text{IrO}_3$  this coupling between magnetic  $\text{Ir}^{5+}$  ions is dominated by the mechanism of Anderson's superexchange mediated by intermediate nonmagnetic  $\text{O}^{2-}$  ions. Particular attention is paid to the role of strong spin-orbit interaction of  $\text{Ir}^{5+}$  valence electrons in the formation of a magnetic moment on this heavy  $5d$  transition metal element in the octahedral oxygen surrounding.

The authors present a review of some of their principal results [1-4]

In general, anisotropic coupling  $\sim \Gamma_{ij}^{\alpha\beta}$  between spins at neighboring lattice sites  $\langle ij \rangle$ , first, depends on the crystallographic  $\langle ij \rangle$ -direction and, second, may even strongly dominate over isotropic exchange  $\sim J_{ij}$  as, for instance, occurs in the Kitaev's spin-1/2 model on hexagonal lattice. Thus, a quantitative justification is given for the validity of various spin models that were proposed on the phenomenological ground, intensely studied and discussed last years.

- [1] V. Katukuri et al., Phys. Rev. X **4**, 021051 (2014).
- [2] S. Nishimoto et al., Nature Comm. **7**, 10273 (2016).
- [3] L. Xu et al., Phys. Rev. B **99**, 115119 (2019).
- [4] M. Eldeeb et al., Phys. Rev. Matt. **4**, 124001 (2020).

## **STRONGLY CORRELATED QUANTUM SPIN LIQUIDS VERSUS HEAVY FERMION METALS**

**V.R. Shaginyan**

*NRC «Kurchatov Institute» - PNPI*

We consider experimental data collected on quantum spin liquid in  $\text{Lu}_3\text{Cu}_2\text{Sb}_3\text{O}_{14}$  and quasi-one dimensional (1D) quantum spin liquid in both  $\text{YbAlO}_3$  and  $\text{Cu}(\text{C}_4\text{H}_4\text{N}_2)(\text{NO}_3)_2$  with the aim to establish a sound theoretical explanation for the observed scaling laws, Landau Fermi liquid (LFL) and non-Fermi-liquid (NFL) behavior exhibited by these frustrated insulators. We show that the thermodynamic and transport properties as well as the empirical scaling laws follow from the fermion condensation theory. We explain how both the similarity and the difference in the thermodynamic and transport properties of heavy fermion (HF) metals and in its sister compounds with quantum spin liquid emerge, as well as establish connection of these HF metals with insulators  $\text{Lu}_3\text{Cu}_2\text{Sb}_3\text{O}_{14}$ ,  $\text{Cu}(\text{C}_4\text{H}_4\text{N}_2)(\text{NO}_3)_2$  and  $\text{YbAlO}_3$ . We demonstrate that the universal LFL and NFL behavior emerge because the HF compounds and the frustrated insulators are located near the topological FCQPT or are driven by the application of magnetic fields.

## COPPER (II) EPR in AMINO PHOSPHONIC POLYAMPHOLYTES

**V.I. Volkov<sup>1</sup>, I.A. Avilova<sup>1</sup>**

<sup>1</sup> Federal Research Center of Problems of Chemical Physics and Medicinal Chemistry of RAS, Chernogolovka, Russia

EPR is the method of choice for paramagnetic metal complexes structure identification in ion exchangers. This kind of investigation is carried out starting by Kazan scientists G. P. Vishnevskaya, R. H. Safin and B. M. Kozyrev.

Aminophosphonic polyampholytes are widely used for selective sorption of polyvalent ions as well as in catalytic processes. The structure of metal ion complexes and kinetics of ligand exchange are fundamental problems. In the case of paramagnetic transition metal ions electron paramagnetic resonance (EPR) technique is a strong tool of this information obtaining. We have investigated structure and sorption-desorption kinetics of copper (II) complexes in polyampholytes containing phosphonic groups only (CMF); phosphonic groups and dimethylamine (PA-1), trimethylamine (PA-2), diethylamine (PA-3), pyridine (PA-4) and ethylenediamine (PA-5) groups. The example of Cu<sup>2+</sup> EPR spectra is shown in Figure 1. At low copper (II) contents spectra are asymmetric lines which are typical for immobile complexes described by the next spin Hamiltonian of axial symmetry (1).

$$\hat{H} = \beta [g_{\parallel} H_{\parallel} S_z + g_{\perp} (H_x S_x + H_y S_y)] + A_{\parallel} S_z I_z + A_{\perp} (S_x I_x + S_y I_y) \quad (1)$$

where  $g_{\parallel}$ ,  $g_{\perp}$  components of  $g$ -factor;  $A_{\parallel}$ ,  $A_{\perp}$  - constants of ultrafine structure in parallel and perpendicular orientations relatively to external magnetic field;  $S_x$ ,  $S_y$ ,  $S_z$ ;  $I_x$ ,  $I_y$ ,  $I_z$  - projections of electron and nuclear spins. It was concluded that in CMF tetragonal Cu<sup>2+</sup> complex forms by two phosphonic groups and four water molecules Cu(R-HPO<sub>3</sub>)<sub>2</sub>(H<sub>2</sub>O)<sub>4</sub>. The same complexes are formed in ampholytes PA-1, PA-2, PA-3, and PA-4. In PA-5 copper (II) forms Cu(R-HPO<sub>3</sub>)<sub>2</sub>(H<sub>2</sub>O)<sub>4</sub>, Cu(R-N)<sub>4</sub>(H<sub>2</sub>O)<sub>2</sub><sup>2+</sup> and Cu(R-N)<sub>2</sub>(H<sub>2</sub>O)<sub>4</sub><sup>2+</sup> complexes where four and two nitrogen atoms coordinate Cu<sup>2+</sup> ion. The example of copper (II) spectra evolution during copper sorption from 0.001 N aqueous CuSO<sub>4</sub> solutions is shown in Figure 1.

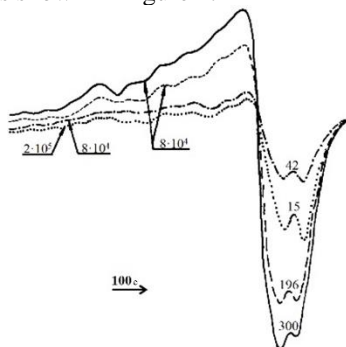
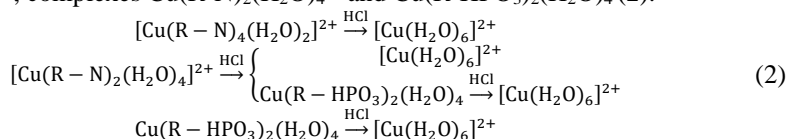


**Fig. 1.** EPR spectra of copper (II) in PA-5 recorded at different sorption time (in minutes) during copper sorption from 0.001 N aqueous solutions CuSO<sub>4</sub>. Figures on the arrow are gains.

On the basis of these data partial sorption and desorption kinetics curves for different copper (II) complexes are obtained. During desorption by hydrochloric acid amino complexes of copper (II)  $\text{Cu}(\text{R-N})_4(\text{H}_2\text{O})_2^{2+}$  transfer in aqua complexes  $\text{Cu}(\text{H}_2\text{O})_6^{2+}$ , complexes  $\text{Cu}(\text{R-N})_2(\text{H}_2\text{O})_4^{2+}$  and  $\text{Cu}(\text{R-HPO}_3)_2(\text{H}_2\text{O})_4$  (2).



The concentrations of  $\text{Cu}(\text{H}_2\text{O})_6^{2+}$  and  $\text{Cu}(\text{R-HPO}_3)_2(\text{H}_2\text{O})_4$  in amphotite grain increase initially as it is shown in Figure 2.

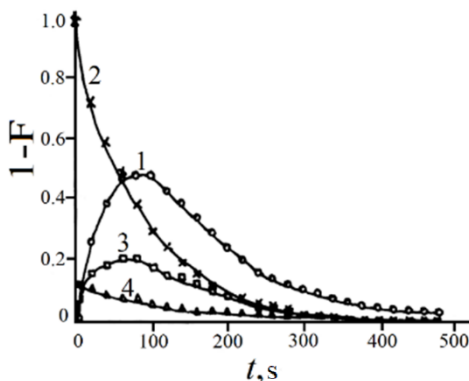


**Fig. 2.** Kinetic curves of copper (II) desorption in PA-5 by 0.1 N aqueous HCl solutions. 1 -  $\text{Cu}(\text{H}_2\text{O})_6^{2+}$ ; 2 -  $\text{Cu}(\text{R-N})_2(\text{H}_2\text{O})_4^{2+}$ ; 3 -  $\text{Cu}(\text{R-HPO}_3)_2(\text{H}_2\text{O})_4$ ; 4 -  $\text{Cu}(\text{R-N})_4(\text{H}_2\text{O})_2^{2+}$  complexes

Dynamic EPR spectra registration gave opportunity to obtain kinetic curves of partial copper (II) complexes sorption and desorption. These partial kinetic was approximated by simple models of ion exchange processes.

#### Acknowledgments

Measurements were performed using equipment of the Multi-User Analytical Center of the Federal Research Center of Problems of Chemical Physics and Medicinal Chemistry RAS with the support of State Assignment of the Federal Research Center of Problems of Chemical Physics and Medicinal Chemistry RAS (state registration No FFSG-2024-0008/124013000743-3).

# ORAL TALKS



## ДОКУМЕНТАЛЬНОЕ НАСЛЕДИЕ АКАДЕМИКА Е.К. ЗАВОЙСКОГО В АРХИВЕ РАН

С.О. Назаров

Архив РАН, Москва, Россия

Личный фонд академика Евгения Константиновича Завойского (1907–1976) (Ф.1943) был передан в Архив РАН его дочерью – Наталией Евгеньевной Завойской. В настоящее время фонд находится на стадии научной обработки и составления описи. Однако процесс комплектования фонда продолжается. В связи с этим, на выставке новых поступлений, открывшейся в Архиве РАН 29 мая 2024 г., были представлены документы Е.К. Завойского. В докладе будут отмечены ключевые разделы описи фонда с кратким описанием содержащихся в них документов.

Первый раздел описи – «Научные труды и другие творческие материалы», включает в себя научные исследования, научно-популярные работы, воспоминания, лекции и рабочие материалы Е.К. Завойского. Научные исследования представлены статьями и докладами за период с 1931 по 1976 г., охватывающими широкий спектр тем, над которыми работал ученый от метода измерения потенциалов возбуждения атомов и молекул, электронного парамагнитного резонанса до проблем физики плазмы. Из лекций особый интерес представляет популярная лекция по теме «Электронный парамагнитный резонанс», подготовленная Е.К. Завойским для поездки в Японию. Рабочие материалы к трудам содержат черновые варианты статей и многочисленные записи результатов экспериментов и расчетов, которые позволяют реконструировать процесс работы физика. Одними из первых таких записей является блокнот под названием «Радиоуголок», который ученый ввел с 1926 по 1928 г. Этому периоду студенчества в Казанском государственном университете посвящены и воспоминания Е.К. Завойского, описывающие также учебу в аспирантуре в начале 1930-х гг.

В раздел «Биографические документы» вошли метрическая книга военной церкви 73-го Крымского пехотного полка за 1907 г. с записью рождения Е.К. Завойского, студенческие тетради с лекциями Я.И. Френкеля, Л.В. Розенкевича, документы о выдаче патента на изобретение «Устройства для управления механизмами на расстоянии» (1927–1933), удостоверения и справки с различных мест работы, постановления об избрании Е.К. Завойского член-корреспондентом и действительным членом АН СССР, грамота о присуждении премии Международного общества магнитного резонанса. В данный раздел также включены многочисленные документы о Е.К. Завойском: воспоминания и статьи разных лиц, стихотворения, либретто оперы-фаду «Евгений Завойский или Эпох Парадоксальный Резонанс» (ЭПР-2)», документы проведения Международной премии имени Е.К. Завойского «Zavoisky Award». Завершают раздел фотографии ученого разных лет с семьей и коллегами, а также рисунки, как самого Е.К. Завойского, так и других лиц.

Не менее значимым представляется раздел описи фонда «Документы о деятельности». Раздел отражает редакционно-издательскую деятельность ученого, в том числе содержит документы о назначении Е.К. Завойского главным редактором журнала «Успехи физических наук». Освещает раздел и его научно-организационную деятельность. Стоит отметить документы академика по работе Сектора № 74 Отдела ядерной физики Института атомной энергии АН СССР, документы по организационным вопросам проведения семинаров «Т» (Термояд) и Всесоюзного семинара по Коллективным взаимодействиям в плазме, а также документы по работам различных комиссий АН СССР с участием или под предводительством Е.К. Завойского, например, документы Комиссии по ознакомлению с научной работой на Физическом факультете МГУ. Наконец, о деятельности в области международного сотрудничества свидетельствуют документы, собранные для выдвижения Е.К. Завойского в кандидаты на Нобелевскую премию по физике, материалы для подготовки участия АН СССР на Всемирной выставке 1958 г. в Брюсселе, приглашение Е.К. Завойского и Б.М. Козырева на Гордоновскую научную конференцию по «Магнитному резонансу» в Нью Хемптоне, документы об участии ученого на конференциях по физике плазмы и управляемым термоядерным реакциям Международного агентства атомной энергии (МАГАТЭ).

Небольшой раздел составила «Переписка» Е.К. Завойского. Однако в ней содержатся письма к таким адресатам, как П.Л. Капица, А.П. Александров и С.А. Альтшулер. Среди корреспондентов стоит отметить Г.Н. Кружилина, А.А. Аникеенка, Х.М. Муштари.

Значительную часть фонда составил раздел «Материалы родственников» Е.К. Завойского. В раздел вошли семейные и личные документы В.К. Труфановой-Завойской, жены ученого, и Н.Е. Завойской. В разделе представлена обширная переписка Завойской Н.Е. с деятелями науки.

Таким образом, личный фонд Евгения Константиновича Завойского в Архиве РАН представляет большую научную ценность. Собранные в фонде документы позволяют с высокой долей подробности воссоздать биографию выдающегося физика. Благодаря сохранившимся многочисленным черновым записям и рабочим материалам возможно проследить принципы работы ученого. В свою очередь, документы о научно-организационной и международной деятельности могут дать историку науки богатый материал по изучению развития физики в XX в. А собранные Н.Е. Завойской материалы родственников содержат уникальную информацию об истории семьи Завойских.

## VISUALISATION of the SURFACE of ISOLATED NERVOUS SYSTEM of a GRAPE SNAIL with FLUORESCENT NANOPROBES

**L.A. Nurtdinova<sup>1</sup>, V.G. Nikiforov<sup>1</sup>, A.V. Leontyev<sup>1</sup>, A.G. Shmelev<sup>1</sup>,  
D.K. Zharkov<sup>1</sup>, R.M. Gataullina<sup>1</sup>, E.O. Mitushkin<sup>1</sup>, A. N. Solodov<sup>1</sup>,  
R. R. Zairov<sup>2</sup>, A.R. Mustafina<sup>2</sup>, V. V. Andrianov<sup>1,3</sup>, L. N. Muranova<sup>3</sup>,  
Kh. L. Gainutdinov<sup>1,3</sup>**

<sup>1</sup>FRC Kazan Scientific Center of RAS, Kazan, Russia

<sup>2</sup>Arbuzov IOPC FRC Kazan Scientific Center of RAS, Kazan, 420029, Russia

<sup>3</sup>Kazan Federal University, Institute of Fundamental Medicine and Biology, Kazan, 420008, Russia

One of the key tasks in biomedicine is visualization, which involves the remote recording of the positions of probes embedded in biological samples using optical methods. This technique enables not only the visualization of individual organs but also facilitates the application of luminescent probes for purposes such as drug delivery and targeted exposure to specific areas of biological tissue.

The following hydrophilic particles were evaluated as luminescent probes:  $[\text{Ru}(\text{dipy})_3]^{2+}@\text{SiO}_2$ ,  $\text{NaYF}_4:\text{Yb,Er}$  coated with L-cysteine,  $\text{NaYF}_4:\text{Yb,Er}$  encased in a  $\text{SiO}_2$  shell, and  $\text{NaYF}_4:\text{Yb,Ho}$  coated with PEI polymer. The first set,  $[\text{Ru}(\text{dipy})_3]^{2+}@\text{SiO}_2$  particles, measuring 50 nm, operates via downconversion, exhibiting a broad emission band in the visible spectrum when excited by a laser at 405 nm. In contrast, fluoride particles,  $\text{NaYF}_4:\text{Yb,Er}$  and  $\text{NaYF}_4:\text{Yb,Ho}$ , 200 nm in size function as upconversion systems with  $\text{Er}^{3+}$  and  $\text{Ho}^{3+}$  ions emitting when stimulated by laser radiation at 980 nm. Utilizing these particles, mapping of the surfaces of living tissues in the isolated nervous system of the grape snail was performed. Their locations within a three-dimensional coordinate system were determined using optical confocal microscopy with a lateral resolution of 10  $\mu\text{m}$ . This approach not only provides detailed morphological analysis of individual tissue sections but also allows for precise exposure of the tissue at the cellular level. Additionally, a series of demonstration experiments were conducted to assess local temperature on the surfaces of individual neurons using the generated 3D surface models.

The synthesis of upconversion nanoparticles was carried out with the support of Russian Science Foundation under grant no 23-42-10012, <https://rscf.ru/project/23-42-10012/>. Spectroscopic studies were supported by the government assignment for the FRC Kazan Scientific Center of RAS.

## ELECTRICALLY TUNABLE SUB-TERAHERTZ RESONANCE IN ANTIFERROMAGNET-BASED HETEROSTRUCTURE

**A.R. Safin, A.Yu. Mitrofanova, A.A. Matveev, S.A. Nikitov**

Kotel'nikov Institute of Radioengineering and Electronics of RAS, Moscow, Russia

Antiferromagnetic (AFM) materials have natural resonance frequencies in the sub-THz or THz ranges. Thus, it is tempting to use antiferromagnets (AFM) as active layers in THz-frequency oscillators [1] and detectors [2]. It has been shown theoretically [2] that both uniaxial and biaxial AFMs can be used for the resonance quadratic rectification of a linearly polarized AC spin current of THz frequency and could have a sensitivity in the range of 100–1000 V/W.

Let us consider the antiferromagnet-normal-metal heterostructure (see the inset in Fig.1) with the antiferromagnetic easy plane (EP) oriented in the angle  $\theta_p$  to the surface plane, and hard axis  $n_h$  is perpendicular to the EP. An additional bias DC current in the normal metal layer (here Pt) is used for tuning the AFM high-frequency mode (near 0.17 THz for  $j_{dc}=0$ ) and for a partial regeneration of the system losses. Based on our previous theoretical analysis [2,3,6] applied to the hematite crystal, we analyzed the so-called “ $\sigma$ -model” equation describing the dynamics of Neel vector  $l(t)$ ; we have found the analytical expressions for both low and high frequencies of hematite as functions of current density for an arbitrary angle of inclination of the easy plane relative to the sample plane.

Our theoretical analysis showed that decreasing the angle between the sample plane and the easy antiferromagnetic plane leads to an increase in the value of threshold current density. Thus, our analysis shows that minimizing the critical tuning current would be desirable for the easy plane to be oriented perpendicular to the sample plane, which can be achieved by choosing a unique substrate.

1. R. Khymyn, et al. Sci. Rep. **7**, 43705 (2017).
2. A.R. Safin, et al. Appl. Phys. Lett. **117**, 222411 (2020).

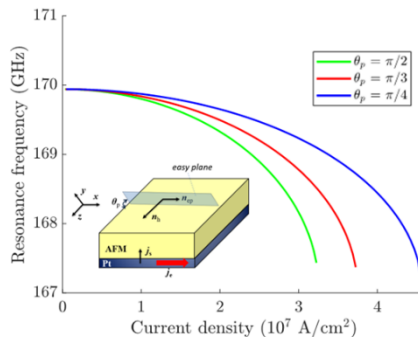


**Fig. 1.** Dependence of the AFMR oscillation frequency on the input bias electrical current density flowing in the Pt layer for different orientations of easy plane relative to the sample plane ( $\theta_p=\pi/2, \pi/3, \pi/4$ ). The inset is an image of the proposed AFM-Pt heterostructure.

## **CORE–SHELL NaYF<sub>4</sub>:Yb<sup>3+</sup>/Tm<sup>3+</sup>@NaGdF<sub>4</sub>:Ce<sup>3+</sup>/Tb<sup>3+</sup> NANOPARTICLES for DUAL-MODE FLUORESCENCE- BASED TEMPERATURE SENSING and ANTI- COUNTERFEITING**

**A.V. Leontyev, R.M. Gataullina, A.N. Solodov, L.A. Nurtdinova, A.G. Shmelev, D.K. Zharkov, V.G. Nikiforov**

FRC Kazan Scientific Center of RAS, Kazan, Russia

Core/shell NaYF<sub>4</sub>:Yb/Er@NaGdF<sub>4</sub>:Ce/Tb nanoparticles were synthesized and their structural and photophysical properties were compared to parent NaYF<sub>4</sub>: Yb/Er and NaGdF<sub>4</sub>:Ce/Tb nanoparticles. The suppression of defects in NaYF<sub>4</sub>:Yb/Er core with the presence NaGdF<sub>4</sub>:Ce/Tb shell is evident as Er<sup>3+</sup> ions emission lines are much sharper resolved when compared to core particles.

If excited by 980nm radiation core/shell nanoparticles exhibit upconverted fluorescent emission with a quantum yield of 0.19% driven by energy transfer between Yb<sup>3+</sup> and Er<sup>3+</sup> ions. Other possible excitation route is Ce<sup>3+</sup> absorption at 266 nm followed by downconverted emission with a quantum yield of 96%. This dual functionality allows for anti-counterfeiting applications, such as creating fluorescent inks active under both UV and IR radiation.

On the other hand, Er<sup>3+</sup> emission is known to be temperature-dependent, making these particles fluorescent nanothermometers. An experiment illustrating this application was conducted with the nanoparticles spread over unevenly heated sample. The surface temperature distribution was mapped with 10 μm lateral resolution and 1.6 K accuracy. And as the excitation wavelength falls within biological tissues transparency window these particles could be potentially used as temperature sensors in living systems, down to intracellular level.

Furthermore, the presence of Gd<sup>3+</sup> ions results in MRI contrasting properties, suggesting the use of these kinds of nanoparticles as multifunctional agents in advanced biomedical imaging and sensing applications.

The synthesis of nanoparticles was carried out with the support of Russian Science Foundation under grant no 23-42-10012, <https://rscf.ru/project/23-42-10012/>. Spectroscopic studies were supported by the government assignment for the FRC Kazan Scientific Center of RAS.

## Electron-nuclear interactions in optically active NV<sup>-</sup> centers in 6H-SiC – a promising material platform for quantum technologies

F. F. Murzakhanov<sup>1</sup>, G. V. Mamin<sup>1</sup>, D. V. Shurtakova<sup>1</sup>, I. N. Gracheva<sup>1</sup>,  
M. A. Sadovnikova<sup>1</sup>, M. R. Gafurov<sup>1</sup>

<sup>1</sup> Institute of Physics, Kazan Federal University, Kazan, Russia

Over the few past decades, spin carrying defects in semiconductors have attracted growing interest as a solid-state ground for quantum technologies [1]. Silicon carbide (SiC) crystals can serve as a host-matrix for a wide variety of color centers. The most studied high-spin ( $S \geq 1$ ) defects in SiC include silicon vacancy centers, paired vacancies and negatively charged nitrogen-vacancy centers (NV), similar to those in diamond. A large-scale study of the properties of color centers allows us to identify those that are promising as qubits. Among the defects in SiC, the NV center stands out especially due to the presence of nuclear spin of the <sup>14</sup>N isotope. Optically active centers in the ground state with coherent electron-nuclear interaction can act as a platform for the implementation of quantum registers. That's why comprehensive study of electron-nuclear interaction in this system is very important and useful.

We present the study of electron-nuclear interactions in optically active NV<sub>hh</sub> centers in 6H-SiC crystals (enriched with <sup>28</sup>Si). In order to determine the hyperfine tensor ( $A$ ) and quadrupole interaction constant ( $Cq$ ) values we perform a complex approach – combination of the electron paramagnetic resonance (EPR), electron nuclear double resonance (ENDOR) techniques and the calculations using the density functional theory method in the Quantum ESPRESSO software package [2].

ENDOR experiments were carried out at different crystal orientations relative to the magnetic field up to 30° degree. Analys of the angular dependence of the ENDOR spectra allows us to determine hyperfine interaction tensor values and  $Cq$  value. Experimental results were compared with the electron – nuclear terms of the spin-Hamiltonian calculated using DFT method. Two sets of the obtained parameters are in good agreement with each other. Additional quantum-chemical calculations using the DFT (density functional theory) method were carried out to clarify the distribution of the electron and spin density of the NV center within the unit cell.

The study was funded by the subsidy allocated to Kazan Federal University for the state assignment in the sphere of scientific activities (Project No. FZSM-2024-0010).

1. Awschalom D. D., Hanson R., Wrachtrup J., Zhou B. B.: Nat. Photon. **12**, 516 (2018)
2. Giannozzi P., Baroni S., Bonini N., et al: J. Phys.: Condens. Matter **21** 395502 (2009)

## STATIC and RESONANT PROPERTIES and MAGNETIC PHASE DIAGRAM of $\text{LiMn}_2\text{TeO}_6$

**E.L. Vavilova<sup>1</sup>, T.M. Vasilchikova<sup>2</sup>, A.N. Vasiliev<sup>2</sup>**

<sup>1</sup> Zavoisky Physical-Technical Institute, FRC Kazan Scientific Center of RAS, Kazan, Russia

<sup>2</sup>Low Temperature Physics and Superconductivity Department, Moscow State University, Moscow, Russia

Physical properties of the mixed-valent  $\text{LiMn}_2\text{TeO}_6$  were investigated by measurements of AC and DC magnetic susceptibility, magnetization, specific heat, electron spin resonance (ESR), and nuclear magnetic resonance (NMR). The study showed that this multicomponent spin system exhibits not only a complex phase diagram in the ordered state [1], but also a field-dependent, nontrivial change in dynamic correlated regimes. The transformation of the magnetic state depending on the field and temperature and its connection with the magnitude, frustration and signs of spin exchanges in the manganese ions system has been studied.

I. Vasilchikova, T.; Vavilova, E.; Salikhov, T.; Nalbandyan, V.; Dengre, S.; Sarkar, R.; Klauss, H.-H.; Vasiliev, A. *Materials* **15**, , 8694 (2022)

## MAGNETIC RESONANCE STUDY OF Fe DOPED TlInTe<sub>2</sub> CRYSTAL

**F. Mikailzade<sup>1</sup>, S. Gökçe<sup>1</sup>, M.Yu. Seyidov<sup>1</sup>,  
T.G. Mammadov<sup>2</sup>, A.I. Nadjafov<sup>2</sup>**

<sup>1</sup> Department of Physics, Gebze Technical University, Gebze, 41400, Kocaeli, Türkiye

<sup>2</sup> Institute of Physics, Ministry of Science and Education, AZ-1143, Baku, Azerbaijan

TlInTe<sub>2</sub> is a compound with a one-dimensional chain-like (fibrous) crystalline structure belonging to the family of thallium based chalcogenide compounds. It is a native *p*-type semiconducting material with an indirect electronic band gap lying between ~ 0.5 - 0.54 eV. According to the structural data, TlInTe<sub>2</sub> crystallizes in centrosymmetric tetragonal structure having space group of *I4/mcm* with *Z*=4 formula units and 16 atoms in the unit cell.

The crystallographic building blocks of TlInTe<sub>2</sub> chain crystal are InTe<sub>4</sub> anionic units linked by edge-sharing telluride atoms and form linear Te<sub>2</sub>-In-Te<sub>2</sub> chains along the tetragonal *c*-axis. The trivalent In cations are located at the centers of InTe<sub>4</sub> tetrahedra, which are surrounded by four Te anions (tetrahedral) by forming covalent (*sp*<sup>3</sup>) bound with 3.6 Å interatomic In-Te distances. The univalent Tl ions are located between four chains and have an octahedral environment consisting of eight Te ions [1]. It can be considered that TlInTe<sub>2</sub> crystal composed of two subsystems, which are indium sublattice inside the chains and weakly bound ionic sublattice comprising of Tl cations located between chains [2].

Fe-doped TlInTe<sub>2</sub> samples were extracted from the single crystalline ingot grown by using the Bridgman-Stockbarger technique. A small amount of Fe used as dopant and purchased in a powder form was added to TlInTe<sub>2</sub> powder during a growth process. Room temperature magnetic resonance measurements have been performed using a JEOL JES-FA 300 EPR spectrometer operated at a fixed microwave frequency of ~ 9.2 GHz (X-band).

The studies revealed the presence of both well-defined EPR peaks originated from paramagnetic Fe<sup>3+</sup> ions located at the centered positions of InTe<sub>4</sub> tetrahedrons and pronounced broadened FMR signal originated from magnetically ordered Fe ions inside the crystal structure. The observed coexistence of EPR and FMR spectra has been attributed to be due to the substitution of Fe<sup>3+</sup> ions into In<sup>3+</sup> sites as well as cluster formation from Fe atoms allocated along Tl chain channels.

1. Orudzhev G.S., Godzhaev E.M., Kerimova R.A., and Allakhyarov E.A.: Physics of the Solid State, **48**, 42–46 (2006)

2. Nadzhafov A.I., Madatov R.S., Khalilova K.G., Iskenderova G.M.: Physics of the Solid State. **64**, 271–277 (2022)



## STUDY OF PECULIARITIES $\text{Co}^{2+}$ and $\text{Co}^{3+}$ EPR SPECTRA IN DIFFERENT SPIN STATES

**R.M. Eremina<sup>1</sup>, I.V. Yatsyk<sup>1</sup>,  
T.I. Chupakhina<sup>2</sup>, Yu.A. Deeva<sup>2</sup>**

<sup>1</sup> Zavoijsky Physical-Technical Institute, FRC Kazan Scientific Center of RAS, Kazan, Russia

<sup>2</sup> Institute of Solid State Chemistry of the RAS (UB), Ekaterinburg, Russia

Recently, great interest in double perovskites has been attracted by the possibility of their use as thermoelectrics. The Seebeck coefficient  $S$  was measured for multiple Ba-based double perovskites at various temperatures. As it has been shown, the properties of thermoelectrics are influenced not only by the processes of diffusion of charge carriers and phonons, but also by the spin components. The goal of our research is to experimentally study the magnetic properties of double perovskite  $\text{Ba}_2\text{CoNbO}_{6-\delta}$  and  $\text{Sr}_2\text{CoNbO}_{6-\delta}$  by ESR method. If the oxygen content is 6, then the valence of cobalt should be 3+. Co in the 3+ oxidation state may be in a high-spin state with  $S = 2$ , an intermediate-spin state with  $S = 1$ , or a low-spin state with  $S = 0$ . As soon as the  $\delta$  is not equal to zero, then part of the cobalt ions goes into the 2+ state with  $S=3/2$ . We consider features of EPR spectra in stoichiometric  $\text{Ba}_2\text{CoNbO}_6$  and oxygen-deficient  $\text{Sr}_2\text{CoNbO}_{6-\delta}$  compounds. A Bruker EMXplus spectrometer was used to record ESR spectra in the X range at a frequency of  $\sim 9.3$  GHz in the temperature range of 5–300 K. The measured ESR spectrum  $d\chi''/dH$  for  $\text{Ba}_2\text{CoNbO}_{6-\delta}$  and  $\text{Sr}_2\text{CoNbO}_{6-\delta}$  where shown in Fig.1.

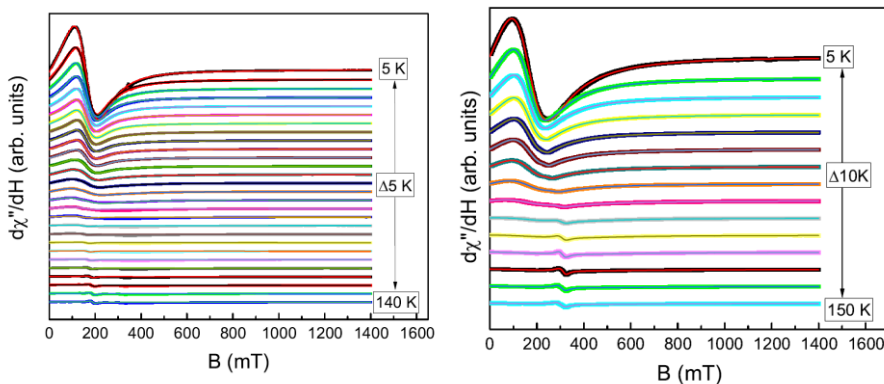


**Fig. 1.** Temperature dependences of ESR spectra in (left)  $\text{Ba}_2\text{CoNbO}_{6-\delta}$  and (right)  $\text{Sr}_2\text{CoNbO}_{6-\delta}$  compounds

Peculiarities of cobalt EPR spectra considering spin-orbit interaction and influence of crystalline field are considered.

This research was supported by the Russian Science Foundation (Project No. 22-42-02014)

## On some properties of the ion spin system in pulsed EPR experiments

Yu.E. Kandrashkin

<sup>1</sup> Zavoisky Physical-Technical Institute, FRC Kazan Scientific Center of RAS, Kazan, Russia

Rare earth ions doped in single crystals are the subject of considerable interest as potential quantum storage elements. The theoretical description of the electron spin properties of the ions, which have the anisotropic Zeeman and strong hyperfine interactions, is presented. Several phenomena, including the reduction of the effective magnetization of the electron spin, the phase memory decay, and the unusual electron spin echo envelope modulation (ESEEM), are described [1-3].

The large values of the zero-field splitting and/or the hyperfine interaction of the ion electron with its own nucleus lead to a nonlinear dependence of the energy of the spin states on the magnetic field. This leads to the formation of anticrossings of some spin sublevels. In the vicinity of the anticrossing region, the effective magnetic moment of the electron spin is reduced, resulting in an increase of the lifetime of the spin coherence and a decrease of the Rabi frequency [1].

Another important property is the anisotropy of the Zeeman interaction, due to which the quantization axis of the electron spin of the ion is tilted with respect to the direction of the external magnetic field. This leads to the appearance of the Zeeman interaction component of the nearby nuclei orthogonal to the quantization axis of the electron spin. This component is responsible for an additional mechanism of coherence formation on the magnetic nuclei in the local environment of the ion [2]. As a result, the ESEEM signal can be formed even in the case of a purely isotropic super-hyperfine interaction. The results of the theoretical analysis are further used to simulate the ESEEM data of an isotopically pure  $Y_2SiO_5$  crystal doped with  $^{173}Yb^{3+}$  ions [3].

1. Kandrashkin Yu. E. Impact of Zeeman and Hyperfine Interactions of the Magnetic Properties of the Ion: I. Local Interactions of the Electron Spin. JMR (2024, accepted)
2. Kandrashkin Yu. E. Impact of Zeeman and Hyperfine Interactions of the Magnetic Properties of the Ion: II. Super-Hyperfine Interactions with Surrounding Nuclei JMR (2024, accepted)
3. Kandrashkin Yu. E.: Impact of Zeeman and Hyperfine Interactions of the Magnetic Properties of the Ion: III. Impact of the Local Interactions of the Doped Yb Ion in  $Y_2SiO_5$  Crystal JMR (2024, accepted)

## Features of modeling the NMR signal shape recorded using the modulation technique from liquid media

**A.A. Gol'dberg<sup>1</sup>, V.V. Davydov<sup>1</sup>, S.A. Klimova<sup>1</sup>, R.V. Davydov<sup>1</sup>**

<sup>1</sup>Peter the Great St.Petersburg Polytechnic University, Saint-Petersburg, Russia

The modulation technique for recording NMR signals from liquid media is applicable in small NMR relaxometers, NMR flowmeters-relaxometers, and magnetometers [1, 2]. Depending on the conditions in which the liquid medium is located (flowing sweat or stationary state), as well as on its composition (for example, oil with water, air, and solid particles), the parameters of the magnetic fields, the modulation frequency and the volume of the medium are selected to obtain the maximum signal ratio /noise to ensure maximum accuracy when conducting research [3, 4]. Unlike classical NMR, in which the spectrum is recorded, in the case of using the modulation technique, a signal is recorded in the form of non-periodic damped oscillations (“wiggles”).

Figure 1 shows an example of a recorded NMR signal from tap water at  $T = 287.3$  K. The repetition period  $T_{nmr}$  of the recorded NMR signal is  $2/f_m$  (where  $f_m$  is the modulation frequency of the constant magnetic field in which the NMR signal is recorded). For these two reasons, for an adequate description of the movement of the magnetization components, it is necessary to transform into a rotating coordinate system around the direction of the field  $H_0$  [5]. New variables  $u(t)$  and  $v(t)$  are introduced to do this, which characterize the dispersion and absorption. Through these components, the magnetization  $M_x$  and  $M_y$  of the medium under study are expressed as:

$$\begin{aligned} M_x &= u(t)\cos(\omega t) - v(t)\sin(\omega t) \\ M_y &= u(t)\sin(\omega t) - v(t)\cos(\omega t) \end{aligned}$$

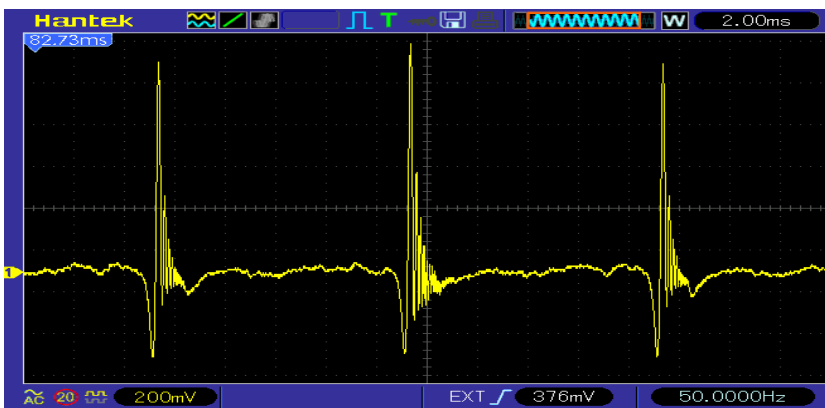


**Fig. 1.** NMR signal recorded using the modulation technique from tap water at  $T = 287.3$  K, at  $f_m = 50$  Hz.

Another feature of the modulation technique, especially in small-sized NMR relaxometers, is registering the NMR signal at the resonant frequency of the magnetic

field  $\omega_0 = \gamma H_0$  to ensure maximum signal-to-noise ratio. In this case, in the classical Bloch equations  $\Delta\omega = 0$ . Considering all the noted features, the system of Bloch equations will take the following form:

$$\begin{aligned} u'(t) + u(t)/T_2 + \gamma H_m \sin(\omega_m t) v(t) &= 0 \\ v'(t) + v(t)/T_2 - \gamma H_m \sin(\omega_m t) u(t) - \gamma H_1 M_z(t) &= 0 \\ M_z'(t) + M_z(t)/T_1 - \gamma H_1 v(t) - M(t)/T_1 &= 0 \end{aligned} \quad (1)$$

where  $M(t) = \chi_0 (H_0 + H_m \sin(\omega_m t))$ ,  $H_m$  and  $\omega_m$  are amplitude and frequency of the modulation field,  $T_1$  and  $T_2$  are the times of longitudinal and transverse relaxation,  $H_1$  is the radio frequency field created by the autodyne detector in the NMR signal recording coil.

An autodyne detector is an integral measuring device [2, 4], therefore the shape  $F(t)$  of the NMR signal recorded by it is expressed by the following relation:

$$F(t) = (v^2(t) \cdot (A_1 / (A_1 + A_2)) + u^2(t) \cdot (A_2 / (A_1 + A_2)))^{1/2} \quad (2)$$

where  $A_1$  and  $A_2$  are coefficients that determine the contribution of dispersion and absorption signals to the recorded NMR signal.

Therefore, to use (2) when describing the NMR signal, it is necessary from (1) to obtain an analytical solution regarding  $u(t)$ ,  $v(t)$ , and  $M_z(t)$ , considering the initial conditions at  $t = 0$ . It should be noted that these conditions are different for stationary and current liquids, which is also a feature. For a stationary liquid:  $u(0) = 0$ ,  $v(0) = 0$  и  $M_z(0) = \chi_0 H_0$ . For a flowing liquid:  $u(0) = 0$ ,  $v(0) = 0$  и  $M_z(0) = \chi_0 H_p \cdot \exp(-\tau/T_1)$ , where  $\tau$  is the time of fluid flow from the polarizing magnet (with field  $H_p$ ) to NMR signal recording coils. It should be noted that for a flowing liquid, the following relationship holds:  $H_p \gg H_0 > H_m$ . For stationary  $H_0 > H_m$ , we cannot exclude the function  $M(t)$  from consideration when solving the Bloch equations. Therefore, the solution for the stationary case will be more general than for a flowing fluid.

By solving (1) for the stationary case of placing a liquid medium, we were able to derive analytical expressions for  $u(t)$ ,  $v(t)$  and  $M_z(t)$ . These expressions are dependent on the parameters of the NMR signal recording fields ( $H_0$ ,  $H_1$ ,  $H_m$  and  $\omega_m$ ) and relaxation times  $T_1$  and  $T_2$ . The formation of the NMR signal line shape using these expressions through relation (2) and comparing it with the experimental one showed their coincidence.

1. Kashaev R.S., Kozelkova V.O., Ovseenko G.A., Karachin V.I., Kozelkov O.V.: *Measurement Techniques*, **66(5)**, 349–358 (2023)
2. Davydov V.V., Dudkin V.I., Vysoczky M.G., Myazin N.S.: *Applied Magnetic Resonance*, **51**, 653–666 (2020)
3. O'Neill K.T., Brancato L., Stanwix P.L., Fridjonsson E.O., Johns M.L.: *Chemical Engineering Science*, **202**, 222–237 (2019)
4. Zhernovoi A.I., D'yachenko S.V.: *Technical Physics*, **60(4)**, 595–599 (2015)
5. Leshe A.: *Nuclear induction*. Veb Deutscher Verlag Der Wissenschaften, Berlin, 1963.

## Analytical prediction of mean interspin distance and its uncertainties in PDS measurements by EPR

V.M. Nekrasov<sup>1</sup>, A.G. Matveeva<sup>1</sup>, V.N. Syryamina<sup>1</sup>, S.A. Agarkin<sup>1</sup>,  
E.A. Golysheva<sup>1</sup>, I.A. Kirilyuk<sup>2</sup> and M.K. Bowman<sup>3</sup>

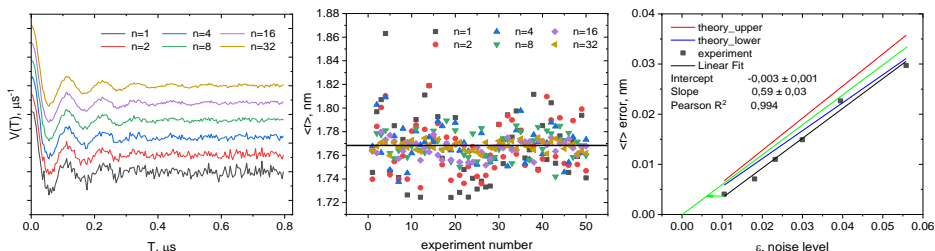
<sup>1</sup>Voevodsky Institute of Chemical Kinetics and Combustion SB RAS, Institutskaya 3, Novosibirsk, 630090, Russia, e-mail: matveeva@solid.nsc.ru

<sup>2</sup>N.N. Vorozhtsov Novosibirsk Institute of Organic Chemistry SB RAS, Ac. Lavrentieva ave. 9, Novosibirsk, 630090, Russia

<sup>3</sup>Department of Chemistry & Biochemistry, University of Alabama, Tuscaloosa, AL, 35487-0336, USA

Pulse dipolar spectroscopy PDS gives information about interspin distances in nanometer scale and therefore is useful for characterization of sizes in dynamically unstable systems. Here analytically demonstrated a new direct way for calculation of mean interspin distance  $\langle r \rangle$  from experimental PDS trace  $V(T)$ , instead of obtaining full distance distribution function. Further, this way allows making upper and lower *a priori* estimation of error for mean distance definition, based only on experimental parameters: noise level  $\varepsilon$ , number of points in PSD trace and on time step of signal acquisition.

We compare obtained estimations with experimental results on model biradical and demonstrate a perfect coincidence. Here  $\varepsilon$  controlled by number of scans  $n$ , so as current  $\varepsilon = \varepsilon_0/\sqrt{n}$ .



Direct definition of mean interspin distance can serve as simple and robust way to compare samples with similar distances and complex form of distance distribution functions. Obtained estimation of mean distance error will additive argument to reliability of small differences between samples. A priory character of error estimation will help us to plan PDS experiments.

This work supported by RSF, project number 24-23-00484.

## Analysis of the trajectory of a symmetrical spinning top in the Earth's magnetic field

**S.A. Klimova<sup>1</sup>, A.A. Gol'dberg<sup>1</sup>, V.V. Davydov<sup>1</sup>, R.V. Davydov<sup>1</sup>**

<sup>1</sup>Peter the Great St.Petersburg Polytechnic University, Saint-Petersburg, Russia

Solving a number of problems associated with launching various rockets from moving objects, lifting underwater vehicles, as well as using torque in work related to drilling, diamond processing and geological exploration of minerals, it is necessary to take into account a number of new circumstances that influence the trajectory of the top. One of them is the magnetic field of the Earth and various objects that can be placed nearby. The modern classical theory of describing the trajectory of a top has a number of shortcomings that do not allow taking into account some physical phenomena, including the magnetic field, which introduces an error when comparing theoretical models and experimental data and creates problems for practical use of calculations in various devices.

Therefore, we propose a new model for analyzing the trajectory of a spinning top in a Cartesian coordinate system and in a system of action-angle variables, the total energy of which is compared to the Lagrange function through Euler angles. In addition, during the calculations, a method is proposed for finding an explicit form of dependence of the total energy on the moments of inertia, as well as three equations describing the symmetry of the spinning top motion with respect to cyclic frequencies  $(\omega_\varphi, \omega_\psi, \omega_\theta)$  expressed in terms of moments of inertia  $(I_\varphi, I_\psi, I_\theta)$ . When considering the motion of a spinning top in a magnetic field, integrals of motion are found, which allows us to say which quantities describing the system are preserved even under the influence of an external magnetic field. Of particular interest is the configuration of the system, in which it will be possible to express the solution analytically. A description of the motion of a spinning top in the case of a nonstationary external magnetic field is proposed using the methods of perturbation theory.

Our model, within the framework of classical theory, is described by three coordinates of the center of inertia of the top and Euler angles  $(\varphi, \psi, \theta)$ , which determine the orientation of the axes of the moving coordinate system relative to the stationary system. Fig. 1 shows the appearance of a spinning top with a coordinate system and a system of acting forces, moments and a magnetic field.

The Lagrange function for describing mechanical motion is expressed in the following form [1]:

$$E = L = \frac{I_x}{2} (\dot{\varphi}^2 \sin^2 \theta + \dot{\theta}^2) + \frac{I_z}{2} (\dot{\varphi} \cos \theta + \dot{\psi})^2 - \frac{eH}{2Mc} \left( (I_x \sin^2 \theta + I_z \cos^2 \theta) \dot{\varphi} + I_z \dot{\psi} \cos \theta \right),$$

As a result, the system was presented as a system of rotating independent three wheels with cyclic frequencies  $(\omega_\varphi, \omega_\psi, \omega_\theta)$ :

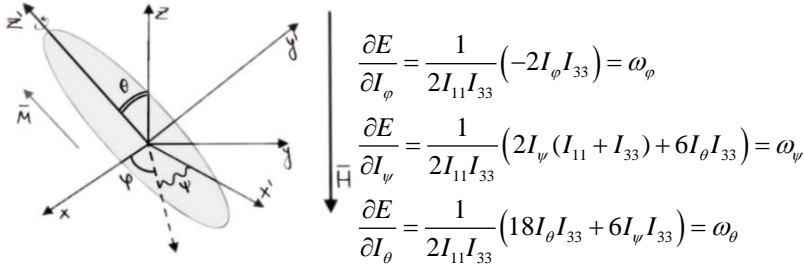


Fig. 1 Model of a spinning top with angles and direction of rotation with orientation of the magnetic field

Further, when considering a spinning top in a uniform magnetic field  $\vec{H} \parallel \vec{M}$ , we use the expression [2], considering that the mutual position of individual moments in the magnetic field remains unchanged.

As a result of the transformations, we obtain a system of equations:

$$\begin{cases} \dot{\phi} = 2 \left| \frac{eH}{2mc} \right| \sin^2 \left( \frac{I_z}{2I_x} \psi_n t \right) \\ \dot{\theta} = \left| \frac{eH}{2mc} \right| \sin \theta_n \sin^2 \left( \frac{I_z}{I_x} \psi_n t \right) \\ \dot{\psi} = \psi_n \left( 1 - \left| \frac{eH}{mc\psi_n} \right| \cos \theta_n \sin^2 \left( \frac{I_z}{2I_x} \psi_n t \right) \right) \end{cases}$$

In an external magnetic field, passing into a rotating coordinate system, we obtain:

$$\vec{M} \times \gamma \left( \vec{H}_0 + \frac{\vec{\Omega}}{\gamma} \right), \quad \vec{\Omega} = -\gamma \vec{H}_0 = \vec{\omega}_L, \quad \vec{H}_{eff} = \vec{H}_0 + \frac{\vec{\omega}}{\gamma} + \vec{H}_{ext}$$

During this work we managed to express the original canonical variables and integrals of motion. Using the generating function of the canonical transformation, a Hamiltonian is obtained whose generalized coordinates are cyclic frequencies. An explicit form of the dependence of the system energy on the moments of inertia in the action-angle variables for this model is found, using the calculations presented above. A top charged uniformly throughout its entire volume in a magnetic field is associated with the Lagrange function through the Euler angles. A system configuration has been found in which the problem is solved analytically. An expression is obtained for the case of a non-stationary magnetic field. An analysis of solved cases is presented

By adding a field  $H_{ext}$ , a “reversal” of the magnetic moment will be observed. When considering an unsteady magnetic field, using the methods of perturbation theory, all forces and phenomena that can have a significant effect on the spinning top will be taken into account. In the future, when improving this model, taking into account the influence of the “neighboring” dipole, it will be possible to describe multiple nuclear resonance, spin wave propagation and other phenomena in magnonics.

1. Landau L. D., Lifshitz E. M., Theoretical physics, Vol. 1, Mechanics, Nauka, Moscow, 1976.
2. Leshe A. Nuclear induction. Veb Deutscher Verlag Der Wissenschaften, Berlin, 1963.
3. Goldstein H., Poole C., Safko J., Classical Mechanics, 3rd edition, USA, 1980.
4. Becker R., Sauter F., Theorie der Elektizitat, Springer Fachmedien Wiesbaden, 1973.
5. Stratton J.A., Electromagnetic Theory, N.Y., 1941.

## **Influence of the «frequency effect» on the Condon form of the electron oscillatory absorption spectrum of the impurity center in the case of a single-oscillator model**

**R.P. Mironov<sup>1</sup>, O.V. Solovyov<sup>1</sup>**

<sup>1</sup>Kazan Federal University, Institute of Physics

The purpose of this study was to obtain analytical expressions for the form of the low-temperature spectrum of the «condone» absorption of impurity paramagnetic ion, taking into account «the frequency effect». The Hamiltonian of the oscillatory subsystem, which is a single oscillator, was considered in a harmonic approximation. The electronic oscillatory interaction, linear in the oscillatory coordinate; within the framework of the adiabatic approximation, the Schrodinger equation for the electronic subsystem was solved in the second order according to the theory of perturbations for the adiabatic potential. As you know, the quadratic dependence of the adiabatic potential on the oscillatory coordinate leads to a «frequency effect» - the renormalization of the oscillatory frequency and normal coordinate. In the course of the work, analytical formulas for the producing function and the form-function of the absorption spectrum in the «Condon» approximation for zero temperature were obtained. The amendment to the absorption form-function due to «the frequency effect» was obtained in the form of a linear combination of the «Condon» form-function (with renormalized) parameters with it, shifted on the frequency scale of the oscillator. The limits of applicability of the set of approximation made in the work and the possibility of going beyond these approximations have been analysed.



## NUMERICAL SIMULATION OF LONG-TIME DYNAMICS OF FINITE DIPOLE ENSEMBLES

**K.B. Tsiberkin, E.I. Kovycheva, V.K. Henner**

Perm State University, Perm, Russia

Collective dynamics of the dipole systems is an important phenomenon that can lead to a number of observable effects. For example, superradiation may occur due to collective spin reversals [1, 2]. If the system has a high initial polarization and small deviations from equilibrium are excited, they may lead to some kind of collective modes similar with the spin waves [3, 4]. These modes are practically unobservable in the nuclear spin systems, but seem to be significant in the ensembles of electronic spins or superparamagnetic particles.

A classical approach uses standard equations of the magnetic moments dynamics in the magnetic field with all-to-all dipole interaction (see [2]). We performed a number of simulations of finite-size spin ensembles with spatial ordering. The numerical method is based on the Runge–Kutta–Merson algorithm of 4–5<sup>th</sup> order with adaptive precision.

The initial state is almost uniform with longitudinal magnetization at 0.99. The system excited by short pulse of the transverse magnetic field; the pulse length is  $0.1\omega_0^{-1}$  time units, where  $\omega_0$  is a Larmor frequency. Two pulse magnitudes were considered; the first one is a strong perturbation with total energy equal to the Zeeman energy, while the second one has only 1% of previous. After the pulse, the system oscillates freely.

We have simulated the 1D, 2D and 3D systems of different size, up to  $30^3$  particles for three-dimensional case. Such size gives an amplitude of remanent magnetization oscillations less than 0.01 of the initial value (Fig. 1). In the quantum-based simulation [5], such a value can be obtained even with  $12\div 13$  particles; of course, collective behavior cannot be achieved at these scale.

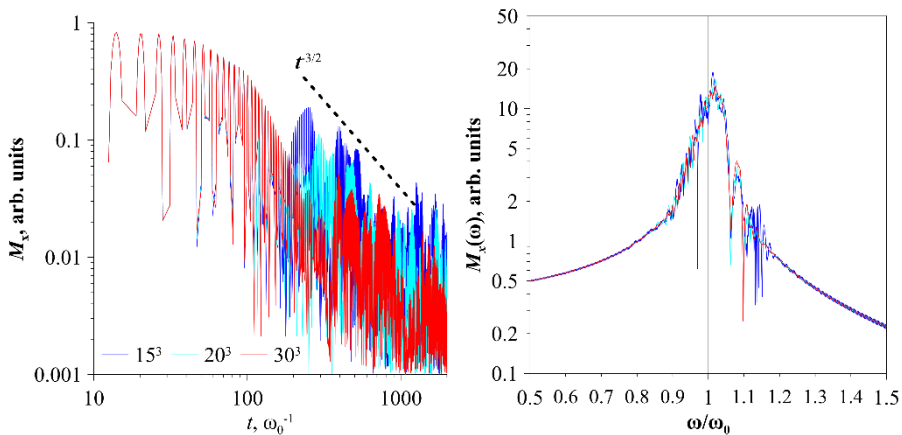


**Fig. 1.** Simulated signals of magnetization decay (left) and Fourier spectra near Larmor frequency (right) for cubic clusters of  $15^3$ ,  $20^3$  and  $30^3$  classical magnetic moments after the strong perturbation

In the case of strong perturbation, during the initial time interval, the magnetization decay matches well the standard picture of free induction decay with a Gaussian envelope; the characteristic time  $T_2$  is inversely proportional to the interaction magnitude. The Fourier spectra of the simulated signal also reproduce the standard data well. After  $T_2$ , an interval with a power-law decay exists. The signal envelope is limited by  $t^{-3/2}$  law (see Fig. 1). The spectral analysis shows that there exist number of equidistant frequencies around the Larmor frequency. We assume that they generated by collective oscillatory modes.

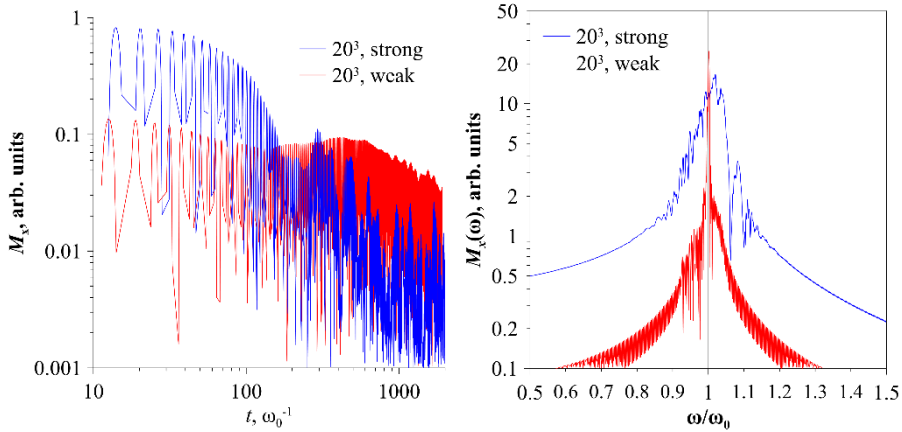


**Fig. 2.** Comparison between the magnetization signal (left) and Fourier spectra (right) for cubic clusters of  $20^3$  classical magnetic moments after strong and weak perturbation

If the initial pulse is weak, there is also a Gaussian-like decay before  $T_2$ , but the initial magnetization is closer to its remanent value (Fig. 2). Both signals at Fig. 2 have the same length, but the “weak pulse” simulation contains long intervals of oscillations with almost constant amplitude. Therefore, the spectrum after weak pulse is narrow, and the collective modes do not realize in given simulation. Here, the power-law decay interval occurs only at large time; the observed power is between  $-1/2$  and  $-1$ . That corresponds better to the signal behaviour determined by long-range contributions of dipole forces, and only the long-wave modes are excited under weak perturbation.

1. Belozerova T.S., Henner V.K., Yukalov V.I.: *Comp. Phys. Commun.* **73**, 151–160 (1992)
2. Yukalov V.I., Henner V.K., Belozerova T.S. et al: *J. Supercond. Nov. Magn.* **29**, 721–726 (2016)
3. Feldman E.B., Khitrin A.K.: *Phys. Lett. A* **153**, 60–62 (1991)
4. Tsiberkin K.B.: *Eur. Phys. J. B*, **89**, 54 (2016)
5. Henner V.K., Klots A., Nepomnyashchy A.A., Belozerova T.S.: *Appl. Magn. Reson.*, **52**, 859–866 (2021)

## PHASE STATE OF POLAR LIQUIDS INSIDE GRAPHENE OXIDE MATERIALS ACCORDING TO SPIN PROBE TECHNIQUE

**N.A. Chumakova<sup>1,2</sup>, D.A. Astvatsaturov<sup>1,2</sup>, T.S. Yankova<sup>2</sup>**

<sup>1</sup> N.N. Semenov Federal Research Center for Chemical Physics of RAS, Moscow, Russia

<sup>2</sup> M.V. Lomonosov Moscow State University, Chemistry Department, Moscow, Russia

Graphene oxide (GO) is a layered material formed by graphene planes randomly decorated with oxygen-containing groups (hydroxyl, carbonyl, epoxy, carboxyl). GO-based materials are of great interest because of high prospects of their practical application. Of particular interest are graphene oxide membranes (GOMs) which were found to possess unique selective permeability for liquids and hydrated ions, so they can be considered as perspective materials for water desalination and water purification. The mechanism of GOMs permeability is still unclear. Moreover, data on the molecular mobility of water and other polar liquids intercalated into the inter-plane space of GO are insufficient and contradictory. Using differential scanning calorimetry (DSC), it was found that polar liquids inside GO do not exhibit the melting/freezing phase transition that is characteristic for bulk liquids [1, 2]. So, the properties of the intercalated substances differ significantly from those of the bulk liquids.

In the present work, the nitroxide spin probe technique was first used for investigation of the molecular mobility of water, ethanol, methanol, and acetonitrile inside powder GO and GOMs with different chemical prehistory. It was revealed that all studied substances can coexist in the inter-plane space of GO as three fractions with different molecular mobility. The relative contribution of the most mobile liquid-like fraction is largely determined by chemical procedure used for GO synthesis. Also, the amount of the liquid-like fraction increases with increasing temperature and/or saturation degree of the material. An intriguing fact is that the molecular mobility of the liquid-like intercalated acetonitrile was found to be significantly lower than that of intercalated water and alcohols, whereas the viscosity of bulk acetonitrile was much lower than that of bulk water, methanol, and ethanol. The molecular structure of GO that determines the coexistence of different phases of intercalated substances will be discussed.

The work was supported by Russian Science Foundation (grant number 23-23-00016).

1. Korobov, M. V., et. al. // *Carbon*, 2016, Vol. 102, pp. 297-303

2. Cerveny, S., et. al., // *J. Phys. Chem.*, 2010, Vol. 114, pp. 2604-2612

## DEVELOPMENT of FREE RADICAL EPR in KAZAN

A.V. Ilyasov<sup>1</sup>

<sup>1</sup> Tatarstan Academy of Sciences, Kazan, Russia

The history of development and application of magnetic resonance methods in the study of the structure and properties of organic free radicals is presented.

Methods of electrochemical generation and photochemistry of free radicals are developed. A new class of phosphorus-containing radicals with high sensitivity of magnetic parameters to environment and temperature is studied, and they represent an effective spin probe in studies of biological structures.

## Study of 3,3-bis-hydroxymethyl sterically shielded nitroxyl radicals of the pyrrolidine series by EPR spectroscopy

**S.Y. Trakhinina<sup>1,2</sup>, A.I. Taratayko<sup>1</sup>, N.B. Asanbaeva<sup>1</sup>, D.A. Kuznetsov<sup>1</sup>,  
E.G. Bagryanskaya<sup>1</sup>, I.A. Kirilyuk<sup>1</sup>**

<sup>1</sup>N.N. Vorozhtsov Novosibirsk Institute of Organic Chemistry SB RAS, Academician Lavrentiev Ave. 9, Novosibirsk 630090, Russia

<sup>2</sup>Novosibirsk State University, Pirogova str. 2, Novosibirsk 630090, Russia

Nitroxyl radicals of the pyrrolidine series with four bulky alkyl substituents near the radical center demonstrate high resistance to bioreduction [1]. For this reason, their use as spin labels and probes for intracellular and in vivo EPR and NMR studies is of great interest [2].

The nature of the immediate environment of the nitroxide fragment can affect its stability, as well as some other properties of the radical. For a more detailed study of this effect, eight new nitroxyl radicals of the pyrrolidine series containing various substituents at ring positions 2 and 5, as well as two geminal CH<sub>2</sub>OH fragments at its 3 position, were studied using CW and pulsed EPR spectroscopy (Fig.1). The presence of the CH<sub>2</sub>OH fragments causes the appearance of additional splitting at  $\gamma$ -hydrogen of one of the alkyl substituents in the CW EPR spectra of nitroxides. It was determined which of the alkyl substituents this splitting relates to. The work also shows that replacing the ethyl group with a propyl group in position 2 of the pyrrolidine skeleton reduces the rate constant of the reduction of nitroxide with sodium ascorbate by 3 times. The influence of the multiple bond in the substituent closest to the radical center on this process was also demonstrated: the triple bond, in contrast to the double bond, significantly reduces the stability of the nitroxide.

1. Jagtap A.P., et al. Sterically shielded spin labels for in-cell EPR spectroscopy: analysis of stability in reducing environment // *Free Radic. Res.*, 2015. Vol. 49. P. 78–85.
2. Pierro A., Drescher M. Dance with spins: site-directed spin labeling coupled to electron paramagnetic resonance spectroscopy directly inside cells // *ChemCommun*, 2023. Vol. 59. P. 1274–1284.

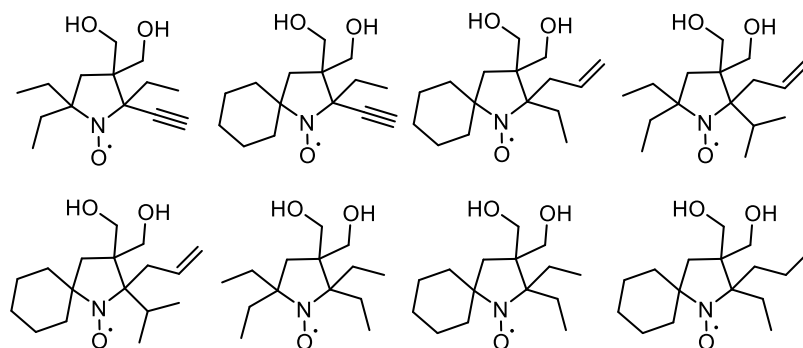


Fig.1. Structural formulas of nitroxyl radicals studied in the work.

## PNIPAM Chains Collapse in Aqueous Solutions in Presence of Proteins: Spin Probe and Spin Label Study

**G. A. Simenido<sup>1</sup>, E. M. Zubanova<sup>1</sup>, E. N. Golubeva<sup>1,2</sup>**

<sup>1</sup>Lomonosov Moscow State University, Faculty of Chemistry

<sup>2</sup>Sechenov University, Moscow, Russia

Poly(*N*-isopropylacrylamide) (PNIPAM) is one of the stimuli-responsive polymers that undergo changes in physical and/or chemical properties in solutions in response to external stimuli. PNIPAM and its copolymers exhibit thermal sensitivity in aqueous solutions. These polymers are soluble in water below the critical temperature and become insoluble due to polymer chain collapse when heated. This critical temperature is denoted as lower critical solution temperature (LCST). Thermoresponsive polymers are used in biomedicine as drug delivery systems, coatings and hydrogels for cell structures. In these applications, polymer is located in multicomponent solutions containing different ions, carbohydrates, proteins etc. Interaction of polymer with proteins can lead to a change in the temperature interval of the chain collapse by shifting the hydrophobic-hydrophilic balance. Bovine serum albumin (BSA) is the most common protein in cell culture media and is also used as a model for human serum albumin. Collagen is one of the components of extracellular matrix and is often used as a coating to enhance cell adhesion and proliferation. The purpose of this work is to establish the effect of BSA and collagen on the polymer chains collapse process, microstructure and microdynamics of aqueous solutions of PNIPAM. The turbidimetry method was used to determine the phase transition temperature, and electron paramagnetic resonance spectroscopy within the framework of spin probe and spin label techniques was used to establish the microstructure and microdynamics of polymer and polymer/protein solutions.

The objects of study were aqueous solutions of PNIPAM in the presence BSA or collagen. Using the TEMPO radical as a spin probe, it was shown that nanoscale inhomogeneities exist in solutions of PNIPAM and BSA. The structure of these inhomogeneities in protein and polymer solutions is different: probe in BSA solutions rotates faster and is located in less polar media in comparison with PNIPAM solutions. At BSA concentrations of ~10%, the formation of inhomogeneities in solution was observed already at 273–295 K. Addition of BSA and collagen to a PNIPAM solution leads to an increase in the proportion of probe molecules located in polymer-protein inhomogeneities along compared to a protein-free solution. In the case of the spin-label technique, a stable radical is covalently attached to the polymer chain. The EPR spectra of spin-labeled polymers allow to determine the dynamics of the polymer chain itself. It was shown by EPR spectroscopy of spin-labeled PNIPAM and turbidimetry that the addition of proteins promotes PNIPAM chains collapse in the temperature interval near LCST: the fraction of slowly rotating label particles in the globule increases with increasing protein concentration. Addition of collagen also decreases PNIPAM LCST to 29 °C.

This research was supported by the Russian Science Foundation (Grant 22-73-00062).

## **Paramagnetic markers in polycystic ovarian syndrome as a possible infertility cause: an EPR study**

**S.N. Arellano-Ahumada<sup>1</sup>, E.A. Aguilar-Roman<sup>1</sup>, C. Villanueva<sup>2</sup>, J.J. Martínez-Maldonado<sup>1</sup>, D. Ramírez-Rosales<sup>1</sup>**

<sup>1</sup>National Polytechnic Institute, Physics and Mathematics School, UPALM, 07738 Mexico City, Mexico.

<sup>2</sup>National Polytechnic Institute, Medical School, Casco de Santo Tomas, 11340 Mexico City, Mexico.

According to the World Health Organization (WHO), infertility affects 48 million couples and 186 million people worldwide. The etiology of female infertility includes ovulatory conditions such as a failure in the maturation and rupture of the follicle (20% of couples); utero-tubal-peritoneal conditions including obstruction at the fallopian tubes, gynecological adhesions, and uterine development. The most common of ovulatory failure conditions is what has been known as polycystic ovarian syndrome (POS).

Electron Paramagnetic Resonance spectroscopy (EPR) reveals information on electronic states of transition metal ions, particularly  $\text{Fe}^{3+}$  in different spin states. It is shown that EPR spectra of blood of patients before examination has signal from metal-protein transferrin ( $g=4.3$ ) and signal of  $\text{Fe}^{3+}$  (methemoglobin) in the high spin state ( $g=6.0$ ).

POS usually coincides with obesity and metabolic syndrome, pathological entities directly related to oxidative stress (OS). OS affects the function of normal cells. The goal of the study was to evaluate, by means of EPR, systemic (blood and plasma) paramagnetic entities in rat Wistar with or without spontaneous infertility and ovary cysts to establish basal conditions of OS in such spontaneous model and later explore new treatments that could overcome infertility. Rats with or without infertility had no differences in transferrin, ceruloplasmin, free radicals, methemoglobin and the adduct nitric oxide-hemoglobin.

It is concluded that the spontaneous infertility-ovary cyst experimental model does not show any difference on systemic OS compared with normal animals. It is necessary to explore if there is any difference on local OS (mainly ovarian).

1. Brugo-Olmedo S, Chillik C, Kopelman S. Definition and causes of infertility. *Reprod Biomed Online*. 2001;2(1):41-53. doi: 10.1016/s1472-6483(10)62187-6. PMID: 12537824
2. [https://www.who.int/health-topics/infertility#tab=tab\\_1](https://www.who.int/health-topics/infertility#tab=tab_1)
3. Svistunenko D. A. EPR spectroscopy of whole blood and blood components: can we diagnose abnormalities? [J]. *The Journal of Biomedical Research*, 2021,35(4): 294-300.doi: 10.7555/JBR.35.20210011

## Electrochemical test cell for in situ and in operando EPR characterization of Li-ion insertion battery electrodes

**D. Ramírez-Rosales<sup>1</sup>, J. Vazquez-Samperio<sup>1,2</sup>, S.N. Arellano-Ahumada<sup>1</sup>, M. A. Martínez-Cruz<sup>3</sup>, I. González<sup>3</sup>**

<sup>1</sup>National Polytechnic Institute, Physics and Mathematics School, UPALM, 07738 Mexico City, Mexico.

<sup>2</sup>National Polytechnic Institute, National Energy Conversion and Storage Laboratory, CICATA-Legaria, 11500. Mexico City, Mexico.

<sup>3</sup>Metropolitan Autonomous University – Iztapalapa, 09340, Mexico City, Mexico.

Understanding the redox mechanisms that occur in the electrodes during the charge / discharge process is an important key to enhance battery performances. In operando Electron Paramagnetic Resonance (EPR) experiments, the fundamental electrochemical redox reactions are monitored by changing the physical and chemical properties of the materials used as electrodes. The combination of two simultaneously recorded analytical methods, for example, spectroscopic and electrochemical data, provides significant information by following the dynamics that are carried out in the materials during the redox reaction.

EPR spectroscopy in situ and in operando has practically not been used for measurements of battery components such as electrodes. Therefore, this way of using EPR spectroscopy is a novel and innovative methodology for obtaining information on the processes that occur in the electrodes of the insertion batteries when the battery is in operation.

EPR spectra and the galvanostatic curve obtained in the in-operation tests of electrochemical cells with different active materials (cobalt oxide, nickel-manganese oxide and Lithium Manganese Nickel Oxide). It is observed in the EPR spectra the signal corresponding to the lithium ion, which increases as the material goes from potentials of 2 to 4.5 V and 3 to 5 V vs. Li/Li+.

We are currently working and focusing on understanding the lithium (Li) storage mechanism in Metal-Organic Frameworks (MOFs) using terephthalic acid as a lamellar ligand and pyrazine as a pillar and manganese and cobalt ions. Here the solvothermal method is used to synthesize the MOFs with Mn, Co and a combination of both Mn-Co.

The aim of this work is to design, manufacture, evaluate and couple an electrochemical cell to an EPR spectrometer to monitor via in-situ and in-operando the local structure of materials used as electrodes in insertion batteries and, therefore, to understand the changes that occur in the materials to propose adjustments and improve their properties.

1. Sathiyam M, Leriche JB, Salager E, Gourier D, Tarascon JM, Vezin H. Electron paramagnetic resonance imaging for real-time monitoring of Li-ion batteries. *Nat Commun.* 2015 Feb 9;6:6276. doi: 10.1038/ncomms7276. PMID: 25662295; PMCID: PMC4347297.



## Potential pharmaceutical pulse EPR applications for detection protein folding and environment upon lyophilization

**Nikolay Isaev<sup>1</sup>, Ken Lo Presti<sup>2</sup>, Wolfgang Frieß<sup>2</sup>**

<sup>1</sup> Voevodsky Institute of Chemical Kinetics and Combustion SB RAS, Novosibirsk, Russia;

<sup>2</sup>Department of Pharmacy; Pharmaceutical Technology and Biopharmaceutics; Ludwig-Maximilians-Universitaet; Munich, Germany

Various methods are used to gain insights into molecular motions and the molecular environment in the solid-state like Fourier-transform infrared spectroscopy (ssFTIR), nuclear magnetic resonance (ssNMR), and hydrogen-deuterium exchange mass spectrometry (ssHDX-MS). Nevertheless, there is still a lack of information correlating protein stability and stabilizing mechanisms in lyophilizates based on the protein folding preservation and molecules' nearest environment. To this end, we evaluated electron paramagnetic resonance (EPR) spectroscopy as a novel technique in this research field in order to gain deeper insights into solid-state protein properties. Double electron-electron resonance (DEER) is used to investigate protein folding, local concentration, and aggregation, whereas the protein nearest shell composition including division by molecular type, and its concentration can be measured by electron spin echo envelope modulation (ESEEM), as it was previously discussed in [1].

In this study, we spin-labeled the Cys34 of human serum albumin (HSA). We deuterated sucrose using Raney-Nickel as a catalyst and successfully performed ESEEM and DEER calibration using glassy water/sucrose formulations containing mentioned labeled components.

In DEER we observed that approx. 50% and 98% of protein molecules were partly unfolded at 2.6 g/l and 84g/l HSA in presence of 100 g/l sucrose. ESEEM signal dependence from HSA/sucrose ratio was approximated by a presence of two HSA types: normally folded with the same ESEEM signal as in glassy formulation and unfolded HSA with 2x ESEEM signal; fractions of folded/unfolded HSA were taken from DEER.

We showed that HSA tends to partially unfold even at very high sugar to protein ratios, which could indicate instabilities in the long term storage. Thus, EPR enables a better understanding of the solid-state stabilization mechanisms in protein lyophilizates.

1. Isaev, N., & Steinhoff, H. J. (2021). Protein and solutes freeze-concentration in water/glycerol mixtures revealed by pulse EPR. *European Journal of Pharmaceutics and Biopharmaceutics*, 169, 44-51.

## The different types of treatment effect on the DyF<sub>3</sub> nanoparticles agglomeration

**E.I. Boltenkova, A.M. Garaeva, A.V. Bogaychuk, E.M. Alakshin**

Kazan Federal University, Kazan, Russia

Lanthanoid-based inorganic nanoparticles are an interesting as a basis for alternative MRI contrast agent [1-3]. For example, the Dy<sup>3+</sup> ion is suitable for use as a T<sub>2</sub> contrast agent in strong magnetic fields, since the Dy<sup>3+</sup> ion has a large magnetic moment without saturating magnetization in very strong magnetic fields [4]. For contrast agents based on nanoparticles, it is also important to pay attention to the processes that occur within the system during synthesis such as the agglomeration processes of nanoparticles because they will affect on nuclear magnetic relaxivity.

It is known that during nanoparticle synthesis the colloidal solution treatment affects the morphology and size of particles, which subsequently can affect the tendency of particles to agglomerate [5].

Basically, the size, shape of particles and the tendency of particles to agglomerate are assessed using microscopy, XRD analysis, and DLS method. But there is an alternative method for studying nanoparticles, such as nuclear magnetic resonance, which can estimate the surface area of nanoparticles by measuring the spin-spin relaxation time. The <sup>1</sup>H NMR based solvent relaxation technique is a non-destructive technique which are sensitive to aggregation as direct measurement of surface area, and available for real-time measurements [6].

In this work the colloidal solutions of DyF<sub>3</sub> nanoparticles with different types of treatments were studied using <sup>1</sup>H NMR. The spin-spin relaxation times were measured for all samples in a field of 3.65 T. T<sub>2</sub> distributions using inverse Laplace transform based on RILT algorithm were obtained. The relationship between T<sub>2</sub> relaxation and primary particle size was studied. The <sup>1</sup>H transverse nuclear magnetic relaxation rates values of the DyF<sub>3</sub> NPs with hydrothermal treatment at magnetic field 3.65 T were evaluated as a function of concentration. Theoretical estimates of transverse nuclear magnetic relaxation rates and agglomeration rates of aqueous colloidal solutions of DyF<sub>3</sub> nanoparticles with various treatments are presented.

This work was supported by the Russian Science Foundation (Project No. 23-72- 01084).

1. Johnson N.J.J., Oakden W., Stanisz G.J. et al.: Chem. Mater. **23**, 3714 (2011)
2. Hu F., Zhao Y.S.: Nanoscale **4**, 6235 (2012)
3. Wang H., Lu W., Zeng T. et al.: Nanoscale **6**, 2855 (2014)
4. Viswanathan S., Kovacs Z., Green K.N.: Chem. Rev. **110**, 2960 (2010)
5. Li C.; Lin J.: J. Mater. Chem. **20**, 6831 (2010)
6. Fairhurst D., Cosgrove T., Prescott S.W.: Magn Reson Chem **54**, 521 (2016)

## RECOVERY OF TEACHER'S VOICE FUNCTION AFTER CHRONIC DISEASES USING SPECTRAL VOICE ANALYSIS AND MRI

**M.Ya. Fattakhova<sup>1</sup>, A.A. Bayazitov<sup>1</sup>, V.L. Odivanov<sup>1</sup>, Ya.V. Fattakhov<sup>1</sup>,  
V.N. Krasnozhen<sup>2</sup>, A.F. Akhatov<sup>3</sup>, E.S. Bekmacheva<sup>3</sup>**

<sup>1</sup>Zavoisky Physical-Technical Institute, FRC Kazan Scientific Center of RAS, Kazan, Russia

<sup>2</sup>Kazan State Medical Academy is a branch of the Russian Medical Academy of Continuing Professional Education of the Ministry of Health of the Russian Federation

<sup>3</sup>Diagnostic Center BarsMed

According to literature data, from 40 to 60% of teachers suffer from diseases of the vocal apparatus. At the same time, there has been an increase in morbidity in recent decades. Therefore, we have paid special attention to this particular group of patients. As a rule, teachers complain of hoarseness of voice and reduced endurance of voice during classes.

We performed the diagnosis using clinical commonly used techniques: magnetic resonance imaging of the cervical spine, video stroboscopy of the larynx, as well as diagnostics using a hardware and software complex for spectral analysis of the voice. Phonation recording was carried out in several stages, since the reduced endurance of the voice did not allow for diagnosis at one time. Studies have shown that the development of voice pathology was influenced by cervical osteochondrosis, a general high stress environment, and a large vocal load.

It is known that with a prolonged pathological condition of the voice, the so-called "habitual hoarseness" occurs, i.e. the sound of an unhealthy apparatus, This complicates the rehabilitation process.

We have finalized a program for recording, processing and analyzing voice. This allowed us to obtain a more detailed digital picture of the voice: the pitch frequency, the frequency range of the voice, the distribution of energy across harmonics, the maximum duration of phonation, etc.

Recovery requires long-term treatment. With the use of a software and hardware complex, it became possible for the patient himself to visually monitor the correctness of performing exercises for rehabilitation.

## **Investigation of NO and Copper Content in Injured and Non-Injured Areas of the Rats Brain by EPR Spectroscopy 24 Hours and 7 Days after Combined Brain and Spinal Cord Injury**

**Kh. L. Gainutdinov<sup>1,2</sup>, V. V. Andrianov<sup>1,2</sup>, G. G. Yafarova<sup>2</sup>, L. V. Bazan<sup>1,2</sup>,  
T. K. Bogodvid<sup>2,3</sup>, I. B. Deryabina<sup>2</sup>, V. S. Iyudin<sup>1</sup>, L. N. Muranova<sup>2</sup>,  
D. I. Silantyeva<sup>2</sup>, S. G. Pashkevich<sup>4</sup>, T. A. Filipovich<sup>4</sup>, V. A. Kulchitchky<sup>4</sup>**

<sup>1</sup> Zavoisky Physical-Technical Institute, FRC Kazan Scientific Center of RAS, Kazan 420029, Russian Federation;

<sup>2</sup> Institute of Fundamental Medicine and Biology of Kazan Federal University, Kazan 420008, Russian Federation;

<sup>3</sup> Volga Region State University of Physical Culture, Sport and Tourism, Kazan 420010, Russian Federation;

<sup>4</sup> Institute of Physiology of Nat. Acad. of Sci. of Belarus, Minsk 220072, Belarus  
kh\_gainutdinov@mail.ru

Nitric monoxide (NO) is one of the key signaling molecules that regulate the physiological functions of the body [1]. Since NO is a chemically highly reactive free radical capable of acting as both an oxidizer and a reducing agent [2], it is assumed that its diverse effects in biological tissues. NO is widespread in the nervous [3], cardiovascular [4] and other functional systems of the body - blood vessel tone, neurotransmission, learning [1, 5]. The involvement of NO in the mechanisms of development of various pathological conditions of the body attracts great interest [6]. It has been shown that the functioning of the NO system is disrupted by ischemia and brain injuries, cerebral ischemia is accompanied by multiple and multidirectional changes in the NO content in the brain and in signal transmission [6, 7]. However, there are contradictions in the information about the role of NO in these processes, which allow us to assert that currently there is no consensus on the role of endogenous NO in the processes occurring with damage to the nervous system [8].

There are many methods of measuring NO production in biological systems. Precise measurement of both the steady concentration of NO and the speed of NO generation in biological systems is a difficult task due to the low activity of NO synthases and its short half-life. In last years electronic paramagnetic resonance (EPR) proved to be one of the most efficient methods for the detection and quantification of nitric oxide in biological tissues [7, 8, 9]. Therefore, we have attempted to detail some biophysical patterns of nitric monoxide formation in case of combined brain and spinal cord injury. We used EPR spectroscopy to study the dynamics of NO in the rat's brain after simulation of combined brain and spinal cord injury. The intensity of NO production by EPR spectroscopy was measured using the spin trap technique [8, 9], which is based on the reaction of a radical (in this case NO) with the spin trap. The complex of Fe<sup>2+</sup> with diethyldithiocarbamate (DETC) was used to capture NO and to form a stable ternary complex (DETC)<sub>2</sub>-Fe<sup>2+</sup>-NO in the animal tissues. Those complexes are characterized by an easily recognizable EPR spectrum with g-factor  $g=2.035 - 2.040$  and a triplet hyperfine structure [2, 7, 9]. Measurements of the spectra of a complex of biological samples (DETC)<sub>2</sub>-Fe<sup>2+</sup>-NO and Cu<sup>2+</sup>-(DETC)<sub>2</sub> was performed on a Bruker X-band spectrometer (9.5320 GHz) EMX/plus.

EPR spectroscopy was used to study the intensity of NO production and copper content in the injured and non-injured areas of the rat brain 1 and 7 days after formation of a combined injury. It was shown that 7 days after the injury, a decrease in NO content was found by 84% in damaged areas of the brain and by 66% in intact areas of the brain. The difference in NO production in the injured and non-injured areas of the brain was also significant. The copper content in the brain remained unchanged a week after the injury simulation. The results demonstrate a significant 30% ( $p < 0.05$ ) decrease in NO production in the injured and non-injured areas of the brain as early as 1 day after the formation of a combined injury. The copper content in the brain remained unchanged 1 day after the formation of the combined injury.

The work was supported by the Russian Scientific Fund No. 23-45-10004 and Belarusian Republican Foundation for Basic Research (grant M23RNF-067).

- [1] Lundberg J.O.; Weitzberg E.: *Cell* **185**, 2853-2878 (2022)
- [2] Vanin A.F.: *Nitric Oxide* **54**, 15-29 (2016)
- [3] Steinert J.R. et al.: *Neuroscientist* **16** 435-452 (2010)
- [4] Zariipova R.I. et al.: *Zhurnal tekhnicheskoy fiziki* **92**(7), 999-1003 (2022)
- [5] Ignarro L.J. et al.: *J Cardiovasc Pharmacol.* **34**(6), 879-886 (1999)
- [6] Pacher P. et al.: *Physiol. Rev.* **87**, 315-427 (2007)
- [7] Gainutdinov Kh.L. et al.: *Technical Physics*, **65**(9), 1421–1426 (2020)
- [8] Wierónska J.M. et al.: *Biomolecules* **11**, 1097 (2021)
- [9] Mikoyan V.D., Kubrina L.N. et al.: *Biochim. Biophys. Acta*, **1336**, No 2, 225-234 (1997)

## Structure determination and study of the internal dynamics of a $\beta$ -enaminone by NMR, UV spectroscopy and DFT

**A. F. Shaidullina<sup>1</sup>, M. Yu. Volkov<sup>2</sup>, A. R. Sharipova<sup>2</sup>, O. A. Turanova<sup>2</sup>,  
L. I. Savostina<sup>1,2</sup>, A. N. Turanov<sup>2</sup>**

<sup>1</sup>Kazan Federal University, Kazan, Russia

<sup>2</sup>Zavoisky Physical-Technical Institute, FRC Kazan Scientific Center of RAS, Kazan, Russia

It is known that  $\beta$ -enaminones are versatile and readily available building blocks for synthesis a wide range of N-heterocycles. Many synthesized enaminones can be used in pharmacology. The structure of 1-phenyl-3-(quinolin-8-ylamino)prop-2-en-1-one was investigated by NMR and UV spectroscopy and DFT calculations. <sup>1</sup>H and <sup>13</sup>C 1D and 2D NMR spectra of the studied substance in different solvents were recorded by a Bruker NMR spectrometer with an operating frequency of 400 MHz. Analysis of 1D and 2D NMR spectra of 1-phenyl-3-(quinolin-8-ylamino)prop-2-en-1-one in different solvents at room temperature showed that the molecules are in the cis-isomeric form.

The solutions of 1-phenyl-3-(quinolin-8-ylamino)prop-2-en-1-one were irradiated with a UV lamp at 365 nm wavelength. It did not lead to the cis-trans isomerization, but it resulted in the formation of a brown precipitate which is poorly soluble in many organic solvents. However, the precipitate is quite soluble in chloroform, therefore its <sup>1</sup>H NMR spectrum was recorder in deuterated chloroform (Fig.1). Signals in the region of 6-11 ppm in this spectrum indicate that most likely it consists of heterocyclic compounds.

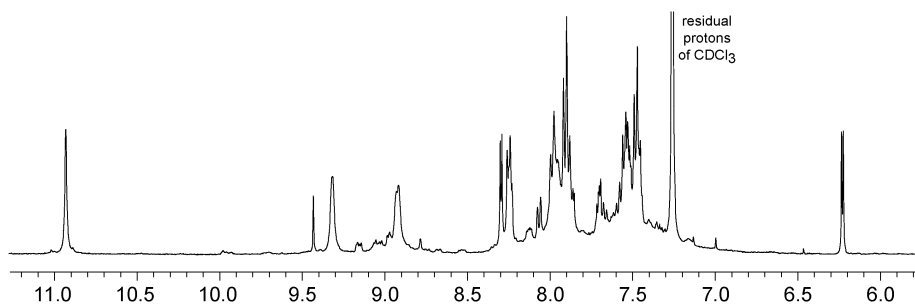


**Fig. 1.** <sup>1</sup>H NMR spectrum of the brown precipitate formed after 365 nm UV-irradiation of 1-phenyl-3-(quinolin-8-ylamino)prop-2-en-1-one in carbon tetrachloride.

Our study involved a meticulous process of optimizing the geometries of all isomers and tautomers of the molecule in the ORCA software package. We used the B3LYP functional and the def2-TZVP basis to calculate ground state energies and absorption spectra. These quantum-chemical calculations were then compared with the experimental data obtained from the NMR and UV spectra, ensuring a comprehensive and rigorous approach to our research [1].

## Pseudospin Quantum Phase Transition Probed by ESR

**S. A. Andreeva<sup>1,2</sup>, A. V. Shchepetilnikov<sup>2</sup>, A. R. Khisameeva<sup>2</sup>, G. Nikolaev<sup>2</sup>,  
I.V. Kukushkin<sup>2</sup>**

<sup>1</sup>Higher School of Economics, Moscow, Russian Federation

<sup>2</sup>Institute of Solid State Physics, Chernogolovka, Russian Federation

Condensed matter physics of strongly correlated two-dimensional electron systems becomes much richer in multi-component systems with a pseudospin degree of freedom. Such systems can be multivalley semiconductors, double quantum wells, van der Waals heterostructures with layers separated by a tunnel barrier, wide quantum wells with several occupied subbands. In this case, pseudospin is an additional degree of freedom that labels the possible states of the electron.

A suitable material platform for studying such effects is AIs, which has a non-trivial valley structure: three ellipsoid valleys are located at X points of the first Brillouin zone. In this case, the pseudospin polarization changes with a change in the relative occupation of the valleys. At the same time, the large effective mass of charge carriers in AIs leads to emergence of many-body effects, such as Stoner ferromagnetism, Wigner crystallization, ferromagnetic phase transition, and valley skyrmions.

In this work, we consider the possibility of observing a quantum phase transitions in the vicinity of filling factors  $\nu = 2$  and  $\nu = 3$  in a heterostructure with an AIs quantum well when strain is applied in the plane of the two-dimensional electronic structure. The in-plane strain applied to the sample makes it possible to lift the degeneracy between in-plane valleys and directly control intervalley splitting, i.e. relative valley occupancy.

To detect relative valley polarization we use resistively detected electron spin resonance (ESR). Due to the anisotropy of the g-factor of AIs, it was possible to achieve maximum splitting in the magnetic field between resonances from each of the valleys at a certain orientation of the magnetic field, making it possible to observe the spin resonances of each of the valleys independently [1].

The existence of several quantum phase transitions in the vicinity of the filling factors 2 and 3 was discovered. Each of the transitions was accompanied by the appearance of a feature in the dependence of the longitudinal resistance of the sample at the minimum of the corresponding filling factor on the applied deformation. It was possible to estimate the change in the pseudospin polarization of the system by analyzing the variation in the relative amplitude of the ESR peaks from each of the valleys. As a result, we demonstrated that these transitions are accompanied with the macroscopic change in pseudospin polarization and are purely pseudospin in nature.

This work was supported by the Russian Science Foundation (Grant No. 20-72-10097).

## LOW-TEMPERATURE SPIN DYNAMICS AND MICROWAVE DIELECTRIC RESPONSE of 2D SQUARE KAGOMÉ LATTICE NABOKOITE FAMILY COMPOUNDS

**V.N. Glazkov<sup>1\*</sup>, Ya.V.Rebrov<sup>1,2</sup>, M.M.Markina<sup>3</sup>, A.F.Murtazoev<sup>3,4</sup>,  
V.A.Dolgikh<sup>3</sup>, P.S.Berdonosov<sup>3</sup>**

<sup>1</sup>P.L.Kapitza Institute for Physical Problems RAS, Moscow

<sup>2</sup>HSE University, Moscow

<sup>3</sup>M.V.Lomonosov Moscow State University, Moscow

<sup>4</sup>National University of Science and Technology “MISiS”, Moscow

\*glazkov@kapitza.ras.ru

2D kagomé lattice is a traditional toy model of the frustrated magnetism. Square kagomé lattice (SKL) [1] is a development of this model, it consists of triangles of spins grouped around alternating square and octagonal voids, as shown at Fig. 1. Ideal 2D equilateral SKL is expected to remain in the spin-liquid state, while complicated forms of order are discussed as a possible scenarios for coupled SKL layers with non-equivalent in-layer couplings [2].

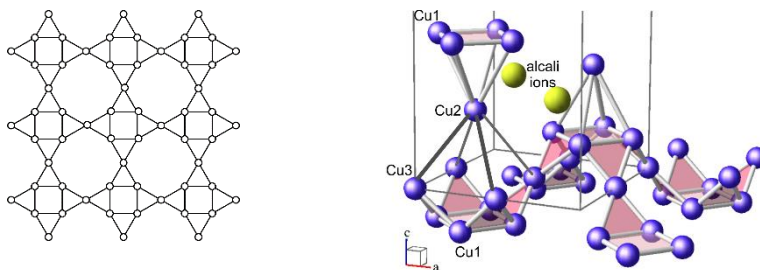


**Figure 1** (left) Fragment of a 2D equilateral square kagomé lattice. (right) Fragment of the nabokoite crystallographic structure (only copper and alkali ions' positions are shown) demonstrating 2D SKL layers formed by copper ions in Cu1 and Cu3 positions and 'decorating' copper ions in inter-layer Cu2 position.

Nabokoite family compounds  $ACu_7(TeO_4)(SO_4)_5Cl$  ( $A=Na, K, Cs, Rb$ ), which were synthesized recently [3], are candidate compounds in the search of the elusive spin-liquid state. Nabokoite crystalline structure (see Fig.1) is beyond the simple SKL model: layers formed by copper ions in Cu1 and Cu3 positions are 'decorated' by the seventh copper ion in the inter-layer Cu2 position. Curie-Weiss temperatures for all compounds from nabokoite family members is around 100-200 K, low temperature magnetic ordering was observed for K and Na compounds only at the temperatures around 3-4 K [3,4]. This proves formation of spin-liquid state in agreement with theoretical predictions [2] for the SKL antiferromagnet.

We have studied low-temperature spin dynamics in  $ACu_7(TeO_4)(SO_4)_5Cl$  family compounds with multi-frequency electron spin resonance technique. Observed microwave response is very unusual indicating possible formation of non-collinear



magnetic ordering and complicating interplay of magnetic and dielectric degrees of freedom.

Magnetization at high temperatures [3,4] corresponds approximately to the total amount of copper ions in the sample. Low temperature paramagnetic resonance signal (see Fig. 2, left panel) corresponds to the 3% of the total amount of copper ions in case of K-compound and slightly less quantity of paramagnetic centers for other members of the family. This means, that supposed spin-liquid state of nabokoites is either ESR-silent, or is affected by strong relaxation processes resulting in very large line-width.

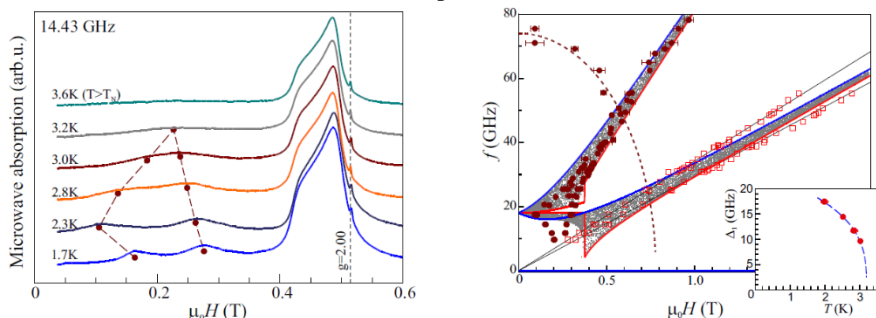


**Figure 2** (left) ESR absorption in K-nabokoite at different temperatures at 14.43 GHz. Symbols mark position of antiferromagnetic resonance absorption (right) Frequency-field diagram of magnetic resonance in K-nabokoite at 1.7K. Closed symbols – antiferromagnetic resonance; open symbols – boundaries of paramagnetic resonance absorption; gray filling – simulation of powder-averaged antiferromagnetic resonance in helicoidal antiferromagnet [4].

Additional antiferromagnetic resonance absorption is observed below the Neel point. Its intensity is very weak, which is in qualitative agreement with the large antiferromagnetic couplings within the 2D layers. Frequency-field diagram of the observed antiferromagnetic resonance signal (Fig.2, right) includes non-Larmor mode with asymptotic slope almost twice as large as that expected for  $\text{Cu}^{2+}$  ion. Such a mode can be explained assuming spiral magnetic ordering [4]. Similar resonance modes were observed in other nabokoite family compounds with Neel point detected in magnetization measurements.

High-frequency ( $\sim 10$  GHz) dielectric properties measurements [5] reveal strong dielectric anomalies (at  $\epsilon''$  and  $\epsilon'$ ) in Na and K-compounds at 26 K (K) and 96 K (Na). These anomalies suggests that minute lattice distortions can be the possible driving force for the magnetic ordering in Na and K-compounds: lattice distortions can lift frustration of the inter-layer couplings via displacement of alkali ions and  $\text{Cu}_2$  ions (see Fig. 1). Additionally high-frequency dielectric anomalies of smaller amplitude were found in all members of nabokoite family at approximately 5 K, which indicates possible close interplay of magnetic and dielectric degrees of freedom at low temperatures [5].

The work was supported by Russian Science Foundation grants 22-12-00259 (V.N.Glazkov, magnetic resonance and dielectric measurements) and 23-23-00205 (P.S.Berdonov, samples preparation).

1. R. Siddharthan, A. Georges, , Phys. Rev. B **65**, 014417 (2001)
2. J. Richter, O. Derzhko, J. Schnack, . Phys. Rev. B **105**, 144427 (2022); M. Gembé et al. Phys. Rev. Res. **5**, 043204 (2023)
3. A.Murtazoev et al., ChemPhysChem **24**, e202300111 (2023)
4. M.Markina et al., Materials Chemistry and Physics **319**, 129348 (2024)
5. Ya.V.Rebrov et al., JMMM **592**, 171786 (2024)

## Magnetic Properties of Rare-earth Trifluoride Nanoparticles

**E.M. Alakshin<sup>1</sup>, A.M. Garaeva<sup>1</sup>, E.I. Boltenkova<sup>1</sup>, V. V. Kuzmin<sup>1</sup>,  
K.R. Safiullin, I.V. Romanova<sup>1</sup>**

<sup>1</sup> Kazan Federal University, Kazan, Russia

The rare earth (RE) elements characterized by unfilled 4f shells (the spin can reach 15/2) which give rise to a variety of interesting electronic and magnetic properties. In terms of their properties, RE magnets differ significantly from those of the iron group and can be classified as a special class, since they can have a significantly higher spontaneous magnetization (or, what is the same, a large atomic magnetic moment) than all previously known magnetic materials. Such unique properties of RE magnets as a large atomic magnetic moment and huge crystallographic magnetic anisotropy make them indispensable for obtaining high-coercivity magnetic materials.

As the particle size decreases, the surface layer begins to play an increasingly important role in the magnetic properties of the sample. In the case of magnetic particles, clustering can be affected by the dipole-dipole interaction and van der Waals forces. Small particles size leads to high surface energy, and nanoparticles tend to aggregate. Since the energy of the magnetic interaction is proportional to the volume, it is therefore well suited for describing the clustering of only sufficiently large particles. In the case of small particles, the dominant role is played by the van der Waals forces acting at fairly close distances. The dipole-dipole attraction is strong if the dipoles are located along the same line, which promotes the assembly of particles into linear or ring-shaped structures. The type of morphology depends on the energy of the magnetic interaction in comparison with thermal fluctuations. An increase in the particle size leads to a further increase in the magnitude of the dipole-dipole interaction. As a result, linear chains acquire a more complex form, and the dimension of clusters increases.

The report will show the effect of size on the magnetic properties of various trifluoride nanoparticles. Some of the experiments were done with helium-3 in contact with rare-earth trifluoride nanoparticles. Helium-3 has unique properties such as good permeability, liquid state at low temperatures, and non-zero nuclear spin, which make it of great interest, especially when considering nuclear magnetic relaxation. For LaF<sub>3</sub> particles, the relaxation of helium-3 on the surface of these particles, in the gaseous and liquid state of helium-3 in contact with these particles, was considered. In all these states the dominant contribution to relaxation is made by relaxation in the adsorbed layer due to the modulation of dipole-dipole interaction by the quantum motion in the adsorbed two-dimensional film.

In case helium-3 nuclei in contact with DyF<sub>3</sub> particles a ferromagnetic phase transition can be observed in the solid matrix. Near the phase transition, fluctuations of the magnetic field induced by Dy<sup>3+</sup> ions in DyF<sub>3</sub> particles increase, which affects the spin kinetics of helium-3 nuclei. The relaxation rate also changes when the particles are covered with nitrogen layers. A possible explanation for these phenomena is proposed.

This work was supported by the Russian Science Foundation (Project No. 23-72-10039).

## Dipolar EPR Spectroscopy of Fullerene and Porphyrin Symmetric Pairs

**R.A. Podarov<sup>1,2</sup>, M.I. Kolokolov<sup>1,2</sup>, E.V. Tretyakov<sup>3</sup>,  
M.V. Fedin<sup>1</sup> and O.A. Krumkacheva<sup>1</sup>**

<sup>1</sup>International Tomography Center, SB RAS, Novosibirsk, Russia

<sup>2</sup>Novosibirsk State University, Russia

<sup>3</sup>N.D. Zelinsky Institute of Organic Chemistry, RAS, Russia

In this work, we introduce for the first time a dipole electron paramagnetic resonance (EPR) approach for measuring distances in symmetric non-orthogonal photoexcited spin pairs. Previous research has effectively explored spin pairs consisting either of a photoexcited triplet state of a molecule paired with a stable radical [1,2], or two photoexcited triplet states of different natures [3]. The subsequent phase involves examining a coupled system containing two photoexcited triplet states to potentially enhance the sensitivity of pulsed EPR techniques through the intensified hyperpolarized signal emanating from two identical components of the pair. Furthermore, such symmetrical systems are increasingly utilized in the efficient conversion of solar energy into electrical energy. Despite the theoretical efficiency limit of contemporary solar cells being only 34%, utilizing the singlet fission process in such symmetric spin pairs could elevate this efficiency to 44%. This increase is facilitated by the generation of two charge carriers rather than one, a process hindered by intersystem crossing (ISC) in spin pairs, which does not contribute to an efficiency gain in solar cells [4].

The aim of this work is to develop an approach for measuring nanometer-scale distances using electron paramagnetic resonance (EPR) in symmetric photoexcited spin pairs based on fullerene and porphyrin. The investigations were conducted using molecules of bisfullerene connected by a fluorinated linker, and pairs of chlorin e6 molecules in complex with human serum albumin.

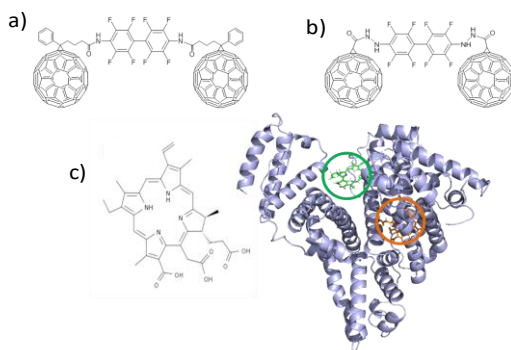


Fig. 1. Structures of the studied spin pairs: a) bisfullerene with a long linker, b) bisfullerene with a short linker, c) chlorine e6 molecule and its complex with human serum albumin.

The echo-detected spectra of the bisfullerene molecules revealed several noteworthy effects and distinctions compared to the monomeric form of PCBM. The spectrum of the bisfullerene was notably broader and featured a distinct set of spectral

lines. Utilizing a theoretical framework that involves strongly interacting spins within fullerene pairs, coupled with considerably weaker dipolar interactions between the fullerenes, enabled the simulation of the echo-detected spectrum and the estimation of inter-fullerene distances using the point dipole approximation. Data derived from nutation experiments and subsequent modeling suggest that the formation of the two triplet states in the system under investigation occurs not via inter-combination conversion, but through the mechanism of singlet fission.

However, not all transitions within the triplet state spectra were accurately described by the existing model. During experiments with a delayed interval post-laser pulse, a spectral line emerged, associated with the coherence transfer of transitions having closely matched frequencies. Throughout the course of the experiments, a general decline in the intensity of the echo-detected spectrum was observed, alongside a notable peak at the center. Additionally, a resolution of the two extreme lines of the original triplet spectrum and a reversal in the sign of one of the spectrum lines were detected. These observed effects could be further modeled by considering an exchange interaction between the paired fullerenes.

We proposed a methodology for measuring distances in symmetric photoexcited spin pairs using the relaxation-induced dipole modulation enhancement (RIDME) pulsed EPR technique. The experimental label spacing determined in bisfullerene aligns with estimates derived from ED spectrum modeling. Additionally, this approach enabled the first-time measurement of the distance between two binding sites of chlorin e6 with albumin. The RIDME technique has thus proven effective for probing nanometer-scale distances in symmetric photoexcited spin pairs, including applications in biological systems. This method utilizes the high quantum yield of photoexcited triplet states and overcomes a significant limitation of dipolar methods—the presence of a broad echo-detected spectrum.

1. Krumkacheva O. A. et al. Triplet fullerenes as prospective spin labels for nanoscale distance measurements by pulsed dipolar EPR spectroscopy // *Angewandte Chemie International Edition*. – 2019. – T. 58. – №. 38. – C. 13271-13275.
2. Di Valentin M. et al. Porphyrin triplet state as a potential spin label for nanometer distance measurements by PELDOR spectroscopy // *Journal of the American Chemical Society*. – 2014. – T. 136. – №. 18. – C. 6582-6585.
3. Bertran A. et al. Light-induced triplet–triplet electron resonance spectroscopy // *The journal of physical chemistry letters*. – 2020. – T. 12. – №. 1. – C. 80-85.
4. Smith M.B., Michl J. Recent advances in singlet fission // *Annu. Rev. Phys. Chem.* 2013. Vol. 64. P. 361–386.

## **$^{15}\text{N}$ Hyperpolarization of Metronidazole Antibiotic in Aqueous Media Using Phase-Separated Signal Amplification by Reversible Exchange with Parahydrogen**

**S.V. Sviyazov<sup>1,2</sup>, D.B. Burueva<sup>1</sup>, N.V. Chukanov<sup>1,2</sup>, I.A. Razumov<sup>2,3</sup>,  
E.Y. Chekmenev<sup>4</sup>, O.G. Salnikov<sup>1</sup>, I.V. Koptyug<sup>1</sup>**

<sup>1</sup>International Tomography Center SB RAS, Novosibirsk, Russia

<sup>2</sup>Novosibirsk State University, Novosibirsk, Russia

<sup>3</sup>Institute of Cytology and Genetics SB RAS, Novosibirsk, Russia

<sup>4</sup>Wayne State University, Detroit, USA

One of the important applications of NMR hyperpolarization methods is the production of hyperpolarized metabolites for their further use in MR diagnostics of various diseases. For this purpose, a promising approach is the SABRE (signal amplification by reversible exchange) method, based on the transfer of nuclear spin order from parahydrogen molecules (nuclear spin isomer of  $\text{H}_2$  molecule with  $I=0$ ) to the nuclei of substrate molecules through spin-spin interactions in the Ir dihydride complex. Nowadays, the literature shows the possibility of hyperpolarization of a wide class of biomolecules using the SABRE method.

Metronidazole is an important drug with antibacterial effect. It is also known that metronidazole is actively metabolized by cancer tumors under hypoxic conditions and therefore metronidazole can be used as a potential marker of tumor hypoxia. However, in the conventional SABER approach, metronidazole is polarized in the methanol solution and the cytotoxic SABRE catalyst is necessarily present in the solution. For further use of metronidazole for *in vivo* MR diagnostics, it is necessary to obtain aqueous solutions of metronidazole with a minimum SABRE catalyst content. Recently, Iali et al. [1] proposed the CASH-SABRE approach based on performing SABRE experiment in a mixture of weakly miscible solvents - water and chloroform. The essence of this approach is that water-soluble substrate molecules are polarized in the organic phase (chloroform) and then extracted into the aqueous phase, while the SABRE catalyst is practically insoluble in water and, therefore, remains in the organic phase.

In this work, we demonstrate a pilot procedure for production of  $\sim 30$  mM hyperpolarized  $[^{15}\text{N}_3]$ metronidazole in aqueous media by using a phase-separated SABRE-SHEATH hyperpolarization method, with  $^{15}\text{N}$  polarization exceeding 2.2% on all three  $^{15}\text{N}$  sites achieved in less than 2 min (the procedure is shown schematically in Fig. 1). The  $^{15}\text{N}$  polarization  $T_1$  of  $\sim 12$  min is reported for the  $^{15}\text{NO}_2$  group at the clinically relevant field of 1.4 T in the aqueous phase, demonstrating a remarkably long lifetime of the hyperpolarized state. The produced aqueous solution of  $[^{15}\text{N}_3]$ metronidazole that contained only  $\sim 100$   $\mu\text{M}$  of residual Ir was deemed biocompatible via validation through the MTT

colorimetric test for assessing cell metabolic activity using human embryonic kidney HEK293T cells. This low-cost and ultrafast hyperpolarization procedure represents a major advance for the production of a biocompatible HP [ $^{15}\text{N}_3$ ]metronidazole (and potentially other hyperpolarized drugs) formulation for MRI sensing applications.

This work was supported by the Russian Science Foundation (grant #24-73-10093)

1. W. Iali, A. Olaru, G. Green, S. Duckett. *Chemistry A European Journal*. 23 (2017) 10491-10495.

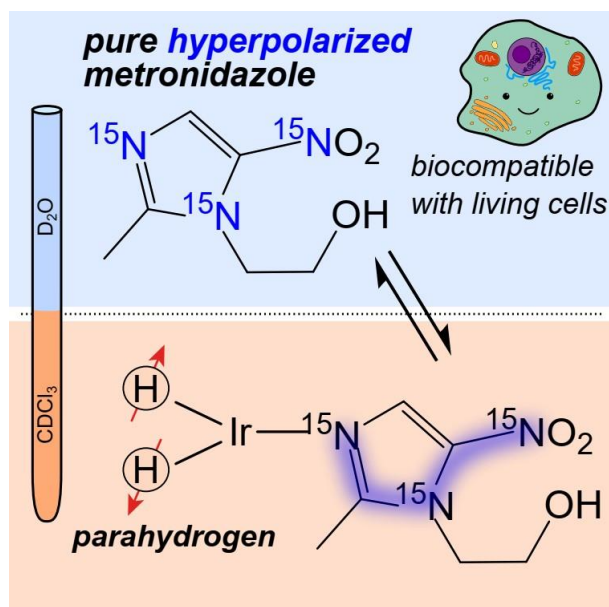


Fig. 1. CASH-SABRE approach for hyperpolarization of [ $^{15}\text{N}_3$ ]metronidazole.

## RESTORATION of OPTICAL ORIENTATION of MANGANESE IONS SPINS in CUBIC ZnSe CRYSTAL in MAGNETIC FIELD

**K.A. Baryshnikov<sup>1</sup>, N.S. Averkiev<sup>1</sup>**

<sup>1</sup> Ioffe Institute, St. Petersburg, Russia

The ground state  ${}^6A_1$  of manganese ions in type II-VI crystals corresponds to a half-filled d-shell of the ion and is described by a full spin of 5/2. A resonant optical transition leads to a flip of one of the electron spins on the d-shell due to spin-orbit interaction, which in a cubic crystal leads to the population of the first excited state of  ${}^4T_1$  symmetry, corresponding to threefold orbital degeneracy and the full spin of 3/2 [1]. It was previously shown that such transitions in a CdMnTe crystal can be described in terms of the total angular momentum of the ground and excited states in the spherical approximation [2] and considering the separation of cubic axes by Jahn-Teller distortions in the excited state [3]. And it was also shown that such resonant intracenter transitions lead to optical orientation of manganese spins in cubic CdMnTe crystal below 8 K.

However, there was found no optical orientation contribution to the photoluminescence (PL) of the manganese ion in zero magnetic field in another cubic ZnSe crystal at 1,5 K. Nevertheless, the appearance of such a contribution in magnetic fields up to 6 T in the Faraday geometry, reaching a value of the order of 3%, was recently observed. Moreover, a strong angular dependence of both the contribution of the optical orientation and the magnetically induced contribution to the PL polarization were experimentally discovered when the orientations of the crystal axes were rotated in the experiment.

To explain these effects, in this work, we propose a theory of optical intracenter transitions in manganese ion in cubic II-VI crystal, considering the presence of the strong Jahn-Teller effect, which couples the orbital degrees of freedom of the center in an excited state with local vibrations of the nearest atomic environment of e-symmetry, and spin-orbit interaction, which results in alignment of spins along corresponding Jahn-Teller distortion axes. Selection rules for optical transitions are obtained and analyzed, and models of the spin relaxation of a center in an excited state are proposed, allowing both the restoration of the optical orientation of the center in a magnetic field (due to selective excitation of different Jahn-Teller distortions and spin alignment in each Jahn-Teller potential well) and a nontrivial angular dependence of the PL polarization (due to dependence of excitation rates and spin alignment on Jahn-Teller distortions orientation).

The work is supported by the Russian Science Foundation grant (Project – 22-12-00139).

1. Agekyan V.F.: Phys. of the Solid State **44**, 2013 (2002)
2. Baryshnikov K.A. et al.: Phys. Rev. B **92**, 204202 (2015)
3. Baryshnikov K.A.: J. Phys.: Condens. Matter **32**, 365503 (2020)

## MAGNETIC PROPERTIES OF LiErF<sub>4</sub> DIPOLAR MAGNET

**G.Iu. Andreev<sup>1</sup>, I.V. Romanova<sup>1</sup>, S.L. Korableva<sup>1</sup>,  
M.A. Cherosov<sup>1</sup>, A.G. Kiiamov<sup>1</sup>, H. Suzuki<sup>2</sup>, M.S. Tagirov<sup>1,3</sup>**

<sup>1</sup>Kazan Federal University, Kazan, Russia

<sup>2</sup>Kanazawa University, Kanazawa, Japan

<sup>3</sup>Institute of Applied Research, Tatarstan Academy of Science, Kazan, Russia

Double fluorides LiREF<sub>4</sub> (RE = Gd-Yb) have gained attention as model objects in physics of dipolar magnetism. These compounds share scheelite type, I4<sub>1/a</sub> crystal symmetry; primitive cell contains two magnetically equivalent rare-earth RE<sup>3+</sup> ions at sites with the S<sub>4</sub> point symmetry that compose two sublattices [1]. LiErF<sub>4</sub> is XY-dipolar antiferromagnet, T<sub>N</sub> = 373(5) mK, magnetic moments are ordering in (001) plane [2].

Single crystal samples are grown using Bridgeman-Stockbarger method, powder sample is synthesized by sintering powders of LiF and ErF<sub>3</sub> in proportions taken from the phase diagram [3]. Magnetization of powder sample is measured (at Kazan Federal University) by vibration sample magnetometer *VSM* at *PPMS*<sup>®</sup> system (*Quantum Design*) in the temperature range of 2-300 K and applied field range of 0-9 T. Magnetization of single crystal samples was measured (at Kanazawa University) in the temperature range of 2-300 K and applied field range of 0-5 T applied along and perpendicular to the *c*-axis using a DC-SQUID magnetometer *MPSM-2* (*Quantum Design*). Theoretical analysis makes use of Er<sup>3+</sup> single ion Hamiltonian, diagonalized in the space of the ground multiplet of the energy states of 4*f*<sup>11</sup> electronic configuration [4], and the set of electron-deformation parameters for LiErF<sub>4</sub> is calculated within the exchange-charge framework, reproducing experimental data at low temperatures not only qualitatively, but also quantitatively, with a satisfactory accuracy in terms of a self-consistent theory that uses a unified set of parameters of the crystal field and electron-deformation interactions.

The work was supported by Kazan Federal University Strategic Academic Leadership Program (PRIORITY-2030).

1. Aminov L.K., Malkin B.Z., Teplov M.A.: Handbook on the Physics and Chemistry of Rare Earths, **22**, 295–506 (1996)
2. Kraemer C., Nikseresht N. et al.: Science, **336**, 1416–1419 (2012).
3. Fedorov P.P., Semashko V.V., Korableva S.L.: Inorg. Mater. **58**, 233–245 (2022).
4. Romanova I.V., M.S. Tagirov M.S.: Magn. Reson. Solids, **21**, 19412 (2019).



## IRON CITRATE COMPLEXES at BIOLOGICALLY RELEVANT CONDITIONS

**Maria Gracheva<sup>1,2,3</sup>, Zoltán Klencsár<sup>1</sup>, Zoltán Homonnay<sup>2</sup>, Ádám Solti<sup>3</sup>,  
Krisztina Kovács<sup>2</sup>**

<sup>1</sup>Nuclear Analysis and Radiography Department, Centre for Energy Research, Hungarian Research Network, Konkoly-Thege Miklós út. 29-33, 1121, Budapest, Hungary

<sup>2</sup>Institute of Chemistry, ELTE Eötvös Loránd University, 1117 Budapest, Pázmány Péter s. 1/A, Hungary

<sup>3</sup>Department of Plant Physiology and Molecular Plant Biology, Institute of Biology, ELTE Eötvös Loránd University, 1117 Budapest, Pázmány Péter s. 1/C, Hungary

Citric acid  $\text{HOC}(\text{COOH})(\text{CH}_2\text{COOH})_2$ , due to its ability to bind metal ions, is well-known for its role in facilitating the bioavailability of iron and promoting the transport of Fe across cell membranes. Consequently, iron(III) citrate complexes are among the most significant coordinated forms of ferric iron involved in biochemical processes across all living organisms. Despite their biological importance, the photochemistry and coordination chemistry of these systems have not been fully elucidated.

In this work, we investigated the speciation of iron(III) citrate in solutions using Mössbauer and electron paramagnetic resonance (EPR) spectroscopies to reveal the structure and nuclearity of the complexes, depending on the pH and iron-to-citrate ratio [1]. By applying the frozen solution technique, the results directly reflect the iron speciation present in aqueous solutions. The slow electronic relaxation relative to the Larmor precession time of the  $^{57}\text{Fe}$  nucleus, expected for mono-iron species, leads to the appearance of paramagnetic hyperfine structure in the Mössbauer spectrum. We have analyzed this in conjunction with the EPR spectroscopy results. At iron-to-citrate molar ratio 1:1, polynuclear species predominated, likely forming a trinuclear structure. In the case of citrate excess, the coexistence of several monoiron species with different coordination environments was confirmed. The stability of the polynuclear complexes was also examined in the presence of organic solvents.

Another significant area of research is the photochemistry of iron(III) citrate. When exposed to light, iron citrate can undergo ligand-to-metal charge transfer, resulting in iron(III) reduction at the expense of oxidative decarboxylation of the carboxylate. The photodegradation of iron citrate under different conditions is discussed with respect to earlier results on crystalline samples, and new aspects were revealed through Mössbauer studies of frozen solutions and plant material [2].

The iron speciation discussed should be considered in biological systems where iron(III) citrate has a ubiquitous role in iron acquisition and homeostasis.

This work was supported by the grant financed by the National Research, Development and Innovation Office, Hungary (NKFIH K-146865) and the Bolyai János Research Scholarship of the Hungarian Academy of Sciences (BO/00113/23/8).

1. Gracheva, M., Klencsár, Z., Homonnay, Z., Solti, Á., Péter, L., Machala, L., Novak, P. Kovács, K.: *Biometals* **37**(2), 461-475 (2024).

2. Gracheva, M., Homonnay, Z., Singh, A., Fodor, F., Marosi, V. B., Solti, Á., Kovács, K.: *Photochemical & Photobiological Sciences*, **21**(6), 983-996 (2022).

## THE EFFECT OF THE SECOND COORDINATION SPHERE OF IRON ON THE $^{57}\text{Fe}$ -MÖSSBAUER ISOMER SHIFTS IN OXIDES

**S.K. Dedushenko<sup>1,2</sup>, V.G. Kostishin<sup>1</sup>, S.V. Stepanov<sup>2</sup>**

<sup>1</sup> NUST MISIS, Moscow, Russia

<sup>2</sup> NRC Kurchatov Institute, Moscow, Russia

Binary and sophisticated iron oxides are a significant subject of Mössbauer spectroscopy. Particularly, they are of interest in terms of studying the relationship between the  $^{57}\text{Fe}$ -Mössbauer isomer shift ( $IS$ ) and the electronic and spatial structure of a substance. In oxides, iron exhibits oxidation states ranging from +2 to +6. While iron is typically found in an octahedral environment, examples of tetrahedral, square planar, and other polyhedra have been observed. At the same time, iron in oxides always is in a high-spin state, and the oxidation state of oxygen is always -2.

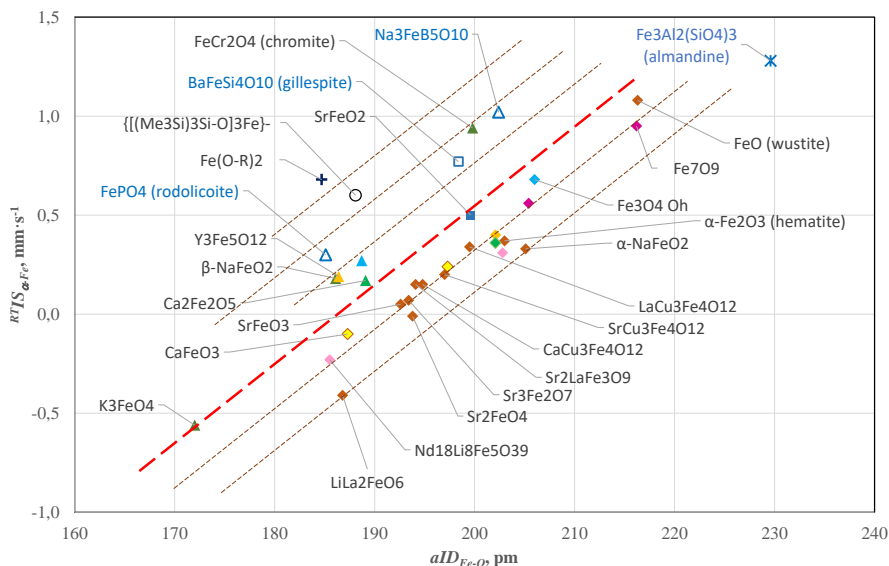


**Fig.1.** The relationship between the Mössbauer isomer shifts of iron oxides and the average Fe-O interatomic distances in them. Octahedral and tetrahedral polyhedra are marked with rhombuses and triangles, respectively. The triangular fragment  $[\text{FeO}_3]$  and the linear fragment  $[\text{O-Fe-O}]$  in organic molecules are represented by  $\circ$  and  $+$  respectively. Pairs of polyhedra corresponding to different sites of iron in the crystal lattice are indicated by the same color. Almandine has an iron coordination number of 8.

In general, the dependence of the *ISs* of iron oxides on the *average Fe-O interatomic distances* ( $aID_{Fe-O}$ ) in them gives a clear picture (Fig.1). An increase in  $aID_{Fe-O}$  leads to an increase in *IS*. It can be noted that, for similar compounds, the dependence is close to linear. The slopes of the corresponding lines are always about  $0.04 \text{ mm s}^{-1} \text{ pm}^{-1}$  [1-3]. It can also be observed that, regardless of  $aID_{Fe-O}$ , an increase in coordination number generally results in a decrease in *IS*. However, octahedral and tetrahedral compounds are clearly separated from each other, and it is important that the pattern is not sensitive to the oxidation state of iron, which is often difficult to determine unambiguously.

Nevertheless, for compounds with the same iron polyhedra, there is a significant variation of the *ISs*. It turns out that the dependencies of the *IS* on the  $aID_{Fe-O}$  for tetrahedra or octahedra are not the lines; there is some straggling of about  $0.4 \text{ mm s}^{-1}$ . This worsens the predictive ability of the plot. To some extent, the spread of the *ISs* is due to two fundamental reasons, which act in the same way. Firstly, when a  $\gamma$ -quantum is emitted without recoil, the momentum of the nucleus does not change, but its mass decreases. This results in an increase of the kinetic energy of the nucleus by  $E_\gamma v^2/2c^2$  (where  $E_\gamma$  is the energy of nuclear transition, and  $v$  is the velocity of the nucleus), and, accordingly, a decrease in the energy of the Mössbauer quantum. Secondly, the relativistic Doppler effect also leads to a decrease in the energy of the emitted Mössbauer quantum. It is caused by the thermal vibrations of the nucleus in the crystal lattice. This circumstance decreases photon energy by  $E_\gamma v^2/6c^2$ . Thus, the total effect on *IS*, which is usually called “the second-order Doppler shift”, is the sum of two above mentioned terms.

It is difficult to say unambiguously how significant this shift may be. According to Menil [4] at sufficiently high temperatures, for example, at room temperature, the effect is minimized and amounts to several hundredths of  $\text{mm s}^{-1}$ .

We suppose that parameters of the second coordination sphere of iron, namely Fe-O and O-M distances and formal charges of the iron and  $M^{n+}$ -ions affect most of all on the *IS*. This approach yielded promising results. For example, if the charge of the  $M^{n+}$ -ion is greater than that of the iron ion, and the M-O distance is shorter (as it happens, for example, in borates, phosphates, and other iron salts of oxygen-containing acids), the *IS* value is higher than in compounds where all relevant distances and charges are equivalent. This can be attributed to the polarization of the  $O^{2-}$ -ions.

The study was supported by the Russian Science Foundation, project no. 24-13-00268, <https://rscf.ru/en/project/24-13-00268/>.

1. Dedushenko S.K., Perfiliev Y.D.: *Hyperfine Int.* **243**, 15 (2022)
2. Dedushenko S.K., Perfiliev Y.D.: *J. Radioanal. Nucl. Chem.* **332**, 2613–2632 (2023)
3. Dedushenko S.K.: *Mendeleev Commun.* **34**, in press (2024)
4. Menil F.: *J. Phys. Chem. Solids* **46**, 763-789 (1985)

## TRANSMISSION OF INFORMATION USING MÖSSBAUER PHOTONS

**F.G. Vagizov<sup>1</sup>, A.L. Zinnatullin<sup>1</sup>, R.N. Shakhmuratov<sup>1,2</sup>**

<sup>1</sup> Institute of Physics, Kazan Federal University, Kazan, Russia

<sup>2</sup> Zavoisky Physical-Technical Institute, FRC Kazan Scientific Center of RAS, Kazan, Russia

Modern communication systems require the creation of new tools that ensure high energy efficiency, cost-effectiveness and resistance to a variety of external disturbance, including targeted ones. Most communication systems are based on the use of radio, microwave, and acoustic and optical frequency bands. At the same time, there is growing interest in information transmission systems using X-ray and gamma radiation sources due to the high noise immunity and penetrating capability of radiation in this frequency range. The last one is of particular importance in connection with the development of communication systems in space where the information carriers of conventional communication systems under certain conditions cannot pass through the media (plasma, dust, etc.) due to frequency limitations and insufficient penetration capabilities. These circumstances prompted NASA and other space agencies around the world to begin developing X-ray based communication systems. NASA recently announced Project XCOM (X-ray communications project) to test the feasibility of X-ray communications in space on the International Space Station [1]. In this project it is planned to use a Modulated X-ray Source (MXS) based on an X-ray tube that is turned on and off many times while encoding digital bits for transmission. However, devices for generating and modulating X-ray radiation using an X-ray tube are very energy-consuming and the efficiency of such sources does not exceed several percent. In our work, we propose a new concept of a communication system based on the use of Mössbauer radiation and quantum interference effects. The feature of our method consist in the fast (compared to the lifetime of the excited state of the resonant nucleus) displacement of nuclei, which leads to the appearance at these instants a gamma-ray burst that exceeds the background radiation due to coherent transient effects [2-4].

In this work, we report the first successful transmission of information using Mössbauer photons. In contrast to previously proposed projects [5], using a mechanical shutter, to modulate gamma radiation we used the effect of quantum interference between the incident and forward-scattered resonant radiation. We transmitted the abbreviation of the Kazan Federal University – “KFU” using random stream of Mössbauer photons. It should be noted that the proposed method based on Mössbauer radiation will have advantages in size and power consumption compared to systems using X-ray tube radiation, and at the same time it will be able to transmit information secretly

This work was supported by Russian Science Foundation (project no. 23-22-00261).

1. <https://www.nasa.gov/technology/nasa-set-to-demonstrate-x-ray-communications-in-space/>
2. Helisto R, Ikonen E., Katila T., Riski K.: Phys. Rev. Lett. **49**, 1209-1213 (1982).
3. Реало Э.Х., Ребане К.К., Хаас М.А., Йьги Я.Я.: Письма в ЖЭТФ, **40**, 477- 480 (1984)
4. Shakhmuratov R.N., et al., Bulletin of RAS, Physics. **78**. 199-202 (2014). Vagizov F., et al., Nature, **508**, 80 (2014)
5. Li F., Wu J., Jiang Q. et al.: Nuclear Inst. and Methods, A. **1039**. 166920(1-7) (2022)

## ON THE MAGNETIC STRUCTURE OF TERNARY ORDERED Fe-Al-B ALLOYS

**E.V. Voronina, A.F. Abdullin**

Kazan Federal University, Kazan, Russia

Magnetic state of ordered Fe-Al alloys containing  $30 < C_{Al} < 50$  at.%, is heterogeneous [1]. In this work, using experimental and theoretical methods, it is shown how replacing aluminum with an isoelectronic analogue, boron, affects the magnetic microstructure of the Fe-Al binary system.

An analysis of XRD, Mössbauer spectroscopy and magnetometry data (at  $4.2 \text{ K} < T < 625 \text{ K}$ , in an external magnetic field  $0 < H_{\text{ext}} < 3 \text{ T}$ ) of ternary  $D0_3$  ordered alloys  $\text{Fe}_{65}\text{Al}_{35-x}\text{B}_x$  ( $x = 5, 10$ ) was carried out. A comparison was made with similar magnetic characteristics of the binary  $\text{Fe}_{65}\text{Al}_{35}$  and the ternary  $\text{Fe}_{65}\text{Al}_{30}\text{Ga}_5$  alloys.

Several variants of statistical models for occupying positions with atoms in the local neighborhood of a resonant atom were considered, namely: random polynomial (trinomial) distribution of atoms over the sites of the *bcc* structure  $A_2$ , random distribution with short-range chemical order in the distribution of atoms over one and two coordination spheres of the *bcc* lattice, distribution of atoms over the  $D0_3$  superstructure for the non-stoichiometric content of components specified by the chemical formula of the alloy. Every model used a statistical weight and a hyperfine magnetic field (HMF) value  $B_{\text{hf}}$  calculated for a specific local configuration, which did not change during the fitting process. It was necessary to know the parameters of hyperfine interactions: local HMF  $B_{\text{hf}}$ , isomer and quadrupole shifts for a specific local environment of the resonant  $^{57}\text{Fe}$  atom. For this purpose, first-principles calculations (Wien2k) of the listed parameters were carried out [2,3].

Next, the hypothesis was assumed about the inhomogeneous local and magnetic structure with a homogeneous chemical composition of the alloys under study. It was possible to obtain a consistent picture for the entire set of available data under the assumption of phase separation.

There are identified two ferromagnetic phases with different types of atomic order: the dominant  $D0_3$  ordered phase ( $\sim 50\%$ ) and the phase of a disordered solid solution ( $\sim 20\%$ , presumably in the boundary distorted zones of crystallites). For the second phase, the values of the  $^{57}\text{Fe}$  HMF and the local magnetic moment of atoms are determined primarily by the characteristics of the local atomic environment. Magnetic moments and HMF on the nuclei of resonant atoms in the  $D0_3$  ordered phase depend on the quantity and position of atoms in several coordination spheres (up to the fourth) [4, 5]. All these values were obtained from *ab initio* calculations.

The value of the average magnetic moment according to Mössbauer spectroscopy data was  $\sim 1.6 \mu_{\text{B}}/\text{Fe}$  atom, and according to magnetometry data  $\sim 1.2 \pm 0.15 \mu_{\text{B}}/\text{Fe}$  atom at  $T = 4.2 \text{ K}$ . These data indicated that in addition to ferromagnetic phases, there is a magnetic phase that does not contribute to the overall magnetization of the sample, but participates in the formation of the average value of the HMF.

In the ground state at the lowest measurement temperature (4.2 K) there is also a magnetic phase, presumably of the spin density wave or spin spiral wave type ( $\sim 30\%$ ), which does not contribute to magnetization and gradually degrades, starting at a temperature of  $\sim 30 \div 35\text{K}$ .

1. Voronina E.V. et al.: *Advances in Condensed Matter Physics*, **2018**, 5781873 (2018).
2. Laskowski R., Blaha P.: *Phys. Rev. B* **69**, 140408 (2004).
3. Blaha P. et al.: *WIEN2k, An Augmented Plane Wave + Local Orbitals Program for Calculating Crystal Properties* (Karlheinz Schwarz, Techn. Universitat Wien, Austria), 2018.
4. Abdullin A.F. et al.: *Uchenye Zapiski Kazanskogo Universiteta. Seriya Fiziko-Matematicheskie Nauki*, **162**(4), 455 – 466 (2020).
5. Arzhnikov A.K. et al.: *JMMM* **320**, 1904 – 1908 (2008).

## SEPARATION OF CONTRIBUTIONS FROM EXCHANGEABLE AND STRUCTURAL FORMS OF IRON IN NATURAL CLAYS

A.A. Zalutskii, V.V. Morozov, A.Y. Sokolov, E.N. Shkolnikov

Yaroslavl State Technical University, Yaroslavl, Russia

In the period of the formation of Mössbauer spectroscopy (MS), its application to natural systems gave an ineffective result. This is clearly evidenced by a series of works on montmorillonite [1] or nontronite [2]. As a result, a discussion arose regarding the reasons for the presence of tetrahedral iron in clay minerals [3].

Based on a critical analysis of the literature data on this issue and studies of natural systems, including model systems [4,5], we have been able to develop a new express method. The content of the methodological approach for quantitative assessment of the separation of the structural and exchangeable state of Fe atoms in clays is as follows:

1. Quantitative estimates of the separation of iron forms in the structure and on the surface of the mineral using EPR spectroscopy (Fig. 1) make it possible to obtain the necessary information that can be effectively used to superimpose connections in the mathematical processing (deciphering) of the Mössbauer spectra of natural systems.
2. Methodologically, it is most effective to describe the partial spectra of bi- and trivalent iron ions within the framework of the quasi-continuous distribution of ultrafine parameters of the Mössbauer spectrum. This mathematical approach leads to a good coincidence of the envelope with the experimental spectrum (Fig. 1). In comparison with the previously used methods, the method makes it possible to obtain a more adequate method for the quantitative separation of "exchangeable" and "structural" iron in clays.

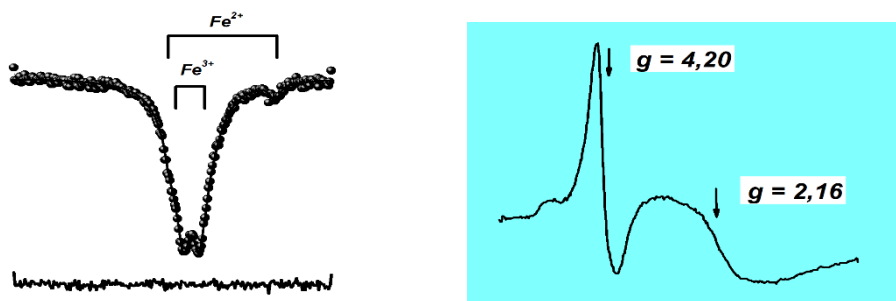


Fig. 1. Characteristic Mössbauer spectrum (left) and EPR spectrum (right) for a typical representative of clay minerals montmorillonite.

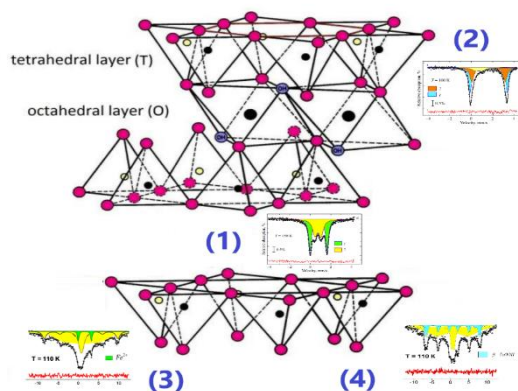
3. From the temperature dependencies of the magnetic susceptibility of iron forms obtained using the Faraday-Sexmit method, on the basis of the application of the Curie-Weiss and Néel laws, it is possible to establish the

"electrical" and "magnetic" nature of the Mössbauer doublet, which cannot be done only within the framework of the MS method. The values of the values of asymptotic Curie temperatures make it possible to quantitatively distinguish between "exchangeable" and "structural" iron in clays.

4. In the absence of positive information on the results of the application of the first three points, which can be characterized as methods of "non-destructive" testing, it is necessary to implement the method of "external influence,  $\leftrightarrow$  object  $\leftrightarrow$  response".

The second part of the report presents experimental data on the behavior of "exchanged" iron adsorbed in four montmorillonite centers (Fig. 2). As a continuation of the solution of the tasks, which are partially described in [4,5], the following results are discussed:

1. On the basis of MS, a methodological approach has been developed and tested, which makes it possible to effectively assess the viscosity value of the medium using the measured diffusion coefficient of the probe in thin films of bound water in a clay mineral.
2. The procedure for restoring a specific type of potential was performed using the analysis of viscosity coefficients and data from measurements of ion mobility associated with diffusion by the Einstein relation.
3. The data of the Mössbauer experiment supplement the missing information that is relevant in the future for the construction of a theoretical model for the formation of natural nanotubes.



Rice. 2. Crystal lattice of montmorillonite indicating the locations of the Messbauer probe: (1) interpacket space (clusters and dimers of  $\text{Fe}^{3+}$ ); (2) chips of the mineral package and well ( $\text{Fe}^{2+}$  compounds); (3), (4) the outer surface of the mineral (ionic form  $\text{Fe}^{3+}$  (3) and acaganeite (4)).

1. Cardile C. M.: Clay Minerals. **22**, 387-394 (1987)
2. Cardile C. M., Johnston J. H.: Clays and Clay Minerals. **33**, 295-300 (1985)
3. Cardile C. M.: Clays and Clay Minerals. **37**, 185-188 (1989)
4. Zalutskii A.A.: Kristallografiya. **65**, 384-389 (2020). (in Russian)
5. Zalutskii A.A., Morozov V.V., Sokolov A.Yu., Shkolnikov E.N.: Physics of the Solid State. **65**, 2052-2055 (2023). (in Russian)



## MOSSBAUER SPECTROSCOPY of the RARE EARTH FERROBORATES $\text{SmFe}_{3-x}\text{M}_x(\text{BO}_3)_4$ ( $M = \text{Al}, \text{Sc}$ )

**K.V. Frolov<sup>1</sup>, E.S. Smirnova<sup>1</sup>, O.A. Alekseeva<sup>1</sup>, E.V. Sidorova<sup>1</sup>, I.A. Gudim<sup>2</sup>**

<sup>1</sup> Shubnikov Institute of Crystallography, KCC&Ph NRC Kurchatov Institute, Moscow, Russia

<sup>2</sup> Kirensky Institute of Physics, FRC KSC SB RAS, Krasnoyarsk, Russia

Rare-earth ferrobates  $R\text{Fe}_3(\text{BO}_3)_4$  ( $R = \text{Y}, \text{La}, \text{Ce} - \text{Lu}$ ) have been actively studied for the last 15 years due to their multiferroic properties arising from the peculiarities of the crystal structure and complex exchange interactions between the magnetic subsystems of  $R$  ions and Fe ions [1-6]. Depending on the radius of the  $R$  ion, a structural phase transition can occur in some of these compounds in the temperature range 80 – 500 K. Below the temperature of 40 K, magnetic ordering of iron ions occurs, and upon further cooling, magnetic ordering of  $R$  ions also occurs, while different types and dimensions of magnetic order are formed, spin reorientation may occur, and magnetoelectric effects are observed.

In this work, single crystals of compounds  $\text{SmFe}_{3-x}\text{M}_x(\text{BO}_3)_4$  ( $M = \text{Al}, \text{Sc}$ ) have been studied in the temperature range 4 – 295 K by Mössbauer spectroscopy on  $^{57}\text{Fe}$  nuclei in combination with single crystal X-ray diffraction analysis. The influence of substitution of iron ions by non-magnetic ions on magnetic properties was studied, the values of the Neel temperature, types and dimensions of the magnetic order have been determined, and the values of the Debye temperature have been calculated.

This work was financially supported by the Russian Science Foundation (Agreement No. 23-22-00286).

1. Kadomtseva A.M., Popov Y.F., Vorob'ev G.P. et al.: Low Temp. Phys. **36**, 511 (2010)
2. Kuz'menko A.M., Mukhin A.A., Ivanov V.Y. et al.: JETP Lett. **94**, 294 (2011)
3. Kuzmenko A.M., Mukhin A.A., Ivanov V.Y. et al.: Solid State Phenom. **190**, 269 (2012)
4. Kurumaji T., Ohgushi K., Tokura Y.: Phys. Rev. B **89**, 195126 (2014)
5. Popova M.T.: Low Temp. Phys. **45**, 1000 (2019)
6. Zhang H., Liu S., Nelson C.S. et al.: J. Phys.: Condens. Matter **31**, 505704 (2019)

## HIGH-ENTROPY SYSTEM $\text{Mg}_{0.2}\text{Co}_{0.2}\text{Fe}_{0.2}\text{Ni}_{0.2}\text{Zn}_{0.2}\text{O}$ : SYNTHESIS, X-RAY DIFFRACTION and MÖSSBAUER STUDIES

V.F. Musin, A.L. Zinnatullin, F.G. Vagizov

Institute of Physics, Kazan Federal University, Kazan, Russia

High-entropy oxides (HEO) are single-phase solid solutions consisting of five or more elements in the cation sublattice in proportions close to equiatomic. The potential applications of HEOs are extremely broad, including catalysts, dielectric materials for supercapacitors, protective coatings, biocompatible materials and etc. Therefore, the synthesis of new HEOs and the study of their properties are important problem, actual both from fundamental and practical sides.

In this work, we present results of synthesis and primary studies of high-entropy oxide  $\text{Mg}_{0.2}\text{Co}_{0.2}\text{Ni}_{0.2}\text{Fe}_{0.2}\text{Zn}_{0.2}\text{O}$ . The choice of such composition was motivated by following reasons. Firstly, this HEO has not been obtained before. Secondly, iron ions in this HEO are in the divalent state. It is well known, that  $\text{Fe}^{2+}$  ion oxidized rapidly to the  $\text{Fe}^{3+}$  state in the most of oxide compounds in native conditions. Therefore, the synthesis of HEO containing of  $\text{Fe}^{2+}$  ions as one of base elements will undoubtedly open new possibilities for the synthesis and study of such materials.

To prepare the HEO of the desired composition, the oxides  $\text{MgO}$ ,  $\text{CoO}$ ,  $\text{NiO}$ ,  $\text{ZnO}$  and divalent iron oxalate  $\text{FeC}_2\text{O}_4 \cdot 2\text{H}_2\text{O}$  were thoroughly mixed and ground in the agate mortar. The obtained powder was pressed into pellet and then was annealed for 1 hour at the temperature of  $1070^\circ\text{C}$  in the pure nitrogen gas stream inside quartz tube. After finishing the annealing, the sample was moved out from heating zone and was cooled achieving room temperature for  $\sim 5$  minutes.

Powder X-ray diffraction studies reveal that the sample has a single-phase composition with the NaCl type face-centered cubic crystal structure with the lattice parameter of  $4.22 \pm 0.01 \text{ \AA}$  (Fig. 1).

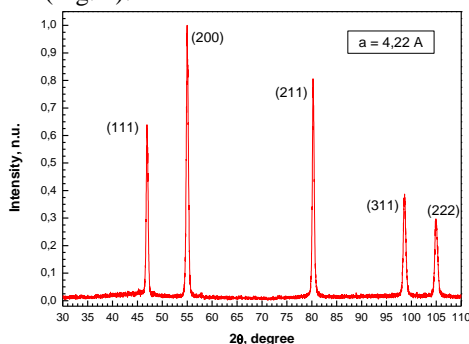


**Fig. 1.** X-ray diffraction pattern of the synthesized sample

Using the lattice parameter value and the known values of the ionic radii for  $\text{Fe}^{2+}$  and  $\text{Fe}^{3+}$  as well as  $\text{O}^{2-}$ , the relative content of ferrous and ferric ions in the sample was calculated as to be 60% and 40%, respectively.

The room temperature Mössbauer spectrum of the sample (Figure 2) was processed by three doublets. It was revealed that the first doublet (isomer shift 0.41 mm/s) should be related with the high-spin ferric ions in the octahedral oxygen environment. The second (isomer shift 0.99 mm/s) and third doublets (isomer shift 1.02 mm/s) correspond to the high-spin ferrous ions in the octahedral oxygen environment. The relative areas of the divalent and trivalent components in the spectrum are 67% and 33%, respectively. These values are close to the ones estimated based on lattice constant.

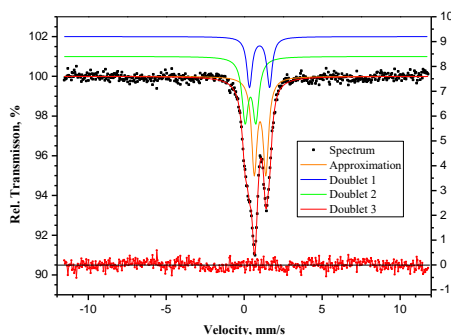


**Fig. 2.** Mössbauer spectrum of the sample

Additionally, Mössbauer measurements of the sample were carried out at lower temperatures (Figure 3).

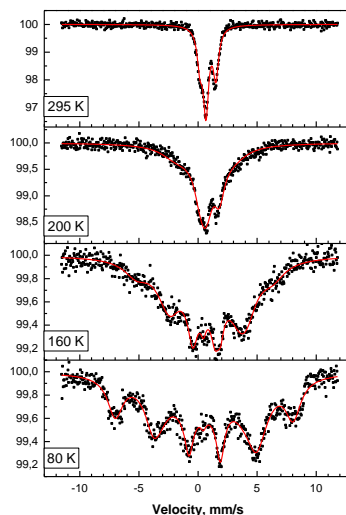


**Fig. 3.** Mössbauer spectra of the sample collected at 295 K, 200 K, 160 K, and 80 K

As the temperature decreases, a smooth transformation of the spectrum is observed with the change of the spectrum shape from the paramagnetic to a more complicated due to gradual onset of the magnetic Zeeman splitting. The appearance of the magnetic components in the spectrum and the further growth of their relative area indicates the transition of Fe ions from the paramagnetic to the magnetically ordered state.

## Microgravity-like Crystallization of Paramagnetic Species in Strong Magnetic Fields

**A.A. Samsonenko<sup>1,2</sup>, N.A. Artiukhova<sup>1,2</sup>, S.L. Veber<sup>1,2</sup>**

<sup>1</sup>International Tomography Center SB RAS, Novosibirsk, Russia

<sup>2</sup>Novosibirsk State University, Novosibirsk, Russia

Crystal growth under microgravity-like conditions has shown a number of benefits. Levitation in a magnetic field gradient can be considered as an approximation of microgravity achieved in laboratory conditions. The levitation of a frog is perhaps the most well-known example of this phenomenon [1]. However, unlike diamagnetic substances, paramagnetic compounds cannot levitate due to fundamental reasons [2]. Although complete compensation of the gravitational force is not achievable for paramagnetic compounds, it is possible to significantly reduce the residual "effective" gravitational acceleration. In addition to compensating for gravitational force, the magnetic field can influence the solution by suppressing convection, which indirectly affects the growth of crystals.

Our investigation provides crucial insights into the growth of crystals in magnetic fields, with a particular focus on copper and cobalt sulfates. We used NMR magnets to generate strong magnetic fields for growing crystals of paramagnetic compounds, specifically utilizing 300 MHz wide-bore NMR magnets (7 T). The research includes thorough characterization of magnetic field profiles and a comprehensive analysis of the factors influencing crystal growth within a magnetic field. For the first time, we achieved the crystallization of copper sulfate, cobalt sulfate, and their mixture under gravitational force compensation in a superconducting magnet. This study experimentally demonstrates the feasibility of growing paramagnetic crystals within the volume of a test tube. A comparison of crystals grown from the solution of a mixture of copper and cobalt sulfates under the identical conditions, both with and without the presence of a magnetic field, revealed differences in the number and size of the crystals [3].

1. M. Simon. A. Geim, *J. Appl. Phys.* **2000**, 87 (9), 6200–6204

2. S. Palagummi, F. Yuan, *Structural Health Monitoring (SHM) in Aerospace Structures*, Elsevier, **2016**, 213-251

3. A. Samsonenko, N. Artiukhova and et. al., *Int. J. Mol. Sci.* **2024**, 25 (10), 5110

## AB INITIO RESEARCH of IMPURITY FERROMAGNETISM of PARAMAGNETIC PALLADIUM IONS

**Z.I. Minnegulova<sup>1</sup>, I.I. Gumarova<sup>1</sup>**

<sup>1</sup> Kazan Federal University, Kazan, Russia

Studying the effect of ferromagnetic impurities on the magnetic properties of binary palladium alloys could lead to the creation of new materials with improved properties, for example, for applying in superconducting magnetic random access memory (MRAM) based on Josephson junctions<sup>1</sup>.

The research included ab initio calculations based on density functional theory with using the MedeA VASP 6 software package to investigate the magnetic properties of palladium-nickel and palladium-manganese alloys in a wide range of concentrations (1–100 at.%). The results confirm the existence of a critical concentration<sup>2</sup> for Pd-Ni (4 at.%), starting from which the anomalously large value of the magnetic moment calculated per nickel atom (about 10  $\mu_B$ ) in the system decreases monotonically with increasing impurity concentration and tends to the value magnetic moment of bulk nickel. For the palladium-manganese alloy, shifting of maxima and minima of magnetization are observed, which is explained by the antiferromagnetic nature of manganese.

1. Soloviev I.I. et al. // Beilstein J. Nanotechnol. 2017. V. 8. P. 2689–2710.

2. Korenblit I.Y. et al.: Ferromagnetism neuporyadochennyh sistem (1978), p 233-238. (In Russian)

## ULTRAFAST LIGHT-INDUCED MAGNETIZATION PRECESSION – A COMPLEMENTARY TOOL TO FMR FOR STUDIES OF THIN FERROMAGNETIC FILMS

**R.V. Yusupov<sup>1</sup>, A.V. Petrov<sup>1</sup>, A.Kh. Kadikova<sup>1</sup>, I.V. Yanilkin<sup>1</sup>,  
A.I. Gumarov<sup>1</sup>, L.R. Tagirov<sup>1,2</sup>**

<sup>1</sup> Kazan Federal University, Kazan, Russia

<sup>2</sup> Zavoisky Physical-Technical Institute, FRC Kazan Scientific Center of RAS, Kazan, Russia

Magnetization precession may be excited by ultrashort laser pulses via light-induced modification of the effective magnetic field direction due to changes in magnetization value and/or magnetocrystalline anisotropy. Studies of this phenomenon can serve a powerful complementary tool to classic ferromagnetic resonance (FMR) as it allows for a wider range of experimental conditions, in particular, accessible frequency and magnetic field combinations. In the talk, we will present the results of an application of this tool to thin epitaxial films of the Pd<sub>0.92</sub>Fe<sub>0.08</sub> alloy and Fe-Al binary systems with compositions close to Fe<sub>3</sub>Al on MgO (001) substrate. In both cases, magnetization precession was excited by 50-fs laser pulses and monitored via the polarization plane rotation of the reflected probe pulse due in the longitudinal magneto-optical Kerr effect arrangement.

Thin epitaxial Pd<sub>0.92</sub>Fe<sub>0.08</sub> film is a soft and relatively weak low-temperature ferromagnet that has an fcc cubic structure and represents an easy-plane system with the four-fold in-plane magnetic anisotropy [1,2]. Here, we find that with a relatively weak magnetic field of 1 kOe applied normal to the film plane, within a temperature range of 5 – 150 K an observed magnetization precession reveals two frequency components while only one is expected for a magnetically homogeneous system. Micromagnetic modelling of both the equilibrium magnetic structure and magnetization dynamics have been performed. It was found that in the described experimental conditions the system is split into the magnetic domains, and the calculated dynamics indeed reveal two frequency components. In the conditions that promote a formation of a single-domain state, only one frequency was predicted. The last has been verified experimentally. Thus, we assign an observed two-frequency magnetization precession to modes arising from a coupled precession of interacting magnetic domains.

A series of Fe-Al films was also studied that differed in the deposition conditions and compositions of the films. We have found a rich variety of magnetization precession manifestations, revealing from one to three frequencies with strongly different damping times and either the Lorentzian or Gaussian line shapes in the results of the Fourier transformations. Some films revealed high-frequency oscillations that we assign to the bcc-Fe precipitates that had not manifested themselves in the classic X-band FMR spectra. A clear correlation between the deposition conditions and the resulting magnetic properties as well as inhomogeneities is established.

## Surface induced anisotropy in MgO single crystals observed by EPR spectroscopy

**B.F. Gabbasov, R.V. Yusupov**

Kazan Federal University, Kremlevskaya 18, 420008 Kazan, Russia

Previously, a lowering the symmetry of  $\text{Fe}^{3+}$  and  $\text{Mn}^{4+}$  impurity ion centers in single-crystalline oriented  $\text{SrTiO}_3$  samples in their nominally cubic phase was discovered by means of EPR spectroscopy [1]. This deformation was tetragonal. Its value depended on the surface roughness and the thickness of the samples. It was further indicated that, according to the data of the electric field effect in EPR, the nature of the distortion was non-polar and a hypothesis was proposed of a symmetry lowering of the host crystal that originated from the surface. Therefore, it is interesting to study a possibility of a similar effect manifestation in other materials. We have chosen MgO single crystals. Primarily due to its use as substrates for thin films, like strontium titanate.

MgO is an ionic oxide with a halite structure (space symmetry  $\text{Fm}\bar{3}\text{m}$ ). Its dielectric permittivity is about 3. Single crystal MgO substrates are a staple of thin film labs for supporting high quality oxide (and metal) epitaxial thin film growth including semiconducting, superconducting, dielectric, ferroelectric, and ferromagnetic oxides. MgO crystals grow nicely with minimal defects meaning it is available up to 2-inch diameter and as a high hardness material that can be polished to near atomic-scale roughness (rms 0.2 nm). Due to its high transparency, it is often used for optical experiments to investigate the film on top, in which case the double side polished substrate is chosen. MgO can be used to produce high-temperature superconducting microwave filters which require large surface area and other devices required for mobile communication equipment.

A study of high-quality commercial MgO single crystal substrates (from Crystal GmbH, Germany) with X-band *cw* electron paramagnetic resonance reveals direct correspondence between a roughness of sample surfaces and magnetic anisotropy of the impurity  $\text{Mn}^{2+}$  and  $\text{V}^{2+}$  centers. In particular, for a sample with the shape of a rectangular prism, a size of ( $a \times a \times h$ ) and faces perpendicular to the  $\langle 100 \rangle$  crystallographic directions, zero-field splitting parameter  $D$  is approximately proportional to  $(a/h - 1)$  quantity. Diminishing of the  $D$  value with the decrease of the surface roughness for a thin (001)-oriented MgO platelet shows that the observed effect originates from the sample surface.

1. Gabbasov, B. F., et al. "Breaking of the Cubic Symmetry in Millimeter-Size  $\text{SrTiO}_3$  Crystals: ESR Manifestations." *Crystallography Reports* 68.5 (2023): 683-694.

## UNUSUAL EPR SPECTRA of $\text{Cu}^{2+}$ DIMER ASSOCIATES in $\text{BaF}_2$ SINGLE CRYSTAL

**V.F. Tarasov, R.B. Zaripov, V.A. Ulanov**

Zavoisky Physical-Technical Institute, FRC Kazan Scientific Center of RAS, Kazan, Russia

Dimer associates (DA) of rare earth ions in dielectric crystals are the object of study for several reasons. An interesting property of these associates is cooperative up-conversion luminescence, when two ions of the dimer associate absorb two photons, and emit the single photon with a frequency exceeding the frequency of exciting photons. These associates were considered as coupled qubits that can be used for implementation of elementary algorithms of quantum computations. With a small concentration ( $C$ ) of impurity ions and their statistical distribution over the crystal lattice, the relative concentration of DA is proportional to  $C^2$ , and it is much less than concentration of single ions. However, in some cases, the statistical distribution of impurity ions in the crystal is disturbed, and during crystal growth, impurity ions forms the DA, concentration of which significantly exceeds the concentration expected with the statistical distribution of the impurity ions. One of these mechanisms is realized for  $\text{Cu}^{2+}$  impurity ions in  $\text{BaF}_2$  single crystals.

Well known Bloch equations are widely used to describe the dynamics of a magnetic moment in nuclear or electron spin resonance. For high-spin systems with  $S > 1/2$ , this simple model cannot fully describe the spin dynamics. It is necessary to introduce spin variables with higher degrees of spin moment. For the spin  $S = 1$ , it is sufficient to include the terms of the second order corresponding to the quadrupole moment [1]. Presence in the same  $\text{BaF}_2$  sample of low-spin ( $S=1/2$ )  $\text{Cu}^{2+}$  single ions and high-spin ( $S=1$ ) dimer associates makes it possible to search and study the difference in spin dynamics of high-spin and low-spin paramagnetic centers of the same origin.

Our measurements were carried out in the continuous wave mode on an ELEXSYS E580 spectrometer with a commercial dielectric resonator ER4118MD5W1 (Bruker). At a relatively high microwave power sufficient for partial saturation of the resonance transitions anomalous resonance lines of the dimer associate appears in the spectra. The phase of this anomalous lines is orthogonal to the phase of the magnetic field modulation. An explanation of this feature is based on the special features of the spin dynamic of high-spin systems, where the transformation of magnetic dipole orientation to quadrupole alignment occurs under intensive resonance excitation of the magnetic dipole transitions [2]. We suppose that the appearance of the unusual resonance lines is due to simultaneous excitation of magnetic dipole resonance transitions and electric quadrupole transitions excited by gradient of the microwave electric field in the dielectric resonator.

1. U. Fano, Phys. Rev. **133**, B828-B830 (1964)
2. K.M. Salikhov, JETP, **135**, 617-631 (2022)



## First-principles investigation of the Rashba–Dresselhaus giant spin splitting in the structure of OsH<sub>2</sub>(bipyridine\_CN)

**E.K. Abdrakhimova<sup>1</sup>, A.A. Evseev<sup>1</sup>, I.I. Gumarova<sup>1</sup>, O.V. Nedopekin<sup>1</sup>**

<sup>1</sup> Kazan (Volga region) Federal University, Kazan, Russia  
Laboratory of computer design of new materials

The search for materials with unique electronic properties for the creation of new electronic devices, including spintronic ones, is an urgent task of modern science. One of the key effects in spintronics is the Rashba–Dresselhaus spin splitting, which occurs in materials with broken inversion symmetry and leads to the separation of energy levels of electrons with different spins<sup>[1]</sup>. Giant spin-orbital splitting can be used to effectively control the spins of electrons, which opens up new possibilities for creating spintronic devices with improved characteristics.

In the search for new materials with giant spin-orbital splitting, two-dimensional chiral metal-organic frameworks (MOFs) have attracted the attention of scientists<sup>[2]</sup>. These materials have a unique structure that combines a high degree of chirality and the presence of heavy atoms, which provides a strong spin-orbit interaction.

To conduct a theoretical study of the production of giant Rashba-Dresselhaus spin splitting in two-dimensional chiral organometallic frameworks using computational methods, we chose osmium (Os) as the base metal in the structure. Osmium, as a heavy transition metal of the platinum group, has a very high value of spin-orbit interaction. This is a key factor in achieving the giant Rashba-Dresselhaus spin splitting. Osmium can also form a variety of chiral metal-organic frameworks due to its ability to coordinate with organic ligands. Chirality of the structure is also a necessary condition for observing Rashba-Dresselhaus splitting.

We calculated the band structure for OsH<sub>2</sub>(bipyridine\_CN), where the valence band exhibits typical Dresselhaus splitting. Since near the point D, the direction of spin changes between the upper and lower branches of the valence band, which indicates a strong spin-orbit interaction in this structure. A good agreement was obtained between the zone structure of OsH<sub>2</sub>(bipyridine\_CN) and the previously published results from the article<sup>[3]</sup>.

1. X. L. Yan, X. Su, J. Chen, C. Jin and L. Chen.: Two-Dimensional Metal-Organic Frameworks Towards Spintronics. *Angew. Chem., Int. Ed.* (2023).

2. H. Furukawa, K. E. Cordova, M. O'Keeffe, O. M. Yaghi.: *The Chemistry and Applications of Metal-Organic Frameworks*. Science (2013).

3. Shanshan Liu, Ke Xu, Xingxing Li.: Obtaining giant Rashba–Dresselhaus spin splitting in two-dimensional chiral metal–organic frameworks. *Chemical Science* (2024).

## FREE RADICAL MECHANISMS of AMORPHIZATION of BIOINORGANIC COMPOUNDS

**D.S. Rybin<sup>1,2</sup>, G.N. Konygin<sup>1</sup>, V.E. Porsev<sup>1</sup>, D.R. Sharafutdinova<sup>3</sup>,  
G.G. Gumarov<sup>4</sup>, A.A. Zhigalova<sup>1</sup>, K.A. Novozhilov<sup>1</sup>, M.M. Akhmetov<sup>4</sup>,  
A.R. Gafarova<sup>4</sup>**

<sup>1</sup>Udmurt Federal Research Center UB of RAS, Izhevsk, RF

<sup>2</sup>Mezomax Inc, San Francisco, CA, US

<sup>3</sup>Arbuzov Institute of Organic and Physical Chemistry, FRC KSC RAS, Kazan, RF

<sup>4</sup>Zavoisky Physical-Technical Institute, FRC Kazan Scientific Center of RAS, Kazan, RF

Solid-state deformation-induced structural transformations are a method used to produce active pharmaceutical substances in an amorphous state. However, it is important to consider the significant drawbacks of this method. It may not be easily scalable and can lead to undesirable chemical changes due to mechanical forces.

The development of amorphization technology is a precise process that requires careful control of reaction products and a detailed study of the morphology of the synthesized samples. The resulting products may not always be amorphous, as they can form low-dimensional crystals.

This paper explores modern concepts related to the mechanisms of amorphization of bioinorganic substances caused by deformation-induced transformations. Understanding these mechanisms is essential for the advancement of our field.

In bioinorganic compounds based on carbohydrate derivatives, the primary mechanism of amorphization resulting from structural transformations is based on free radical reactions.

The paper discusses the features of the emergence of free radicals, their stability, the kinetics of chemical conversions and amorphization, the processes of structural relaxation in an amorphous state, and the stability of the final products.

*Acknowledgment: The studies were carried out within the grant of the MSHE of the RF (project FUUE-2024-0011).*

## VARIATION OF THE EPR SPECTRA OF NON-MORPHOGENIC BUCKWHEAT CELL CULTURE DURING GROWTH AND CELL DIVISION

**S.V. Yurtaeva<sup>1</sup>, I. V. Yatsyk<sup>1</sup>, A.I. Valieva<sup>2</sup>, A.N. Akulov<sup>2</sup>,  
N.I. Rumyantseva<sup>2</sup>**

<sup>1</sup> Zavoisky Physical-Technical Institute, FRC Kazan Scientific Center of RAS, Kazan, Russia

<sup>2</sup> Kazan Institute of Biochemistry and Biophysics, FRC Kazan Scientific Center of RAS, Kazan, Russia

Since 1960s it is known the phenomenon of “wide EPR signals” arising in yeast cell cultures [1,2]. The origin of ferromagnetic signal during cell division is still not quite understood. In this study, this phenomenon is first investigated in dividing cells of non-morphogenic culture of buckwheat *Fagopyrum tataricum*.

The changes in EPR spectra in samples of dividing cells were studied. A strong transformation of the EPR spectrum was detected in the process of cell growth and division, which is the appearance of new signals, depended on magnetic field orientation, which are not present in cell culture in the stationary phase. These signals are of maximum intensities when the number of dividing cells is maximal.

After cells are transferred to fresh nutrient medium during growth and division in cell samples, signals of three types I, II and III appear sequentially. The characteristics of these signals were studied in detail. The temperature behavior of an isotropic signal of type I ( $g=2.08\div 2.1$ ,  $\Delta H \approx 1000$  Oe) of a symmetrical shape is close to the behavior of superparamagnetic particles incorporated in a diamagnetic matrix.

Signals of type II ( $g > 2.1$ ,  $\Delta H = 150\div 350$  Oe) and type III depend on orientation and are characterized with an angular dependence of  $H_{res}$ . The temperature behavior of signal II in the range 5-300 K corresponds to the behavior of  $Fe_3O_4$  [3,4]. The angular dependence of signal II is well described by the equation for a suspension of ferromagnetic particles. The behavior of the type III signal is close to “noise-like spectra” inherent in dispersed ferromagnetic systems. Signals of II and III type were recorded in the phase of the maximum number of dividing cells. Signals similar to I and II types were previously recorded in isolated DNA samples [5,6]. The possible relation of all 3 types of signals and the stages of DNA compaction is supposed.

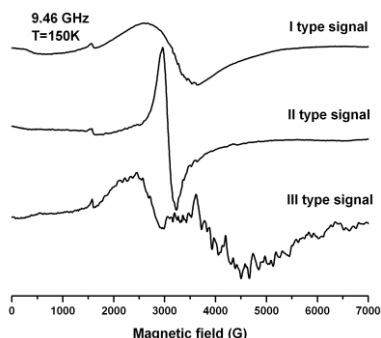


**Fig. 1.** Three types of signals emerging in fast growing cell culture of *Fagopyrum tataricum*.

## STRUCTURE of ZINC FINGER of the *E. COLI* FPG in the SOLUTION

**N.E. Litovskikh<sup>1,3</sup>, A.V. Shernyukov<sup>1</sup>, D.O. Zharkov<sup>2</sup>, N.A. Bulgakov<sup>2,3</sup>,  
E.G. Bagryanskaya<sup>1</sup>**

<sup>1</sup>Vorozhtsov Novosibirsk Institute of Organic Chemistry of the Siberian Branch of the RAS, Novosibirsk, Russia

<sup>2</sup>Institute of Chemical Biology and Fundamental Medicine of the Siberian Branch of the RAS, Novosibirsk, Russia

<sup>3</sup>Novosibirsk State University, Novosibirsk, Russia

The zinc finger is a small structural motif that allows proteins to bind to DNA, RNA, other proteins and molecules. A distinctive feature of zinc fingers is that they contain one or more zinc ions ( $Zn^{2+}$ ) bound to amino acid residues of cysteines and/or histidines. Zinc ion plays a strengthening role in the zinc finger structure. Zinc fingers are found in the structure of many proteins involved in catalysing biochemical reactions and regulating RNA synthesis. In particular, these motifs are DNA-binding elements of enzymes involved in base excision repair of DNA. Such enzymes are called DNA glycosylases. This class of proteins includes the FPG enzyme (formamidopyrimidine DNA glycosylase) of *E. Coli*. The main feature of the FPG is that it removes oxidized damage 8-oxoguanine from DNA, the accumulation of which leads to an increased risk of mutagenesis. In the present work, the structure of zinc finger, which is a fragment of the mentioned protein, was studied.

The crystal structure of the FPG in complex with a DNA fragment is known, obtained using X-ray diffraction analysis [1]. The analysis showed that the zinc finger is a  $\beta$ -sheet consisting of two antiparallel  $\beta$ -strands connected by a flexible hairpin, where the  $Zn^{2+}$  ion is coordinated to the sulfhydryl groups of four cysteines (Fig. 1 (a)). It was hypothesised that there is a difference between the structure of the isolated zinc finger in solution and its structure as part of the full-length protein in the crystal. To test this hypothesis, nuclear magnetic resonance (NMR) methods were used, which allows to determine the structure and dynamics of biological molecules in solution with atomic resolution. In addition, the choice of NMR is justified by the fact that there is a large accumulated experience of studying zinc fingers by this method.

To determine the structure of the zinc finger, NMR spectra were recorded using different techniques such as COSY, TOCSY, NOESY, HSQC, TOCSY-HSQC and HMBC. The signals of protons and  $^{13}C$  nuclei of the backbone and side chains were assigned, structural constraints were extracted, and the structure of the zinc finger was modelled using molecular dynamics methods. NMR data and simulated annealing with restricted molecular dynamics showed that the isolated zinc finger in solution is a disordered peptide, in which elements of the secondary structure are not observed (Fig. 1 (b)). A suggested explanation for the difference between the structures in solution and crystal is that the structure of the zinc finger in the crystal is stabilized by other domains of the protein and the DNA fragment to which the zinc finger is attached.

This work was supported by the state task of N.N. Vorozhtsov Novosibirsk Institute of Organic Chemistry of Siberian Branch of Russian Academy of Sciences in the area of basic research (registration number 122040800265-0).

I. Gilboa R., Zharkov D.O., Golan G., Fernandes A.S., Gerchman S.E., Matz E., ... & Shoham G.: Structure of formamidopyrimidine-DNA glycosylase covalently complexed to DNA. *M.: Journal of Biological Chemistry*, **277**(22), 19811-19816 (2002).

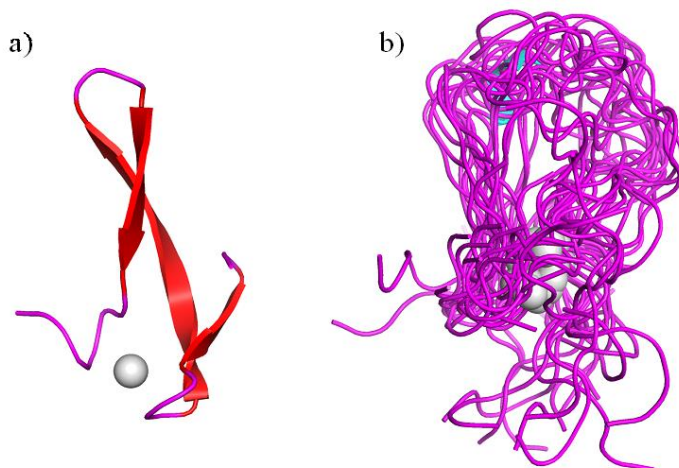


**Fig. 1. a)** Zinc finger structure of FPG protein extracted from X-ray diffraction analysis data of the full-length protein in crystal. **b)** Results of molecular modeling for an isolated zinc finger in solution based on NMR constraints.

## MUTUAL DEPENDENCES OF DYNAMICAL PROPERTIES OF $\text{Mn}^{2+}$ AND $\text{Gd}^{3+}$ IMPURITY CENTERS IN $\text{Pb}_{1-x-y-z}\text{Cu}_x\text{Mn}_y\text{Gd}_z\text{S}$ NARROW-BAND SEMICONDUCTOR: RESULTS OF EPR STUDY

**V.A. Ulanov<sup>1,2</sup>, I.V. Yatzyk<sup>1</sup>, R.R. Zainullin<sup>2</sup>**

<sup>1</sup>Zavoisky Physical-Technical Institute, FRC Kazan Scientific Center of RAS, Kazan, Russia

<sup>2</sup>Kazan State Power Engineering University, Kazan, Russia

In this work the mixed  $\text{Pb}_{1-x-y-z}\text{Cu}_x\text{Mn}_y\text{Gd}_z\text{S}$  crystal was synthesized on the basis of a galena ( $\text{PbS}$ ), a member of the group of lead chalcogenides ( $\text{PbS}$ ,  $\text{PbSe}$ ,  $\text{PbTe}$ ) [1]. Even though lead chalcogenides have long been the focus of attention of many researchers, interest in them remains unabated due to new possibilities of using lead chalcogenides as effective thermoelectric converters and materials for creating new nanoelectronic and spintronic devices.

Unlike other crystals of the lead chalcogenide group, the physical properties of galena remain poorly studied. While studies performed so far allow one to predict some results from doping galena with impurity atoms of the same type, one cannot foresee those of doping with several impurities simultaneously. All attempts to predict the results from the double or triple doping of galena with different types of paramagnetic ions have failed. In this work, interest arose in the mechanisms of interaction between impurity paramagnetic ions of different nature at different concentrations and types of free charge carriers. Of particular interest was the case where one of the doping components is a paramagnetic ion from the iron group (e.g.,  $\text{Mn}^{2+}$ ), while the other is a rare-earth ion (e.g.,  $\text{Gd}^{3+}$ ).

Typically, galena crystals are characterized by an electronic type of conductivity, since during their growth there is a high probability of the formation of donor defects (sulfur vacancies). Therefore, it was interesting to study the possibilities of controlling the concentrations of free charge carriers by additionally doping the synthesized material with copper.

The crystal studied in present work was grown using the vertical Bridgman method. Conical quartz crucible was used. The crystals corresponded to the chemical formulas  $\text{Pb}_{1-x-y-z}\text{Cu}_x\text{Mn}_y\text{Gd}_z\text{S}$  ( $x = 3 \times 10^{-3}$ ,  $y \approx z \approx 1,5 \times 10^{-4}$ ). Copper impurity was introduced into the furnace charge using a  $\text{Cu}_2\text{S}$  compound. Gadolinium and manganese impurities were introduced in the form of fine powders of the corresponding metals. The amount of sulfur required to ensure stoichiometry was also included in the furnace charge. All components of the furnace charge were chemically pure. The prepared furnace charge was loaded into a quartz crucible, and annealed for 3 h at  $T = 250^\circ\text{C}$ , and evacuated with a vacuum pump. The crucible was sealed and placed in the growth chamber of the Donets-2 setup, where it moved downward vertically in a thermal field with a temperature gradient of 250 deg/cm. The rate at which the crucible was lowered was 1.2 cm/h. The EPR experiment was performed on an ER200SRC spectrometer (EMX/plus, Bruker) with an ITC503S temperature controller (Oxford instruments) in the X range.

EPR spectra of  $\text{Pb}_{1-x-y-z}\text{Cu}_x\text{Mn}_y\text{Gd}_z\text{S}$  ( $x = 3 \times 10^{-3}$ ,  $y \approx z \approx 1.5 \times 10^{-4}$ ) crystal recorded in orientation  $H_0 \parallel \langle 001 \rangle$  at microwave power  $P = 2$  mW are presented in Fig. 1. The Fig. 1 shows spectra recorded at various temperatures from 5K to 77K. As it can be seen, the observed spectra of  $\text{Gd}^{3+}$  centers ( $S_{\text{Gd}} = 7/2$ ) consist of seven lines with relative characteristic intensities corresponding approximately to the series 7:15:12:16:12:15:7. The angular dependences of positions of these lines demonstrate the cubic symmetry of the  $\text{Gd}^{3+}$  centers. In addition to the lines of  $\text{Gd}^{3+}$  centers, the EPR spectra in Fig. 1 contain six lines of the same intensity which belong to  $\text{Mn}^{2+}$  centers of cubic symmetry with  $S = 5/2$  and  $I = 5/2$ .

In Fig. 1 it can be seen that with increasing temperature the intensities of the lines of the manganese and gadolinium spectra rapidly decrease so that already at  $T > 77\text{K}$  they are practically unobservable. This temperature dependence of the EPR line intensities for cubic  $\text{Gd}^{3+}$  and  $\text{Mn}^{2+}$  centers is unusual. The shapes of the EPR spectra lines of these centers at low temperatures also turn out to be unexpected.

Obviously, the unusual shapes of the EPR lines of the  $\text{Mn}^{2+}$  and  $\text{Gd}^{3+}$  centers and the unusual temperature-related changes in the shapes of these lines demonstrate the mutual dependences of dynamic properties of the  $\text{Mn}^{2+}$  and  $\text{Gd}^{3+}$  centers. The experimental facts got in the present study are discussed.

1. Kaidanov, V.I., Ravich, Yu.I.: Sov. Phys. Usp. **145**, 51-86 (1985)

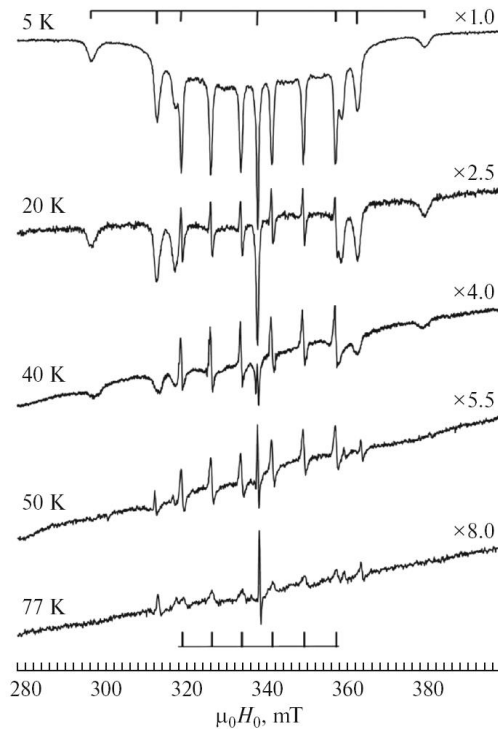


Fig. 1. Temperature-related changes in the intensities and shapes of EPR spectra lines of  $\text{Gd}^{3+}$  and  $\text{Mn}^{2+}$  centers in  $\text{Pb}_{1-x-y-z}\text{Cu}_x\text{Mn}_y\text{Gd}_z\text{S}$  crystal in  $\bar{H} \parallel \langle 110 \rangle$  orientation.

## NEW PROPERTIES OF TITANIUM DIOXIDE HEAT-TREATED IN VARIOUS ENVIRONMENTS ACCORDING TO ELECTRON MAGNETIC RESONANCE DATA

**A.M. Ziatdinov<sup>1</sup>, D.A. Saritsky<sup>1</sup>, N.S. Saenko<sup>1</sup>, D.P. Opra<sup>1</sup>, A.A. Sokolov<sup>1</sup>, S.V. Gnedenkov<sup>1</sup>**

<sup>1</sup>Institute of Chemistry, Far Eastern Branch of the Russian Academy of Sciences, Vladivostok, Russia

Non-stoichiometric modifications of TiO<sub>2</sub> containing intrinsic and/or impurity structural defects attract significant attention due to their improved properties [1]. Doping with impurities of the cationic or anionic type is one of the promising ways to create defects in TiO<sub>2</sub>. On the other hand, the formation of structural defects in TiO<sub>2</sub> can be achieved without changing the chemical composition (i.e., by a non-doping method) due to heat-treatment under specific conditions – namely in certain inert atmosphere [2]. In this work we used electron magnetic resonance (EMR) for the investigation of the possibility of creating structural defects in nanoribbon-like TiO<sub>2</sub>(B) by heat treatment in vacuum, in nitrogen and argon atmospheres. The EMR spectra were recorded with the JES-X330 (Japan) spectrometer at the X-band frequency.

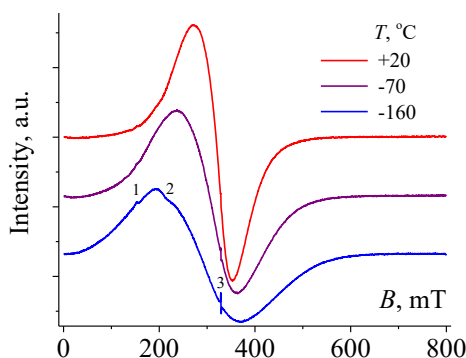


**Fig. 1.** The EMR spectra of TiO<sub>2</sub>(B) powder heat-treated in nitrogen atmosphere. The labels 1, 2 and 3 indicate weak signals.

The EMR spectrum of TiO<sub>2</sub>(B) powder heat-treated in nitrogen atmosphere contains an intense broad signal (**Fig. 1**), whose parameters change significantly with temperature (**Figs. 1** and **2**). In addition to that, the spectrum contains three more narrow, low-intensity signals, which are superimposed on the main resonance (**Fig. 1**). The parameters of these signals change insignificantly with temperature. The low-intensity asymmetric component with  $g \sim 4.32(1)$  (signal 1) in the spectra corresponds to ions having a 3d<sup>5</sup> configuration (i.e., Mn<sup>2+</sup> or Fe<sup>3+</sup>), which are under the influence of crystal fields with a significant rhombic component [3]. Taking into account the small width of this line, it should be



considered as a resonance on  $\text{Fe}^{3+}$  ( $3d^5$ ,  $S = 5/2$ ,  $I = 0$ ), which is present as a small impurity in the precursors. The nature of signal 2 with  $g=3,16(2)$  has not yet been established. The  $g$ -factor value of the third signal, equal to  $1,996(1)$ , is characteristic of  $\text{Ti}^{3+}$  ions located in regular positions or in lattice interstitial sites ( $1,945 < g < 1,999$  [4]). As the temperature decreases, the parameters of the main signal (Fig. 2) change qualitatively in the same way as the parameters of superparamagnetic resonance [5]. Consequently, during heat treatment, nitrogen ions are introduced into the titanium dioxide lattice, possibly forming magnetic compounds (quasi-molecules) and their ferromagnetic clusters. The temperature dependence of the integral intensity of the main signal reaching a plateau below  $-150\text{ }^\circ\text{C}$  (Fig. 2c). Obviously, this is due to the achievement of the blocking temperature of the superparamagnetic fragments of the compound.

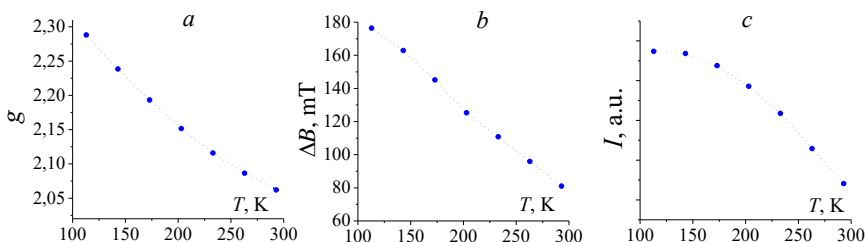


**Fig. 2.** The temperature changes in the  $g$ -factor (a), width  $\Delta B$  (b) and integral intensity  $I$  (c) of the EMR signal of the  $\text{TiO}_2(\text{B})$  powder heat-treated in nitrogen atmosphere.

The **Fig. 3** shows the EMR spectrum of  $\text{TiO}_2(\text{B})$  powder heat-treated in vacuum, recorded at  $-160\text{ }^\circ\text{C}$ . The analyzed spectrum contains an intense narrow symmetric component with  $g = 2,0037(1)$ , low-intensity asymmetric component with  $g \sim 4,32$ , belonging to  $\text{Fe}^{3+}$  ions added from precursors, and group of three close low-intensity resonances marked as 'a', 'b' and 'c' with  $g$ -factors of 2,063, 2,056, and 2,044, respectively. The  $g$ -factor value of the main component in the EMR spectra is close to that of the electrons localized in oxygen vacancies of titanium dioxide (so-called F-centers) [6]. On the other hand, absent or weak temperature dependence of integral intensity of the EMR signal (**Fig. 4**) is characteristic for spin resonance on conduction electrons [7]. Consequently, after heat treatment in vacuum, areas with electronic conductivity appear in the  $\text{TiO}_2(\text{B})$  powder particles. The values of the  $g$ -factors of lines 'a', 'b' and 'c' are close to those of  $\text{O}^-$  and  $\text{O}^-\text{H}^-$  radicals in titanium dioxide [8].

The characteristics of EMR spectrum of  $\text{TiO}_2(\text{B})$  powder heat-treated in argon atmosphere are similar to those of the spectrum of  $\text{TiO}_2(\text{B})$  powder heat-treated in vacuum. Indeed, along with other signals, it contains a signal with  $g = 2,001(1)$ , whose integral intensity varies slightly with temperature (**Fig. 5**). This observation suggests that in the particles of  $\text{TiO}_2(\text{B})$  powder, during its heat treatment in argon atmosphere, regions with electronic conductivity are also formed.

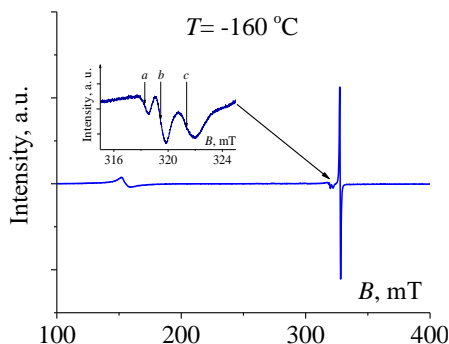


**Fig. 3.** The EMR spectrum of  $\text{TiO}_2(\text{B})$  powder heat-treated in vacuum. The inset shows a fragment of the spectrum with low-intensity components 'a', 'b' and 'c'.

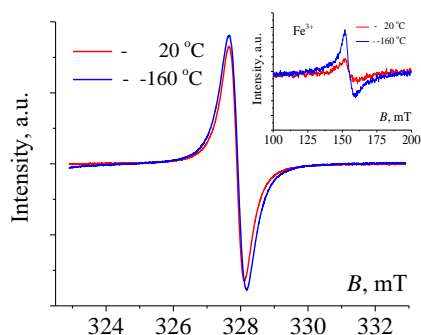


**Fig. 4.** The temperature change of the main EMR signal of  $\text{TiO}_2(\text{B})$  powder heat-treated in vacuum. The inset shows the change in the  $\text{Fe}^{3+}$  EMR signal with temperature in the same sample.

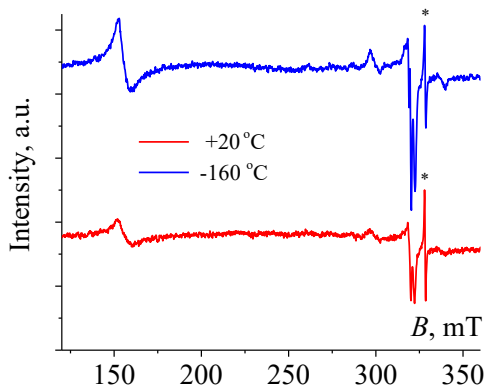


**Fig. 5.** The EMR spectra of  $\text{TiO}_2(\text{B})$  powder heat-treated in argon atmosphere. The asterisk marks a signal whose intensity varies slightly with temperature.

The work was carried out within the framework of state assignments to the Institute of Chemistry, Far Eastern Branch of the Russian Academy of Sciences (projects: No. FWFN(0205)-2022-0003 and FWFN(0205)-2022-0004).

1. Tan H., Zhao Z., Niu M., Mao C., Cao D., Cheng D., Feng P., Sun Z.: *Nanoscale*. **6**, 10216–10223 (2014).
2. Janczarek M., Kowalska E.: *Catalysts*. **11**, 978 (2021).
3. Castner T., Newell G.S., Holton W.C., Slichter C.P.: *J. Chem. Phys.* **32**, 668–673 (1960).
4. Mohajernia S., Andryskova P., Zoppellaro G., Hejazi S., Kment S., Zboril R., Schmidt J.: *J. Mater. Chem. A*. **8**, 1432–1442 (2020).
5. Berger R., Bissey J.-C., Kliava J., Daubric H., Estourmes C.: *J. Magn. Magn. Mat.* **234**, 535–544 (2001).
6. Serwicka E., Schindler R.N.: *Z. Naturforsch. A*. **36**, 992–995 (1981).
7. Winter J.: *Magnetic Resonance in Metals*. Oxford, UK: The Clarendon Press (1971), 206 p.
8. Yang G., Jiang Z., Shi H., Xiao T., Yan Z.: *J. Mater. Chem.* **20**, 5301 (2010).

## DFT INVESTIGATION of MAGNETOELECTRIC COUPLING in Fe/BaTiO<sub>3</sub> HETEROSTRUCTURE

**K.V. Evseev<sup>1,2</sup>, R.F. Mamin<sup>2</sup>, I.I. Piyanzina<sup>1,2</sup>, O.V. Nedopekin<sup>1</sup>**

<sup>1</sup> Kazan Federal University, Kazan, Russia

<sup>2</sup> Zavoisky Physical-Technical Institute, FRC Kazan Scientific Center of RAS, Kazan, Russia

Magnetolectric coupling, which is observed in multiferroics, is the topic of many studies today [1, 2]. This is not surprising, since control of the magnetic properties of a material by an external electric field and control of electrical properties by a magnetic field provides a large number of opportunities for solving the problems of modern electronics [3]. Materials exhibiting magnetolectric coupling can become components for magnetoresistive memory devices and spin valves.

Possible way to change the magnetic properties of a thin ferromagnetic film in ferromagnet/ferroelectric (FM/FE) heterostructures is the effect of reverse magnetostriction. Works [4, 5] show that when mechanical deformation is applied to a ferroelectric, an electric field arises in it, which might affect the magnetization of the neighboring ferromagnetic film.

In this work, the Fe/BaTiO<sub>3</sub> (Fig. 1) thin film heterostructure was studied using density functional theory (DFT) calculations. *bcc* Fe is a well-studied ferromagnetic material, with known values of the lattice parameter and magnetic moment in the bulk phase. BaTiO<sub>3</sub> (BTO) has a perovskite crystal structure and exhibits piezoelectric properties and spontaneous polarization at room temperature. Due to the small lattice mismatch (1.324%) of these materials, it is possible to epitaxially grow a thin Fe film on a BaTiO<sub>3</sub> substrate, which makes it possible to construct a model for *ab initio* calculations as well as experimentally grow and check the predictions. To study the possibility of controlling the magnetic properties of a ferromagnet using an external electric field, we carried out calculations with a given displacement value of Ti and Ba atoms from the O plane and two different directions of ferroelectric polarization. To investigate the effect of mechanical deformation of the BTO on the magnetization of Fe layers, the entire Fe/BaTiO<sub>3</sub> heterostructure was built with striction along the *xy* – axes parallel to the interface.

1. R. Revathy et al., Exotic magnetic properties and enhanced magnetolectric coupling in Fe<sub>3</sub>O<sub>4</sub>-BaTiO<sub>3</sub> heterostructures, *J. All. Compd.* **889**, 161667 (2021)
2. Y. Zhao et al., Ultraflexible and Malleable Fe/BaTiO<sub>3</sub> Multiferroic Heterostructures for Functional Devices, *Adv. Funct. Mater.* **31**, 2009376 (2021)
3. Ortega et al., Multifunctional magnetolectric materials for device applications, *J. Phys.: Condens. Matter.* **27**, 504002 (2015)
4. O. Tumentsereg, et al., Electrically Driven Magnetization Reorientation at the Fe/PbTiO<sub>3</sub> Interface, *J. Phys. Chem.* **127**, 24467 (2023)
5. Y. Zhang, et al., Electric-field induced strain modulation of magnetization in Fe-Ga/Pb (Mg<sub>1/3</sub>Nb<sub>2/3</sub>)-PbTiO<sub>3</sub> magnetolectric heterostructures, *J. Appl. Phys.* **115**, 084101 (2014)

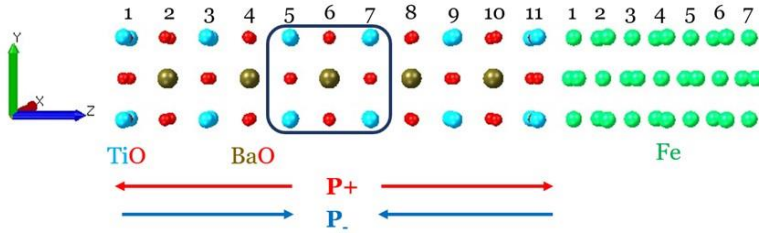


**Fig. 1.** Fe/BaTiO<sub>3</sub> heterostructure, the numbers 1-11 show the atomic layers BTO, interfacial layers are 1 and 11; the numbers 1-7 show the atomic layers Fe, interfacial layers are 1 and 7 due to the periodicity of the structure. Layers with frozen atoms are highlighted by a frame. The red (blue) arrow indicates the ferroelectric polarization directed towards (away from) the interface and denoted as P<sub>+</sub> (P<sub>-</sub>). Titanium (Ti), oxygen (O), barium (Ba) and iron (Fe) atoms are represented in blue, red, brown and green respectively

## Electron Paramagnetic Resonance in Nanocrystalline Potassium Tetratitanate Doped with Copper Ions

**D.A. Saritsky, V.V. Zheleznov, D.P. Opra, A.M. Ziatdinov**

Institute of Chemistry, Far Eastern Branch of the RAS, Vladivostok 690022, Russia.  
denissaricki@mail.ru

In this study, we present the results of determining the magnetically nonequivalent states of impurity copper ions and the nature of charge compensation in potassium tetratitanate ( $K_2Ti_4O_9$ ) using electron paramagnetic resonance (EPR). The EPR spectra were recorded using a JES-X330 spectrometer.

Analysis of the second derivative of the microwave absorption spectrum of copper-doped potassium tetratitanate powder (**Fig. 1**) indicates that copper impurity ions exist in three magnetically nonequivalent states (**Tab. 1**). Two of these states correspond to  $Cu^{2+}$  ions substituting  $Ti^{4+}$  ions in the crystal lattice, within a tetragonally-distorted oxygen octahedron. This environment stabilizes the unpaired hole of copper ion predominantly on the  $d_{x^2-y^2}$  atomic orbital. Differences in the distortion of the oxygen environment of these  $Cu^{2+}$  centers can be explained by their location in different parts of the particle. Specifically, centers of lower concentration are likely distributed within the particle volume, whereas those of higher concentration are likely concentrated near the particle surface. Significant differences in the resonance widths of the magnetically nonequivalent  $Cu^{2+}$  centers also confirm their preferential localization in different regions of the particle.

Analysis of the EPR spectra parameters of  $Cu^{2+}$  centers substituting  $Ti^{4+}$  ions, using molecular orbital theory, shows that the delocalization of the hole (spin density) from the  $d_{x^2-y^2}$  orbital to the four  $\sigma$ - orbitals of the equatorial oxygen ions is  $\sim 19\%$ . The contribution of the excited  $d_z^2$  orbital to the ground state is negligibly small, indicating the absence of vibronic interaction between these orbitals.

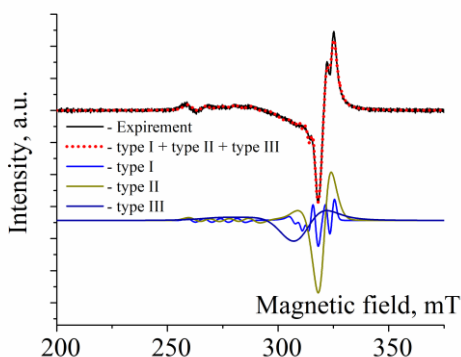


**Fig. 1.** Second derivatives of theoretical and experimental EPR spectra of  $K_2Ti_4O_9$  powder doped with copper ions;  $T = -160$  °C, X-band

**Table 1.** Parameters of the spin Hamiltonian of rhombic symmetry ( $g_i, A_i, P_{\parallel}/h, \eta$ ), electric field gradient in the region of the nucleus of copper ions ( $eq$ ), the widths of the Lorentz ( $\Delta B_L$ ) and Gaussian ( $\Delta B_{Gi}$ ) components of the Voigt resonance contours and contributions of different types of  $\text{Cu}^{2+}$  centers to the integral intensity of the theoretical spectrum presented in **Fig. 1**.

Type of center	$g_i$	$A_i$ , mT	$P_{\parallel}/h$ , MHz ( $\eta$ )	$eq \cdot 10^{21}$ , V/m <sup>2</sup>	$\Delta B_L$ , mT	$\Delta B_{Gi}$ , mT	Contribution, %
I	$g_x=2,085$ $g_y=2,066$ $g_z=2,415$	$A_x=4,305$ $A_y=3,716$ $A_z=9,003$	45,6 (0,13)	36,6	0,20	$\Delta B_{Gx}=3,17$ $\Delta B_{Gy}=2,22$ $\Delta B_{Gz}=4,61$	6,74
II	$g_x=2,064$ $g_y=2,062$ $g_z=2,383$	$A_x=2,933$ $A_y=1,239$ $A_z=10,35$	50,6 (0,33)	40,7	0,71	$\Delta B_{Gx}=5,52$ $\Delta B_{Gy}=5,11$ $\Delta B_{Gz}=7,26$	28,56
III	$g_x=2,123$ $g_y=2,123$ $g_z=2,276$	$A_x=2,344$ $A_y=2,344$ $A_z=8,876$	-	-	8,87	$\Delta B_{Gx}=10,2$ $\Delta B_{Gy}=10,2$ $\Delta B_{Gz}=14,4$	64,70

The absence of resonance absorption on electrons trapped by oxygen vacancies in the EPR spectra of copper-doped potassium tetratitanate samples indicates that the charge imbalance resulting from the substitution of matrix  $\text{Ti}^{4+}$  ions by impurity  $\text{Cu}^{2+}$  ions is compensated without the formation of new oxygen vacancies. Comparative analysis of the parameters of the three types of signals shows that charge compensation occurs mainly through type III ions located in the interlayer spaces. Moreover, as the concentration of the impurity ion increases, the contribution to the intensity of the type III signal grows, in contrast to our previously studied sodium trititanate also doped with  $\text{Cu}^{2+}$  ions [2]. This is possible in nanocrystalline materials if the charge imbalance occurring on the material surface, due to uncompensated  $\text{O}^{2-}$  ions, is balanced by additional incorporation of  $\text{Cu}^{2+}$  ions into interstitial positions.

The authors are grateful to N.S. Saenko for help in recording the EPR spectra. The work was carried out within the framework of state assignments to the Institute of Chemistry, Far Eastern Branch of the Russian Academy of Sciences (projects: No. FWFN(0205)-2022-0003 and FWFN(0205)-2022-0004).

1. Narayana P. A., Sastry K. V. L. N.: J. Chem. Phys. **57**, 3266-3268 (1972)
2. Opra D. P., Zhelezov V. V., Sinebryukhov S. L., Sokolov A. A., Ziatdinov A. M., Podgorbunsky A. B., Gerasimenko A. V., Ustinov A. Yu., Kuryavy V. G., Saritsky D. A., Neumoin A. I., Zaytsev N. I., Polyakova N. V., Gnedenkov S. V.: J. Power Sources. **600**, Article Number 234230 (2024)

## POLARIZED NEUTRON REFLECTOMETRY FOR INVESTIGATION OF LOW-DIMENSIONAL 2D MAGNETIC & SUPERCONDUCTING HETEROSTRUCTURES

V.D. Zhaketov<sup>1,2</sup>

<sup>1</sup> Joint Institute for Nuclear Research, Dubna, Russia

<sup>2</sup> Moscow Institute of Physics and Technology, Dolgoprudny, Russia

Low-dimensional magnetic and superconducting heterostructures, due to the presence of a large number of interesting phenomena, are currently being actively studied. One of the effective methods for studying magnetism is polarized neutron reflectometry, which makes it possible to obtain isotopic and magnetic depth profiles with nanometer resolution. Low-temperature studies of proximity effects in superconducting-ferromagnetic systems [1] and rare-earth films with nontrivial magnetic ordering [2] were carried out using the REMUR reflectometer of the IBR-2 reactor (Dubna).

Proximity effects at the interface between two media are currently being actively studied. Of particular interest are layered low-dimensional structures with superconducting (S) and ferromagnetic (F) properties, in which the interaction of two antagonistic order parameters is realized. Promising systems for studying proximity effects are S/F heterostructures made of niobium and rare earth (RE) metals [3]. As example for the layered heterostructure  $\text{Al}_2\text{O}_3/\text{Nb}(40 \text{ nm})/[\text{Dy}(6 \text{ nm})/\text{Ho}(6 \text{ nm})]_{34}/\text{Nb}(10 \text{ nm})$  it was found that at a temperature below the superconducting transition, the magnetic state of the helimagnet was affected by superconductivity, namely the fan-shaped magnetic state the ordering was rearranged into helimagnetic ordering [4].

The described periodic layered systems are artificial layered crystals. When neutrons are reflected from a periodic layered structure, Bragg peaks are observed. Layered artificial quasicrystals are also of particular interest. It is possible to create artificial layered systems with quasicrystallinity in the direction perpendicular to the plane of the structure. The possibility of creating layered quasicrystals from alternating superconducting and ferromagnetic layers is considered. These model systems are simple to manufacture and research, but will make it possible to study non-trivial phenomena, such as fractal superconductivity and long-range magnetic order in a quasiperiodic system, as well as their coexistence. Of course, the creation of Fibonacci structures using magnets with helical magnetic order is of particular interest.

1. Yu.V. Nikitenko et al. // *Physics of Particles and Nuclei*, v. 53, No. 6, pp. 1089-1125 (2022).
2. D.I. Devyaterikov et al. // *Journal of Surface Investigation*, v. 16, № 5, pp. 839-842 (2022).
3. Khaydukov Yu.N. et al. // *Phys. Rev. B*, vol. 99, pp. 140503(R) (2019).
4. Zhaketov V.D. et al. // *Physics of the Solid State*, Vol. 65, No. 7 (2023).

## Effective Spin Traps for Singlet Oxygen Detection in Physiological Conditions

**S.A. Dementev<sup>1,2</sup>, R.A. Podarov<sup>1,2</sup>, N.E. Sannikova<sup>1</sup>, Y.F. Polienko<sup>3</sup>,  
I.A. Kirilyuk<sup>3</sup>, O.A. Krumkacheva<sup>1,2</sup>**

<sup>1</sup> International Tomography Center SB RAS, 630090 Novosibirsk, Russia

<sup>2</sup> Novosibirsk State University, 630090 Novosibirsk, Russia

<sup>3</sup> N.N. Vorozhtsov Novosibirsk Institute of Organic Chemistry, 630090 Novosibirsk, Russia  
email: dementev.epr@gmail.com

Reactive oxygen species (ROS) remain a relevant target of scientific research. In particular, they play a pivotal role in photodynamic cancer therapy (PDT): under illumination, the photosensitizer (PS) enters the triplet state. It generates ROS, which leads to apoptosis and necrosis of surrounding cells. Singlet oxygen ( $^1\text{O}_2$ ) is considered to be the most effective agent for PDT. The new advancements in PDT inherently hinge on the search for new promising PSs. An important step in assessing the applicability of new PSs is to determine the efficiency of their ROS generation; therefore, it is crucial to refine the existing experimental techniques, to achieve a more precise testing. One of the most prominent experimental techniques in this area is the spin trapping (ST) methodology combined with electron paramagnetic resonance (EPR).

A diamagnetic spin trap (ST) captures reactive oxygen species (ROS) and becomes a paramagnetic stable radical (SR), which can be detected by EPR. Typically, 2,2,6,6-Tetramethylpiperidine and 2,2,6,6-tetramethylpiperidine-4-ol are used as STs for the detection of singlet oxygen. However, these spin traps are not effective at physiological pH. Additionally, their use causes a significant increase in the pH of the medium, even in buffer solutions, which may distort the data obtained, lead to various side reactions in the system, and cause the aggregation of various promising photosensitizers, such as cationic porphyrins. Thus, the search for STs effective at physiological pH is an urgent task.

In this work, we studied new STs (Fig. 2) characterized by trimethylammonium substituent in the 4th position of the piperidine cycle with improved functional properties. Using the model porphyrin meso-5,10,15,20-tetrakis(N-methylpyridyl-4')porphyrin, the efficiency of  $^1\text{O}_2$  registration was determined by EPR during steady-state photolysis at room temperature with pH control. Additional studies at different pH levels revealed their range of applicability. The high selectivity of STs to  $^1\text{O}_2$  was confirmed by control studies in a deuterated buffer solution and by the addition of  $\text{NaN}_3$ . Thus, the most promising ST structures for studying the functional properties of photosensitizers were identified. Additionally, the capability for quantitative detection of  $^1\text{O}_2$  at physiological pH was demonstrated for the first time.



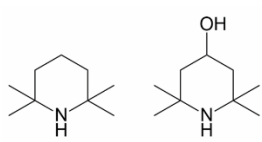


Fig.1. 2,2,6,6-tetramethyl-piperidine on the left and 2,2,6,6-tetramethylpiper-idine-4-ol on the right.

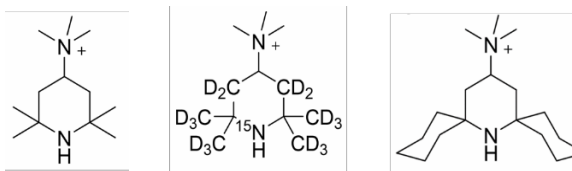


Fig. 2. The new STs studied in current work.

## Investigation of the HTel-22 G-quadruplex Complex with Cationic Porphyrin by EPR and Optical Spectroscopy Methods

**T.A. Khlynova<sup>1,2</sup>, N.E. Sannikova<sup>1,2</sup>, M.I. Kolokolov<sup>1,2</sup>, O.A. Krumkacheva<sup>1,2</sup>**

<sup>1</sup> International Tomography Center SB RAS, 630090 Novosibirsk, Russia

<sup>2</sup> Novosibirsk State University, Novosibirsk 630090, Russia

Telomerase is an enzyme responsible for maintaining the telomere ends of chromosomes, which shorten during cell division. While telomerase activity is not observed in somatic cells, its high expression has been detected in cancer cells. Inhibiting telomerase activity by stabilizing G-quadruplexes (G4) via ligand binding has been proposed as a potential cancer treatment. Due to their high selectivity for G4, cationic porphyrins are widely studied as ligands. Porphyrins are also actively used in therapy as photosensitizers (PSs), capable of generating reactive oxygen species upon excitation to the triplet state. Ligand interaction and light exposure can lead to structural changes in G-quadruplexes. Therefore, it is necessary to investigate the structure of the G4 complex with cationic porphyrin and its changes resulting from photolysis for successful therapeutic application.

The high polymorphism of G-quadruplexes complicates structural examination due to the presence of multiple conformations in samples. Electron paramagnetic resonance (EPR) is an informative method for studying biopolymer structures. Double electron-electron resonance is a pulsed EPR technique that can extract distance distributions in the range of 1.5–10 nm between stable spin labels. The recently proposed laser-induced magnetic dipole spectroscopy (LaserIMD) method allows the measurement of distances between the spin label and photoexcited triplet states of the photosensitizer. This approach has not previously been used in the study of nucleic acids and PS complexes with G-quadruplexes.

In this study [1], we introduce, for the first time, the application of laser-induced dipolar EPR as a method to characterize G-quadruplex DNA complexes containing photosensitizer and to investigate light-induced structural modifications in these systems. To demonstrate the feasibility of this approach, we studied complexes of the human telomeric G-quadruplex (HTel-22) with cationic 5,10,15,20-Tetrakis(1-methyl-4-pyridinio) porphyrin tetra(p-toluenesulfonate) (TMPyP4). In addition to showcasing a new methodology, we also aimed to provide insights into the mechanisms underlying photoinduced HTel-22/TMPyP4 structural changes, thereby aiding in the advancement of approaches targeting G4s in photodynamic therapy. EPR revealed G-quadruplex unfolding and dimer formation upon light exposure. Our findings demonstrate the potential of EPR spectroscopy for examining G4s complexes with photosensitizers and contribute to a better understanding of G4s interactions with ligands under light.

[1] Sannikova, N. E., Kolokolov, M. I., Khlynova, T. A., Chubarov, A. S., Polienko, Y. F., Fedin, M. V., & Krumkacheva, O. A. (2023). Revealing light-induced structural shifts in G-quadruplex-porphyrin complexes: a pulsed dipolar EPR study. *Physical Chemistry Chemical Physics*, 25(33), 22455-22466.

## JOINT USE OF SPIN PROBE TECHNIQUE AND SCANNING ELECTRON MICROSCOPY TO STUDY THE INTERNAL STRUCTURE OF GRAPHENE OXIDE MEMBRANES

**M.V. Matveev<sup>1,2</sup>, N.A. Chumakova<sup>1,2</sup>, N.A. Marnautov**

<sup>1</sup> M.V. Lomonosov Moscow State University, Chemistry Department, Moscow, Russia

<sup>2</sup> N.N. Semenov Federal Research Center for Chemical Physics of RAS, Moscow, Russia

Graphene oxide membranes (GOMs) have attracted a lot of attention in the last decades, in particular, because of its unique selective permeability [1] for polar liquids and hydrated ions. Graphene oxide nonstoichiometry and complex lamellar structure of the membranes make it difficult to study the mechanism of the liquid permeation. Some factors that determine the permeability of GOMs, according to the literature, are orientational ordering of the oxidized graphene layers [2] and their relief (degree of corrugation [3]).

Recently, we worked out two novel methods for investigation of the GOMs orientational ordering on the different scales. The first method, based on the quantitative analysis of scanning electron microscopy (SEM) images using the machine learning technology, allows determining the orientational ordering of lamellas (layer-packs) inside the membrane and, so, studying the microscopic structure of the membrane. The second method, based on the spin probe technique, permits investigating of the layers ordering and corrugation. For this aim, stable nitroxide radicals with different structure are inserted into the membrane and sorbed on the surface of the layers. Orientational distribution of the radicals, which reflects the orientational alignment of the layers, can be defined from the angular dependence of EPR spectra of the spin-contained membrane. Thus, the combined use of the spin probe technique and the numerical analysis of the SEM images makes it possible to perform a detailed quantitative analysis of the internal structure of GOMs.

In the present study, the proposed methods were used to characterize a number of GOMs with different synthetic background (Fig. 1). A qualitative correlation was observed between the internal structure of the membranes and their functional characteristics.

The work was supported by Russian Science Foundation (grant number 23-23-00016).

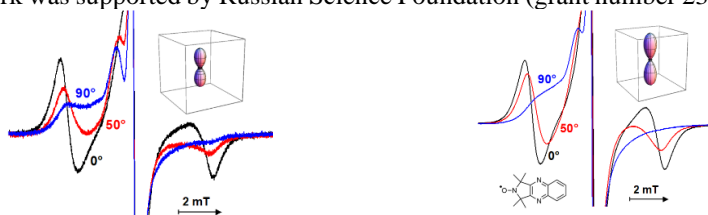


Fig. 1 Angular dependence of EPR spectra of stable nitroxide radical in two GOMs with different synthetic background; orientation distribution function (upper right corner) reflects ordering of spin probe in GOM

1. Nair, R. R., et al. // *Science*, 2012, Vol. 335, pp. 442–444.
2. Akbari, A., et al. // *Nat. Commun.*, 2016, Vol. 7 no. 10891
3. H. Huang et al. // *Nat. Commun.*, Vol. 4, pp. 1–9.

## LIGHT-INDUCED TWO-CYCLE RADICAL FORMATION in SUPRAMOLECULAR CRYSTALLINE MATRIX

**A.A. Timralieva<sup>1</sup>, A.I. Kokorin<sup>1,2,3</sup>, E.V. Skorb<sup>1</sup>**

<sup>1</sup> Infochemistry Scientific Center, ITMO University, St. Petersburg, Russia

<sup>2</sup>N. N. Semenov Federal Research Center for Chemical Physics, Russian Academy of Sciences, Moscow, Russia

<sup>3</sup>Plekhanov Russian University of Economics, Moscow, Russia

Alkylation is an efficient tool to achieve functional properties of several heterocycles e.g. barbituric acid [1]. Barbituric acid forms a binary supramolecular assembly with melamine based on hydrogen bonding, also as methylated close analog 1,3-dimethylbarbituric acid [2-4]. For both binary assemblies radical activity was identified as a functional property caused by a formation of two radical centers. One of the radical centers for both assemblies was determined by electron paramagnetic resonance (EPR) spectroscopy as oxygen radical, e.g. superoxide radical. Doublet EPR signal with g-factors 2.0058 and 2.0018 (Figure 1) was obtained for both assemblies and associated with the formation of superoxide radical through the sorption of oxygen molecules on the supramolecular oxygen matrix and electron transfer to it under UV-visible irradiation.

Despite the non-advanced surface of 1,3-dimethylbarbituric acid and melamine assembly crystals (Figure 1), experiments with vacuum showed that degassing the samples causes complete disappear of EPR spectra. It is associated with the weakly sorbed paramagnetic oxygen detachment. However, some diamagnetic oxygen species are stronger chemisorbed as light irradiation in vacuum leads to a formation of new radical centers.

Thus, the alkylation of barbituric acid leads to a significant transformation of binary supramolecular assembly with melamine followed by drastic morphology and surface change and opens a way of two-cycle radical formation through samples degassing and further UV-visible light irradiation.

1. Y. Shu, A. Mikosch, K. Winzenberg, P. Kemppinen, C. Easton, A. Bilic, C. Forsyth, C. Dunn, Th. Singh and G. Collis, *Journal of Materials Chemistry C*, 2014, 2, 3895-3899.
2. V. V. Shilovskikh, A. A. Timralieva, E. V. Belogub, E. A. Konstantinova, A. I. Kokorin and E. V. Skorb, *Applied Magnetic Resonance*, 2020, 51, 939-949.
3. V. V. Shilovskikh, A. A. Timralieva, P. V. Nesterov, A. S. Novikov, P. A. Sitnikov, E. A. Konstantinova, A. I. Kokorin and E. V. Skorb, *Chemistry – A European Journal*, 2020, 26, 16603-16610.
4. A. A. Timralieva, I. V. Moskalenko, P. V. Nesterov, V. V. Shilovskikh, A. S. Novikov, E. A. Konstantinova, A. I. Kokorin and E. V. Skorb, *ACS Omega*, 2023, 8, 8276-8284

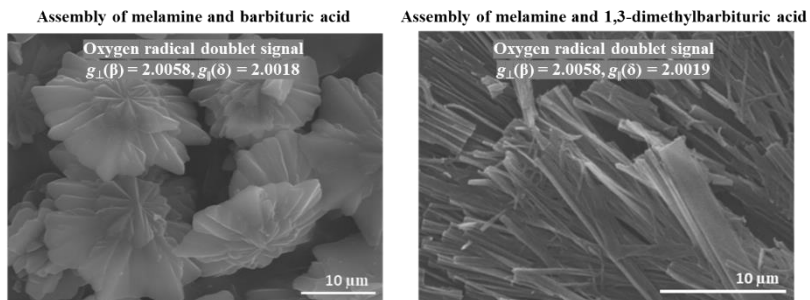


**Fig. 1.** Morphology changes of melamine-based assembly and preservation of oxygen radical EPR doublet signal due to N-methylation of barbituric acid.

# POSTERS

## **The Dipole-Dipole Interaction Contribution to EPR Spectra of Nitroxyl Free Radical Solution**

**M.M. Bakirov, I.T. Khairutdinov , R.B. Zaripov, K.M. Salikhov**

Zavoisky Physical-Technical Institute, FRC Kazan Scientific Center of Russian Academy of Sciences,  
Kazan 420029, Russia, pinas1@yandex.ru

Nitroxide free radical in 60% water glycerol solution are studied to separate a dipole-dipole contribution due to bimolecular collisions between radicals and another one due to rotational modulation of interactions between the unpaired electron and the magnetic nucleus in a single radical. The last contribution is not well studied. The third mechanism that contribute to spin coherence transfer is Heisenberg Spin Exchange. There is three mechanisms that require separation.

New protocol was used to analyze radical concentration and temperature dependences of dispersion contribution to EPR spectra. The manifestation of dispersion in form of resonance lines of EPR spectrum in solutions, caused by random modulation of the resonance frequency of electron spin by process of spin-lattice relaxation of nuclear spin are shown experimentally. For  $^{15}\text{N}$  nitroxide free radical solution modified kinetic equations for the magnetization of spins were constructed, that take into account three contributions to decoherence of spins of unpaired electrons and to transfer of quantum coherence of spins in different components of the hyperfine structure of the EPR spectrum.

## New Fe(III) complexes of NNO tridentate $\beta$ -enaminone in solutions: EPR research and molecular docking

**E.E. Batueva<sup>1</sup>, A.R. Sharipova<sup>2</sup>, E.N. Frolova<sup>2</sup>, O.A. Turanova<sup>2</sup>,  
L.I. Savostina<sup>2</sup>, R.B. Zaripov<sup>2</sup>, A.N. Turanov<sup>2</sup>**

<sup>1</sup> KFU Kazan (Volga region) Federal University, Kazan, Russia

<sup>2</sup> Zavoisky Physical-Technical Institute, FRC Kazan Scientific Center of RAS, Kazan, Russia

Preliminary quantum chemical calculations of the interaction between potential biologically active complexes with biological macromolecules are necessary for the development of new therapeutic reagents. Since biological processes in organisms mainly occur in solutions, it is of interest to study the effect of solvation on the structure of synthesized metal complexes.

The results of the study of the properties of solutions of new Fe(III) complexes with tridentate  $\beta$ -enaminones with the composition  $[\text{FeL}_2]\text{Y}$  ( $\text{L} = 1$ -phenyl-3-(quinolin-8-ylamino)prop-2-en-1-onato, and  $\text{Y} = \text{PF}_6, \text{SbF}_6$ ), modeling their interaction with DNA and the urease of *Helicobacter pylori* (*H-Pylori*) using molecular docking programs AutoDockTools [1] and AutoDock Vina [2] have been considered in this work.

The leveling of the structural differences between the studied complexes with different counterions in solutions has been revealed by the EPR method. This is due to the dissociation of coordination compounds, the destruction of intermolecular interactions forming channels of indirect exchange between Fe(III) ions in molecular crystals and the formation of new exchange channels with solvent molecules. The parameters of the basic low-spin electron state for the studied complexes in molecular crystals and vitrified solutions have been determined.

The studied docking conformation of the complex has been selected based on the calculated binding probability of the complex to DNA and *H-Pylori*. The information and types of interactions between the complex and DNA are shown in Fig. 1a, while Fig. 1b illustrates the interactions between the complex and *H-Pylori*. Affinities of the complexes for DNA has been 8.1 kcal/mol and 9.1 kcal/mol for *H-Pylori*.

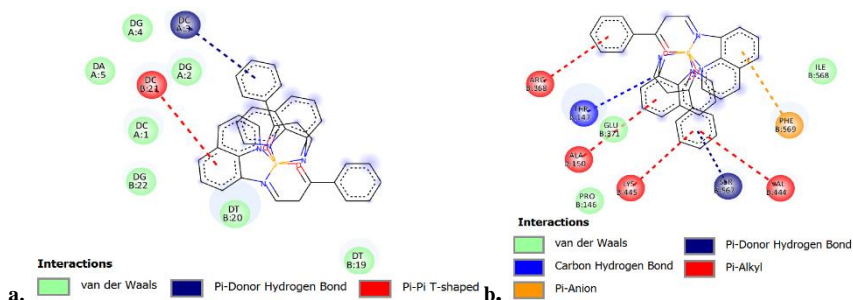


**Fig. 1.** 2D graph showing various interactions and interacting residues: **a)** DNA with Fe(III) complex; **b)** *H-Pylori* with Fe(III) complex

1. AutoDockTools. G.R. Nielubowicz, H.L.T. Mobley, Nat. Rev. Urol. 7(8), 430–441 (2010)
2. O. Trott, A.J. Olson, J. Comput. Chem 31(2), 455–461 (2010)



## Heptanuclear Fe(II)–Fe(III) complex as a multifunctional magnetic material

**E.E. Batueva<sup>1</sup>, A.R. Sharipova<sup>2</sup>, E.N. Frolova<sup>2</sup>, A.A. Sukhanov<sup>2</sup>,  
O.A. Turanova<sup>2</sup>, A.N. Turanov<sup>2</sup>**

<sup>1</sup> KFU Kazan (Volga region) Federal University, Kazan, Russia

<sup>2</sup> Zavoisky Physical-Technical Institute, FRC Kazan Scientific Center of RAS, Kazan, Russia

Iron complexes with Schiff bases, exhibiting spin-crossover and ferromagnetic properties, are promising for the creation of new materials controlled by external factors (temperature, pressure, irradiation, *etc.*). We have recently shown by magnetometry and CW EPR methods that the heptanuclear mixed-valence complex  $[\text{Fe(II)(CN)}_6\{\text{Fe(III)(L)}\}_6]\text{X}_2$ , where L = dianion N,N-bis(1-hydroxy-2-benzyliden)-1,7-diamino-4-azaheptane, X = NCS, exhibits spin-crossover properties ( $S = 1/2 \leftrightarrow 5/2$ ).

This work presents the results of the influence of laser radiation with wavelengths of 355 and 580 nm on the properties of this complex according to CW and TR EPR data. It was found that the intensity of the lines in CW EPR spectra of the iron ion decreases symbatically by  $\sim 35\%$  upon irradiation at  $T = 20$  K. This may be due to the ligand-metal electron transfer and the formation of a metastable state, which is not recorded in the spectra due to the short lifetime. The option of the transition of iron ions to a state with a spin of  $3/2$  cannot be excluded. The polarized signal in the form of emission was observed in TR EPR spectra after a laser pulse at  $T = 25$  K. The shape of the spectrum changed, and both emission and absorption signals were observed at  $T = 40$  K.

The  $[\text{Fe(II)(CN)}_6\{\text{Fe(III)(L)}\}_6]\text{X}_2$  complex may be promising as a contrast agent in MRI due to its large magnetic moment  $\mu = 14.5 \mu_B$ . The longitudinal relaxation time of HDO in a colloidal solution of this molecular magnet with SDS was measured by  $^1\text{H}$  NMR spectroscopy at various concentrations, and its relaxivity was also calculated.

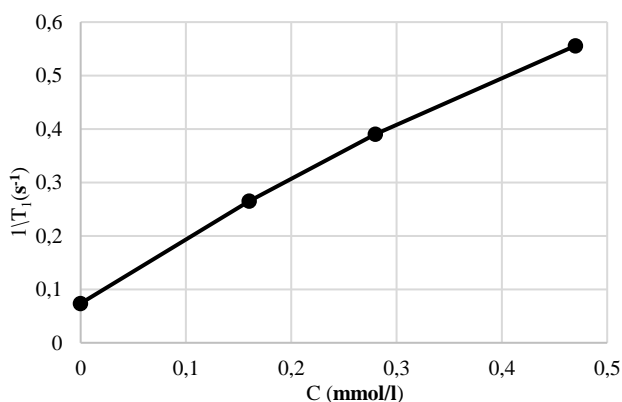


Fig. Relaxivity of the water (HDO) signal at different concentrations of the iron complex

## ***AB INITIO* INVESTIGATION OF RASHBA SPLITTING HETEROSTRUCTURES FOR SPINTRON APPLICATIONS**

**A.A. Evseev<sup>1</sup>, I.I. Gumarova<sup>1</sup>, O.V. Nedopekin<sup>1</sup>**

<sup>1</sup> Institute of Physics, Kazan Federal University, Kazan, Russia

Materials used in spintronic devices and for detecting Majorana fermions in solids must have significant and ideal Rashba-type spin-orbit splitting. Recently, a combination of ordered surface fusion and interface engineering, that is, the growth of alloy monolayers on a polar insulating surface, has been proposed [1]. The Rashba effect is defined as the spin-orbit splitting at surfaces/interfaces due to inversion symmetry breaking [2].

In this work, we studied film heterostructures with various combinations of components, which, as expected, would have a Rashba-type spin-orbit splitting [2, 3]. In these heterostructures, due to the electron density gradient at the interfaces, an eddy current associated with electron spins arises. The structural and electronic properties of these systems were investigated. An electronic calculation of DFT+U was carried out taking into account the spin-orbit interaction. All calculations were performed using the VASP program [4], integrated into the MedeA software [5].

For heterostructures CuO/Cu, Cu<sub>3</sub>N/Cu, Bi/BaTiO<sub>3</sub>, Bi/PbTiO<sub>3</sub>, Bi/HfO<sub>2</sub>, La/BaTiO<sub>3</sub>, La/PbTiO<sub>3</sub>, band structures were calculated taking into account the spin-orbit interaction, and on this basis the values of the Rashba parameter were obtained  $\alpha_R$ , which characterizes the magnitude of spin-orbit splitting [6]. The influence of interfacial contact layers, drainage parameters, thickness, interface polarity and ferroelectric polarization on the values of the Rashba parameter was investigated.

The results of this study can be used in the development of functional materials for spintronics based on the properties of these compounds.

Calculations were supported by the Kazan Federal University within the Laboratory of Computer design of new materials and machine learning.

1. Chen M. and Liu F.: Natl. Sci. Rev. **8** (2021).
2. Rashba E.I. and Sheka V.I.: Fiz. Tverd. Tela – Collected Papers (Leningrad) **II**, 162–176 (1959) (in Russian).
3. Caviglia A.D., Gabay M., Gariglio S. et al.: Phys. Rev. Lett. 126603 (2010).
4. Kresse G. and Furthmüller J.: Phys. Rev. B **54**, 11169–11186 (1996).
5. MedeA version 3.; MedeA is a registered trademark of Materials Design, Inc., San Diego, USA.
6. Bychkov Yu. A. and Rashba E. I.: Sov. Phys. - JETP Lett. **39**, 78–81 (1984) (in Russian).

## Impact of spin correlations on resistivity and microwave absorption of iron pnictides doped with cobalt

**I.I. Gimazov<sup>1</sup>, D.E. Zhelezniakova<sup>1,2</sup>, Yu.I. Talanov<sup>1</sup>**

<sup>1</sup>Zavoisky Physical-Technical Institute, FRC Kazan Scientific Center of RAS, Kazan, Russia

<sup>2</sup>Kazan Federal University, Kazan, Russia

In iron arsenide compounds, superconductivity occurs near the antiferromagnetic phase, which may indicate the magnetic nature of this state [1]. With increasing temperature in iron pnictides, a magnetic transition precedes a structural transition from an orthorhombic to a tetragonal lattice. During the transition to the orthorhombic phase, the rotational symmetry of the crystal lattice is broken, and all parameters of the crystal obtain  $C_2$  symmetry. The symmetry breaking is detected as resistivity anisotropy of  $\rho_a$  and  $\rho_b$  [2], and also as enhancement of anisotropic magnetic fluctuations in neutron studies [3]. In the literature, such a state with anisotropy of the corresponding  $C_2$  symmetry, formed due to elongated electronic and magnetic formations, is usually called nematic ordering.

In our work, to study the transport properties of iron pnictides, the temperature dependences of resistivity at direct current and microwave absorption at a frequency of  $10^{10}$  Hz were obtained (Fig. 1). Analysis of the results obtained for samples with different cobalt concentrations (from overdoped to underdoped) suggested that the deviation of  $\rho(T)$  and  $A_{MWA}(T)$  from the linear behavior below 100 K is not related to transition to the Fermi liquid regime, but is associated with the emerging nematic fluctuations.

1. Wang. X.F., et al.: Phys. Rev. Lett. **102**, 117005 (2009)

2. Ishida S., et al.: Phys. Rev. Lett. **110**, 207001 (2013)

3. Wang. Q., et al.: Nature Comm. 7, 12182 (2016).

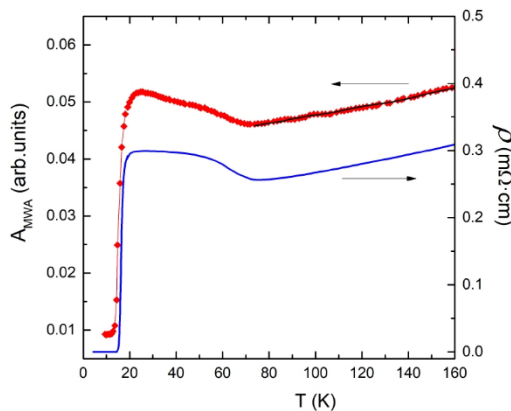


**Fig. 1.** Temperature dependences of microwave absorption (left) and resistivity (right) for an underdoped sample.

## EPR in polymer composites with carbon black

A.M. Zyuzin<sup>1</sup>, K.E. Igonchenkova<sup>1</sup>, A.A. Karpeev<sup>1</sup>, N.V. Yantsen<sup>1</sup>,  
S.S. Gostyushov<sup>1</sup>.

<sup>1</sup> National Research Mordovia State University, Saransk, Russia

In this work, the main characteristics of EPR spectra in composites based on an ethylene vinyl acetate matrix filled with technical carbon (CB) brands C40 and P267E are investigated. The composites were obtained by mixing on a laboratory extruder and subsequent pressing. The CB content of one and the other brands varied from 5 to 35% wt. (mass fractions). The spectra were recorded at a frequency of 9.4 GHz in the temperature range of 77÷420 K.

The identification of the nature of paramagnetic centers (PC) and the features of their states in carbon structures seems to be an urgent task despite the large number of works devoted to this topic [1, 2]. Depending on the technology of obtaining carbon material, the nature of paramagnetic centers can be significantly different. The structure of the particle surface and its features significantly affect the conductivity of composites in which they are used as a filler. The main possible types of PC in carbon black include: conduction electrons in CB particles and their agglomerates, broken C-C bonds, especially at the boundaries of graphite planes, which can be both broken valences and attached, for example, oxygen or OH-groups. Each of the listed types of PC will determine its own set of line parameters, as well as their temperature and concentration dependences. The relaxation time of the corresponding spin system and, consequently, the width of the EPR line will depend on the nature of the unpaired spin and its environment. Depending on which uncompensated spins cause resonant absorption, free electrons or localized ones, magnetic susceptibility will obey the Pauli or Curie-Weiss laws, respectively. In the general case, when several types of paramagnetic centers contribute to resonant absorption, the expression for magnetic susceptibility can be written as:

$$\chi'' = \chi_p'' + \frac{C}{T - \Theta}$$

where  $\chi_p''$  is the Pauli susceptibility,  $C$  is the Curie constant, and  $\theta$  is the Weiss constant.

The conducted researches has allowed us to establish the following. In both composites with C40 and with P267E, the spectra consisted of a single line with a shape close to Lorentzian, with g-factor values close to 2, while the line width  $\Delta H_{pp}$  differed by about an order of magnitude and amounted to  $\sim 37$  Oe and 4.3 Oe, respectively. The next difference was that in composites with C40, with an increase in temperature from 77 K to 295 K, there was a slight ( $\sim 10\%$ ) decrease in  $\Delta H_{pp}$ , in samples with P267E, on the contrary, an increase of approximately 15% was observed. This behavior occurred for composites in the entire studied range of CB concentrations. There was also a slight decrease in  $\Delta H_{pp}$  at high concentrations of CB.

Temperature studies have allowed us to establish the following. With an increase in the temperature of the samples from 77 K to 295 K, the area under the absorption

line curve, which for the Lorentz line can be expressed as  $S \sim I' \cdot \Delta H_{pp}^2$ , where  $I'$  is the amplitude of the derivative, decreased by about 4 times, which corresponds to Curie's law for the temperature dependence of localized PC and indicates the invariance of their total concentration with temperature change. Only the difference in the population of energy levels in the magnetic field changes in accordance with the Boltzmann distribution. In composites with C 40, the decrease in  $S$  with a change in  $T$  from 77 K to 295 K was significantly lower  $S(77)/S(295)=1.5$ . This behavior can be explained either by an increase in the total concentration of PC in such samples, or by the presence of a more efficient exchange interaction between localized PC and conduction electrons in CB particles.

Thus, the detected differences in the values of  $\Delta H_{pp}$  and the behavior of  $S(T)$  allow us to conclude that there is a significant difference in the nature of paramagnetic centers in CB brands C40 and P267E.

1. Chipara M., Brittain W.J., Lau K., Chipara M.D.: *Polymers & Polymer Composites* 16, 519–526 (2008)
2. Weinger A.I., Shanina B.D., Danishevsky A.M., Popov V.V., Gordeev S.K., Grechinskaya A.V.: *Physics of the Solid State* 45, 1197-1206 (2003)

## Magneto resonant properties and spin-Hall effects in epitaxial $\text{Pd}_{1-x}\text{Fe}_x$ and $\text{Pd}_{1-x}\text{Fe}_x/\text{Pt}$ thin film structures

**Zh.K. Pulotov<sup>1</sup>, A.K. Kadikova<sup>1</sup>, B.F. Gabbasov<sup>1</sup>, I.V. Yanilkin<sup>1</sup>,  
A.I. Gumarov<sup>1</sup>, A.G. Kiiamov<sup>1</sup>, L.R. Tagirov<sup>1,2</sup>, R.V. Yusupov<sup>1</sup>**

<sup>1</sup>Kazan Federal University, Kazan, Russian Federation

<sup>2</sup>Zavoisky Physical-Technical Institute, Kazan, Russian Federation

Spin-Hall effects (SHE) are phenomena originating from the coupling of charge and spin currents in media with strong spin-orbit interaction. SHE consists in the occurrence of a spin current during the flow of a charge current, which leads to a spatial redistribution of charge carriers (electrons) with oppositely directed spins. In elements of superconducting spintronics, this would provide a possibility to switch the magnetization of the ferromagnetic layer without an involvement of a magnetic field. Functioning of superconducting elements is possible only at cryogenic temperatures, therefore one of the most promising materials for ferromagnetic layers is a solid solution of palladium and iron. Magnetic ordering in these materials occurs at temperatures much lower than the room temperature. We did not find any studies of spin-Hall effects in structures with magnetic layers based on Pd-Fe alloys, so the subject of the studies presented in this work was the direct and inverse spin-Hall effects (ISHE) in heteroepitaxial thin-film structures of  $\text{Pd}_{0.90}\text{Fe}_{0.10}/\text{Pt}$  and  $\text{Pd}_{0.88}\text{Fe}_{0.12}/\text{Pt}$  and their magneto resonant properties.

$\text{Pd}_{0.90}\text{Fe}_{0.10}$ ,  $\text{Pd}_{0.90}\text{Fe}_{0.10}/\text{Pt}$ ,  $\text{Pd}_{0.88}\text{Fe}_{0.12}$  and  $\text{Pd}_{0.88}\text{Fe}_{0.12}/\text{Pt}$  thin film structures were synthesized by molecular-beam epitaxy. Structural studies by low-energy electron diffraction (LEED) and X-ray diffraction (XRD) methods revealed the epitaxial nature of these structures. XRD analysis revealed a total mixing of Pt and Pd-Fe layers of the  $\text{Pd}_{0.90}\text{Fe}_{0.10}/\text{Pt}$  bilayer during annealing at 800°C for 1 h, which was not observed in the  $\text{Pd}_{0.90}\text{Fe}_{0.10}/\text{Pt}$  sample, for which the Pt-layer was deposited at a substrate temperature of 300 degrees C. Mixing of the Pt and Pd-Fe layers was confirmed by the ferromagnetic resonance (FMR) spectroscopy: the lines revealed a significant broadening and a reduction of the magnetization compared with the FMR spectra of the as-deposited heteroepitaxial  $\text{Pd}_{0.90}\text{Fe}_{0.10}/\text{Pt}$  structure. Studies of the  $\text{Pd}_{0.88}\text{Fe}_{0.12}/\text{Pt}$  sample by FMR revealed a broadening of the absorption line compared to the resonance line of a single  $\text{Pd}_{0.88}\text{Fe}_{0.12}$  layer, which was attributed to losses due to the generation of charge currents in the normal metal under spin pumping conditions as a result of the ISHE. Investigation of the orientation dependences of the FMR spectra of samples  $\text{Pd}_{0.90}\text{Fe}_{0.10}$  and  $\text{Pd}_{0.88}\text{Fe}_{0.12}$  confirmed the trend of decreasing magnetocrystalline anisotropy constants with iron content increase, which is opposite to previously investigated Pd-Fe alloy films with iron below 8 at. % [1]. The  $\text{Pd}_{0.88}\text{Fe}_{0.12}$  thin film is characterized by the presence of uniaxial magnetocrystalline anisotropy of small magnitude equal to  $K_u = -6,3 \cdot 10^3 \text{ erg/cm}^3$ , characteristic of ferromagnetic thin films, and zero in-plane anisotropy. The sample  $\text{Pd}_{0.90}\text{Fe}_{0.10}$  has uniaxial magnetocrystalline anisotropy and small values of anisotropy constants in the sample plane, the values of which will be presented.

Experiments have been carried out to observe a direct and inverse spin-Hall effects in the heteroepitaxial structure  $\text{Pd}_{0.88}\text{Fe}_{0.12}/\text{Pt}$ . SHE is manifested in the observation of FMR spectra when an alternating electric current is passed through the

sample instead of modulating the magnetic field. SHE leads in these conditions to the modulation of the magnetization value of the ferromagnetic layer and, accordingly, to the shift of the resonance line. In experiments with a  $\text{Pd}_{0.88}\text{Fe}_{0.12}/\text{Pt}$  bilayer heteroepitaxial structure, an estimate of the effective magnetic field modulation of 50 mG was obtained when an alternating in-plane electric current with an amplitude of 5 mA was passed through the heterostructure. However, the passage of a charge current through the heterostructure, in addition to the occurrence of the desired spin Hall effect, also leads to the generation of an alternating magnetic field due to electromagnetic induction (Oersted field). To establish the fact of SHE manifestation, the spatial distribution of the magnetic field generated by the electric current in the ferromagnetic layer  $\text{Pd}_{0.88}\text{Fe}_{0.12}$  of the  $\text{Pd}_{0.88}\text{Fe}_{0.12}/\text{Pt}$  bilayer heteroepitaxial structure was calculated. Comparison of the magnetic field value obtained from the calculation with the effective modulation field showed that at least 70% of the effective modulation field is due to SHE. SHE studies in  $\text{Pd}_{0.90}\text{Fe}_{0.10}/\text{Pt}$  heterostructure will be presented at poster.

The inverse spin-Hall effect (ISHE) manifests itself in the voltage generation in the course of spin-dependent scattering of electrons under spin pumping conditions. A voltage signal of the order of 1  $\mu\text{V}$  was detected from the ISHE of a  $\text{Pd}_{0.88}\text{Fe}_{0.12}/\text{Pt}$  heteroepitaxial structure at temperatures from 20 to 150 K. A weak dependence of the voltage amplitude on the sample temperature is observed. This, in our opinion, is due, on the one hand, to a decrease in magnetization with increasing temperature, thus reducing the spin current under conditions of spin pumping, and on the other hand, the sample is a metal, whose resistance increases with increasing temperature. Thus, the two effects cancel each other out in a given temperature range. The Hall angle for platinum was calculated, which at a temperature of 20 K was:  $\alpha_{\text{SHE}} = (0.35 \pm 0.02) \%$ . The Hall angle is the conversion coefficient between the charge and spin currents.

I. Yanilkin I.V., Yusupov R.V. et al.: Epitaxial thin-film  $\text{Pd}_{1-x}\text{Fe}_x$  alloy: a tunable ferromagnet for superconducting spintronics. *Science China Materials* **63**, p. 1-10 (2020)

## Magnetotransport Investigation of Pb/Bi<sub>1.08</sub>Sn<sub>0.02</sub>Sb<sub>0.9</sub>Te<sub>2</sub>S Heterostructures

**V.O. Sakhin, E.F. Kukovitsky, I.I. Gimazov, A.A. Kamashev,  
N.N. Garif'yanov, Yu. I. Talanov**

Zavoisky Physical-Technical Institute, FRC Kazan Scientific Center of RAS, Kazan, Russia

Topological insulators (TI) are known for their conductive surface properties. The combination of TI and superconductor properties in one system promises to introduce an intriguing phenomenon: topological superconductivity [1]. This specific type of superconductivity is proposed for use in quantum computing to create qubits [2]. However, achieving topological superconductivity is a complicated task. Among various approaches, we have chosen to create a heterostructure and investigate the proximity effect between a thin layer of metallic superconductor and a 3D topological insulator.

We have created a series of superconductor-topological insulator heterostructures by depositing a thin Pb layer on the surface of Bi<sub>1.08</sub>Sn<sub>0.02</sub>Sb<sub>0.9</sub>Te<sub>2</sub>S (BSSTS) flakes. Pb was chosen due to its relatively high bulk  $T_C=7.2$  K and it is known to be successfully deposited on the surface of bismuth chalcogenides [3]. A popular choice for TI in such heterostructures is Bi<sub>2</sub>Se<sub>3</sub> or Bi<sub>2</sub>Te<sub>3</sub> [4], but in our approach we have used BSSTS due to its low bulk carrier concentration. Because of this the transport properties of BSSTS at  $T<100$  K are determined by surface contribution.

The proximity effect in the Pb/BSSTS heterostructure was studied mainly using the standard four-probe technique. Additionally, we have used the non-resonant microwave absorption method because the amplitude of microwave absorption is known to be proportional to sample resistance [5]. This allows us to measure the resistance of the sample at high frequency (X-band, 9.6 GHz). We obtained temperature and magnetic field dependences of resistance for heterostructures with varying Pb layer thicknesses. When the Pb layer thickness is smaller than 30 nm it becomes fractured and a continuous superconducting channel through the lead layer is not formed. Contrary to what one may suppose, this doesn't lead to decrease of  $T_C$ , it remains close to that of bulk Pb. Moreover, samples with discontinuous thin Pb layer exhibit complex superconducting transition which we believe to be a sign of superconducting correlations in the topological insulator surface layer. To study proximity effect in such system series of heterostructures was created using masks, allowing us to controllably create separate Pb islands on the surface of BSSTS.

1. Hosur P., Ghaemi P., Mong R., Vishwanath A., PRL **107** 097001 (2011)
2. Fu L., Kane C. L., Phys. Rev. Lett. **100** 096407 (2008)
3. Stolyarov V., Pons S., Vlaic S., Remizov S. et al., J. Phys. Chem. Lett. **12** 9068 (2021)
4. Surnin Y., Klimovskikh I., Sostina D., Kokh K., Tereshchenko O., Shikin A., JETP **126** 535 (2018)
5. Golosovsky M., Monod P., Mududli P.K. et al., Phys. Rev. **76** 184414 (2007)



## COMPUTER DESIGN OF NEW ORGANIC MATERIALS FOR METAL-ION BATTERIES

**A.I. Shamsieva<sup>1</sup>, I.I. Gumarova<sup>1</sup>**

<sup>1</sup> Institute of Physics, Kazan Federal University, Kazan, Russia

Covalent Organic Frameworks are a class of polymers with a high structural order. Unlike conventional polymers, the structure of COF can be pre-designed, and various combinations of monomers and bonds allow the synthesis of COF with limited molecular space, regular crystal structure and precise pores, creating an interface for interaction with electrons, ions and molecules. Due to their molecular diversity and functional design, COFs can be used in particular as efficient energy storage materials. In today's world, highly efficient batteries that can withstand high charges, have a long service life and remain stable are very important. One promising option is the use of porous organic polymers, which have advantages such as light weight, flexibility, environmental friendliness, stability and ease of structure optimization. Covalent organic frameworks are environmentally friendly, have controlled theoretical capacitances and redox potentials, making them attractive as electrode materials. They can play an important role in the development of electrodes due to their flexible structure, permeable framework and diverse functional groups.

In this work, the structures of covalent triazine frameworks were studied as electrodes for the accumulation, storage and conversion of energy for the purpose of its further use. Covalent triazine frameworks are a promising subclass of covalent organic frameworks for use as electrode materials in lithium-ion batteries. Their exceptional chemical and physical stability, provided by rigid triazine bonds, guarantees excellent cyclic stability. The inclusion of ions such as fluorine, silicon and other ions can significantly improve energy storage capabilities. By comparing the pristine and doped CTF structures, the geometric properties, chemical/thermal stability, open circuit voltage, theoretical specific capacitance, volume change rate, and diffusion behavior of lithium ions were studied. In addition, the electronic properties were assessed by studying the partial density of states, electronic band structure and charge transfer analysis. The results of this work provide information on the effect of joint doping of fluorine and silicon on the electrochemical properties of CTFs as anode materials for lithium-ion batteries.

1. Lv X., Li F., Gong J., Gu J., Lin S., Chen Z. :Phys. Chem. Chem. Phys., **22**, 8902–8912 (2020).

2. Xu, J., Xu Y., Lai C., Xia T., Zhang B., Zhou X. - Science China Chemistry, **64**, 1267–1282 (2021).

## OBSERVATION OF A GRIFFITHS PHASE AND ANALYSIS OF THE CRITICAL EXPONENTS IN THE MAGNETIC BEHAVIOR OF $\text{La}_{0.7}\text{Sr}_{0.3}\text{Mn}_{0.9}\text{Fe}_{0.1-x}\text{Zn}_x\text{O}_3$ ( $x = 0.05, 0.075, 0.1$ )

**A.V. Shestakov<sup>1</sup>, Z.Y. Seidov<sup>2</sup>, I.V. Yatsyk<sup>3</sup>, A.S. Ovchinnikov<sup>4</sup>,  
F.G. Vagizov<sup>5</sup>, V.A. Shustov<sup>3</sup>, A.G. Badelin<sup>6</sup>, V.K. Karpasyuk<sup>6</sup>,  
H.-A. Krug von Nidda<sup>7</sup>, R.M. Eremina<sup>3</sup>**

<sup>1</sup>Prokhorov General Physics Institute of the RAS, Moscow, Russia

<sup>2</sup>Institute of Physics, Ministry of Science and Education, Baku, Azerbaijan

<sup>3</sup>Zavoisky Physical-Technical Institute, FRC Kazan Scientific Center of RAS, Kazan, Russia

<sup>4</sup>Institute of Natural Sciences and Mathematics, Ural Federal University, Ekaterinburg, Russia

<sup>5</sup>Institute of Physics, Kazan Federal University, Kazan, Russia

<sup>6</sup>Astrakhan State University, Astrakhan, Russia

<sup>7</sup>Experimental Physics V, Center for Electronic Correlations and Magnetism, University of Augsburg, Augsburg, Germany

The magnetic properties and the critical behavior in  $\text{La}_{0.7}\text{Sr}_{0.3}\text{Mn}_{0.9}\text{Fe}_{0.1-x}\text{Zn}_x\text{O}_3$  ( $x = 0.05, 0.075, 0.1$ ) have been investigated by dc susceptibility and magnetization measurements. All samples show a paramagnetic-to-ferromagnetic phase transition. The Curie temperature  $T_C$  decreases on increasing Fe content. The Griffiths phase is identified by the downturn of the inverse susceptibility versus temperature plot from the Curie-Weiss law ( $T_G \approx 364\text{K}$ ), which is best visible in case of small external magnetic fields, but suppressed with the increase of the field strength due to saturation of its magnetization contribution. The critical properties of  $\text{La}_{0.7}\text{Sr}_{0.3}\text{Mn}_{0.9}\text{Fe}_{0.1-x}\text{Zn}_x\text{O}_3$  ( $x = 0.05, 0.075, 0.1$ ) were investigated by analysis of the magnetization measurements in the vicinity of their critical temperature. By means of Arrott plots, the nature of the magnetic transition is found to be of second order. The critical exponents  $\beta$ ,  $\gamma$  and  $\delta$  were evaluated using modified Arrott plots (MAP) [1]. The values of the critical exponents for the doped compounds are in fair agreement with the 3D-Heisenberg model. Slight deviations of  $\beta$  and  $\gamma$  from the exact theoretical values may be due to the presence of the Griffiths phase.

1. Arrott A. and Noakes J. E.: Phys. Rev. Lett. **19**, 786 (1967).

## HIGH TEMPERATURE ESR ABSORPTION of $\text{Fe}_{45}\text{Co}_{30}\text{Si}_{10}\text{B}_{15}$ MICROWIRE

A.V. Shestakov<sup>1</sup>, I.I. Fazlizhanov<sup>2</sup>, R.M. Eremina<sup>2</sup>,  
S.V. Demishev<sup>3</sup>, V.V. Rodionova<sup>4</sup>, V.G. Kolesnikova<sup>4</sup>

<sup>1</sup>Prokhorov General Physics Institute of the RAS, Moscow, Russia

<sup>2</sup>Zavoisky Physical-Technical Institute, FRC Kazan Scientific Center of RAS, Kazan, Russia

<sup>3</sup>Institute for High Pressure Physics of the RAS, Troitsk, Moscow, Russia

<sup>4</sup>Immanuel Kant Baltic Federal University, Kaliningrad, Russia

Thin ferromagnetic metallic glass-coated microwire of  $\text{Fe}_{45}\text{Co}_{30}\text{Si}_{10}\text{B}_{15}$  was produced by the Taylor-Ulitovsky method under water or air cooling. It demonstrated various types of the magnetization reversal: bistable, stepwise, and S shape with a highly enhanced coercivity [1]. It was found that a system of Co-based microwires with nearly zero magnetostriction coefficient exhibits a step-like hysteresis loop [2]. The hysteresis loops of microwires magnetostrictive exhibit strong sensitivity to the ratio  $d/D$  [3]. The influence of post-processing conditions on the magnetic properties of amorphous and nanocrystalline microwires have been thoroughly analyzed, paying attention on the influence of magnetoelastic, induced and magnetocrystalline anisotropies on the hysteresis loops of Fe-, Ni- and Co-rich microwires [4].

Using the EPR equipment (Varian-12, X-band 9.48 GHz), first derivative of microwave absorption spectra were obtained at temperatures from 290 to 620 K and in magnetic fields up to 10 kOe (Fig. 1a). The microwire was located vertically in the central part of the rectangular resonator ( $\text{TE}_{102}$ ), i.e. along the MW magnetic component and perpendicular to the external magnetic field. The spectrum shows two pairs of lines, probably parallel and perpendicular components of the ferrimagnetic resonance from the core-shell phases. At temperatures above 1400–1800 K, the core and shell transform into a paramagnetic state (Fig. 1b).

5. Rodionova V.V., Baraban I.A., Panina L.V., Bazlov A.I., Perov N.S.: IEEE Trans. of Magn. **99**, 1-6 (2018)

6. Rodionova V.V. et al.: J Supercond Nov Magn. **28**, 977-981 (2014)

7. Zhukov A., Ipatov M., Zhukova V.: Abstract II-Moscow Readings (MISIS), Chernogolovka **62** (2011)

8. Zhukova V. et al.: Opt. of Magn. Properties of Magn. Microwires by Post-Processing **8**, 1006 (2020)

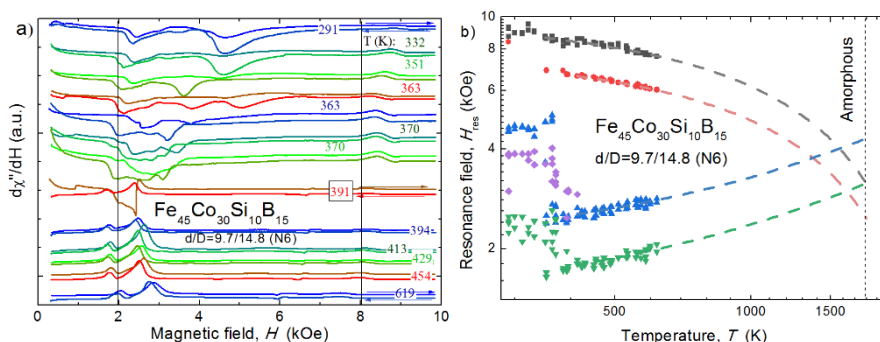


**Fig. 1.** (a) Magnetic resonance spectrum in  $\text{Fe}_{45}\text{Co}_{30}\text{Si}_{10}\text{B}_{15}$  microwire at  $290 \leq T(\text{K}) \leq 620$  (b) temperature dependence of line positions.

## STUDY of LOW-TEMPERATURE SPIN FLUCTUATION TRANSITION in the CONICAL PHASE of MnSi and ANISOTROPY FEATURES

**S.V. Demishev<sup>1</sup>, A.V. Shestakov<sup>2</sup>, I.V. Yatsyk<sup>3</sup>,  
R.M. Eremina<sup>3</sup>, A.V. Semeno<sup>2</sup>, S.V. Grigoriev<sup>4</sup>**

<sup>1</sup>Institute for High Pressure Physics of the RAS, Troitsk, Moscow, Russia

<sup>2</sup>Prokhorov General Physics Institute of RAS, Moscow, Russia

<sup>3</sup>Zavoisky Physical-Technical Institute, FRC Kazan Scientific Center of RAS, Kazan, Russia

<sup>4</sup>Petersburg Nuclear Physics Institute of NRC «Kurchatov Institute», Gatchina, Russia

Spin fluctuation transitions (SFTs) constitute a novel and interesting direction of research in the field of various magnetic materials [1]. One of the possible experimental tools for studying SFT is electron spin resonance (ESR) line width, as long as just this parameter provides information about spin fluctuations magnitude [1,2]. A promising object for the realization of the spin fluctuation transitions is the spiral magnet, MnSi, known for its rich physics related to the formation of skyrmion states and the dynamic reorientation of spins with varying temperatures [3]. Indirect evidence for exist SFT in MnSi was recently demonstrated in Ref. [4], where the high-frequency (60 GHz) ESR study of the spiral magnet MnSi was performed. The authors described the ESR spectrum with only one line, the temperature dependence of which showed two characteristic temperatures of 15 and 25 K, where a change in the nature of its behavior was observed. The SFT point, characterized by additional broadening of the ESR line width accompanied by a change in the ESR line position, was detected at temperatures much lower than the transition temperature into spin-polarized phase (field induced ferromagnetic phase). In the seminal work [5], the H-T diagram consists of paramagnetic (P), spiral (S), conical spiral (C), and spin polarized (SP) magnetic phases. The transition C→SP (at  $T \ll T_C$ ) occurs at ~6 kOe [6]. Therefore, in view of the aim of our study, the ESR experiment should be performed at relatively low frequencies and, consequently, at low magnetic fields, which allow probing the conical spiral phase.

A Bruker EMXplus spectrometer was used to record ESR spectra in the X range at a frequency of ~9.3 GHz in the temperature range of 5–30 K (external magnetic field oriented along the crystallographic direction [100]) and at different angles (at 5 and 15 K). The measured ESR spectrum  $d\chi''/dH$  for MnSi (Fig. 1 (a, insert)) consists of several asymmetric lines, each of which was described using the relation obtained in [7].

It is found that in the range  $26 < T < 30$  K the ESR spectrum is formed by one main line with a weak satellite. It is also established that in the temperature range  $T < T^* = 25$  K, located 4 K below the paramagnetic phase-conical phase transition temperature  $T_C = 29$  K, a complex ESR spectrum consisting of several lines appears: two main most intense lines (line 1 and line 2) and several lines of lower amplitude, observed in the range of magnetic fields below 3 kOe. At  $T_f \sim 16$  K, one of the main lines in the ESR spectrum with the highest integrated intensity demonstrates a maximum in the temperature dependence of the line width  $W(T)$ , corresponding to a change in  $W$  by a factor of ~2.8. We argue that this unusual behavior appears as a consequence of a spin fluctuation transition in the conical spiral magnetic phase with

long range magnetic order. Additionally, it was found that the same line at a temperature of 5 K has a stronger angular anisotropy than that at 15 K (Figure 1(b)). Other lines do not demonstrate a pronounced angular dependence either at 5 or 15 K.

We thank V.A. Shustov<sup>3</sup> for determining the crystallographic axes of the crystal by X-ray diffraction analysis. Financial support from the government assignment for FRC Kazan Scientific Center of RAS is acknowledged.

1. Demishev S.V., et al.: Phys. Rev. B **85**, 045131 (2012)
2. Demishev S.V., et al.: JETP Lett. **115**, 673–678 (2022)
3. Date M., Okuda K., Kadowaki K.: J.Phys.Soc.Jpn. **42**, 1555-1561 (1977)
4. Demishev S.V., et al.: JETP Lett. **98**, 829-833 (2014)
5. Demishev S.V.: Applied Magnetic Resonance, **51**, 473–522 (2020)
6. Demishev S.V.: Physics-Uspekhi, **194**, 23–47 (2023)
7. Joshi J.P., Bhat S.V.: J. Magn. Reson., **168** (2), 284-287 (2004)

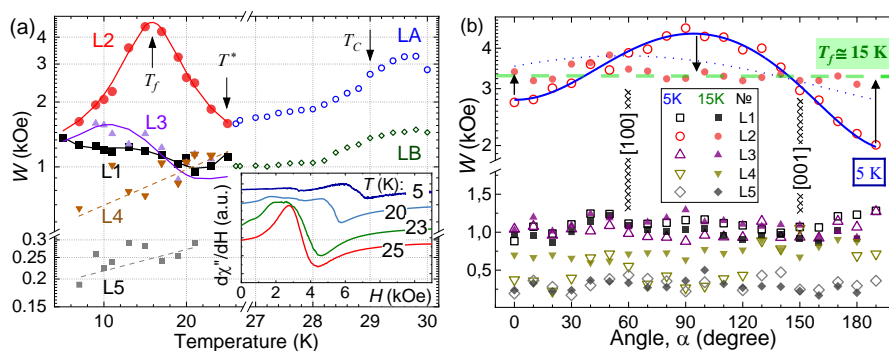


**Fig. 1.** Temperature (a) and angular (b) dependences of the line widths  $W(T)$  in ESR spectra in MnSi. Inset: ESR spectra of MnSi.

## Comprehensive study of magneto-resonance properties of dendrimer metal complexes of polydentate N,O-ligands using the example of a new Fe<sup>3+</sup> $\beta$ -diketonate

**Denis V. Starichenko<sup>1</sup>, Valerya E. Vorobeva<sup>2</sup>, Matvey S. Gruzdev<sup>3</sup>,  
Ulyana V. Chervonova<sup>3</sup>, Aleksey S. Volegov<sup>4</sup>, Ivan V. Yatsyk<sup>2</sup>**

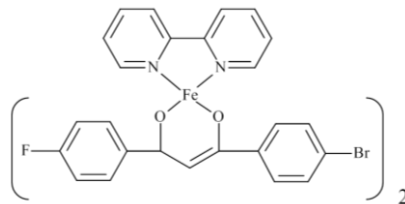
<sup>1</sup>M.N. Mikheev Institute of Metal Physics of the Ural Branch of the Russian Academy of Sciences, 620108 Ekaterinburg, Russia, starichenko@imp.uran.ru

<sup>2</sup>Zavoisky Kazan Physical-Technical Institute, Russian Academy of Science, 420029 Kazan, Russia

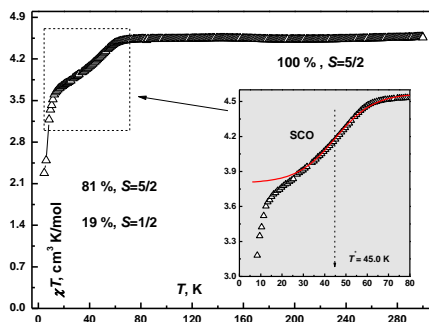
<sup>3</sup>G.A. Krestov Institute of Solution Chemistry of Russian Academy of Sciences, 153045 Ivanovo, Russia

<sup>4</sup>Institute of Natural Sciences and Mathematics, Ural Federal University, 620083 Ekaterinburg, Russia

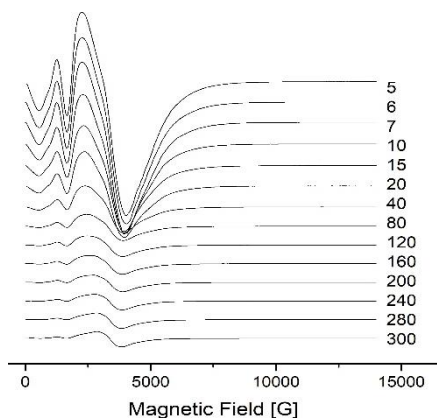
The development of heterofunctional metal complexes with controlled specified properties is an actual scientific problem. One of these are iron-containing structures, in which the magnetically active properties of Fe<sup>3+</sup> ions (in particular, spin crossover (SCO)) can cooperate with the luminescent properties of dendrons based on N, O-ligands coordinated to the metal (Fig. 1). According to differential scanning calorimetry data the complex is characterized by an amorphous glassy phase without a clearly defined melting point. Solutions of the Fe complex in dichloromethane have weak fluorescence (QYFL = 1%) with an emission maximum at 435 nm. The substance also exhibits solid-state emission when irradiated at a wavelength of 356 nm. In this work, to study the magnetic properties of the complex, a combination of two experimental techniques was used - EPR spectroscopy and SQUID magnetometry, which made it possible to obtain complete and self-consistent information about the magnetic state of the substance.



Magnetic measurements,  $\chi(T)$ , showed that complex at room temperature in a single-phase high spin (HS) state of Fe<sup>3+</sup> ions ( $S = 5/2$ ). In the range 100 ÷ 300 K, weak AFM correlations are observed with a Weiss temperature  $\theta_1 = -0.8$  K. At  $T^* \sim 45$  K a partial SCO transition ( $5/2 \leftrightarrow 1/2$ ) occurs (Fig. 2). This process is accompanied not only by a change in the magnetic state (81% HS, 19% LS), but also by the emergence of strong AFM interactions between neighboring Fe<sup>3+</sup> ions with  $\theta_2 = -2.3$  K. Analysis of the ground spin state at 2.0 K indicates that not all of the Fe<sup>3+</sup> ions participate in the interactions; some of them remain in a paramagnetic state, the share of which is  $\sim 60\%$ .



X-band EPR as a locally sensitive technique allow to study in detail the individual HS and LS contributions of  $\text{Fe}^{3+}$  ions and its temperature evolution from 5 to 300 K. The spectra (Fig. 3) were simulated by Lorentzian line shape by using EasySpin Matlab toolbox. EPR measurements confirmed the presence of magnetically active HS and LS  $\text{Fe}^{3+}$  ions states and made it possible to distinguish two HS types: I-type with strong low-symmetry and II-type with weak, distorted octahedral environments. SCO was also detected and the temperature dependences of the integral EPR intensities,  $I(T) \sim \chi(T)$ , of the HS and LS contributions were analyzed.



This work was supported by the Russian Science Foundation (Project no. 23-13-00015).

## Ferromagnetic resonance in Co-ions implanted SnO<sub>2</sub> films: Effects of oxygen vacancies

**A. A. Sukhanov, V. V. Bazarov, V. F. Valeev, V. I. Nuzhdin, R. I. Khaibullin**

Zavoisky Physical-Technical Institute, FRC Kazan Scientific Center of RAS, Kazan, Russia

Semiconducting tin dioxide (SnO<sub>2</sub>) doped with a magnetic 3d-elements reveals room-temperature ferromagnetism [1]. However, the origin of the observed ferromagnetism and its relationship with structural point defects is still a subject of discussion. In this work, we present a ferromagnetic resonance (FMR) study of SnO<sub>2</sub> films heavily doped with cobalt (up to 15 at.%) by using ion implantation. The influence of oxygen vacancies in oxide structure on FMR of Co-ions implanted SnO<sub>2</sub> films is also shown.

The experimental samples were obtained by the implantation of 40 keV Co<sup>+</sup> ions into epitaxial SnO<sub>2</sub> films grown on c-cut Al<sub>2</sub>O<sub>3</sub> substrates using reactive magnetron sputtering. The ion implantation was carried out with Co ions fluence of  $1.0 \times 10^{17}$  ion/cm<sup>2</sup> at room (300 K) or at the elevated (750 K) substrate temperatures. Our recent studies [2] showed that the most of cobalt implant exists predominantly in the form of metallic Co hcp nanoparticles in SnO<sub>2</sub> sample implanted at room substrate temperature. On the other hand, the content of metallic Co atoms is sufficiently lower, and the implanted cobalt mainly occur in the 2+ valence state in SnO<sub>2</sub> film implanted at the elevated temperature. These Co<sup>2+</sup> ions form a magnetically ordered solid solution in the SnO<sub>2</sub> host, and the presence of a certain concentration of oxygen vacancies plays a crucial role in producing ferromagnetism, according to FC exchange mechanism [3]. In our experiments, the content of oxygen vacancies in the Co-implanted films was changed either by high-temperature annealing of the samples in an air atmosphere (the filling of oxygen vacancies), or by annealing in a high vacuum (the creation of vacancies), or by storing the thin-film samples in an ethanol medium containing the dissolved atoms and molecules of oxygen [4].

FMR spectra were taken on a Bruker Elexsys-E580 X-band spectrometer (9.64 GHz) in the temperature range of 77-300 K. The angular dependences of the FMR spectra were recorded by rotating of the applied DC magnetic field in plane perpendicular to the sample plane (“out-of-plane” geometry). Three FMR signals were clearly observed in the magnetic resonance spectra of Co-ions implanted SnO<sub>2</sub> films when the magnetic field is perpendicular to the sample plane (not shown here). The first two signals out of three observed ones exhibit strong angular dependences of the resonant field and the signals broaden with decreasing temperature. On the contrary, the third signal has a very weak angular dependence. Moreover, its integral intensity decreases with decreasing temperature at a constant line width. The observed angular and temperature dependences of the first two FMR signals are typical for thin granular magnetic films with strong magnetic anisotropy [5]. In contrast, the weak angular dependence of the third signal is characteristic of isotropic bulk ferromagnetic materials. Thus, our FMR studies indicate the formation of two different magnetic phases (anisotropic Co nanoparticles and a magnetically isotropic solid solution of Co<sup>2+</sup> ions) in Co-ions implanted SnO<sub>2</sub> films.

All three FMR signals disappear in the samples after annealing in air at a temperature of 875 K for 30 minutes. However, subsequent second annealing of the



same samples under high vacuum conditions at same temperature of 875 K leads to the restoration of the third signal with a weak angular dependence. The last observation indicates on the crucial role of oxygen vacancies in producing ferromagnetism of solid solutions of  $\text{Co}^{2+}$  ions in the implanted  $\text{SnO}_2$  films.

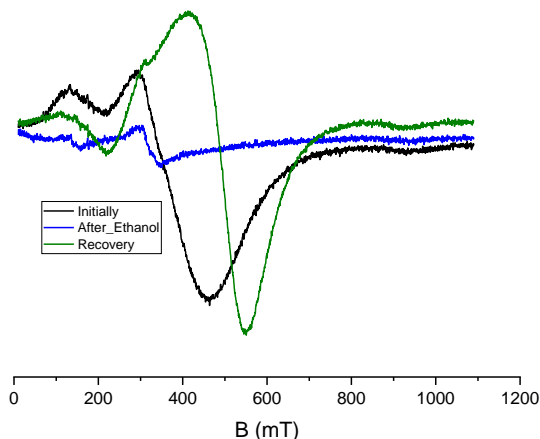


**Fig. 1.** FMR spectra of Co-implanted  $\text{SnO}_2$  sample for the orientation of magnetic field perpendicular to the sample plane recorded before (black curve) and after (blue curve) storage of sample in ethanol. The green curve represents the FMR spectrum after the vacuum annealing of sample stored in ethanol.

A strong effect of organic solvents on FMR was observed for the first time. For example, this chemical effect of ethanol on the FMR spectrum is shown in Fig. 1 for  $\text{SnO}_2$  sample implanted with Co ions at the elevated substrate temperatures. It should be noted that this effect was observed for samples subjected to double annealing, first in air and then in vacuum. After keeping the sample in ethanol for more than 2 hours, the FMR spectrum completely disappears (marked as “After ethanol” in Fig. 1). Then the sample was again annealed in vacuum, the FMR spectrum was restored (marked as “Recovery” in Fig. 1), for which an angular dependence was also observed (not shown here). However, the “restored” FMR spectrum differs from the “Initial” spectrum.

The study was supported by the Russian Science Foundation (project number 22-19-00712, <https://rscf.ru/project/22-19-00712/>).

1. Worku Y., Sahu D. R., Srinivasu V. V.: Ferromagnetism in  $\text{SnO}_2$  Doped with Transition Metals (Fe, Mn and Ni) for Spintronics Application: A Review of Experimental Status. In *Magnetic Materials and Magnetic Levitation* (2020), Chapter 7, pp. 1–14.
2. Khaibullin R. I., Gumarov, A. I., Vakhitov I. R., Sukhanov A.A. et al., *Condensed Matter (MDPI)*, **9**, art. 27 (2024).
3. Coey J. M. D., Douvalis A. P., Fitzgerald C.B., Venkatesan M. *Applied Physics Letters*, **84**, 1332–1334 (2004).
4. Shchukarev S. A., Tolmacheva T. A. *Journal Structural Chemistry*, **9**, 16–21 (1968).
5. Okay C., Vakhitov I. R., Valeev, V.F., Khaibullin R. I., Rameev B. *Applied Magnetic Resonance*, **48**, 347–360 (2017).

## RESONANCE CONDUCTANCE of ELECTRONS on INTERFACES of MAGNETIC TUNNEL JUNCTION

N.Kh. Useinov<sup>1</sup>

<sup>1</sup> Institute of Physics, Kazan Federal University, Kazan, Russia

Our research is devoted to the calculation of spin-polarized dynamic conductance  $G = dI/dV$  in point magnetic tunnel junctions (PMTJs) which have a structure: Left ferromagnetic metal/dielectric/Right ferromagnetic metal ( $FM^L/I/FM^R$ ). These PMTJs are widely used in modern spintronics nanodevices, particularly in the field of data storage: MRAM devices, read heads of hard disk drives, and programmable logic gates [1].

While much research has been carried out on experimental study the fundamental electronic structure-related from magnetic field dependence of the conductance in PMTJs, but relatively little has been assessed on their room-temperature properties and bias dependence which are important for memory applications. Moreover, theoretical investigations of spin-polarized conductance in PMTJ have been mostly overlooked.

It is well known that PMTJ has high conductance in the case of parallel (P) alignment of magnetizations of the nanocontact sides. If their magnetizations are antiparallel (AP) then the situation can be interpreted within the framework of band theory as a mutual exchange of spin-subbands (minority or majority of electrons) in one of the magnetic domains. In this case, additional resistance arises associated with the processes of electron spins interactions with magnetic moments of domain atoms and the conductance is low.

This work examines the conductance properties of PMTJ taking into account gradients of the electrochemical potentials at the ferromagnetic metal/dielectric interface [2, 3]. The calculation of the conductances was carried out within the framework of the quasiclassical theory [4] for an arbitrary ratio of the contact size (its radius  $a$  and thickness  $d$ ) and the mean free paths  $l$  of conduction electrons in the  $FM^L$  and  $FM^R$ .

Expression for the  $G = dI/dV$  was obtained based on solutions to the system of Boltzmann equations for quasiclassical Green's functions and a system of quantum mechanical equations that determine the transmission coefficients of an electron through the energy barrier taking into account the spin directions  $s = (\uparrow, \downarrow)$  and applied voltage  $V$  [3, 4].

The results of calculations of conductances  $G$  for an asymmetric PMTJ with different values of Fermi wave vectors  $k_{F,s}^{L(R)}$  and the mean free paths  $l_s^{L(R)}$  of conduction electrons are shown in Figure 1. Here also shows the radius  $a$  and thickness  $d$  of the dielectric layer, the height of the energy barrier  $U_B$ , the effective mass  $m_B$  of electrons in the dielectric in units of free electron mass  $m_e$ . Note that the effective masses of conduction electrons in  $FM^{L(R)}$  electrodes were equal to  $m_e$ .

In Figure 1 shows the dynamic conductance  $G = dI/dV$  of point magnetic tunnel junctions for P and AP alignment of magnetization of the contact sides of different ferromagnetic metals  $FM^L$  and  $FM^R$ . These curves are calculated taking into account gradients of electrochemical potentials on interfaces, and the curve at P alignment of magnetization have unusual peak at an applied voltage of  $V \sim 0.9$  V.

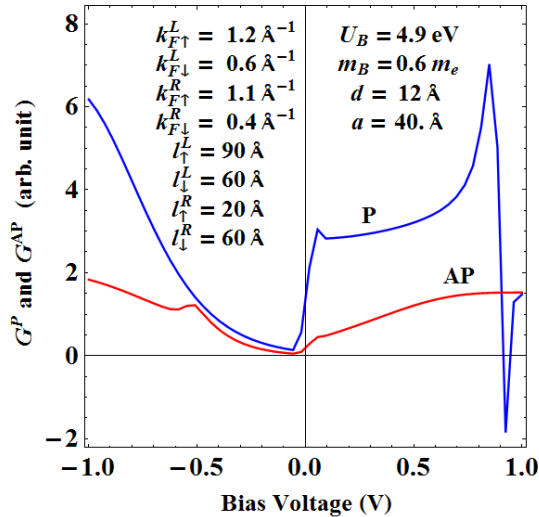


**Fig. 1.** Dynamic conductances  $G$  as functions of the dc bias voltage are shown for the parallel P and antiparallel AP alignment of magnetizations of the sides PMTJ.

In our opinion, this peak is associated with the quantization of the energy of conduction electrons near the FM/dielectric interfaces and with the narrowing of the contact area. Here the accumulation of electrons with one spin projection and its spin flip from one spin-subband to another occurs. At the FM/dielectric interface, the spin-dependent electrochemical potentials have different gradients (or opposite curvatures) above and below the Fermi energy and, together with the exchange energy, enhance the conductivity of the electrons with one spin projection. These effects, at a certain combination of parameters of the PMTJ with the restricted geometry, lead to the resonance of the conductance at a certain voltage.

The author hopes that these theses will be noticed by researchers to interpret the spectra of inelastic electron tunneling, which is a powerful method to detect various sorts of elementary excitations at magnetic tunnel junctions interfaces.

This work was supported by the Priority-2030 program of Kazan Federal University.

1. Tsymbal E., Žutić I.: Spintronics Handbook, Second Edition, Spin Transport and Magnetism. CRC Press Taylor & Francis Group, Boca Raton, London, New York (2019), 735 p.
2. Useinov N. K.: Theoret. and Math. Phys. 183, 705 (2015).
3. Useinov A. N., Lin H.-H., Useinov N. K., Tagirov L. R.: J. Magn. Magn. Mater. **508**, 166729 (2020).
4. Useinov N. K.: Quasiclassical theory of spin-polarized conductivity and magnetoresistance in magnetic nanoheterocontacts. Kazan: KFU (2023), 445 p. (In Russian)



## Electron Spin Polarization Dynamics of the Photoexcited Triplet States of the organic chromophores and donor-acceptor Dyads: Analysis of the TREPR spectra Evolution

**V. Voronkova<sup>1</sup>, A. Sukhanov<sup>1</sup>, A. Mambetov<sup>1</sup>, Jianzhang Zhao<sup>2</sup>**

<sup>1</sup> Zavoisky Physical-Technical Institute, FRC Kazan Scientific Center of RAS, Kazan, Russia

<sup>2</sup> State Key Laboratory of Fine Chemicals, School of Chemical Engineering, Dalian University of Technology, Dalian, China

To date, there are several examples of observing the polarization inversion of photoexcited triplet state TREPR spectra, for example [1-3]. For the first time, S. Yamauchi et al. presented the decay properties of the short-lived triplet (T) states of pyridazine and 3,6-dichloropyridazine (DCP) studied by means of time-resolved EPR with laser excitation [1]. The population ratios and the decay rate constants of the triplet sublevels have been determined from the analysis of the time profile of the transient EPR signals on the assumption that the spin-lattice relaxation (SLR) rates are much slower than the triplet decay rates. It was shown that the decay rate constant for one of the principal orientations of the triplet D-tensor ( $k_y$ ) is an order of magnitude higher than that for the other two orientations. Simplified diagram explaining the inversion of electron spin polarization of triplet state for magnetic field  $\mathbf{B}_0 \parallel Y$  is presented Fig. 1.

Here we present a study of the dynamics of the photogenerated electron spin polarization of the triplet states of some BODIPY and Aminoanthraquinone (AQ) derivatives and some Donor-Acceptor Naphthalimide-Phenothiazine Dyads. Pulsed laser excited time-resolved electron paramagnetic resonance (TREPR) spectra shows inversion of the electron spin polarization (ESP) phase pattern of the triplet state at longer delay-time.

An efficient algorithm for the exact numerical solution of the equation of motion of the spin density matrix of an ensemble of photoexcited triplets, taking into account the anisotropy of the decay rates of the triplet state sublevels, spin-lattice and spin-spin relaxations for analyzing the inversion of the ESP spectra of TREPR was used to calculate the time evolution of the TREPR spectra and match it with the experimental spectra [3]. The dependence of the effect on various factors is discussed.

1. M. Terazima, S. Yamauchi and N. Hirota: Chem.Phys.Letters **120**, 321-326 (1985)

2. Zh. Wang, A. Toffoletti, Yu. Hou, J. Zhao, A. Barbon and B. Dick, Chem. Sci., **12**, 2829-2840 (2021)

3. A. Mambetov · A. Sukhanov · Xue Zhang · Jianzhang Zhao · V. Voronkova: Appl. Magn. Reson. <https://doi.org/10.1007/s00723-024-01654-y>

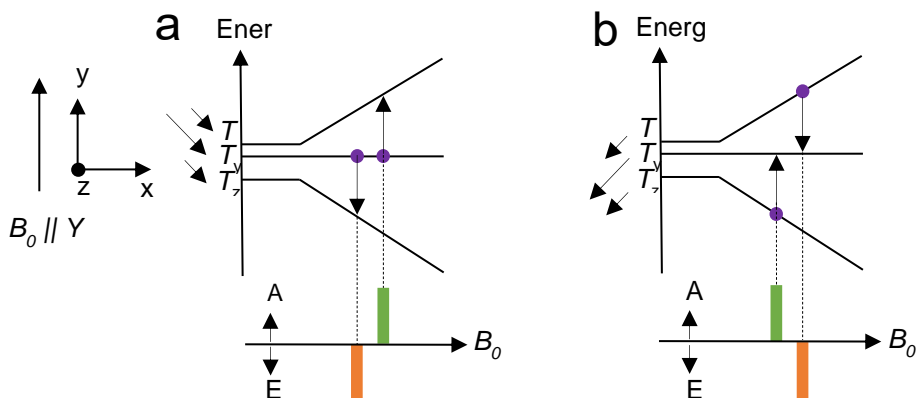


**Fig. 1.** Diagram explaining the inversion of electron spin polarization of triplet state : (a) Just after the laser excitation,  $T_y$  sublevel of the  $T_1$  state is over populated and mainly produces an **E/A** pattern. (b) Sufficiently later (longer delay time), the rapid decay rate of the  $T_y$  sublevel of the  $T_1$  state makes the population of the  $T_y$  sublevel deplete selectively and the observed polarity becomes an **A/E** pattern.

## **Effect of carbon black content on the EPR linewidth in a composite based on an ethylene vinyl acetate matrix EPR**

**A.M. Zyuzin<sup>1</sup>, K.E. Igonchenkova<sup>1</sup>, A.A. Karpeev<sup>1</sup>, N.V. Yantsen<sup>1</sup>,  
S.S. Gostyushov<sup>1</sup>.**

<sup>1</sup> National Research Mordovia State University, Saransk, Russia

One of the important materials of scientific and practical interest are polymer composites filled with carbon black, which is added to impart the necessary mechanical and electrical properties. In this work, we investigated the effect of carbon black (CB) content on the ESR resonance absorption linewidth in composites based on an ethylene vinyl acetate matrix in two frequency ranges: X-band (9.4 GHz) and Q-band (34 GHz).

For the study, samples of composites were made with different concentrations of carbon black from 5 to 35 wt.% (mass fractions). CB brand C40 was used as a filler providing electrical conductivity. The composites were prepared by mixing on a laboratory extruder and subsequent pressing. EPR spectra were recorded at room temperature on a Bruker EMX Plus spectrometer in the X- and Q-bands. The resonance absorption linewidth was determined as the peak-to-peak width  $\Delta H_{pp}$  of the first derivative of the EPR absorption line.

It was observed in [1] that the resonance linewidth decreases as the carbon nanofiber content in the polycarbonate matrix increases. A correlation was also established between the EPR linewidth and the resistivity of polycarbonate-based composites with carbon nanofibers.

The results of our studies showed that when the microwave field frequency changes from 9.4 to 34 GHz in samples with the same CB content, there is no noticeable change in the EPR absorption linewidth. In both the X- and Q-bands, a decrease in the resonance absorption linewidth was detected at carbon black concentrations greater than 25 wt.%. Note that it is precisely this concentration that determines the upper boundary of the percolation region. A particularly noticeable decrease was observed at 9.4 GHz (X-band).

The main factor explaining the observed decrease in linewidth with increasing CB content may be a change in the magnitude of the spin-spin interaction of uncompensated spin magnetic moments. Carbon black brand C40 has electron delocalization, which reduces the likelihood of spin-spin interactions leading to line broadening. In particular, CB particles can act as relaxation centers by changing the spin-spin relaxation time.

With an increase in the concentration of carbon black, the paramagnetic centers located in CB can come closer and interact with each other. This leads to an increase in exchange interaction, which can reduce the width of the EPR line due to exchange narrowing. This phenomenon occurs when the exchange interaction between spins becomes dominant, thereby averaging the magnitude of the change in local magnetic fields.

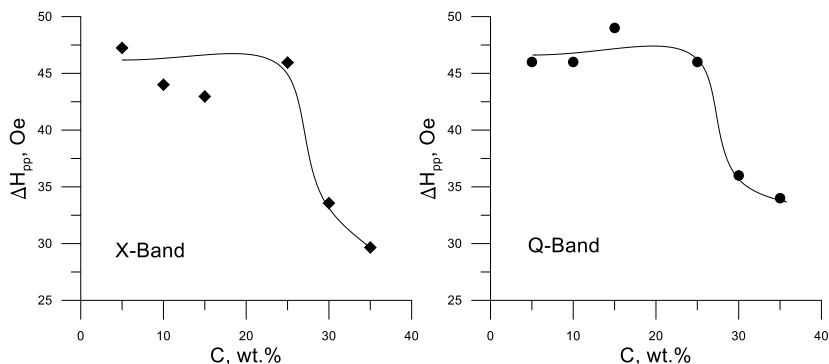


Fig. 1. Dependence of linewidth on CB concentration in the X- and Q-range.

Also, with an increase in the concentration of carbon black in the composite, the distribution of distances between paramagnetic centers changes. If these distances become more uniform, this may reduce the contribution of random interactions to the EPR linewidth. A more uniform distribution of distances between spins leads to a decrease in inhomogeneous broadening.

Thus, in this study, the dependence of the EPR resonance absorption linewidth on the concentration of carbon black in the polymer matrix of ethylene vinyl acetate was revealed. It has been established that with increasing concentration of carbon black, the EPR linewidth decreases both in the X-band and in the Q-band. This behavior of  $\Delta H_{pp'}$  can be explained by a change in the magnitude of the spin-spin interaction of magnetic moments.



## ESEEM study of $Y_3N@C_{80}$ under photoexcitation

**R.B. Zaripov, Yu.E. Kandrashkin**

Zavoisky Physical-Technical Institute, FRC Kazan Scientific Center of RAS, Kazan, Russia

The fullerene cage is an excellent container to isolate the atoms and molecules from the influence of the environment. The encapsulated systems exhibit a number of interesting phenomena, including the unusual properties of electron and nuclear spins [1, 2]. The fullerenes are very good chromophores and are characterized by the efficient generation of the triplet state under photoexcitation. Therefore, additional properties are expected for the photoexcited endohedral fullerenes due to the interactions between the unpaired electrons of the fullerene and its encapsulated fragment. Our interest in such systems is motivated by their potential application in quantum storage protocols that use both microwave and radiofrequency pulses to interplay the coherences of the electron and nuclear spin sublevels.

The endohedral fullerene  $Y_3N@C_{80}$  [3, 4] was chosen as the object of study. A three-pulse electron spin echo envelope modulation (ESEEM) signal of the photoexcited endohedral fullerenes was recorded by the EPR machine operating in the X- and Q-bands. Different light sources were used for the experiments, the continuous laser (532 nm and 90 mW) and the pulsed laser (Nd:YAG, 532 nm). The Fourier transform of the ESEEM data shows several distinct frequencies. The hyperfine interactions with the carbon isotope ( $^{13}C$ ) localized on the cage of the fullerene and with the yttrium nuclei ( $^{89}Y$ ) of the encapsulated fragment are identified.

**Acknowledgments:** The research was supported financially by Russian Science Foundation (project #23-22-00402).

1. Zaripov R.B., Kandrashkin Yu.E., Salikhov K.M., Büchner B., Liu F., Rosenkranz M., Popov A.A., Kataev V.: *Nanoscale* **12**, 20513-20521 (2020)
2. Kandrashkin, Yu.E., Zaripov, R.B.: *Phys. Chem. Chem. Phys.* **25**, 31493–31499 (2023)
3. Zalibera M., Krylov D.S., Karagiannis D., Will P.-A., Ziegs F., Schiemenz S., Lubitz W., Reineke S., Savitsky A., Popov A.: *Angew. Chem. Int. Ed.* **57**, 277-281 (2018)
4. Zalibera M., Ziegs F., Schiemenz S., Dubrovin V., Lubitz W., Savitsky A., Deng Sh.H.M., Wang X.-B., Avdoshenko S.M., Popov A.A.: *Chem. Sc.* **12**, 7818-7838 (2021)

## EPR study of iron impurities in BaF<sub>2</sub> single crystal under X-ray irradiation

**R.B. Zaripov<sup>1</sup>, V.A. Ulanov<sup>1,2</sup>, R.R. Zainullin<sup>2</sup>**

<sup>1</sup>Zavoisky Physical-Technical Institute, FRC Kazan Scientific Center of RAS, Kazan, Russia

<sup>2</sup>Kazan State Power Engineering University, Kazan, Russia

Interest in fluorite-type crystals is associated with the use them as ionic conductivity elements, the properties of which depend on the type of ions. In this paper, we studied the effect of an additional iron impurity on the properties of an iron associate. This is a continuation of the works [1,2].

In the crystal of BaF<sub>2</sub>:Fe pairs of iron ions [Fe<sup>+</sup>-Fe<sup>2+</sup>] are formed under the influence of X-ray radiation. The ground state of the studied pairs corresponds to an electronic spin multiplet with spin 7/2, split so that the Kramers doublet turned out to be the ground one. It is found that the energy difference between the ground and the next spin doublet corresponds approximately to 125 GHz. The paper defines the parameters of the superhyperfine interaction with the magnetic moments of fluorine nuclei. It is shown that the observed experimental facts clearly indicate that the exchange between iron ions in the studied pairs is realized mainly by the mechanism of double Zener exchange.

The figure 1 shows the angular dependence of the "center of gravity" of the EPR spectra of BaF<sub>2</sub>:Fe in the X and Q frequency ranges in the crystallographic axis  $\langle 1\bar{1}0 \rangle$ . Curve number 1 corresponds to an ensemble of radiation centers, which at an angle 0° turn out to be oriented parallel to the direction of the external magnetic field. Curve 2 corresponds to the other two ensembles oriented differently in the crystal. The squares and circles correspond to the resonant values of the constant external magnetic field, and the lines correspond to the theoretical values. It can be seen that the theoretical values coincide very well with the experimental ones (despite the fact that splits in a zero magnetic field were described only by the operator  $B_2^0 O_2^0$ ).

Acknowledgments: The research was supported financially by Russian Science Foundation (project #23-22-00402).

5. Zhiteitsev, E.R., Ulanov, V.A., Zaripov, M.M., Zheglov E.P.: Phys. Solid State **47**, 1254–1257 (2005)
6. Zhiteitsev, E.R., Ulanov, V.A., Zaripov, M.M., Zheglov E.P.: Phys. Solid State **48**, 1887–1892 (2006)

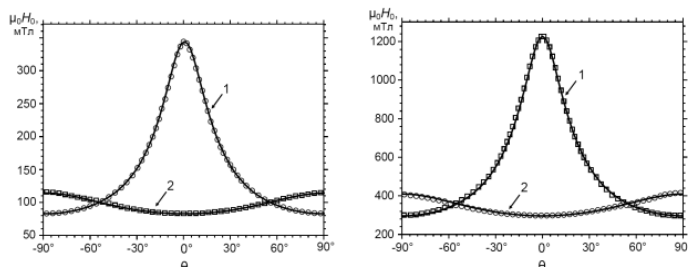


Fig. 1. Angular dependence of the BaF<sub>2</sub>:Fe crystals registered in  $\overline{H} \parallel \langle 1\bar{1}0 \rangle$  orientation at 80K: right – X-band, left – Q-band data.

## Cylindrical and sphere Halbach magnet arrays

**A.V. Bogaychuk**

Institute of Physics, Kazan Federal University, Kremlyovskaya str. 18, Kazan, Russia

One of the most common methods for achieving the greatest magnetic field homogeneity in low field NMR systems with permanent magnets is the use of Halbach magnet array. The usual form of implementation of this array is in the form of a cylinder. However, there are also a number of theoretical works [1] suggesting a design in the form of a sphere, which allows for an increase of the average value and improvement of the homogeneity of the magnetic field within the working area of magnet. A Halbach sphere has  $4/3$  more internal flux than an ideal ring with the same shell thickness and additionally a strong stray field. But, according to recent reviews [2], this design has not yet been put into practice. A significant disadvantage of sphere may be, for example, the difficulty of accessing the working area from outside the magnetic assembly.

In this work presents a comparison of the calculated parameters of cylindrical and spherical Halbach magnetic arrays. A simplified implementation of the discrete Halbach sphere is also presented. Also, to reduce the influence of the imperfection of magnetic materials, approaches to accounting for defects presented in our previous works were used [3].

1. Leupold H., Tilak A., Potenziani E.: *J. Appl. Phys.* **87**, 4730–4734 (2000).
2. Blümmler P., Soltner H.: *Appl Magn Reson* **54**, 1701–1739 (2023)
3. Bogaychuk A., Ivshin E. *Rev. Sci. Instrum.* **95**, 055107 (2024)

## PECULIARITIES OF PORE SPACE INVESTIGATION BY NMR RELAXOMETRY AND CRYOPOROMETRY METHODS

**D.S. Ivanov, A.N. Afanas'eva, V.D. Skirda**

Institute of Physics, Kazan Federal University, Kazan, Russian Federation

The strategy of scientific and technological development of the Russian Federation implies the use of scientific achievements and developments in the applied plane. One of the methods actively developing in recent years is the method of nuclear magnetic resonance (NMR). Today, the NMR method is actively used in various fields: from magnetic resonance imaging (MRI) to oil field studies (logging studies). Over the last decade, the development of special techniques for NMR equipment aimed at investigations of porous media (core material) has become more and more relevant. This is primarily due to the possibility of determining pore sizes from nanometers to hundreds of micrometers. At the same time pore size determination is performed by non-invasive method.

In this paper, we demonstrate the results of application of special methods of porous media analysis: NMR cryoporometry and a method based on the use of internal gradients of the porous medium magnetic field (DDif). To obtain information about the presence of pores in the core sample, the size of which varies in the range from several units to tens of nanometers, the NMR cryoporometry technique was applied. To implement this method, a core sample saturated with water was frozen to a temperature of 228 K. Figure 1 shows the differential pore size spectrum obtained from NMR cryoporometry data.

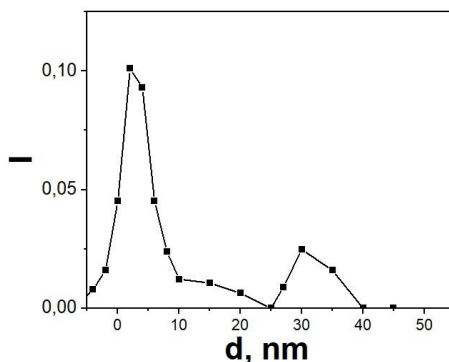


**Fig. 1.** Differential spectrum of pore size distribution obtained from NMR cryoporometry data

The analysis of the dependence of the share of the solid-state component of the NMR signal allows us to characterize the porous space of the core. The differential spectrum shown in Figure 3.6 demonstrates the presence of two different sized regions: 2 and 30 nm. According to the pore size classification we discussed in Section 1.1, mesopores are present in the core where molecular adsorption can preferentially occur. The size constraints of 2 nm according to the classification are micropores.

Nevertheless, in our opinion, such a small size can also be related to the roughness of the pore surface [1, 2].

To characterize the translational mobility of water in the core, the DDif technique was applied. Figure 2 shows the dependence of the stimulated echo amplitude on the diffusion time, as well as the relaxation attenuation characterizing the spin-lattice relaxation process obtained by the Inversion-Recovery pulse sequence.

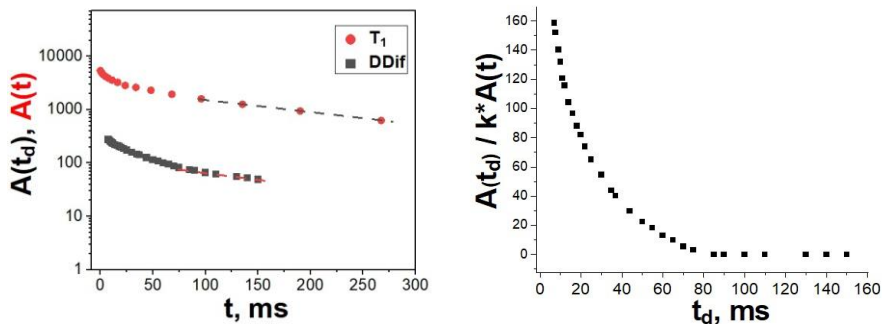


**Fig. 2.** a) Relaxation attenuation characterizing the spin-lattice relaxation process (red symbols); Dependence of the stimulated echo amplitude on the diffusion time. Dotted lines indicate parallel sections. The temperature of the studies is 293 K

To obtain the size of diffusion restrictions it is necessary to determine from the data presented in Figure 2 the time of reaching the restriction for the diffusant molecule. In the case of the studied porous space, reaching of the constraints is observed after diffusion time of 80 ms. Taking into account that the diffusant molecule is water, the size of the constraints is 36  $\mu\text{m}$  according to the Einstein-Smoluchowski equation.

This work was funded by the subsidy allocated to Kazan Federal University for the state assignment in the sphere of scientific activities number FZSM-2023-0016.

1. Nikoo, A. H. On the affinity of carbonate and sandstone reservoir rocks to scale formation—Impact of rock roughness / A. H. Nikoo, M. R. Malayeri // *Colloids and Surfaces A: Physicochemical and Applied*
2. Chen, Y. Effect of water–rock interaction on the morphology of a rock surface / Y. Chen, P. Cao, R. Chen, Y. Teng // *International Journal of Rock Mechanics and Mining Sciences*. – 2010. – V. 47. – №. 5. – P. 816-822.

## Simulation of CPMG Sequence Echo Signals with Gaussian Pulse Shape

**I.T. Khairutdinov, R.B. Zaripov, M.M. Bakirov, M. Yu. Volkov**

Zavoisky Physical-Technical Institute, Russian Academy of Sciences  
Sibirsky trakt 10/7, 420029, Kazan, Russian Federation, [semak-olic@mail.ru](mailto:semak-olic@mail.ru)

The Carr-Purcell-Meiboom-Gill (CPMG) pulse sequence is useful to minimize the influence of decoherence processes on the spin system [1,2]. These processes are characterized by spin-spin ( $T_2$ ) and spin-lattice ( $T_1$ ) relaxation times. EPR spectrum line width usually is one order or larger than the microwave field amplitude  $B_1$ . This is called the case of selective excitation. In this case the magnetization will be particularly on longitudinal direction along external magnetic field  $B_0$ . This leads to a large number of echo signals [3]. These signals have own magnitude and decay time. Time decay of echo signals looks like exponential combination of relaxation times  $T_1$  and  $T_2$  in different proportions. Appearance of stimulated and other unwanted echoes can be a drawback in practice because they may interfere with the refocused primary echo (Hahn echo). This signal mixing makes it very difficult to obtain  $T_1$  and  $T_2$  relaxation times from CPMG experiments.

The magnitude of  $B_1$  does not change with the duration of the pulse. This is typical for rectangular pulse shapes. In this work we describe way to build CPMG phase cycle sequences using gaussian pulses. Phase cycling allows us to eliminate unwanted echo signals and increase the desired ones against their background. In this case, pulses with a Gaussian shape should be more effective than pulses with a rectangular shape. For the N-pulse sequence the number of necessary cycles increases to  $2^N$  and thus for large N values the measuring times become unrealistically long. Numerical calculations of echo signals in CPMG gaussian pulse sequence within the spin density matrix formalism were performed and analyzed. We performed numerical simulation of CPMG experiment for different durations of gaussian pulses and relaxation times values.

The Fig.1 shows sequences of 7 gaussian pulses with excitation of the inhomogeneous width of the EPR spectrum. To determine the time  $T_2$  from a monoexponential decay (red line), signals such as the Hahn echo and its refocused signals are needed. In the case of incomplete excitation using rectangular pulses unwanted echo signals appear. These unwanted signals overlap in the classical CPMG method and make it difficult to determine  $T_2$ . CPMG sequence with gaussian pulses reduces the contribution of unwanted signals. One can determine the time  $T_2$  in this case more accurately from the monoexponential decay in CPMG pulse train.

The reported study was funded by RSF according to the research project № 22-72-10063. Web: <https://rscf.ru/en/project/22-72-10063/>

[1] H. Y. Carr, E. M. Purcell Phys. Rev. **94**, 630 (1954).

[2] S. Meiboom, D. Gill Rev. Sci. Instrum. **29**, 688 (1958).

[3]. Y.-Q. Song Journal of Magnetic Resonance **157**, 82–91 (2002).

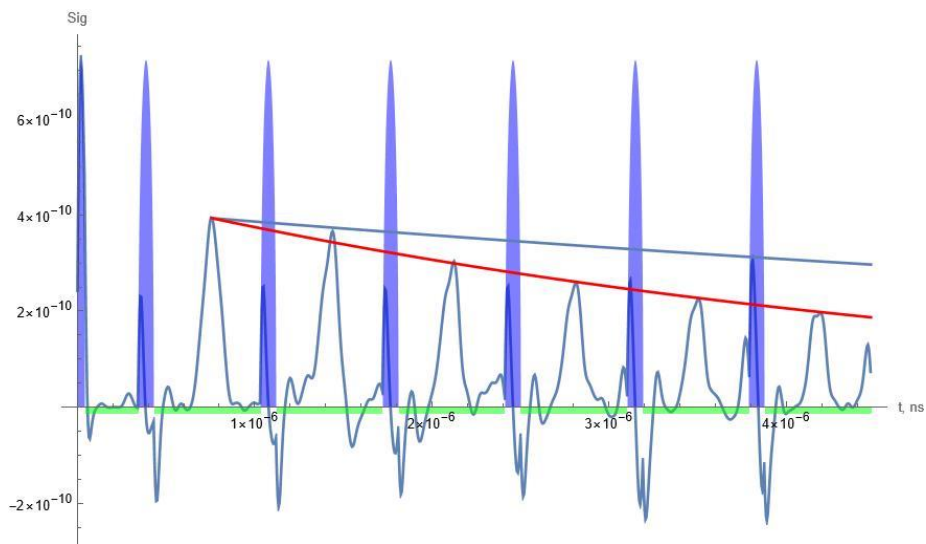


**Fig 1.** Simulation CPMG pulse echo train sequence with gaussian shapes of pulses.

## Electrochemical test cell for in situ and in operando EPR characterization of Li-ion insertion battery electrodes

**D. Ramírez-Rosales<sup>1</sup>, J. Vazquez-Samperio<sup>1,2</sup>, S.N. Arellano-Ahumada<sup>1</sup>, M. A. Martínez-Cruz<sup>3</sup>, I. González<sup>3</sup>**

<sup>1</sup>National Polytechnic Institute, Physics and Mathematics School, UPALM, 07738 Mexico City, Mexico.

<sup>2</sup>National Polytechnic Institute, National Energy Conversion and Storage Laboratory, CICATA-Legaria, 11500. Mexico City, Mexico.

<sup>3</sup>Metropolitan Autonomous University – Iztapalapa, 09340, Mexico City, Mexico.

Understanding the redox mechanisms that occur in the electrodes during the charge / discharge process is an important key to enhance battery performances. In operando Electron Paramagnetic Resonance (EPR) experiments, the fundamental electrochemical redox reactions are monitored by changing the physical and chemical properties of the materials used as electrodes. The combination of two simultaneously recorded analytical methods, for example, spectroscopic and electrochemical data, provides significant information by following the dynamics that are carried out in the materials during the redox reaction.

EPR spectroscopy in situ and in operando has practically not been used for measurements of battery components such as electrodes. Therefore, this way of using EPR spectroscopy is a novel and innovative methodology for obtaining information on the processes that occur in the electrodes of the insertion batteries when the battery is in operation.

EPR spectra and the galvanostatic curve obtained in the in-operation tests of electrochemical test cells with different active materials (cobalt oxide, nickel-manganese oxide and Lithium Manganese Nickel Oxide). It is observed in the EPR spectra the signal corresponding to the lithium ion, which increases as the material goes from potentials of 2 to 4.5 V and 3 to 5 V vs. Li/Li+.

We are currently working and focusing on understanding the lithium (Li) storage mechanism in Metal-Organic Frameworks (MOFs) using terephthalic acid as a lamellar ligand and pyrazine as a pillar and manganese and cobalt ions. Here the solvothermal method is used to synthesize the MOFs with Mn, Co and a combination of both Mn-Co.

The aim of this work is to design, manufacture, evaluate and couple an electrochemical cell to an EPR spectrometer to monitor via in-situ and in-operando the local structure of materials used as electrodes in insertion batteries and, therefore, to understand the changes that occur in the materials to propose adjustments and improve their properties.

1. Sathiyam M, Leriche JB, Salager E, Gourier D, Tarascon JM, Vezin H. Electron paramagnetic resonance imaging for real-time monitoring of Li-ion batteries. *Nat Commun.* 2015 Feb 9;6:6276. doi: 10.1038/ncomms7276. PMID: 25662295; PMCID: PMC4347297.



## LOW TEMPERATURE NMR PROBE with VARIABLE FREQUENCY

**K.O. Sannikov, A.V. Klochkov, D.G. Zverev, P. Mampua**

Institute of Physics, Kazan Federal University, Kazan, Russia

A low-temperature NMR probe with variable frequency (Fig.1a) has been designed and created for the LH-311-1.5K-MRI cryostat, operating in the temperature range from 1.5 to 325 K and magnetic fields up to 0.8 T. The frame of the structure is assembled on M3 threaded rods, thanks to which it was possible to make the structure light and rigid. The frequency of the probe is adjusted using two variable capacitors KPK-MT and shafts extending beyond the cryostat. In the upper part of the probe, shown in Fig.1b), there are three vacuum sealed RSGS-10 connectors and two vacuum sealed BNC connectors. Also, a capillary is provided through the upper part for the condensation of gases into the experimental cell, for example,  $^3\text{He}$  and Xe. The versatility of the design makes it possible to conduct experiments at low temperatures with a variety of samples: from crystalline samples to porous systems. At the moment, the sensor is in the final assembly and testing stage.

a)

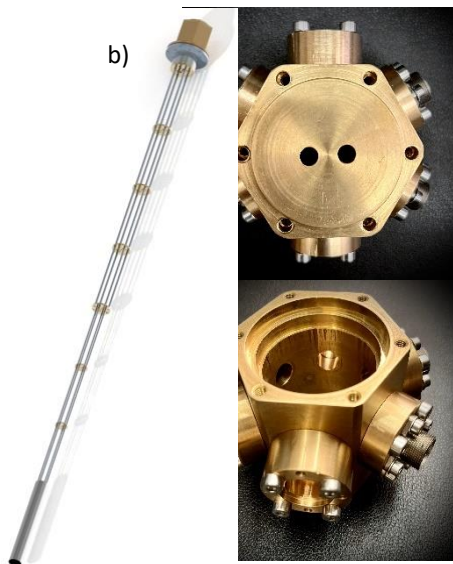


**Fig. 1.** a) The model of the probe; b) the upper part of the probe with connectors

## THE PROMISES OF LOW-FIELD MAGNETIC RESONANCE IMAGING

**A.V. Tuckachev, A.S. Alexandrov, D.L. Melnikova, V.D. Skirda**

Institute of Physics, Kazan Federal University, Kazan, Russia

Today Magnetic Resonance Imaging (MRI) is one of the main non-invasive methods of visualization, which has found wide application not only in medicine, but also in other fields of science and technology. Magnetic resonance imaging (MRI) has traditionally been associated with high-field systems that operate in the magnetic field range of 1.5 to 3 T and above. However, in recent years, there has been a growing interest in the use of low-field magnetic resonance imaging (LFMRI) [1-2], which operates in the magnetic field range of 0.15 to 0.5 T. Low-field MRI systems have a number of unique features and advantages that make them promising for a variety of applications.

One of the key advantages of LFMRI is its cost-effectiveness, such systems are generally less expensive to both purchase and operate [3]. This is because they do not require complex and energy-intensive cryogenic equipment, making them more affordable for small clinics, research laboratories and mobile research stations. Low-field MRI machines are generally smaller in size and weight than their high-field counterparts, what makes them easier to transport and install. However, there are a number of disadvantages associated with the use of low magnetic fields in MRI. These disadvantages include a significant deterioration of the spatial resolution of the obtained images due to the relationship between the signal/noise ratio of the obtained signal and the magnitude of the magnetic field [4]. Permanent magnet systems used in LFMRI are characterized by larger values of magnetic field inhomogeneity and are subject to thermal drift without proper thermal stabilization.

The aim of this work was to find out whether it is possible to develop such a set of tomographic techniques to use a compact commercial permanent magnet system without prior fine shimming to obtain MR images of small objects ( $\leq 30$  mm) with sufficient quality. To answer this question, we used a magnetic system on a Halbach structure with a magnetic field of 150 mT and an average inhomogeneity value of  $10^{-3}$  in a 100 mm diameter region. Next, we designed and constructed all the necessary RF blocks – probe, probe coupler, preamplifier, power amplifier – to operate at 6.5 MHz. We also calculated and constructed a new set of gradient coils X, Y, Z for efficient operation in a smaller volume. Then we reconfigured our 1.5 T MR scanner “MobiRT-122x” to register signals at the new 6.5 MHz frequency.

After tuning the system as a whole and tuning the pulse sequence, as preliminary experiments we were able to obtain a number of projections of the test phantom (Figure 1). Two 500  $\mu$ l Eppendorf tubes placed parallel to each other at a distance of 1 cm were used as a phantom. A Spin Echo (SE) pulse sequence with time  $TE = 5.5$  ms and repetition time  $TR = 1$  s and classical phase-frequency encoding was used for image acquisition. The obtained preliminary images, in our opinion, are quite encouraging and at this stage allow us to expect that magnetic systems of this type, even without

fine shimming, can be used to build on their basis LFMRI systems for tomographic studies of small objects and small animals.

This work was funded by the subsidy allocated to Kazan Federal University for the state assignment in the sphere of scientific activities number FZSM-2023-0016

1. Hori, M., et al. *Investigative radiology*, **56**(11), 669-679 (2021)
2. Marques, J. P., et al. *Journal of magnetic resonance imaging*, **49**(6), 1528-1542 (2019)
3. Arnold, T. C., et al. *Journal of Magnetic Resonance Imaging*, **57**(1), 25-44 (2023)
4. Klein, H. M. *Clinical low field strength magnetic resonance imaging: a practical guide to accessible MRI*. Springer (2015)

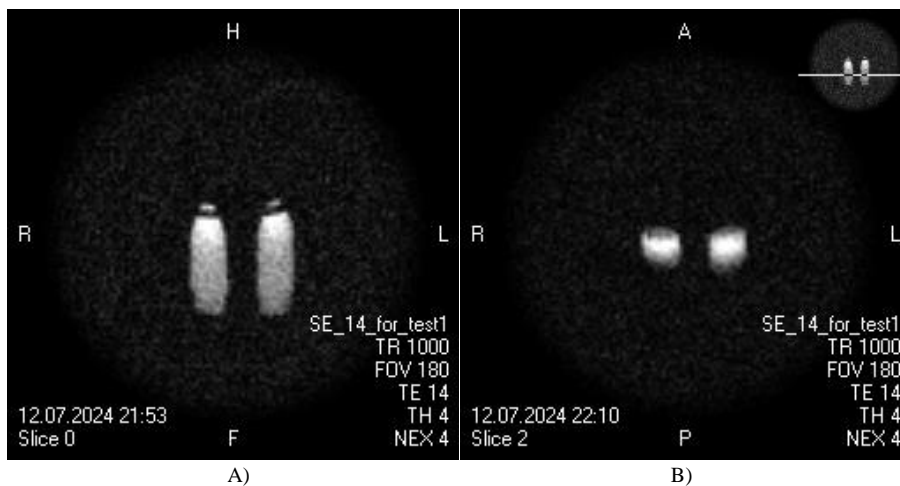


**Fig. 1.** Coronal (A) and transversal (B) projections of the test phantom obtained with a 6.5 MHz Spin Echo sequence with TE = 5.5 ms, TR = 1 s, number of averages – 4.

## Development of a software product for design gradient systems in nuclear magnetic resonance equipment

**A.L. Valiullin, V.D. Skirda, D.S. Ivanov, A.S Alexandrov, O.I. Gnezdilov, M.M. Doroginizky, T.A. Kazbaev**

Institute of Physics, Kazan Federal University, Kazan, Russian Federation

Gradient coils are an integral part of nuclear magnetic resonance (NMR) equipment and, above all, magnetic resonance imaging (MRI). By creating an inhomogeneous magnetic field, gradient coils allow the NMR signal to be spatially encoded. In classical methods, linear gradients are used, the field of which is directly proportional to the coordinates. Due to this, they allow you to uniquely encode the study sample and obtain its image. Nevertheless, classical methods based on linear magnetic field gradients have a number of disadvantages: the duration of the study, as well as insufficient spatial resolution in some cases. In this regard, the use of nonlinear magnetic field gradients, which have uneven spatial resolution, makes it possible to focus research in the area of interest, becomes promising. This idea is implemented in a technique called Patloc [1], based on the formation of several separate zones in the object under study at once, but not with a linear, but with a quadratic gradient of the magnetic field. This approach makes it possible to significantly increase the quality of the resulting image by registering the NMR signal from these zones in parallel mode. The complexities of calculating and modeling nonlinear gradient coils lead to the need to use numerical analytical methods and specialized software. The purpose of this work is to develop a universal software product for calculating gradient coils for a given target field, with specified dimensions and optimized for inductance and resistance.

The MATLAB software package is used as the development environment. The flow function method was used for the calculation [2]. In the process of calculating the gradient coil, the functional is minimized, which includes: deviation of the generated field from the target, inductance and electrical power. Considering the modeling process, we note that the optimization of the current density occurred on the entire surface of the coil. In this regard, when allocating a certain number of current lines, it is necessary to take into account the possible deviation of the created magnetic field from the target. To do this, we used an additional calculation model based on the Bio-Savard-Laplace law, which allowed us to control the magnetic field created by gradient coils. For a qualitative assessment of the calculated gradient coils, the following criterion was chosen: the relative deviation of the created field from the target field should be less than 5%.

The developed program makes it possible to determine the optimal winding configuration of a conductor with current on the cylindrical surface of the coil using a given field, minimizing its inductance and resistance. As an example of how the program works, Figure 1 shows the results of calculating the configuration of coils that create gradients  $G_x, G_{xz}$  (the X-axis is directed along the axis of the coils). For both gradients, the deviation of the received field from the target field does not exceed 5%, and the size of the homogeneous region is  $\sim 75\%$  of the radius of the coil.

In addition to standard linear and nonlinear gradients, the program also allows you to calculate coils that create fields whose configuration is absent in the decomposition

of the field into spherical harmonics [3]. So, the use of a gradient  $G_{x|x|}$  is promising in NMR, the winding for which was defined in the developed program. The calculation result is shown in Figure 2A. Figure 2B shows the surface of the coil and the area in which the field was calculated. The deviation of the received field from the target is ~4%.

The peculiarity of such gradient fields is that they exist in areas of much smaller dimensions than those of classical gradients. So for the gradient  $G_{x|x|}$  this is a layer ~7% thick of the coil radius.

The developed application allows you to calculate coils of cylindrical shapes with great accuracy, creating the necessary fields. In addition to the standard set of gradients, it becomes possible to calculate coils to create nonlinear gradients of arbitrary shape, such as  $x|x|$ .

This work was funded by the subsidy allocated to Kazan Federal University for the state assignment in the sphere of scientific activities number FZSM-2023-0016.

1. Schultz G. Magnetic resonance imaging with nonlinear gradient fields: signal encoding and image reconstruction. – Springer Science & Business Media, 2013. – 343 p.
2. Sánchez C. C. Forward and inverse analysis of electromagnetic fields for MRI using computational techniques: diss. – University of Nottingham, 2008. – 183 p.
3. Jezzard P. Shim coil design, limitations and implications //International Society of Magnetic Resonance in Medicine (ISMRM) Annual Meeting. – 2006.

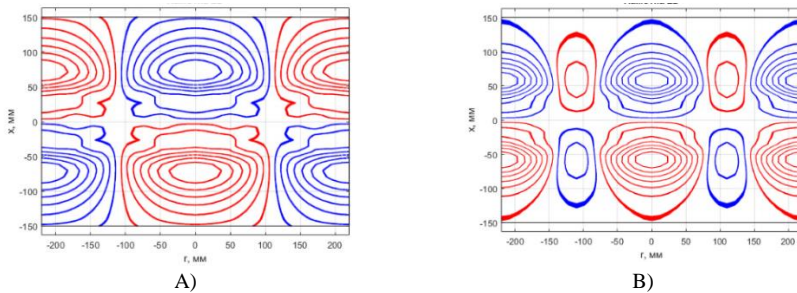


**Figure 1.** Configuration of windings of gradient coils: A)  $G_x$ , B)  $G_{xz}$ . The radius of the coils is 70 mm, the length is 300 mm

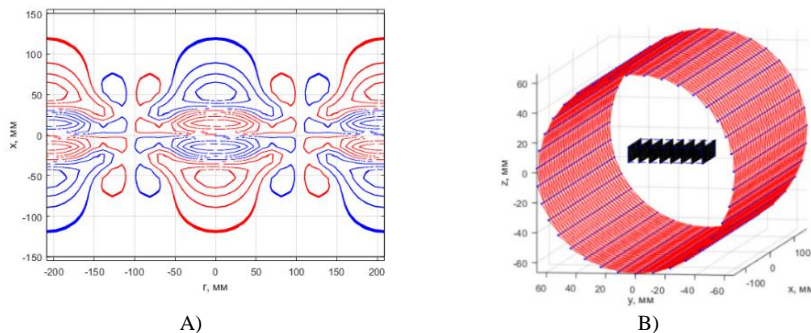


**Figure 2.** A) The configuration of the coil winding  $G_{x|x|}$  (the radius of the coils is 70 mm, the length is 300 mm), B) the surface of the coil and the calculation area (the dimensions of the calculation area are 50 mm \* 50 mm \* 10 mm)

## SURFACE AND VOLUME CENTERS IN LaF<sub>3</sub> PARTICLES

**A.M. Garaeva, F.F. Murzakhanov, E.I. Boltenkova,  
G.V. Mamin and E.M. Alakshin**

Kazan Federal University, Kazan, Russia

The study of rare earth compounds is of great interest due to their unique properties and application possibilities. In this regard, more and more works are devoted to the study of such substances. Rare earth materials can be used in lasers [1], luminophores [2], electronic devices [3], biological markers [4], permanent magnets [5], and so on. In particular, LaF<sub>3</sub> doped with rare earth elements such as Nd, Dy, Yb, Er, Tm, Ho have high potential as optical media [6].

It is known that the method of thermal treatment during synthesis affects the size and morphology of particles [7,8], which affects the physical properties of the sample [8,9]. Therefore, the study of the effect of hydrothermal treatment temperature on the structure of synthesized particles is of great interest.

In this work, LaF<sub>3</sub> particles were studied using electron paramagnetic resonance (EPR). LaF<sub>3</sub> particles were synthesized through a chloride reaction followed by hydrothermal treatment in an autoclave for 24 hours at temperatures of 120°C, 160°C, 200°C and 230°C. Control of the chemical composition and confirmation of crystallinity were carried out using X-ray phase analysis on a Bruker D8 Advance Cu K $\alpha$  diffractometer,  $\lambda=1.5418$  Å. Photographs obtained by transmission electron microscopy on a Hitachi HT Exalens microscope were used to determine the shape and characteristic size of particles in the obtained powders. The effect of the temperature of hydrothermal treatment in an autoclave on the particle size is observed.

EPR measurements were carried out at temperatures (10 K – 300 K) in the X-band with an operating frequency ( $\nu_{mw} = 9.6$  GHz) on a commercial spectrometer Bruker Elexsys E580. A model of the distribution density of paramagnetic centers in the volume and on the surface of particles was compiled. It was found that most of the paramagnetic centers are located in the volume of particles. The dependence of the paramagnetic centers concentration in particles on an increase in the temperature of hydrothermal treatment in an autoclave is analyzed.

This work was financially supported by the Russian Science Foundation (Project No. 23-72-10039).

1. Auzel F.: Chemical reviews, **104** (1), 139-174 (2004).
2. Zeng J. H. et al, Advanced Materials: **17** (17), 2119-2123 (2005).
3. Downing E. et al.: Science: **273** (5279), 1185-1189 (1996).
4. Diamante P. R., van Veggel F. C. J. M.: Journal of fluorescence, **15** (4), 543-551 (2005).
5. Burzo E.: Reports on Progress in Physics: **61** (9), 1099 (1998).
6. Hong J. Q. et al.: Journal of Alloys and Compounds, **646**, 706-709 (2015).
7. Angewandte Chemie International Edition, **42** (30), 3497-3500 (2003)
8. Alakshin, E., Kondratyeva, E., Garaeva et al.: Nanoscale, **14** (31), 11353-11358 (2022).
9. Garaeva, A., Romanova, I., Boltenkova, E. et al.: Nanoscale, **15** (29), 12366-12374 (2023).

## Sorption-Oxidation Mechanism for the Removal of Arsenic (III) Using Cu-Doped ZnO in an Alkaline Medium

**T.P. Gavrilova<sup>1</sup>, A.R. Yagfarova<sup>1</sup>, O.I. Gyrdasova<sup>2</sup>, I.V. Yatsyk<sup>1</sup>**

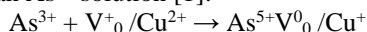
<sup>1</sup>Zavoisky Physical-Technical Institute, FRC Kazan Scientific Center of RAS, Kazan, Russia

<sup>2</sup>Institute of Solid State Chemistry of the Ural Branch of RAS, Ekaterinburg, Russia

Arsenic contamination of water is a serious environmental problem caused by anthropogenic and natural activities. Arsenic enters waterways and soils through the use of pesticides, mine drainage, and geothermal discharges. Adsorption is often used to remove arsenic, and mixed metal oxide composites such as ZnO, CuO and TiO<sub>2</sub> are particularly effective, being able to effectively remove both forms of arsenic (As<sup>3+</sup> and As<sup>5+</sup>). Pre-oxidation of As<sup>3+</sup> to As<sup>5+</sup> followed by adsorption is a key step in removing arsenic from water. In this work, we studied the mechanism of the adsorption process for ZnO and Zn<sub>0.95</sub>Cu<sub>0.05</sub>O samples using electron spin resonance method.

The experimentally detected ESR spectra of ZnO, copper-doped Zn<sub>0.95</sub>Cu<sub>0.05</sub>O samples in initial form and after sorption in As<sup>3+</sup>/As<sup>5+</sup> solutions are presented in Fig. 1 and Fig. 2, respectively. One can see that the ESR spectra consist of a single narrow absorption line of the Lorentzian lineshape (line 1) and a low-field broad absorption line of complex shape (line 2). Line 1 was observed for all samples except the copper-doped sample after sorption in As<sup>3+</sup> solution, Zn<sub>0.95</sub>Cu<sub>0.05</sub>O/As<sup>3+</sup> (Fig. 2). For other samples, the ESR linewidth ( $\Delta H=0.3$  mT) and position ( $g$ -factor  $g=2.002$ ) of this signal do not depend on the method of further processing of the initial ZnO and Zn<sub>0.95</sub>Cu<sub>0.05</sub>O samples. Based on the literature and our experimental data, it is assumed that this signal may be associated with defects in the anion sublattice—singly charged oxygen vacancies. In addition to vacancies (line 1), the low-field EPR signal (line 2) is also due to other intrinsic defects (embedded in the ZnO lattice both in the bulk and on the surface), which have magnetic properties and can be recorded during EPR experiments. As for samples doped with copper (Fig. 2), the ESR signal due to the presence of copper ions in the ZnO sample often appears in a weak magnetic field compared to the narrow ESR line (line 1) from vacancies, and the intensity of this ESR signal increases with increasing copper concentration. Since there were defects in the original sample, it is most likely to assume that the ESR signal in the Zn<sub>0.95</sub>Cu<sub>0.05</sub>O samples arises from the Cu<sup>2+</sup>-V<sup>+</sup><sub>0</sub> and Cu<sup>2+</sup>-V<sup>2+</sup><sub>0</sub> centers (or other pair defects), or it is caused by two simultaneously existing magnetic sublattices Cu<sup>2+</sup> and V<sup>+</sup><sub>0</sub> (or V<sup>2+</sup><sub>0</sub>, etc.) whose magnetic centers interact with each other.

The main focus of this work was the investigation of possible impact of As<sup>3+</sup>/As<sup>5+</sup> sorption on the physical properties of Zn<sub>0.95</sub>Cu<sub>0.05</sub>O samples. Figure 1 shows a significant impact on the ESR spectra of all solutions (As<sup>3+</sup>/As<sup>5+</sup>). However, as for the oxygen vacancy, only the sorption of As<sup>3+</sup> leads to the disappearance of the corresponding line in the ESR spectrum (line 1). It can be concluded that in the case of “photosorption”, the oxidation of As<sup>3+</sup> involves vacancies directly associated with Cu, since in other cases the narrow ESR line from a singly charged vacancy (line 1) practically does not change. Based on obtained experimental results, we can conclude that the following schematic reaction occurs on the surface of the Zn<sub>0.95</sub>Cu<sub>0.05</sub>O sample in an As<sup>3+</sup> solution [1]:



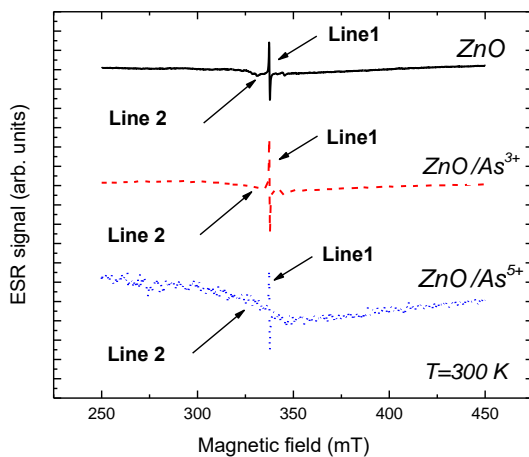


**Fig. 1.** Electron spin resonance spectra of ZnO, ZnO/As<sup>3+</sup> and ZnO/As<sup>5+</sup> in X-band measured at T = 300 K

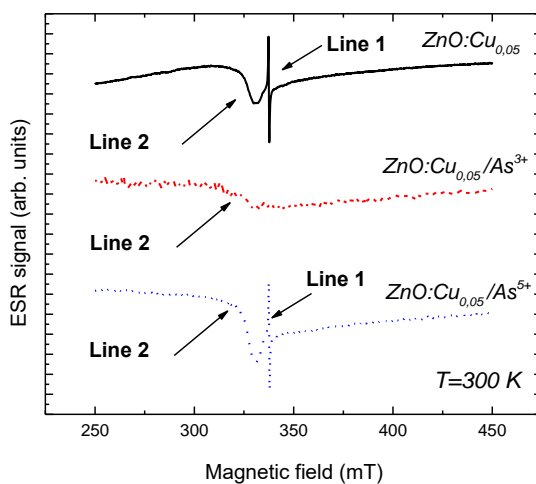


**Fig. 2.** Electron spin resonance spectra of Zn<sub>0.95</sub>Cu<sub>0.05</sub>O, Zn<sub>0.95</sub>Cu<sub>0.05</sub>O/As<sup>3+</sup> and Zn<sub>0.95</sub>Cu<sub>0.05</sub>O/As<sup>5+</sup> measured in X-band at T = 300 K.

1. Gyrdasova O. I., Pasechnik L. A., Krasil'nikov V. N., Gavrilova T. P., Yatsyk I. V., Kuznetsova Yu. V., Kalinkin M. O., Kuznetsov M. V. Water environment research. **95**, e10956 1–15 (2023).



## NMR and MOSSBAUER SPECTROSCOPY STUDY of the POSSIBILITY of OBTAINING HOMOGENEOUS NANOPARTICLES BASED on FeCu ALLOYS

A.Yu. Germov, Ye.V. Suvorkova

M.N. Miheev Institute of Metal Physics of the Ural Branch of the Russian Academy  
of Sciences, Yekaterinburg, Russia

The FeCu alloys and nanoparticles are of interest due to unique properties, application possibilities and relatively low cost. However, the synthesis of these alloys is difficult because of the immiscibility of the Fe and Cu components [1]. In the past studies, the FeCo@C nanoparticles obtained by gas-phase synthesis [2]. Annealing allowed the production of nanoparticles with a high degree of composition homogeneity [3].

In order to study the possibility of producing FeCu nanosized alloys, the combination of NMR and Mössbauer spectroscopy methods have been used to determine the phase composition. The Fe<sub>x</sub>Cu<sub>1-x</sub> powder nanoparticles ( $x = 0.36 - 0.85$ ) in the oxide ( $d = 38$  nm) and carbon ( $d = 6$  nm) shell have been studied.

The <sup>63</sup>Cu NMR spectra of nanoparticles in the oxide or carbon shell are similar and, according to the value of the chemical shift, belong to metallic copper. Based on the presence of quadrupole splitting, a copper-iron solid solution is formed to a certain concentration, but this does not exclude the presence of phase separation.

The Mössbauer spectra of <sup>57</sup>Fe indicate a large part of the ferromagnetic  $\alpha$ -Fe phase, as well as the presence of iron atoms dissolved in the copper lattice. This is partially in agreement with magnetization data. The strong broadening of the sextets in lower fields can be attributed to the solid solution of copper in iron, or to the ferromagnetic state of the particles near the blocking temperature. In the carbon encapsulated FeCu@C nanoparticles, iron carbides have been observed. The similar phases were detected in Fe@C nanoparticles [4], which also points out to composition's inhomogeneity.

Analyzing a complex of resonance methods, we concluded that the FeCu nanoparticles have a heterogeneous structure containing individual phases of iron with inclusions of copper and vice versa. In this case, gas-phase synthesis does not allow us to obtain the homogeneous FeCu nanoparticles, and annealing only increases the inhomogeneity.

The study was carried out within the state assignment of the Ministry of Science and Higher Education of the Russian Federation (theme "Function", No. 122021000035-6).

e-mail: germov@imp.uran.ru

1. Alami A. H., Hawili A. A., Applied Surface Science Advances **1**, 100027 (2020).
2. Tsurin V. A., et al., Physics of the Solid State **56**, 287 (2014).
3. A. Yu. Germov, et al., Journal of Magnetism and Magnetic Materials **588**, 171391 (2023).
4. A. Yu. Germov, et al., Materials Today Communications **27**, 102382 (2021).

## The $\text{Mn}^{2+}$ EPR study of $\text{Cd}_3\text{P}_2$ for topological tuning with 3D Dirac semimetal $\text{Cd}_3\text{As}_2$

Yu. Goryunov<sup>1</sup>, A. Nateprov<sup>2</sup>

<sup>1</sup>Zavoisky Physical-Technical Institute, FRC Kazan Scientific Center of RAS, Kazan, Russia

<sup>2</sup>Institut of Applied Physics, Moldova State University, Chisinau, Moldova

At recent years, it has been increased significantly interest in the arising of 3D topological states in the band structure of semimetals and, in particular, in tuning topological transitions in alloys by introducing magnetic impurities or changing crystal lattice parameters. In the latter case, the alloy system of  $\text{Cd}_3\text{P}_2$  and  $\text{Cd}_3\text{As}_2$  aroused theoretical interest [1].  $\text{Cd}_3\text{P}_2$  is narrow-gap semiconductor.  $\text{Cd}_3\text{As}_2$  is well-known 3D Dirac semimetal. Previously, we studied the influence of impurities topological state in the cadmium arsenide (incl. Mn) [2]. Here we made an attempt to study the magnetic resonance on  $\text{Mn}^{2+}$  in  $\text{Cd}_3\text{P}_2$ , which has a crystal structure identical to  $\text{Cd}_3\text{As}_2$ .

We observed an intense signals is from the  $\text{Mn}^{2+}$  ion, which has the pure spin state  $3d^5$  with  $S=5/2$  and  $L=0$  for  $g=2.0026$  and  $g \sim 2.2$ .  $g = 2.0026$  is almost coincides with the  $g$  - factor of a free electron. This indicates on the absence of a density of  $s$ -electrons at the crystal lattice sites at the locations of cadmium ions. Those, the conduction electrons do not interact with the localized magnetic moments located in these positions. The spectrum also shows a admixture of a signal with a significant different  $g$ -factor from ions in tetrahedral vacancies. This electronic Knight shift indicates the presence in this position of the crystal lattice of the density of  $s$ -electrons.

1. Awadhesh Narayan, et.al., arXiv:1408.3509v3 [cond-mat.mes-hall] 17 Dec 2014

2. Yu.V. Goryunov, A. N. Nateprov, Phys. Sol. St., **63**, 223 (2021)

## Electron paramagnetic resonance investigations of $\beta$ -Ga<sub>2</sub>O<sub>3</sub> single crystals doped with chromium

**A. S. Gurin<sup>1</sup>, R. A. Babunts<sup>1</sup>, A. V. Batueva<sup>1</sup>, D. D. Kramushchenko<sup>1</sup>, P. G. Baranov<sup>1</sup>, D.Yu. Panov<sup>2</sup>, V.A. Spiridonov<sup>2</sup>, D.A. Bauman<sup>2</sup>, A.E. Romanov<sup>2,1</sup>**

<sup>1</sup> Ioffe Institute, Saint Petersburg, Russia

<sup>2</sup> ITMO University, Saint Petersburg, Russia

Gallium oxide in the  $\beta$  phase is a wide-bandgap semiconductor with a bandgap width of 4.7 eV. Both single crystals and thin films of beta-gallium oxide ( $\beta$ -Ga<sub>2</sub>O<sub>3</sub>) can be used in various fields: from high-power electronics to solar-blind UV detectors. One of the attractive features of the Ga<sub>2</sub>O<sub>3</sub> system is its high radiation resistance, which makes it suitable for space applications.

Impurities determine the electrical and optical properties of the crystal. Chromium-doped  $\beta$ -Ga<sub>2</sub>O<sub>3</sub> single crystals were grown at ITMO by the Czochralskii method [1].

Recently, the results of electron paramagnetic resonance (EPR) studies of nominally undoped  $\beta$ -Ga<sub>2</sub>O<sub>3</sub> single crystals have been published, where Cr<sup>3+</sup> ion signals in the octahedral environment were detected [2].

EPR studies were carried out using high-frequency EPR/ODMR W/D-band spectrometer in continuous wave mode at 94 GHz and a 6K with a closed-cycle magneto-optical cryostat. The spectrometer was developed at the Ioffe Institute [3] and it can operate in 1.7-300 K temperature range and a wide range of magnetic fields with a zero-value crossing.

In addition to the three EPR signals of the Cr<sup>3+</sup> ion ( $S = 3/2$ ) in the octahedral environment, three other less intense signals were observed. Using analysis of anisotropic spectra and numerical modeling we can established that Cr<sup>3+</sup> ions in gallium oxide crystal occupy two positions: octahedral and tetrahedral.

The research was supported by the Ministry of Science and Higher Education of the Russian Federation (FFUG-2024-0046)

1. D.A. Bauman, D.I. Panov, D.A. Zakgeim, V.A. Spiridonov, A.V. Kremleva, A.A. Petrenko, P.N. Brunkov, N.D. Prasolov, A.V. Nashchekin, A.M. Smirnov, M.A. Odnoblyudov, V.E. Bougrov, A.E. Romanov. *Phys. Status. Solidi A*, 218, 2100335 (2021).

2. R. A. Babunts, A. S. Gurin, E. V. Edinach, H.-J. Drouhin, V. I. Safarov, P. G. Baranov. *J. Appl. Phys.*, 132, 155703 (2022).

3. R. A. Babunts, A. G. Badalyan, A. S. Gurin, N. G. Romanov, P. G. Baranov, A. V. Nalivkin, L. Yu. Bogdanov, D. O. Korneev, *Appl. Magn. Reson.*, 51, 1125 (2020).

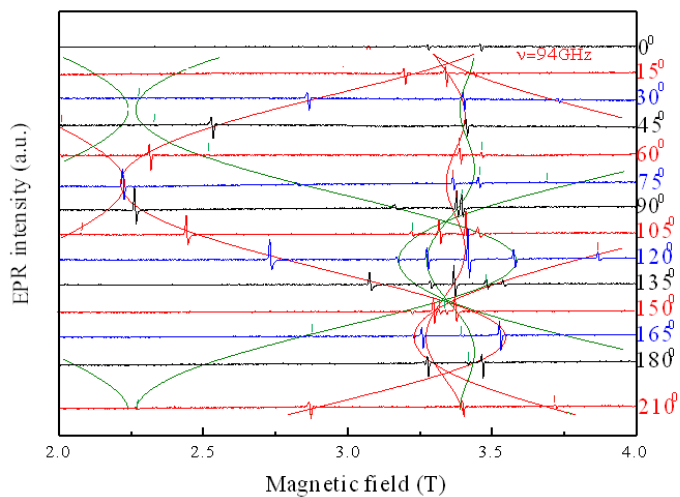


**Fig. 1.** Angular dependences of EPR signals in  $\beta\text{-Ga}_2\text{O}_3$  at  $T=6\text{K}$ . The red lines indicate the simulated EPR octahedral position and the green ones show the simulated EPR tetrahedral chromium position.

## Magnetic anisotropy in rutile (TiO<sub>2</sub>) heavily implanted with cobalt ions: FMR, VSM and TEM studies

Ö. Karataş<sup>1</sup>, C. Okay<sup>2</sup>, B. Özkal<sup>3</sup>, S. Kazan<sup>3</sup>, B.Z. Rameev<sup>3,4,5</sup>,  
N. Cherkashin<sup>6</sup>, E.M. Begishev<sup>5</sup>, R.I. Khaibullin<sup>5</sup>

<sup>1</sup> Konya Technical University, Department of Electrical and Energy, Konya, Turkey

<sup>2</sup> Marmara University, Department of Physics, Göztepe, Istanbul, Turkey

<sup>3</sup> Gebze Technical University, Department of Physics, Gebze, Kocaeli, Turkey

<sup>4</sup> Kazan State Power Engineering University, Kazan, Russia

<sup>5</sup> Zavoisky Physical-Technical Institute, FRC Kazan Scientific Center of RAS, Kazan, Russia

<sup>6</sup> CEMES-CNRS and Université de Toulouse, Toulouse, France

Single rutile (TiO<sub>2</sub>) heavily implanted with cobalt ions reveals room-temperature anisotropic ferromagnetism [1,2]. However, up until now, a systematical study of the magnetic anisotropy in cobalt-ions implanted TiO<sub>2</sub> has been missing. In this work, the magnetic crystalline anisotropies of the Co-ions implanted TiO<sub>2</sub> rutile plates with different crystallographic orientations have been studied in detail by ferromagnetic resonance (FMR) and vibrating sample magnetometry (VSM) methods supported by high-resolution transmission electron microscopy (HRTEM).

The Co<sup>+</sup> ions with energy of 40 keV were implanted into (100), (001) and (110) single-crystalline plates of rutile to a high fluence of  $1.5 \times 10^{17}$  ions/cm<sup>2</sup> at room temperature by using an ion-beam implanter (ZPTI of RAS). HRTEM study showed that the high-fluence implantation of Co ions into the TiO<sub>2</sub> results in the formation of hcp-Co nanoparticles in the surface layer with a thickness of about 50 nm. The angular dependences of FMR spectra have revealed the room-temperature ferromagnetic behaviour with extraordinary magnetic anisotropies. VSM measurements taken at different temperatures support FMR observations of magnetic anisotropy in Co-ions implanted TiO<sub>2</sub> plates. It was noted that in-plane magnetic hysteresis curves for the (100) and (110) TiO<sub>2</sub> samples reveal the behaviour which is typical to orientations near the hard axes. On the other hand, the (001) TiO<sub>2</sub> sample shows a hysteresis shape closer to the rectangular one which is a typical feature of easy axis direction.

The general analysis of FMR, VSM and HRTEM data indicates that strongly anisotropic room-temperature ferromagnetism is induced by the textured growth of magnetic cobalt nanoparticles. The possible growth directions of the Co nanoparticles with respect to crystal axes of the TiO<sub>2</sub> rutile matrix are discussed.

The authors from ZPTI of RAS (E.M.B and R.I.K.) acknowledge the support of the Russian Science Foundation (project number 22-19-00712, <https://rscf.ru/project/22-19-00712/>).

1. Khaibullin R.I, Tagirov L.R., Rameev B.Z. et al.: J. Phys. Cond. Matter **16**, L443-L449 (2004).

2. Akdogan N., Rameev B.Z., Khaibullin R.I. et al.: J. Magn. Magn. Mater. **300**, e4-e7 (2006).

## MODELING THE MAGNETIC RESPONSE OF FUNCTIONALIZED CARBON STRUCTURES

E.I. Kovycheva, K.B. Tsiberkin, V.K. Henner

Perm State University, Perm, Russia

The properties of highly porous carbon materials can be controlled by inserting metal cores into shells or by depositing magnetic ions on the carbon surface. For example, adding an impurity in a high concentration leads to the opening of a band gap in the energy spectrum of carbon, and the material becomes close to a semiconductor in its properties. In addition, the described materials can find applications in the development of new systems for storing, processing and transmitting information using spin magnetic moments. [1]. The study of composites with properties that are controlled by an applied magnetic field, is an urgent task. In this work, we analyze the dynamics of the spin clusters magnetization with a ring structure in different states, as well as their combination in the form of a spherical carbon nanoshell formed by rings of different numbers of spins.

In this work, the model of the dynamics of the spin clusters magnetization in various states for spin 1/2 is improved. The dynamics of the lattices magnetization with various geometries, in addition to ring structures, are considered. In addition, a new method of modeling a spherical structure, which is closer to reality, has been developed. Here is have been performed a series of calculations of the spin systems transverse magnetization evolution, that make up a two-dimensional rectangular lattice and a hexagonal lattice element.

In previous work [5], the calculated magnetization signals from individual rings were summed to simulate the dynamics of the spherical structure according to the method described in [2, 3]. The total signal shows a monotonic decay; the exact dependence requires additional analysis.

Using the same technique, the magnetization signal was calculated for a rectangular flat lattice consisting of nine spins (Fig. 1):

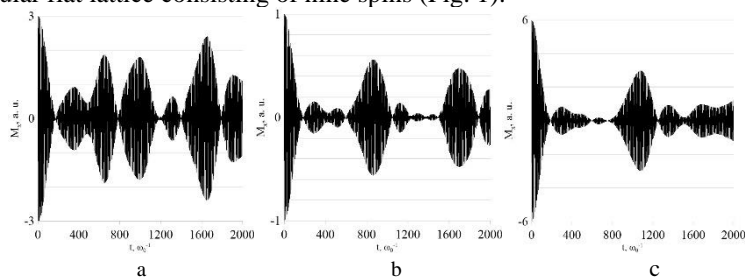


**Fig. 1.** Magnetization of a rectangular lattice of a - 6 spins, b - 9 spins, c - 12 spins

During the work, there was found a maximum number of spins that the machine used can count - 13 particles. The following calculation simulates the structure of graphene - a hexagonal lattice consisting of three rings is reproduced. This structure contains 13 spins. The magnetic response of such a grating is shown in Fig. 2:

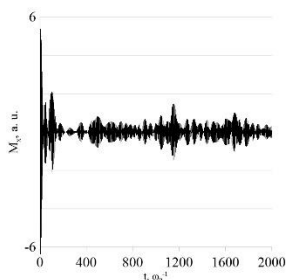


Fig. 2. Magnetization of a hexagonal lattice of 13 spins

Next, the existing model was improved. Instead of obtaining the response of a spherical system by summing the magnetization signals of individual rings, a spherical shell was modeled, created by a random distribution of spins over the surface. Unlike the previous model, in the new one all particles interact with each other. Thus, a model of a spherical shell that is closer to reality was obtained. For this model, a function is used that returns a random floating number of the von Mises distribution [6]. The angles that define the location of particles on the surface of the sphere are obtained by generating random numbers with a uniform distribution. Fig. 3 shows the responses of spherical structures for different numbers of spins:

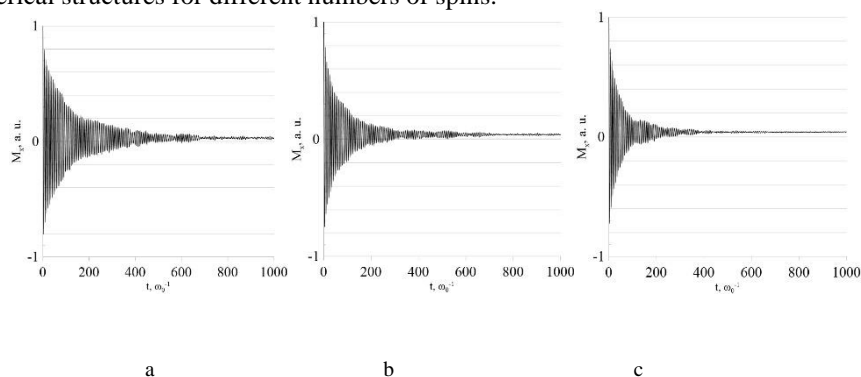


Fig. 3. Sphere magnetization a – 6 spins, b – 8 spins, c – 10 spins

On Fig. 3 it can be seen that the exponential dependence is preserved in the same way as when modeling the response of a sphere by adding the individual responses of the rings.

1. G.A. Rudakov, A.V. Sosunov, R.S. Ponomarev, V.K. Khenner, M.S. Reza, G. Sumanasekera. *Phys. Solid State* **60** (1), 167 (2018)
2. E.K. Henner, I.G. Schaposhnikov, *Radiospectroscopy* **10**, 74–81 (1976)
3. Henner V. K., Klots A., Nepomnyashchy A. A., Belozerova T. S. *Applied Magnetic Resonance*. **52**, 859–866 (2021).
4. A. Abragam, *The principles of nuclear magnetism* (Clarendon Press, Oxford, 1961), p.599
5. E.I. Kovycheva, K.B. Tsiberkin, *Bull. Perm Univ. Phys.* **2**, 26–35 (2022).
6. Python documentation, The Python Standard Library, Numeric and Mathematical Modules, random. Available at: <https://docs.python.org/3/library/random.html>

## ESR of Yb<sup>3+</sup> ION at CUBIC SITES in Cs<sub>2</sub>NaScF<sub>6</sub> CRYSTALS

M.L. Falin<sup>1</sup>, V.A. Latypov<sup>1</sup>, N.M. Khaidukov<sup>2</sup>

<sup>1</sup> Zavoisky Physical-Technical Institute, FRC Kazan Scientific Center of RAS, Kazan, Russia

<sup>2</sup> Kurnakov Institute of General and Inorganic Chemistry, Moscow, Russia

Hexafluorides (fluoroelpasolites) A<sub>2</sub>BLnF<sub>6</sub> (A<sup>+</sup>, B<sup>+</sup> = Na, K, Cs, Rb; Ln<sup>3+</sup>) have good optical and thermomechanical properties. This leads to widespread applications of such crystals doped with impurity ions in lighting, lasers and displays, sensing, imaging and photodynamic therapy for silicon solar cells, etc. [1–4]. Crystals, in which ions of the matrix crystal can be replaced by isovalent triply charged impurity ions, have attracted much attention. On the one hand, there is no multicentricity, which greatly simplifies spectroscopic studies; on the other hand, it is possible to activate such crystals with high concentrations of impurity ions, in some cases up to 100%, which is of great practical importance. It is known that crystals have a cubic elpasolite structure with the space symmetry group  $O_h^5$  down to low temperatures [5], where dopant impurity centers mainly have cubic symmetry and are good model systems for experimental and theoretical studies of the interactions of dopant impurity ions with each other and with ions of the matrix crystal, for the further development of the theory of calculating the electronic structure of crystals activated by impurity ions, etc. Recently, attention has been attracted to crystals of hexafluoroscandates (e.g., Cs<sub>2</sub>NaScF<sub>6</sub>) with photo-active lanthanide ions for backlighting devices of liquid crystal displays, mobile phones, TV sets, etc. [6].

The crystals were synthesized by a direct temperature-gradient method as a result of a reaction of aqueous solutions containing 35–40 mol% CsF and 8–10 mol% NaF with oxide mixtures 0.999Sc<sub>2</sub>O<sub>3</sub> – 0.001Yb<sub>2</sub>O<sub>3</sub> (purity: 99.9% for Sc<sub>2</sub>O<sub>3</sub> and 99.999% for Yb<sub>2</sub>O<sub>3</sub>) at a temperature of 750 K in the upper growth region, temperature gradient along the reactor body of up to 3 K/cm, and pressure of 100 MPa. Spontaneously nucleated Cs<sub>2</sub>NaSc<sub>0.999</sub>Yb<sub>0.001</sub>F<sub>6</sub> crystals of up to 0.5 cm<sup>3</sup> were obtained in the upper crystallization region of the autoclave for 200 h.

EPR measurements were carried out on a modified X-band spectrometer ERS-231 (Germany), which used a helium flow thermostat CRYO202ESR (Russia) at temperatures of 4.2–300 K.

The parameters of the corresponding spin Hamiltonians, the ground states and their wave functions were determined. Structural model of the observed complex was proposed. The experimental results were analyzed in comparison with those for the same paramagnetic ion in other hosts [7-9].



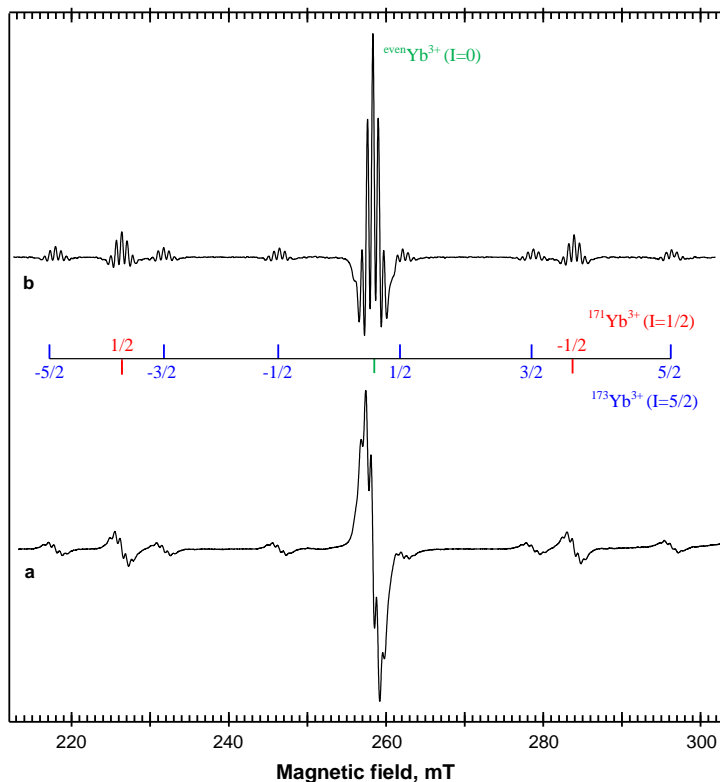


**Fig.** EPR spectrum of the  $\text{Yb}^{3+}$  ion in  $\text{Cs}_2\text{NaScF}_6$  (**a** and **b** – the first and second derivatives of the absorption EPR lines, respectively).  $T = 4.2$  K.  $\nu = 9.360$  GHz.

1. Makhov V.N., Khaidukov N.M., Lo D., Krupa J.C., Kirm M., Negodin E.: *Opt. Mater.* **27**, 1131 (2005)
2. Mroczkowski S., Dorain P.: *J. Less. Common Met.* **110**, 259-265 (1985)
3. Vrielinck H., Izeddin I., Ivanov V.Y., et al: *MRS Online Proceedings Library* **866**, 7 (2005)
4. Khaidukov N., Makhov V., Guckan V., Altunal V., Ozdemir A., Kurt K., Abusaid W.: *J. Lumin.* **239**, 118391 (2021)
5. He X., Yan B.: *Journal of Materials Chemistry C*, **2**, 2368 (2014)
6. Zhou Y.Y., Song E.H., Brik M.G., Wang Y.J., Hu T., Xia Z.G., Zhang Q.Y.: *Journal of Materials Chemistry C*, **7**, 9203 (2019)
7. Falin M.L., Latypov V.A., Khaidukov N.M.: *Appl. Magn. Reson.* (2024) (in press)
8. Falin M.L., Anikeenok O.A., Latypov V.A., Khaidukov N.M. et al: *Phys. Rev. B* **80**, 174110 (2009)
9. Falin M.L., Meiklyar V.P., Konkin A.L.: *J. Phys. C: Solid St. Phys.* **13**, 1299 (1980)

## $^{59}\text{Co}$ CENTERS IN MONOCLINIC $\text{Sc}_2^{28}\text{SiO}_5$ SINGLE CRYSTAL: CW EPR STUDY

**R. F. Likerov<sup>1</sup>, I. V. Yatsyk<sup>1</sup>, D. V. Popov<sup>1</sup>, A. V. Shustov<sup>1</sup>, R. M. Eremina<sup>1</sup>**

<sup>1</sup> Zavoisky Physical-Technical Institute, FRC Kazan Scientific Center of RAS, Kazan, Russia

Monoclinic orthosilicates doped with rare-earth and transition metal ions are actively studied by numerous groups for at least few decades. The main reason for interest in these materials is that such materials have promising properties for quantum memory applications [1].

The scandium orthosilicate with pure silicon by isotope content,  $\text{Sc}_2^{28}\text{SiO}_5$  is one of two actively studied orthosilicate mediums for quantum memory materials, the other being  $\text{Y}_2^{28}\text{SiO}_5$ . By excluding other isotopes of silicon, we removing the influence of nuclear magnetism of  $^{29}\text{Si}$  on the impurity ion's properties.

Previously, we studied both scandium and yttrium orthosilicates, doped with Nd, Yb, Cr and V ions. In this work we studied  $^{59}\text{Co}$  impurity centers with CW EPR method. From the fitting of angular dependencies of EPR spectrum for  $^{59}\text{Co}:\text{Sc}_2^{28}\text{SiO}_5$ , obtained in three orthogonal planes, we derived parameters of the spin Hamiltonian, such as g-tensor main values, hyperfine tensor main values and zero-field splitting parameters.

1. Likerov R., Eremina R., Yatsyk I., et. al. // Appl. Magn. Reson. – 2023. – v. 54. – p. 477 – 489.

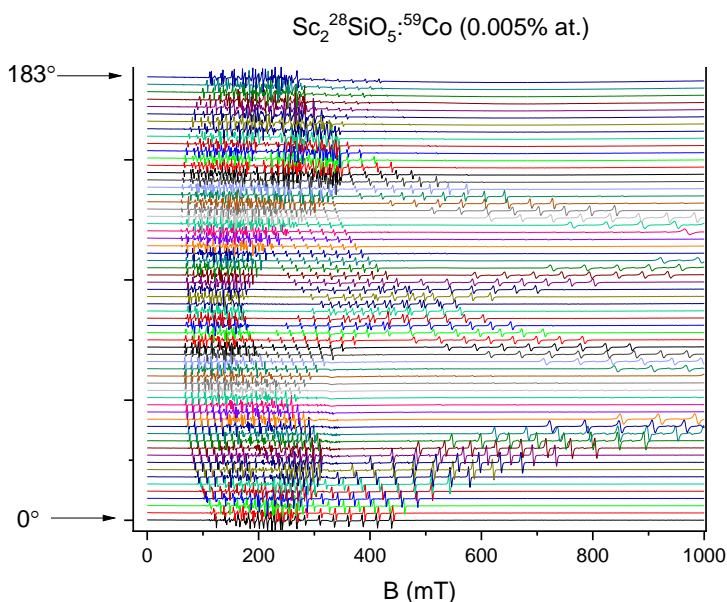


**Fig. 1.** Angular dependence of EPR spectrum for  $\text{Sc}_2^{28}\text{SiO}_5: ^{59}\text{Co}$  (0.005% at.) obtained with external magnetic field  $\mathbf{B}$  rotated in the  $bD2$  – plane

## Electron nuclear double resonance of $^{14}\text{N}$ nuclei coupled to the $\text{V}_\text{B}^-$ defect in hBN crystals

**G.V Mamin<sup>1</sup>, F.F. Murzakhanov<sup>1</sup>, I.N. Gracheva<sup>1</sup>, M.R. Gafurov<sup>1</sup>,  
V.A. Soltamov<sup>2</sup>**

<sup>1</sup> Institute of Physics, Kazan Federal University, Kremlyovskaya 18, Kazan 420008, Russia

<sup>2</sup> Ioffe Institute, Polytekhnicheskaya, 26, St. Petersburg 194021, Russia

The negatively charged boron vacancy ( $\text{V}_\text{B}^-$ ) in hexagonal Boron Nitride (hBN), featuring a triplet ( $S=1$ ) ground spin state, is emerging as a promising candidate in advanced quantum technologies based on van der Waals (vdW) materials. Its spin can be precisely controlled and read out using microwave and optical methods [1], making it ideal for applications as qubits and for quantum sensing to detect minute variations in magnetic, electric, and other physical fields. The robustness of this defect and compatibility of hBN with graphene and other vdW materials further enhance its potential for practical sensing of quantum phenomena in vdW-based devices. Understanding electron-nuclear interactions between  $\text{V}_\text{B}^-$  electron spin with surrounding nuclei is nowadays of core interest [2]. Currently, understanding is limited to the three nitrogen atoms nearest to the vacancy, for which the following interactions have been established: hyperfine interaction (HFI) with  $A_{\text{iso}}=59.3$  MHz and dipole-dipole  $A_{\text{dd}}=13.8$  MHz, nuclear quadrupole interaction (NQI) with  $C_q=1.96$  MHz and  $\eta=0.07$ [3].

The exploration of nitrogen nuclear spins, particularly for applications in coherent control, nuclear hyperpolarization, is a key focus of current research worldwide [4]. Here we extend the study of electron-nuclear interactions involving the  $\text{V}_\text{B}^-$  electron spin and N atoms by expanding our understanding beyond the nearest three nitrogen nuclei. Specifically, we use high-frequency ENDOR techniques to investigate the HFI and NQI with more distant nuclear spins on the nitrogen sublattice of hBN. Our findings reveal that the hyperfine coupling constant with these distant nitrogen spins is an order of magnitude smaller than that with the nearest nitrogen spins. Furthermore, the corresponding NQI allows us to extract fundamental property of the hBN crystal, such as the native electric field gradient experienced by the nitrogen nuclei.

This work has been supported by the grants the Russian Science Foundation, RSF 24-12-00151.

1. Gottscholl, A., Kianinia, M., Soltamov, V., Orlinskii, S., Mamin, G., Bradac, C., Kasper, C., Krambrock, K., Sperlich, A., Toth, M., Aharonovich, I., Dyakonov, V: *Nature Materials*. **19**, 540-545 (2020) <https://doi.org/10.1038/s41563-020-0619-6>

2. S. Ru, Z. Jiang, H. Liang et al. Robust Nuclear Spin Polarization via Ground-State Level Anticrossing of Boron Vacancy Defects in Hexagonal Boron Nitride, *Phys. Rev. Lett.* **132**, 266801 (2024) <https://doi.org/10.1103/PhysRevLett.132.266801>

3. Gracheva, I.N., Murzakhanov, F.F., Mamin, G.V., Sadovnikova, M.A., Gabbasov, B.F., Mokhov, E.N., Gafurov, M.R.: *The Journal of Physical Chemistry C*, **127**, 3634–3639 (2023) <https://doi.org/10.1021/acs.jpcc.2c08716>

4. Gao, X., Vaidya, S., Li, K. *et al.*: Nuclear spin polarization and control in hexagonal boron nitride. *Nat. Mater.* **21**, 1024–1028 (2022). <https://doi.org/10.1038/s41563-022-01329-8>

## Optical Spin Initialization of Nitrogen Vacancy Centers in a $^{28}\text{Si}$ -Enriched 6H-SiC Crystal for Quantum Technologies

**F.F. Murzakhonov<sup>1</sup>, G.V. Mamin<sup>1</sup>, D.V. Shurtakova<sup>1</sup>, M.A. Sadovnikova<sup>1</sup>,  
E.N. Mokhov<sup>2</sup>, O.P. Kazarova<sup>2</sup>, M.R. Gafurov<sup>1</sup>**

<sup>1</sup> Institute of Physics, Kazan Federal University, Kazan, Russia

<sup>2</sup> Ioffe Institute, St. Petersburg, 194021 Russia

Intrinsic or artificially induced point defects in various materials are of particular interest because even extremely low their concentrations can significantly affect various physicochemical characteristics of materials. A number of vacancy defects (color centers) promote the variation of the visible and near-infrared optical properties of crystals [1]. The presence of a high-spin state (electron spin  $S \geq 1$ ) in combination with optical, charge, and coherent properties makes it possible to consider color centers as candidates for a quantum bit (qubit), which a basic computing unit of a quantum computer. Silicon carbide (SiC) with color centers can be a possible alternative of diamond (NV centers) because it doesn't have the diamond's demerits and has sufficient mechanical, temperature, chemical, and radiation strengths [2]. It is known that SiC can be used as a reliable matrix for many high-spin ( $S = 1$  and  $3/2$ ) defects such as a silicon vacancy  $V_{\text{Si}}$ , divacancy  $VV$ , and negatively charged nitrogen-vacancy centers NV, which are direct "twins" in microscopic structure of NV centers in diamond [3, 4].

In this work, optically active nitrogen-vacancy color centers NV in a  $^{28}\text{Si}$ -enriched (nuclear spin  $I = 0$ ) 6H- $^{28}\text{SiC}$  crystal have been studied using the photoinduced ( $\lambda = 980$  nm) high-frequency (94 GHz, 3.4 T) pulsed electron paramagnetic resonance method at a temperature of  $T = 150$  K. Three structurally nonequivalent types of NV centers with axial symmetry have been identified and their spectroscopic parameters have been determined. Long spin–lattice,  $T_1 = 1.3$  ms, and spin–spin,  $T_1 = 59$   $\mu\text{s}$ , ensemble relaxation times of NV centers with extremely narrow (450 kHz) absorption lines allow highly selective excitation of resonant transitions between sublevels ( $m_l$ ) caused by the weak hyperfine interaction ( $A = 1.1$  MHz) with  $^{14}\text{N}$  ( $I = 1$ ) nuclei for the quantum manipulation of the electron spin magnetization.

The study was funded by the subsidy allocated to Kazan Federal University for the state assignment in the sphere of scientific activities (Project No. FZSM-2024-0010).

1. V. M. Acosta, E. Bauch, M. P. Ledbetter, A. Waxman, L.-S. Bouchard, and D. Budker, Phys. Rev. Lett. 104, 070801 (2010)
2. M. Xu, Y. R. Girish, K. P. Rakesh, P. Wu, H. M. Manukumar, S. M. Byrappa, Sh. M. Udayabhanu, and K. Byrappa, Mater. Today. Commum. 28, 102533 (2021)
3. F. F. Murzakhonov, B. V. Yavkin, G. V. Mamin, S. B. Orlinskii, H. J. von Bardeleben, T. Biktagirov, U. Gerstmann, and V. A. Soltamov, Phys. Rev. B 103, 245203 (2021)
4. R. A. Babunts, Yu. A. Uspenskaya, A. P. Bundakova, G. V. Mamin, E. N. Mokhov, and P. G. Baranov, JETP Lett. 118, 629 (2023)

## STUDIES OF STATIONARY SATURATION OF INHOMOGENEOUSLY BROADENED EPR LINES OF N-V CENTERS IN HPHT DIAMOND

**A.V. Nikitina<sup>1,2</sup>, Yu.V. Bogachev<sup>1</sup>, V.I. Zubkov<sup>1</sup>, A.V. Solomnikova<sup>1</sup>,  
S.M. Suharzevskiy<sup>2</sup>**

<sup>1</sup>St.-Petersburg Electrotechnical University, St.-Petersburg, Russia

<sup>2</sup>Magnetic Resonance Research Centre, St.-Petersburg State University, St.-Petersburg, Russia

The estimation of spin-lattice  $T_1$  and spin-spin  $T_2$  relaxation times plays an important role in the EPR research of semiconductor diamonds properties.

EPR studies of synthetic diamond samples of NDT company (Sestroretsk, Russia) grown by the HPHT method were carried out. EPR experiments were performed on EPR spectrometer Bruker Elexsys E580 in the Magnetic Resonance Research Centre of St.-Petersburg State University, Russia.

We have analyzed the stationary saturation of inhomogeneously broadened EPR lines of N-V centers in HPHT diamond sample using the method proposed in [1].

In accordance with [1], we assume that the inhomogeneously broadened resonance line consists of non interacted spin packets, each of which is characterized by a Lorentz absorption line. The frequency distribution function of the packets is approximated by a Gaussian curve. The analysis of the experimental saturation curves for EPR signals of hyperfine structure of EPR spectra for N-V centers of HPHT diamond and comparison with the results of computer simulation of the saturation curves of the first harmonic of the absorption signal shown that the number of spin packets involved in the shape of inhomogeneous broadened EPR line is equal to 25 with a sufficiently high degree of accuracy. Calculations in accordance with the formulas in [1] give the values of  $T_2 = 2,5 \cdot 10^{-6}$  s and  $T_1 = 5,4 \cdot 10^{-5}$  s. The values of relaxation times found in our experiment are consistent with the values of  $T_1$  and  $T_2$  found by the pulsed EPR method [2] for the N-V centers in diamonds. The difference in the values of  $T_1$  may be due to the different nature and concentration of the studied paramagnetic centers, different structures of the sample matrices.

In this study we also observed the effect of a dip in the saturation curve and the effect of transformation of the shape of the absorption lines of the EPR signal into the shape of the radiation line under strong microwave saturation of the EPR spectra.

### **Acknowledgments**

*This study was supported by the state assignment for the Saint Petersburg Electrotechnical University "LETI" (theme No. FSEE-2024-0005).*

1. Bogachev Yu.V., Nikitina A.V.: *LETI Transactions on Electrical Engineering and Computer Science*, **8**, 16-20 (2016).
2. S. Kollarics, F. Simon, A. Bojtor, K. Koltai, et al.: *Carbon*, **188**, 393-400 (2022).

## INFLUENCE OF THE INTERFACE ON MAGNETIC RESONANCE IN FILMS OF THE Fe-Bi SYSTEM

**G.S. Patrin<sup>1,2</sup>, E.N. Volchenko<sup>1,2</sup>, Ya.G. Shiyan<sup>1,2</sup>,  
V.Yu. Yakovchuk<sup>2</sup>, V.R. Churkin<sup>1</sup>**

<sup>1</sup> Siberian Federal University, Svobodny pr., 79, Krasnoyarsk, 660041, Russia

<sup>2</sup> L.V. Kirensky Institute of Physics, Federal Research Center KSC SB RAS, Akademgorodok, 50/38, Krasnoyarsk, 660036, Russia

Magnetic nanosized layered structures with a semi-metallic interlayer are poorly studied objects and are of significant interest for condensed matter physics. Most of the research is devoted to the study of Bi-containing semiconductor alloys as materials for infrared detectors or multilayer 3d-metal–bismuth films. Many properties of film systems are determined by interactions at the interface of different materials. Interfaces change not only bulk magnetic properties, but are also capable of inducing magnetism in non-magnetic layers, changing the nature of the magnetic state.

The films were obtained by thermal evaporation at a base vacuum of  $P \sim 10^{-6}$  Torr. In one cycle, films of Fe/Bi, Bi/Fe and Fe compositions were deposited onto glass substrates. For all films, the thickness of the magnetic layer was  $t_{\text{Fe}} \approx 10$  nm, and the bismuth thickness was  $t_{\text{Bi}} = 15$  nm. To measure the resonance properties, we used a Bruker E 500 CW EPR spectrometer operating at a frequency  $f_{\text{MWF}} = 9.48$  GHz.

It was previously discovered that the magnetic properties of two-layer films in the Fe-Bi system strongly depend on the order of deposition of layers on the substrate. If we compare the resonant absorption of the reference film of pure iron with other films, it is found that the deposition of the second layer of bismuth changes the magnetic resonance spectrum differently depending on the order of deposition of the magnetic and non-magnetic layers. In the case of the Fe/Bi film, the resonance field and the shape of the absorption curve do not differ much from the resonance in the Fe film, and the most dramatic change is observed for the film of the Bi/Fe composition. To determine the role of the interface at the iron-bismuth interface, the resonance properties of a pure iron film were studied in detail. It was found that uniaxial anisotropy is observed in the film plane with the easy axis directed along the magnetic field during deposition. The difference in the magnetic resonance parameters for Fe/Bi and Fe films in the temperature range up to the temperature of liquid nitrogen differs only slightly. The  $\Delta H_{\text{pp}}$  linewidth for a film of composition Bi/Fe is approximately an order of magnitude greater than that of a film of the Fe/Bi composition. For the Bi/Fe structure highly heated, high-energy iron ions fall onto a layer of bismuth, which is fusible. Iron penetrates quite deeply into the thickness of the bismuth layer. As a result, nano-sized iron granules are formed. It is known that in the nanogranular state, iron particles have much greater anisotropy.

The research was conducted according to the state assignment of the Ministry of Science and Higher Education of the Russian Federation and the Federal State Autonomous Educational Institution of Higher Education Siberian Federal University (No. FSRZ-2023-0008).

## LONG-RANGE INTERLAYER COUPLING IN [(CoP)<sub>hard</sub>/(NiP)<sub>am</sub>/(CoP)<sub>soft</sub>]<sub>n</sub> STRUCTURES

**G.S. Patrin<sup>1,2</sup>, Ya.G. Shiyan<sup>1,2</sup>, V.A. Orlov<sup>1,2</sup>, V.G. Plekhanov<sup>1</sup>**

<sup>1</sup> Siberian Federal University, Svobodny pr., 79, Krasnoyarsk, 660041, Russia

<sup>2</sup> L.V. Kirensky Institute of Physics, Federal Research Center KSC SB RAS, Akademgorodok, 50/38, Krasnoyarsk, 660036, Russia

Film systems consisting of alternating layers with different properties provide the possibility of obtaining synthetic materials that are promising for solving spin electronics problems [1]. In this series, systems can be distinguished where ferromagnetic layers are coupled with non-magnetic semiconductor (or semi-metallic) layers [2]. Systems with magnetic layers having different magnetic order [3] or with strongly differing magnetic anisotropies are of interest [4]. We have already shown [5] that in the [(CoP)<sub>soft</sub>/(CoP)<sub>hard</sub>]<sub>n</sub> structure, when the direct coupling of magnetically hard and magnetically soft layers occurs and through the NiP interlayer, the resulting magnetization curve is not an algebraic sum of the magnetization curves of the initial layers. An increase in the number of blocks (n) in the structure of ferromagnetic magnetically soft and magnetically hard layers results in an increase in the influence of the magnetically soft layer on the magnetization process of the film structure.

Multilayer structures with the number of blocks  $n = 1, 5, 10, 15, 20, 40$  have been synthesized. The entire series of multilayer films was deposited in one cycle. Both magnetic layers had a thickness of  $t_{\text{CoP}} = 5$  nm and a non-magnetic layer had a thickness of  $t_{\text{NiP}} = 2$  nm. In this case, the Zeeman interaction energies of each type of layer give approximately the same contribution. The thicknesses of the layers were also controlled by X-ray spectroscopy with a measurement accuracy of  $\pm 0.5$  nm. The electron magnetic resonance spectra were measured by using a Bruker E 500 CW EPR spectrometer operating at a frequency of  $\omega_{\text{MWF}} = 9.49$  GHz. The spectra were processed by fitting the experimental absorption line curve into components from the Lorentz-type curves.

When studying the magnetostatic properties of multilayer films [(CoP)<sub>soft</sub>/(NiP)<sub>am</sub>/(CoP)<sub>hard</sub>/(NiP)<sub>am</sub>]<sub>n</sub>, it has been found that depending on the number of structural blocks (n), oscillations of the saturation field of magnetization ( $H_s$ ) and coercive force ( $H_c$ ) take place. According to it, it is possible to suggest that there is a change in both interface anisotropy and interlayer interactions in the films. If the magnetic layers are identical layers of amorphous cobalt [24], only one microwave absorption line is observed in a three-layer film at a given frequency. This indicates that there is a strong ferromagnetic interaction between the amorphous cobalt layers. In our case, when one of the layers is magnetically hard, the magnetic layers become different not only because of the large difference in the anisotropies but because of the possible change in the interlayer interaction. For this reason, the spectrum consists of two lines spaced at a fairly significant distance along the magnetic field. . When the number of blocks in the film structure ( $n \geq 5$ ) increases, another line appears and later there are 3 microwave absorption lines in the resonance spectrum. The experimental results do not fit into the scheme of alternating identical magnetically soft and

magnetically hard layers, which can be represented as magnetic sublattices. In the two-sublattice model, the third peak of microwave absorption is not obvious. In the case of the  $[(\text{CoP})_{\text{soft}}/(\text{NiP})_{\text{am}}/(\text{CoP})_{\text{hard}}/(\text{NiP})_{\text{am}}]_n$  structure, the question arises about the reason for the third peak of resonant absorption. Obviously, additional interaction is necessary for such behavior of resonant properties.

It can be considered that a possible mechanism for long-range interaction is the effect of magnetic proximity. The essence of the effect is that in a paramagnetic metal layer in contact with a ferromagnetic layer spin polarization occurs extending a considerable distance ( $t_{\text{SM}}$ ) from the interface of materials [7]. In our case, the distance between the nearest soft magnetic layers is  $t_{\text{SS}} = 2 \cdot t_{\text{NiP}} + t_{\text{hard}} \approx 9$  nm, which fits perfectly into the spatial scale where magnetic proximity can occur.

Finally, it has been established that processes in interfaces between different materials play a significant role in the formation of magnetic properties in multilayer film superlattices  $[(\text{CoP})_{\text{soft}}/(\text{NiP})_{\text{am}}/(\text{CoP})_{\text{hard}}/(\text{NiP})_{\text{am}}]_n$ .

Firstly, a perpendicular magnetic anisotropy occurs at the interface between the magnetic and non-magnetic layers, the their magnitude increases together with an increase in the number of blocks  $n$ .

Secondly, at the interface of the NiP and CoP layers, a CoNiP sublayer is presumably formed, which is magnetically soft. It is revealed in a decrease in the magnetization of that part of the magnetization curve that the magnetically hard subsystem is responsible for.

Thirdly, the fact that the deposition of layers occurs practically under equilibrium conditions may be the reason for long-range interlayer interaction, since the loss of spin polarization of electrons at the intersection of the interface of materials is minimal. As a result, three peaks of microwave absorption are observed in the magnetic resonance spectrum.

At the same time, antiferromagnetic interaction takes place between the nearest magnetically hard and soft magnetic layers, and ferromagnetic interaction takes place between the nearest soft magnetic layers. It is the reason for the system of soft magnetic layers to be divided into two subsystems. Under the conditions of magnetostatic measurements, the behavior of magnetization shows signs inherent in magnetic springs with moderate interaction.

1. Zutic, J. Fabian, S. Das Sarma, *Rev. Mod. Phys.* **76**, 323 (2004).
2. G.S. Patrin, O.V. Vas'kovskii. *The Physics of Metals and Metallography*. **101**, S63 (2006).
3. Florin Radu and Hartmut Zabel Exchange Bias Effect of Ferro-/Antiferromagnetic Heterostructures P.97), in book *Magnetic Heterostructures. Advances and Perspectives in Spinstructures and Spintransport* H. Zabel and S. D. Bader (Eds.) Springer-Verlag Berlin Heidelberg, 2008.
4. Z.M. Dai, W. Liu, X.T. Zhao, Z. Han, D. Kim, C.J. Choi, Z.D. Zhang. *J. Appl. Phys.* **120**, 163906(7) (2016).
5. G. S. Patrin, Ya. Shiyan, K. G. Patrin, and G. Yu. Yurkin, *J. Low Temp. Phys.* **182**, 73 (2016).
6. G.S. Patrin, Ya.G. Shiyan, A.V. Chzhan, S.A. Podorozhnyak. *Mater. Res. Express.*, **8**, 056102 (2021).
7. M.J. Zuckermann. *Sol.St. Commun.* **12**, 745 (1973).



## MAGNETIC RESONANCE STUDIES OF BIQUADRATIC INTERLAYER COUPLING IN CoNi/Si/FeNi FILMS

**G.S. Patrin<sup>1,2</sup>, Ya.A. Vakhitova<sup>2</sup>, Ya.G. Shiyan<sup>1,2</sup>,  
A.V. Kobyakov<sup>1,2</sup>, V.I. Yushkov<sup>1,2</sup>**

<sup>1</sup> Siberian Federal University, Svobodny pr., 79, Krasnoyarsk, 660041, Russia

<sup>2</sup> L.V. Kirensky Institute of Physics, Federal Research Center KSC SB RAS, Akademgorodok, 50/38, Krasnoyarsk, 660036, Russia

Due to the specific nature of their structure, nanomagnetic materials have a set of unusual properties, which arouses interest in them, both in terms of fundamental research and in terms of possible practical applications. Interlayer interaction in such systems is responsible for the formation of the magnetic state. To control the interlayer interaction, as a determining parameter when creating structures such as a magnetic spring with given characteristics, attempts are being made to introduce additional layers, for example, from a semiconductor material, between the magnetic layers.

The films were sputtered onto a glass substrate using an ultrahigh vacuum magnetron sputtering system from Omicron NanoTechnology (Taanusstein, Germany) with Pfeiffer Vacuum turbomolecular pumps. The deposition was carried out at a base pressure of  $10^{-10}$  Torr in an argon atmosphere. The nickel content in the CoNi layer was 19.5 at. %, and in the FeNi layer there was 83 at. %. The thickness of the CoNi layer was  $t_h = 53$  nm and was chosen so that it would exhibit the properties of a magnetically hard layer when measured in available magnetic fields. The thickness of the soft magnetic FeNi layer was  $t_s = 72$  nm. The thickness of the non-magnetic semiconductor layer was variable and varied in the range  $t_{Si} = 0 - 23$  nm. Magnetization measurements were carried out using an MPMS-XL setup in the temperature range from helium temperature to room temperature. Electron microscopic studies of the cross section were performed on a JEOL JEM-2100 electron microscope. To measure the resonance properties, we used a Bruker E 500 CW EPR spectrometer operating at a frequency  $f_{MWF} = 9.48$  GHz.

Along with magnetostatic studies of the magnetic spring properties of the films, magnetic resonance spectra were measured. It was discovered that, depending on the thickness of the silicon layer, the angular dependences of the resonant field behave in an unusual way. Between the lines responsible for absorption in different materials, there is an angular shift of the resonant field in the plane of the film, the magnitude of which depends on the thickness of the silicon layer and temperature. In the limiting case, the shift is 90 degrees. This behavior cannot be associated with magnetic anisotropy, since the anisotropy of the FeNi layer is practically zero at room temperature, and the magnitude of the line shift, on the contrary, increases with temperature. The observed resonance properties are explained within the framework of a model with negative biquadratic interlayer interaction.

## THE INFLUENCE OF CENTRIFUGATION ON DOSIMETRIC PROPERTIES OF SYNTHETIZED HYDROXYAPATITE

**Podshivalov A.P.<sup>1</sup>, Bajtimirov D.R.<sup>1</sup>, Konev S.F.<sup>1</sup>, Ivanov D.V.<sup>1, 2</sup>, Slesarev G.P.<sup>1</sup>**

<sup>1</sup>Ural Federal University, Ekaterinburg, Russia

<sup>2</sup>M.N. Mikheev Institute of Metal Physics, Ural Branch of the Russian Academy of Sciences, Ekaterinburg, Russia

The research is aimed to study of the centrifugation procedure influence on the structure of synthesized hydroxyapatite samples, and their sensitivity to ionizing radiation in the dose range from 10 to 40 kGy.

The hydroxyapatite samples synthesized by precipitation from solution were studied. A saturated solution of calcium hydroxide was used as a calcium-containing reagent, while a solution of orthophosphoric acid with a mass fraction of 1.5 percent was used as a phosphate-containing reagent. During the entire synthesis, the hydroxyapatite solution was bubbled with carbon dioxide.

The hydroxyapatite synthesized in this way was separated into two parts: the first was dried at room temperature in a precipitated form (control group), and the second was subjected to centrifugation in plastic tubes before drying. After that, all centrifuged samples were removed from the test tubes and divided into three groups - upper, central and lower (samples of A, B and C groups respectively). Then all samples were irradiated by a linear electron accelerator in the dose range of 10–40 kGy.

As a result, it was shown that noticeable differences in the characteristics of the EPR spectra were observed in the centrifuged samples. Group A demonstrated the lowest radiation sensitivity, and the most sensitive were group B samples. Group C demonstrated the most similar behavior of the EPR signal dose response as natural hydroxyapatite (tooth enamel), showing an increase of signal up to 30 kGy with subsequent saturation.

12 days after the last irradiation of the samples with a total dose of 40 kGy, EPR spectra for all groups were recorded to determine the relaxation of radiation-induced signal. For the control group, a significant relaxation of the EPR signal was observed within the range of 25-35%, for the A group - about 37%, and for B and C groups the relaxation of the EPR signal was less than the method error.

The work was partially supported by the Ministry of Science and Higher Education of the Russian Federation (through the basic part of the government mandate, project No. FEUZ-2023-0013).

## Combined equation of semiclassical spin dynamics and electron paramagnetic resonance

S.V. Demishev<sup>1,2</sup>, A.V. Popov<sup>1,2</sup>

<sup>1</sup> Vereshchagin Institute for High Pressure Physics of the Russian Academy of Sciences, Troitsk, Moscow, Russia

<sup>2</sup> National Research University Higher School of Economics, Moscow, Russia

In a recent paper [1] it is shown that the equations of semiclassical spin dynamics with Landau-Lifshitz (LL) and Hilbert (G) relaxation terms are not equivalent in general case. When calculating the EPR spectrum, both variants of accounting for spin relaxation give a close line shape only in the limit of weak relaxation. In the case of significant dumping, the effect of the relaxation parameter on the maximum position of the absorption line turns out to be different, which may reflect different possible physical situations in systems with strong electron correlations [1].

In this work, we consider for the first time an equation for semiclassical magnetization  $\mathbf{M}$  dynamics in a magnetic field  $\mathbf{H}$  with a combined term representing a weighted sum of LL and G relaxation terms,  $\mathbf{R}_{LL}=\lambda[\mathbf{M}, [\mathbf{M}, \mathbf{H}]]$  and  $\mathbf{R}_G=\gamma\eta[\mathbf{M}, d\mathbf{M}/dt]$ :

$$\frac{d\mathbf{M}}{d\mathbf{H}} = \gamma[\mathbf{M}, \mathbf{H}] - (\delta \cdot \mathbf{R}_{LL} + (1 - \delta) \cdot \mathbf{R}_G) \quad (1)$$

where  $0 \leq \delta \leq 1$  sets relative contribution  $R_{LL}$ , и  $\gamma$  is gyromagnetic ratio. Following [1], it is possible to introduce relaxation parameters  $\alpha_{LL}=\eta\chi_0\omega$  and  $\alpha_G=\lambda\chi_0\omega/\gamma^2$  and, for simplicity, we will put  $\alpha_{LL}=\alpha_G=\alpha$ . In linear approximation  $\mathbf{M}=\chi_0\mathbf{H}$ , the calculation of absorbed power  $P$  for EPR in Faraday's geometry gives:

$$P = \chi_0 h_0^2 \frac{\alpha(x^6 + (1 + (1 - \delta)^2 \alpha^2)x^4 + (\delta\alpha x)^2)}{(x^4 - (1 - (1 - \delta)^2 \alpha^2)x^2 - (\delta\alpha)^2)^2 + (2\alpha x)^2}, \quad (2)$$

where  $x=\omega/(\gamma H_0)=\omega/\omega_H$  is the reduced frequency of microwave radiation and  $h_0$  stands for the amplitude of variable magnetic field. The shape of the EPR line in coordinates  $P/\chi_0 h_0 = f(x, \alpha)$  is shown in Fig.1 for case  $\delta=0,5$  by three-dimensional graph and contour graph. It is visible that at  $\alpha \sim 2$  there is a sharp change in the position of the EPR line maximum  $x_{max}$ , at which the value of  $x_{max}$  changes 1.8 times. This effect is accompanied by an increase in EPR line width  $W$  and resulting  $W(\alpha)$  turns out to be non-monotonous: there is a maximum on curve  $W(\alpha)$  in the range  $2 < \alpha < 3$  (Fig. 1).

The obtained result is of interest from the point of view of a new group of magnetic phenomena – spin-fluctuation transitions (SFT) [2], which are characterized by a sharp change in amplitude of magnetic fluctuations  $\Delta M$  under variation of a control parameter. According to [1], a change in the relaxation parameter may be due to change in the amplitude of magnetic fluctuations. Then, in the model under consideration, a monotonous change in  $\Delta M$  will lead to a maximum in EPR linewidth. Interestingly, this type of SFT was recently discovered in the spiral magnet MnSi [3].

1. Demishev S.V.: *Appl. Magn. Reson.* (2024). <https://doi.org/10.1007/s00723-023-01638-4>
2. Demishev S.V.: *Physics – Uspekhi*, **67**, 22-43 (2024)
3. Demishev S.V., Shestakov A.V., Yatsyk I.V., Semeno A.V., Grigoriev S.V., Eremina R.M.: *Sol. State Commun.* **385**, 115501 (2024)

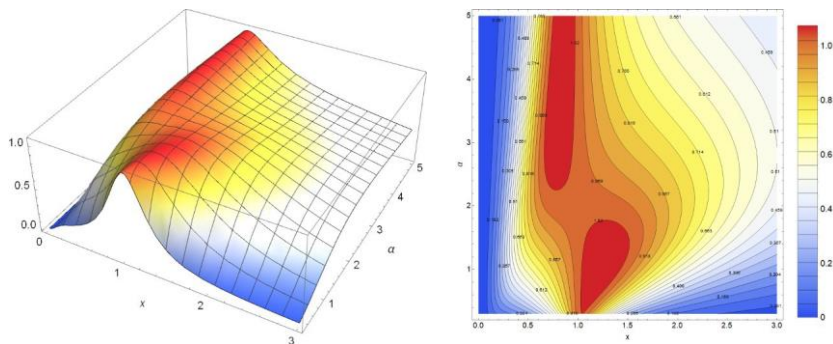


**Fig. 1.** 3D plot and  $P/\chi_0 H_0^2 = f(x, \alpha)$  map for the simulated EPR line with the combined relaxation term.

## ADDITIONAL EPR LINE IN Mn-CONTAINING DOUBLE PEROVSKITES

**Popov D.V.<sup>1</sup>, Batulin R.G.<sup>2</sup>, Yatsyk I.V.<sup>1</sup>, Maiti T.<sup>3</sup>, Eremina R.M.<sup>1</sup>**

<sup>1</sup>Zavoisky Physical-Technical Institute, FRC Kazan Scientific Center of RAS, Kazan 420029, Russian Federation,

<sup>2</sup>Kazan (Volga Region) Federal University, Kazan 420111, Russian Federation

<sup>3</sup>Department of Materials Science and Engineering, Indian Institute of Technology Kanpur, Kanpur 208016, UP, India

e-mail: kazan-city.dvpopoff@yandex.ru

Perovskites are oxides with formula  $ABO_3$ , where A is alkaline earth metal ion, B is transition metal ion. Perovskites have octahedral oxygen framework built around B ions [1]. Double perovskites are the type of perovskites, that consist of two aforementioned formulas at once. Their major difference from complex single perovskites is an ordering in the arrangement of B ions – in double perovskite, B ions can form chains or planes.

The aim of this work is investigation and comparison of  $Sr_2MnNbO_6$  and  $Sr_2MnTiO_6$  double perovskites' magnetic and EPR properties. AC and DC magnetization dependences from temperature and external magnetic field were measured, using PPMS-9 device in Kazan Federal University. Temperature dependences were measured in zero field cooling (ZFC) and field cooling (FC) modes at range 2-300K. External magnetic field dependences were measured in fields up to 9T.

EPR spectra were measured using a Bruker spectrometer. The measurements were performed at temperature range from 10 to 340K. The same unusual effect was observed at  $H_{res} \approx 600$  Oe for  $Sr_2MnNbO_6$  at temperatures 38-42K and at  $H_{res} \approx 500$  Oe for  $Sr_2MnTiO_6$  at temperatures 35-40K.

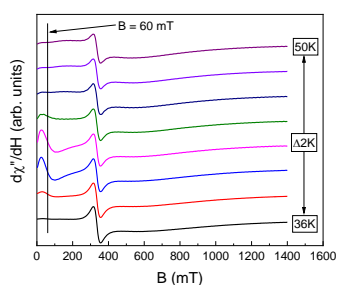


Fig. 1. EPR spectra of  $Sr_2MnNbO_6$  at temperature range of  $T = 36-50K$

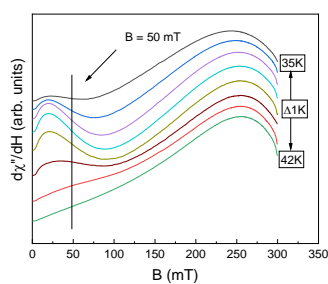


Fig. 2. EPR spectra of  $Sr_2MnTiO_6$  at temperature range of  $T = 35-42K$

This research was supported by the Russian Science Foundation (Project No. 22-42-02014) and DST Project number DST/INT/RUS/RSF/P-55/2021.

## SYNTHESIS AND STUDY OF MAGNETIC PROPERTIES OF [La<sub>0.5</sub>Dy<sub>0.5</sub>]ES AND [La<sub>0.99</sub>Dy<sub>0.01</sub>]ES COMPOUNDS

**I.V. Romanova<sup>1</sup>, S.V. Stazharova<sup>1</sup>, R.G. Batulin<sup>1</sup>,  
M.S. Tagirov<sup>1,2</sup>, R.V. Yusupov<sup>1</sup>**

<sup>1</sup>Kazan Federal University, Kazan, Russia

<sup>2</sup>Institute of Applied Research, Tatarstan Academy of Science, Kazan, Russia

Dysprosium ethyl sulfate Dy(C<sub>2</sub>H<sub>5</sub>SO<sub>4</sub>)<sub>3</sub>·9H<sub>2</sub>O is one of the promising materials for use in magnetic technologies, for example, for changing temperature under the influence of a magnetic field to accelerate gas cooling. This chemical compound has high magnetic susceptibility and magnetic anisotropy, which makes it attractive for use in various instruments and devices [1]. The space group of crystal symmetry Ln(C<sub>2</sub>H<sub>5</sub>SO<sub>4</sub>)<sub>3</sub>·9H<sub>2</sub>O is hexagonal P6<sub>3</sub>/m, with two magnetically equivalent complexes in the unit cell of the crystal [2]. The Dy(C<sub>2</sub>H<sub>5</sub>SO<sub>4</sub>)<sub>3</sub>·9H<sub>2</sub>O crystal is an Ising ferromagnet with an ordering temperature T<sub>c</sub> = 0.13 K [3]. Interest in this substance is due to the colossal effective magnetic moment of the dysprosium ion in the ground state. In this work, single crystals of lanthanum ethyl sulfate and dysprosium La(C<sub>2</sub>H<sub>5</sub>SO<sub>4</sub>)<sub>3</sub>·9H<sub>2</sub>O (LaES), [La<sub>1-x</sub>Dy<sub>x</sub>]ES (x = 0.01, 0.5) were grown, where ES=(C<sub>2</sub>H<sub>5</sub>SO<sub>4</sub>)<sub>3</sub>·9H<sub>2</sub>O. The magnetic properties of the synthesized compounds were also studied by measuring magnetization with a vibrating magnetometer in a wide range of temperatures and fields, as well as comparing the data obtained with theoretical calculations.

The work was supported by Kazan Federal University Strategic Academic Leadership Program (PRIORITY-2030).

1. H.B. Brom, W.J. Huiskamp: *Physica*, **60**, 163-198, (1972).
2. D. R. Fitzwater, R.E. Rundle: *Zeitschrift für Kristallographie-Crystalline Materials*, **112**, 362-374 (1959).
3. A.H. Cooke, Donald T. Edmonds, C. B. P. Finn, W. P. Wolf: *Proceedings of the Royal Society of London. Series A. Mathematical and Physical Sciences*, 306, 335-353 (1968).

## Modeling of Magnetic Resonance Spectra of $\text{La}_{1-x}\text{K}_x\text{MnO}_3$

**N.S. Saenko, N.I. Steblevskaya, M.V. Belobeletskaya, A.M. Ziatdinov**

Institute of Chemistry, Far Eastern Branch of the RAS, Vladivostok, Russia,  
saenko@ich.dvo.ru

At present, there has been continued interest to study the properties of materials potentially suitable for use both in information storage devices and in magnetic field sensors. The compounds based on lanthanum manganite  $\text{LaMnO}_3$ , obtained by partial replacement of lanthanum in the structure of this compound with mono- ( $\text{Li}^+$ ,  $\text{K}^+$ ,  $\text{Na}^+$ ,  $\text{Ag}^+$ ), di- ( $\text{Ca}^{2+}$ ,  $\text{Sr}^{2+}$ ,  $\text{Ba}^{2+}$ ,  $\text{Pb}^{2+}$ ), trivalent ( $\text{Cr}^{3+}$ ,  $\text{Co}^{3+}$ ,  $\text{Bi}^{3+}$ ,  $\text{Ce}^{3+}$ ,  $\text{Pr}^{3+}$ ) ions, as well as their combinations are among them. The main objectives in studying systems of this kind are to reveal relations between physical properties, chemical composition, synthesis method, valence state of manganese and the type of crystal structure. Electronic and magnetic properties of manganites are rather various and sensible to the chemical composition and doping extent of compounds. Particularly, depending on doping element concentration, they can exhibit transitions between different magnetically ordered states [1-5]. The following methods are most often used in the scientific literature for the synthesis of lanthanum manganites, including doped ones: 1) solid-phase synthesis with different types of atmosphere, at different temperature and pressure, and with optional additional physical effect to reagents (mechanical, ultrasonic, irradiation); 2) chemical deposition; 3) sol-gel method; 4) hydrothermal synthesis; 5) sorption method 6) pyrolysis [6]. This work examines samples of undoped and doped with potassium ions lanthanum manganite, which were synthesized by the low-temperature extraction-pyrolytic method [7]. Analysis of temperature changes in magnetic characteristics was carried out using computer simulation of the spectra of electron paramagnetic and ferromagnetic resonances (further, united under the general name: electronic magnetic resonance – EMR). All spectra were recorded on a JEOL-X330 spectrometer equipped with variable temperature unit DVT5 (ES-13060).

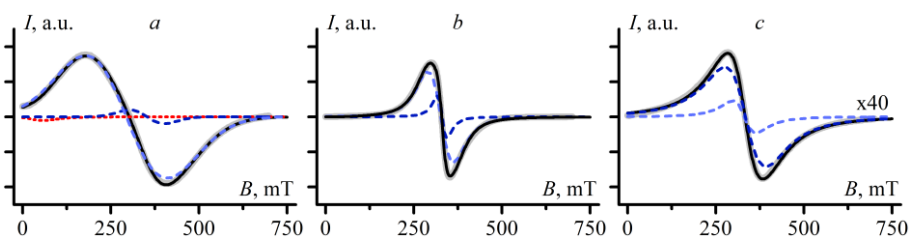


**Fig. 1.** Approximation of EMR spectra of  $\text{La}_{0.85}\text{K}_{0.15}\text{MnO}_3$  at temperatures  $-160$  (a),  $0$  (b) and  $+160$  °C (c).

In all  $\text{La}_{1-x}\text{K}_x\text{MnO}_3$  samples, where  $x = 0.0, 0.1, 0.15$ , at temperatures above  $25^\circ\text{C}$ , the EMR spectrum can be approximated by the sum of two components of the Lorentzian form (Fig. 1c). The latter indicates that magnetic resonance at high temperatures is observed predominantly on paramagnetic particles. In the spectrum of undoped  $\text{LaMnO}_3$ , the narrow and broad components of approximation simultaneously

broaden with increasing temperature with various changes in the  $g$ -factor value (Fig. 2*a, b*). At the same time, for potassium-doped lanthanum manganites, the lines in the approximation of EMR spectrum are also broaden, and the changes in the  $g$ -factor of both components do not exceed 0.03 (Fig. 2*a, b*).

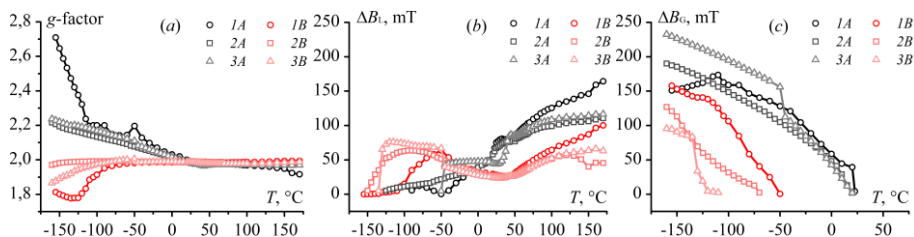


**Fig. 2.** The temperature dependences of the  $g$ -factor (*a*), Lorentz linewidth  $\Delta B_L$  (*b*) and Gauss linewidth  $\Delta B_G$  (*c*) for two Voigt function components in decomposition of EMR spectra of the compounds  $\text{La}_{1-x}\text{K}_x\text{MnO}_3$ . Curves 1, 2 and 3 correspond to  $x = 0.0, 0.1, 0.15$ , respectively; A and B – to the parameters of first and the second Voigt function components.

As the temperature decreases, the shapes of the lines under consideration are transformed, and in such a way that their approximations by the sum of lines with a Lorentzian shape become less and less satisfactory (Fig. 1, *a, b*). In this case, a transformation of the spectrum to a form characteristic of ferromagnetic resonance is observed [8-9]. It turned out that the EMR spectra of  $\text{La}_{1-x}\text{K}_x\text{MnO}_3$  at low temperatures can be expressed using the sum of two components with the Voigt function (Fig. 1*a, b*). What is common to all samples with increasing temperature is an increase from zero in the Lorentzian contribution to the linewidth (Fig. 2*b*), as well as a decrease in the Gaussian contribution to the linewidth down to zero (Fig. 2*c*). In the spectra of all compounds at a temperature of about  $-100^{\circ}\text{C}$ , absorption of microwave power is clearly observed at zero external magnetic field (Fig. 1*a*), which increases with decreasing temperature. This is a characteristic feature of the EMR spectra of ferromagnetic materials with residual magnetization [8-9]. An additional component (also by Voigt function) was used to describe it in the approximations (Fig. 1*a*). All of the above indicates the presence of ferromagnetic phase clusters in the samples, the proportion of which increases with decreasing temperature. The report plans to discuss the possible reasons for temperature changes in the parameters of the components in the approximations of the EMR spectra of these compounds.

The work was carried out under a state assignment of the Institute of Chemistry, Far Eastern Branch of the Russian Academy of Sciences, Vladivostok, Russia (project FWFN(0205)-2022-0003).

1. Guan X., Li H., Jin Sh. et al.: *Ceram. Int.* **47**, N. 13, 18931 (2021).
2. Gluchowski P. et al.: *Materials* **13**, N. 7, 1788 (2020).
3. Eremina R.M. et al.: *Phys. Rev. B.* **84**, N. 6, 064410 (2011).
4. Bouzid S.A. et al. *J. Alloys Compd.* **839**, 155546 (2020).
5. Deisenhofer J. et al.: *Phys. Rev. B.* **66**, N. 5, 054414 (2002).
6. Rudskaya A. et al.: *Inž. vestn. Dona* **25**, N. 2, 1-21 (2013). (In Russian)
7. Steblevskaya N.I. et al.: *Russ J. Inorg. Chem.* **68**, N. 12, 1737–1743 (2023).
8. Castel V., Youssef J.B., Brosseau C. J.: *Nanomaterials.* **2007**, P. 27437 (2007).
9. Guskos N. et al.: *Nanotechnol. Secur. Syst.* **2015**, P. 33–47 (2015).



## ANTI-SITE DEFECTS and TRIGONAL CENTER of HOLMIUM in $\text{Y}_3\text{Al}_5\text{O}_{12}:\text{Ho}^{3+}$ CRYSTAL ACCORDING to the RESULTS of WIDEBAND EPR SPECTROSCOPY

**G.S. Shakurov<sup>1</sup>, N.M. Lyadov<sup>1</sup>, G.R. Asatryan<sup>2</sup>, A.G. Petrosyan<sup>3</sup>, K.L. Hovhannesyan<sup>3</sup>**

<sup>1</sup> Zavoisky Physical-Technical Institute, FRC Kazan Scientific Center of RAS, Kazan, Russia

<sup>2</sup>Ioffe Institute, St-Petersburg, Russia

<sup>3</sup>Institute for Physical Research, Ashtarak-2, Armenia

The YAG:Ho<sup>3+</sup> crystal is a well-known laser material that allows generation on many channels in the wavelength range from ~0.55 to ~3 μm. Of particular interest is laser radiation on the <sup>5</sup>I<sub>7</sub>–<sup>5</sup>I<sub>8</sub> channel in the two-micron region, which corresponds to the window of absolute transparency of the atmosphere and is less dangerous for human eyes. YAG:Ho crystals are used in surgery, lidar systems, and mechanical processing of materials. Crystals of aluminum garnets Re<sub>3</sub>Al<sub>5</sub>O<sub>12</sub>, where Re is a rare-earth element or Y, obtained by the melt method contain an excess of Re, even if the melt corresponds to the stoichiometric composition. Based on X-ray diffraction and spectroscopic measurements, it was found that the excess Re<sup>3+</sup> fills a part of octahedral a-sites of Al<sup>3+</sup>. The concentration of such non equivalent substitutions (Re<sub>a</sub>3+), later called anti-site, in YAG crystals is 2–3%. According to theoretical calculations, the formation energy of anti-site defects is lower than that of Frenkel and Schottky defects, so the probability of their presence in the garnet lattice during synthesis at high temperatures is high. The energy of formation of anti-site defects “aluminum in place of yttrium” is greater, so their expected concentration is much lower. Anti-site defects play a negative role in scintillators, creating electron traps and slowing down the scintillation process.

Previously, we studied Ho<sup>3+</sup> impurity centers occupying dodecahedral positions of yttrium in a YAG crystal [1]. However, it was not possible to study in detail the centers associated with anti-site defects because of the weak signals and the overlap of their spectra with the lines of the main holmium center. In the present work, the study is supplemented by measurements on two new crystals. Using the method of wideband EPR spectroscopy information was obtained on the energy interval between the ground and first excited nondegenerate sublevels of the ground multiplet <sup>5</sup>I<sub>8</sub> of Ho<sup>3+</sup> ion. In addition, a trigonal holmium center was discovered and its spectroscopic parameters were determined.

## DISTRIBUTION OF $Ce^{3+}$ IMPURITY CENTERS IN HIGHLY DOPED $LiCaAlF_6$ CRYSTALS

**A. A. Shavelev<sup>1</sup>, A. S. Nizamutdinov<sup>1</sup>, A. A. Shakirov<sup>1</sup>, S. L. Korableva<sup>1</sup>,  
D. G. Zverev<sup>1</sup>, A. A. Rodionov<sup>1</sup>, E. V. Lukinova<sup>2</sup>, V. V. Semashko<sup>3</sup>**

<sup>1</sup> Kazan (Volga Region) Federal University, Kazan, Russia

<sup>2</sup> Belgorod State University, Belgorod, Russia

<sup>3</sup> Kazan Institute of Physics and Technology, Federal Research Center KazSC RAS, Kazan, Russia

In this work, crystals of the active media of  $Ce^{3+}:LiCaAlF_6$  UV lasers, which are characterized by the formation of several types of  $Ce^{3+}$  ion centers, are studied [1,2]. This was confirmed by us as a result of the detection of zero-phonon lines for two centers in low-temperature luminescence spectra, as well as in ESR spectra for different orientations of the magnetic field relative to the crystallographic axes of the samples. We have shown that for  $Ce^{3+}:LiCaAlF_6$  crystals, with an increase in the concentration of  $Ce^{3+}$  ions in the melt, crystallization occurs in such a way that the concentration of impurity centers of lower symmetry increases to a greater extent than that of centers of higher symmetry. Moreover, laser generation belongs to precisely this type of center.

1. The magnetic and optical properties of  $Ce^{3+}$  in  $LiCaAlF_6$ , M. Yamaga, D. Lee, B. Henderson, T. P. J. Han, H. G. Gallagher, T. Yosida, *J. Phys.: Condens. Matter* 10 (1998) 3223–3237

2. Investigation of multisite activation in  $LiCaAlF_6:Ce^{3+}$  Crystals using stimulated quenching of luminescence / V. V. Semashko et al. // *Laser Phys.* – 1995. – V. 5. – P. 69-72.

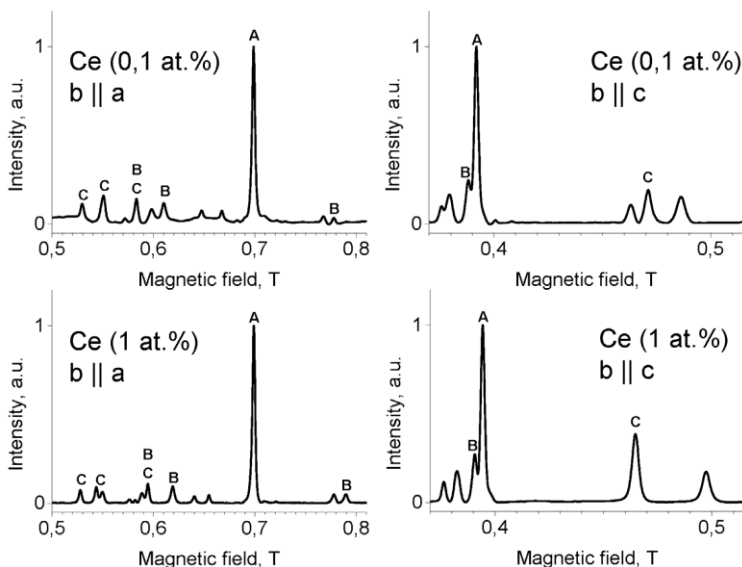


**Fig. 1.** ESR spectra of  $Ce^{3+}:LiCaAlF_6$  crystals doped with  $Ce^{3+}$  ions at low (0.1 at.% in the melt) and high (1 at.% in the melt) doping degrees, with different crystal orientations in a magnetic field

## ESR IN $\text{EuSn}_2\text{As}_2$ CRYSTALS CLOSE TO MAGNETIC ORDERING TEMPERATURE

**D.E. Zhelezniakova<sup>1</sup>, I.I. Gimazov<sup>1</sup>, K.S. Pervakov<sup>2</sup>, V.A Vlasenko<sup>2</sup>,  
V.M. Pudalov<sup>2</sup>, Y.I. Talanov<sup>1</sup>**

<sup>1</sup> Zavoisky Physical-Technical Institute, FRC Kazan Scientific Center of RAS, Kazan, Russia

<sup>2</sup> P.N. Lebedev Physical Institute of the Russian Academy of Sciences

Magnetic topological insulators attract significant interest of researchers due to their potential applications in spintronics. The  $\text{EuSn}_2\text{As}_2$  compound is one of the recently discovered promising magnetic topological insulators.  $\text{EuSn}_2\text{As}_2$  crystallizes in a  $\text{Bi}_2\text{Te}_3$ -type structure with rhombohedral (R-3m) symmetry and consists of layers of SnAs bilayers connected by hexagonal crystalline layers of Eu through Van der Waals bonding. Overall, the electronic and magnetic properties of the compound are well studied. However, some features of its magnetic structure remain unclear and continue to be discussed.

The main goal of this study is to investigate the magnetic state peculiarities of the crystal  $\text{EuSn}_2\text{As}_2$  below the ordering temperature of the europium magnetic moments ( $T_m \sim 24\text{K}$ ). Within this study, the temperature dependencies of the parameters of the electron spin resonance (ESR) spectra were examined, and their analysis was done to determine the nature of the magnetic anomalies. ESR spectra obtained at temperatures of 14 and 40 K are shown in Fig. 1. Above the magnetic ordering temperature  $T_m \sim 24\text{K}$  there is one signal, and below  $T_m$  the line splits into two signals. These signals asynchronously shift to lower fields. Data obtained with electron microscopy revealed planar defective areas. The appearance of the second signal is possibly due to these defects.

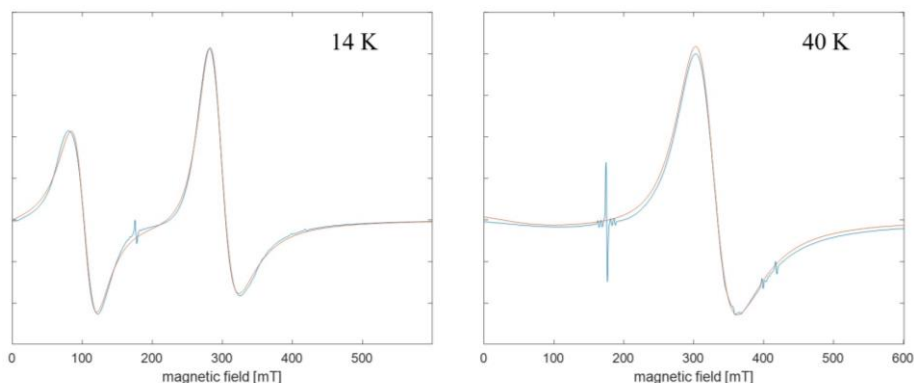


**Fig. 1.** ESR spectra of  $\text{EuSn}_2\text{As}_2$  crystal at temperatures of 14 and 40 K shown with blue line. Fitting using Dyson line shape shown with red line

## STUDYING PORE SPACE of a CORE by NUCLEAR MAGNETIC RESONANCE METHOD

A.N. Afanaseva, D.S. Ivanov, V.D. Skirda

Institute of Physics, Kazan Federal University, Kazan, Russia

One of the unique states of solid state is the porous body. The NMR relaxometry method is claimed as a technique by which information about micrometer range pores can be obtained. In most works, additional factors [1] that may affect, for example, relaxation time ( $T_1$ ,  $T_2$ ), relaxivity ( $\rho$ ) are not considered. One such factor could be the presence of paramagnetic impurities located in the pore space [2]. Therefore, the questions of the correctness of the pore space data obtained by NMR and also study of the pore space saturated with fluid with different paramagnetic concentrations remains open.

To obtain information about the studied sample of dolomite core saturated with water, relaxation attenuation was recorded using a CPMG sequence, which was characterized by a nonmonoexponential signal form. The spectrum of spin-spin relaxation times obtained from the attenuation can be used to obtain the pore size distribution (1).

$$\frac{3}{r} = \frac{1}{T_2 \rho} \quad (1)$$

To calculate the pore size from nuclear magnetic relaxation data, the value of relaxivity  $\rho$  is necessary. For the dolomite core sample, which is investigated in this work, the average value of  $\rho \approx 1 \mu\text{m}/\text{ms}$  was taken from the analysis of various works [3, 4, 5].

Figure 1 shows the spectrum of spin-spin relaxation times as well as the pore size distribution.

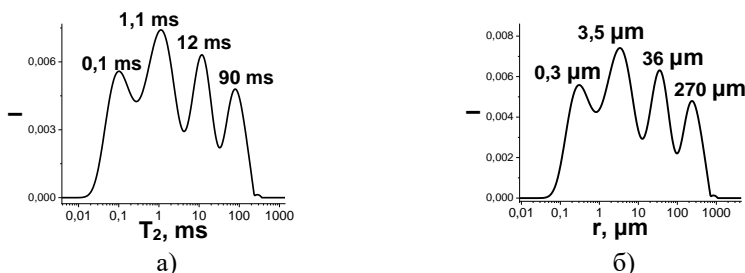


**Fig. 1** - a) Differential spectrum of spin-spin relaxation times for a core sample saturated with water; b) Pore size distribution. Each peak is labeled with the mean value of spin-spin relaxation time (a) and the mean value of pore size (b)

In the core sample under study, pore sizes with a maximum value of  $\sim 270 \mu\text{m}$  and a minimum value of  $\sim 0.3 \mu\text{m}$  were recorded. However, the issue with the correctness of the determined pore size of  $270 \mu\text{m}$  using spin-spin relaxation time  $T_2=90 \text{ ms}$  is not clear. Further investigation of the pore space is necessary for unambiguity. The relaxation processes are influenced by paramagnetic impurities, which can be located on the pore surface or dissolved in the fluid itself. Therefore, let

us consider the influence of copper sulfate concentration in the saturating fluid on the NMR characteristics of the pore space (Fig. 2).

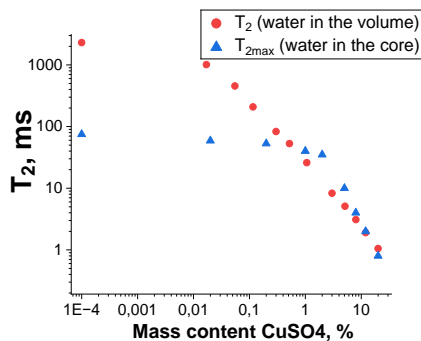


**Fig. 2** - Dependence of spin-spin relaxation times on copper sulfate concentration. Red symbols indicate the behavior of relaxation time of water with copper sulfate in the volume ( $T_2$ ), blue symbols - the value of the largest transverse relaxation time for water molecules in the core ( $T_{2max}$ )

Increasing the concentration of copper sulfate up to 1% practically does not affect the values of time  $T_{2max}$ , although for free water in the same concentration range the value of time  $T_2$  decreases about 30 times. The presented results suggest that the maximum value of  $T_{2max} \approx 90$  ms found above is indeed related to the characteristics of the porous structure. However, the estimate of the pore size of  $270 \mu\text{m}$ , made for  $T_{2max} \approx 90$  ms at the value of  $\rho = 1 \mu\text{m/ms}$ , seems to be implausible, because to reach by diffusion the corresponding pore boundaries with such dimensions requires a time significantly longer than 90 ms. By calculating the diffusion time required to reach the  $270 \mu\text{m}$  pore boundary, we obtain a value of 4.5 s. This value exceeds the time recorded by the NMR signal. For a time of 90 ms with a value of the self-diffusion coefficient of  $2.7 \cdot 10^{-9} \text{ m}^2/\text{s}$ , the size of the constraints is obtained as  $38 \mu\text{m}$ . Such inconsistency of the results may be due to the fact that the value  $\rho = 1 \mu\text{m/ms}$ , taken from literature data as typical for dolomites, does not correspond to the sample studied by us. In order the obtained estimate for the maximum pore size ( $38 \mu\text{m}$ ) determined from the relaxation time spectrum to be consistent with theoretical calculations, it is necessary to take  $\rho = 0.14 \mu\text{m/ms}$ . Then, the pore sizes determined from the data of the relaxation time spectrum (Fig. 1) by means of expression (1) at  $\rho = 0.14 \mu\text{m/ms}$  will have the following values: 0.04; 0.49; 5 and  $38 \mu\text{m}$ .

This work was funded by the subsidy allocated to Kazan Federal University for the state assignment in the sphere of scientific activities number FZSM-2023-0016.

1. Livo, K. Effect of paramagnetic mineral content and distribution on nuclear magnetic resonance surface relaxivity in organic-rich Niobrara and Haynesville shales / K. Livo, M. Saidian, M. Prasad // *Fuel*. – 2020. – V. 269. – P. 117417.
2. Saidian, M. Effect of mineralogy on nuclear magnetic resonance surface relaxivity: A case study of Middle Bakken and Three Forks formations / M. Saidian, M. Prasad // *Fuel*. – 2015. – V. 161. – P. 197-206.
3. Rogozin A. A. Integration of NMR relaxometry data and electrometric studies using the example of reservoir rocks in the Timan-Pechora oil and gas province / - A. A. Rogozin, T. S. Ignatieva, A. V. Churkov // *Exposition Oil Gas*. – 2021. – No. 6 (85). – P. 62-66.
4. Peesu R. R. et al. Automated Image Processing of Petrographic Thin Sections for Digital Reservoir Description: A Bridge to Correlate with Core and NMR Data // Abu Dhabi International Petroleum Exhibition and Conference. – SPE, 2022. – C. D012S145R004,
5. Wang H. et al. Study on SWCC and PSD evolution of compacted loess before and after drying-wetting cycles // *Bulletin of Engineering Geology and the Environment*. – 2023. – V. 82. – №. 5. – P. 180

## W-BAND EPR OF RADICALS IN CALCIUM GLUCONATE

**M.M. Akhmetov<sup>1</sup>, G.G. Gumarov<sup>1</sup>, R.B. Zaripov<sup>1</sup>, G.N. Konygin<sup>2</sup>,  
D.S. Rybin<sup>2</sup>**

<sup>1</sup> FRC Kazan Scientific Center of RAS, Kazan, 420029, Russia

<sup>2</sup> UdmFRC Ural Branch of RAS, Izhevsk, 426067, Russia

One of the most common and simplest carbohydrates are metal gluconates (Na, Ca, Fe, Cu, etc.). Being non-toxic and completely biodegradable, they are widely used in medicine, pharmaceuticals, food, feed and chemical industries [1]. In addition, it was found that mechanochemical processing of calcium gluconate in a planetary ball mill leads to a significant increase in therapeutic efficacy in the treatment of a number of diseases associated with calcium deficiency [2]. It is also known that during mechanochemical treatment free radicals are formed, the study of which has been the subject of a number of works [3]. This paper presents the results of studies using the EPR method in the millimeter range.

As measurements in the millimeter range show, the spectrum consists of two parts. The results of quantum chemical calculations showed that the most suitable for describing experimental EPR spectra in the high-field part were the calcium radical and in the low-field part, carbon radicals on the C3 and C2 carbon atoms, respectively. In carbon radicals, 3 hydroxyl oxygen atoms (at the C2, C3 and C4 atoms) form a covalent bond with the calcium atom according to the donor-acceptor mechanism. As a result, the radical turns out to be “closed,” which leads to the relative stability of this radical and the high intensity of the corresponding EPR line (about 60% of the spectrum intensity).

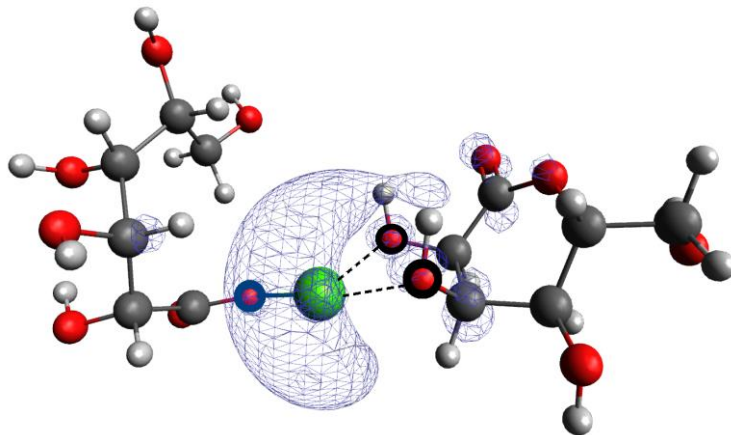


**Fig. 1.** Spin density distribution of the calcium radical

The spin density for such a molecular structure turns out to be concentrated mainly around the calcium atom. For the molecular structure under consideration (Fig. 1), the g-tensor was calculated using quantum chemistry methods; the difference

between quantum chemistry calculations (ORCA) and experimental data (Easyspin) turns out to be extremely small and does not exceed  $3-8 \cdot 10^{-4}$ .

Thus, mechanical activation leads to the formation of two types of free radicals: carbon radicals (Lactone 1 and Lactone 2) formed as a result of the abstraction of a proton from a carbon atom and a calcium radical formed as a result of the cleavage of the Ca-O bond.

1. I. Mariam, S.A. Nagra, I. Haq, S. Ali: *Bioresour. Technol.* **101**, 4075-4080 (2010).
2. D.S. Rybin, G.N. Konygin, V.E. Porsev [et. al.]: *Acta Physica Polonica A* **126**, 1014-1018 (2014).
3. G.G. Gumarov, V.Yu. Petukhov, G.N. Konygin [et. al.]: *Jour. Phys. Chem.* **87**, 1-4 (2013).

## STUDY by EPR SPECTROSCOPY of BRAIN TISSUE SAMPLES in MODELS with BRAIN DISORDERS

**V. V. Andrianov<sup>1,2</sup>, G. G. Yafarova<sup>1,2</sup>, L. V. Bazan<sup>1,2</sup>, T. K. Bogodvid<sup>2,3</sup>,  
A. I. Arslanov<sup>1</sup>, M. M. Bakirov<sup>1</sup>, N. G. Shayakhmetov<sup>4</sup>, S. V. Yurtaeva<sup>1</sup>,  
S. G. Pashkevich<sup>5</sup>, T. A. Fillipovich<sup>5</sup>, Kh. L. Gainutdinov<sup>1,2</sup>**

<sup>1</sup> Zavoisky Physical-Technical Institute, FRC Kazan Scientific Center of RAS, Kazan 420029, Russia

<sup>2</sup> Institute of Fundamental Medicine and Biology of Kazan Federal University, Kazan 420008, Russia

<sup>3</sup> Volga Region State University of Physical Culture, Sport and Tourism, Kazan 420010, Russia

<sup>4</sup> Interregional Clinical Diagnostic Center, Kazan 420101, Russia

<sup>5</sup> Institute of Physiology of Nat. Acad. of Sci. of Belarus, Minsk 220072, Belarus  
vvandrianov@kpfu.ru

Hypoxia is a precursor to many pathological processes in the body [1]. It occurs when the body tissues are insufficiently supplied with oxygen or its utilization is disrupted during biological oxidation; this is a key component of the pathogenesis of many diseases [2]. With hypoxia and ischemia of the brain, the functioning of neurotransmitter systems, including the nitrogen monoxide system, is disrupted. Nitric oxide (NO) is known as one of the most important signaling molecules regulating the physiological functions of the body and cell metabolism [3, 4]. Research on the role of NO in signaling in the nervous system began shortly after its discovery [5]. Since then, it has been demonstrated that NO is involved in various functions of the nervous and cardiovascular systems, performs the function of a neurotransmitter that provides relaxation of smooth muscles [4, 6, 7].

In recent years, many facts have emerged indicating that NO biosynthesis is one of the key factors in the pathophysiological response of the brain to hypoxia-ischemia [8, 9]. However, there is a number of evidence that other elements are involved in pathological processes, which can also be determined by EPR spectroscopy [6, 10, 11].

The issue of quantifying NO in living systems is relevant. Recently, one of the most effective methods for determining NO in biological tissues is the method of electron paramagnetic resonance (EPR) [3, 9, 12, 13]. This happened thanks to the technique developed by A.F. Vanin et al. [14], in which they used the spin capture method. The spin capture method is based on the reaction of a radical (in this case NO) with a spin trap. As a result of the reaction, an adduct with a characteristic EPR spectrum is formed. The authors applied the Fe<sup>2+</sup> complex with diethyldithiocarbamate (DETC) to capture NO and form a stable triple complex samples (DETC)<sub>2</sub>-Fe<sup>2+</sup>-NO in various animal tissues. These complexes are characterized by an easily recognizable EPR spectrum with a g-factor value of g=2.035 – 2.040 and a triplet hyperfine structure. The method has a sensitivity of 0.04–0.4 nM, allows direct measurements, and is highly sensitive [3].

By EPR spectroscopy we investigated NO content in biological tissues after some disorders of the normal activity of the body. These were models of ischemia, ischemia-reperfusion, combined brain and spinal cord injuries, model of motor activity restriction. The spectra of human malignant brain tumor samples were also obtained.

It has been shown that after an ischemic stroke of the brain, the amount of NO in brain tissues decreases by about 40%, which is partially restored after 3 days. In models of cerebral ischemia-reperfusion, the amount of NO decreases by 30-50% in



hippocampal tissues. In the model of combined brain and spinal cord injury, a decrease in NO production in the tissues of the injured and symmetrical non-injured areas of the brain was also found (by about 60-80%). In the model of restriction of motor activity, an increase in the amount of NO in the tissues of the rat heart with a deficit of movements for periods from 21 days to 1 month was shown, while it was shown that this increase may be due to the contribution of NOS.

Electron spin resonance measurements were performed with the financial support from the government assignment for FRC Kazan Scientific Center of RAS.

- [1] Kumar H., Choi D.-K.: Mediators of Inflammation Article ID 584758 (2015)
- [2] Manukhina E.B. et al.: Nitric Oxide **3**(5), 393-401 (1999)
- [3] Vanin A., Poltorakov A.: Front. Biosci. **14**, 4427-4435 (2009)
- [4] Steinert J.R. et al.: Neuroscientist, **16**(4), 435-452 (2010)
- [5] Boehning D., Snyder S.H.: Annu. Rev. Neurosci. **26**, 105-131 (2003)
- [6] Lundberg J.O.; Weitzberg E.: Cell **185**, 2853-2878 (2022)
- [7] Lakomkin V.L. et al.: Nitric Oxide: Biology and Chemistry. **16**(4), 413-418 2007
- [8] Chen Z.Q. et al.: Med Gas Res. **7**(3), 194-203 (2017)
- [9] Gainutdinov Kh.L. et al.: Technical Physics, **65**(9), 1421-1426 (2020)
- [10] Klare J.P.: Biomedical Spectroscopy and Imaging **1** (2), 101-124 (2012)
- [11] Yurtaeva S.V. et al.: Appl. Magn. Reson. **47**(6), 555-565 (2016)
- [12] Vanin A.F.: Biofizika **62**(4), 629-656 (2017)
- [13] Wierónska J.M. et al.: Biomolecules **11**, 1097 (2021)
- [14] V.D. Mikoyan, L.N. Kubrina, et al.: Biochim. Biophys. Acta, **1336**, 225-234 (1997)

## DFT CALCULATION as a TOOL to FIND C-CENTERED RADICALS LOCALIZATION in SUPRAMOLECULAR ASSEMBLIES

**M.A. Demekhin<sup>1</sup>, A.A. Timralieva<sup>1</sup>, A.I. Kokorin<sup>1,2,3</sup>, E.V. Skorb<sup>1</sup>**

<sup>1</sup> Infochemistry Scientific Center, ITMO University, St. Petersburg, Russia

<sup>2</sup>N. N. Semenov Federal Research Center for Chemical Physics, Russian Academy of Sciences, Moscow, Russia

<sup>3</sup>Plekhanov Russian University of Economics, Moscow, Russia

Binary assemblies of N-heterocycles show a wide range of functional activity, e.g. quite strong radical activity confirmed by electron paramagnetic resonance (EPR) spectroscopy [1-2]. Two radical centers were identified for melamine barbiturate supramolecular assembly, e.g. associated with superoxide radical and C-atoms. Experimental EPR spectra have shown that C-centered radical is generated in barbituric acid molecule or at least associated with it [3].

In case of assembly complexation *via* barbituric acid methylation at N-atoms, C-centered radicals still present also as superoxide radicals. Experimental g-factors were identified as 2.0032 and 2.0034 with accuracy  $\pm 0.0003$  for melamine-based assembly with barbituric acid and 1,3-dimethylbarbituric acid correspondingly. Density functional theory (DFT) calculations were performed to identify the localization of C-centered radicals in these two assemblies. Quantum-chemical calculations were performed using the ORCA software, while the visualization of spectra was conducted with the aid of MATLAB and EasySpin. The full geometry optimization for all model structures was carried out at the B3LYP/def2-TZVP level of theory. After that, single point geometries were calculated for predicting EPR spectra using B3LYP as model Hamiltonian and EPR-III basis. All calculations were performed within Orca 5.0.4 program package.

Three structures were selected for modelling C-centered radicals within an increase of system's complexity from one acid molecule to the assembly. For melamine barbiturate the close g-factor was obtained for melamine barbiturate tetramer with two deprotonated barbituric acid molecules with radical also at C5 (Figure 1 C). It is in a good accordance to experimental data that showed barbituric acid also has a weak EPR signal similar to the one in the assembly with melamine. For melamine assembly with 1,3-dimethylbarbituric acid the structure is not as clear as wanted, and the calculations were performed only for systems with an increase in acid molecules number. The best g-factor fit is for system where all 1,3-dimethylbarbituric acid molecules are deprotonated and with radicals at C5 (Figure 1 E).

Thus, DFT calculations were shown as an efficient tool to identify and confirm the localization of C-centered radicals in supramolecular assemblies of N-heterocycles.

1. V. V. Shilovskikh, A. A. Timralieva, E. V. Belogub, E. A. Konstantinova, A. I. Kokorin and E. V. Skorb, *Applied Magnetic Resonance*, 2020, 51, 939–949.

2. V. V. Shilovskikh, A. A. Timralieva, P. V. Nesterov, A. S. Novikov, P. A. Sitnikov, E. A. Konstantinova, A. I. Kokorin and E. V. Skorb, *Chemistry – A European Journal*, 2020, 26, 16603–16610.

3. A. A. Timralieva, I. V. Moskalenko, P. V. Nesterov, V. V. Shilovskikh, A. S. Novikov, E. A. Konstantinova, A. I. Kokorin and E. V. Skorb, *ACS Omega*, 2023, 8, 8276–8284

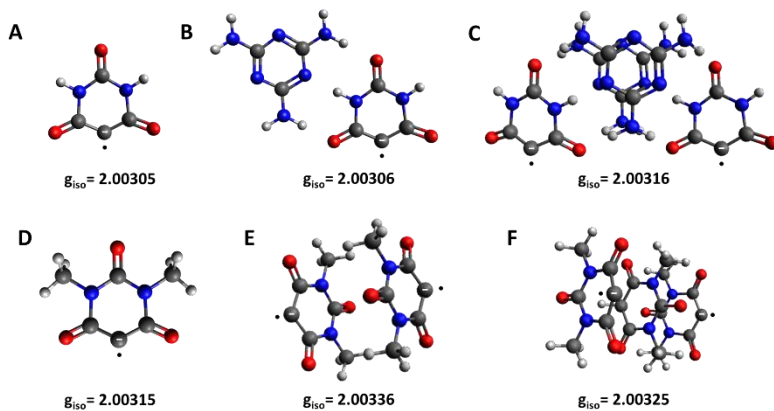


**Fig. 1.** C-centered radical localization for deprotonated barbituric acid (A), its dimer with melamine (B), tetramer with melamine (C) and for one deprotonated 1,3-dimethylbarbituric acid molecule (D), two molecules (E) and three molecules (F).

## CALCIUM FREE RADICAL FORMATION at IRRADIATION and MECHANOACTIVATION of CALCIUM GLUCONATE

**A.R. Gafarova<sup>1</sup>, G.G. Gumarov<sup>1</sup>, R.B. Zaripov<sup>1</sup>, D.S. Rybin<sup>2</sup>, G.N. Konygin<sup>2</sup>**

<sup>1</sup> Zavoisky Physical-Technical Institute, FRC Kazan Scientific Center of RAS, Kazan, Russia

<sup>2</sup> UdmFRC Ural Branch of RAS, Izhevsk, Russia

The possibility of obtaining a calcium radical was demonstrated by the gas-phase reaction of metal vapors with  $\text{Hg}(\text{CH}_3)_2$  vapors [1]. As is known, a calcium atom has two 4s electrons in its outer electron shell. In calcium monomethyl ( $\text{CaCH}_3$ ), one of the electrons forms a chemical bond with carbon, and the second is unpaired. Quantum chemical calculation for the  $\text{CaCH}_3$  radical gives the g-tensor values [1.997217 1.997217 2.002335]. The model EPR spectrum in the W band (constructed on the basis of calculations) of such a radical is similar to the signal in the high-field part of the spectrum from irradiated (Fig. 1). However, for the  $\text{CaCH}_3$  radical, a significantly greater anisotropy is observed compared to the anisotropy characteristic of irradiated calcium gluconate. Another work demonstrated the possibility of obtaining the  $\text{CaOCH}_3$  radical in the gas phase [2]. The model spectrum of this radical is much closer to the spectra of the studied calcium gluconate samples.

This paper presents the results of a quantum chemical calculation of the g-tensor for the calcium radical in the structure of calcium gluconate. Atomic coordinates are taken from the work [3]. There is good agreement with the results obtained by the W-band EPR. The mechanism of calcium radical formation during mechanical activation and irradiation with gamma quanta is discussed.

1. C.R. Brazier, P.F. Bernath Observation of gas phase organometallic free radicals: Monomethyl derivatives of calcium and strontium / C.R. Brazier, P.F. Bernath // *The Journal of Chemical Physics*. – № 86. – 1987. – P. 5918-5922.
2. M. Elhanine, R. Lawruszczuk, B. Soep Laser spectroscopy of metallic free radicals: the observation of the C–X vibronically allowed electronic transition for  $\text{Ca-OCH}_3$ ,  $\text{Ca-OC}_2\text{H}_5$  and  $\text{Ca-CCH}$  / M. Elhanine, R. Lawruszczuk, B. Soep // *Chemical Physics Letters*. – 288. – 1998. – P. 785–792.
3. Crystal and solution structures of calcium complexes relevant to problematic waste disposal: calcium gluconate and calcium isosaccharinate / V. Bugris, Cs. Dudas, B. Kutus, [at al.] // *Acta Crystallographica* - 74(6) - 2018 - P. 598-609

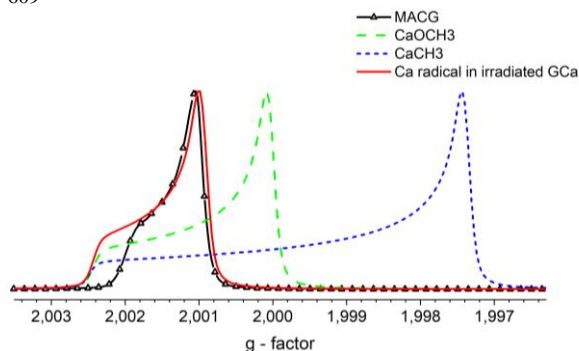


**Fig. 1.** Comparison of the EPR spectrum of MACG with the spectra of  $\text{CaOCH}_3$  and  $\text{CaCH}_3$  radicals and the spectrum of calcium radical in irradiated calcium gluconate

## **STUDY OF BIRADICALS BY THE TRANSIENT NUTATION METHOD**

**Galeev R.T., Zaripov R.B., Salikhov K.M.**

Zavoisky Physical-Technical Institute, FRC Kazan Scientific Center of RAS, Kazan, Russia  
e-mail: galeev\_rt@rambler.ru

In this work, the transient nutation method was used to determine the exchange interaction between unpaired electron spins in a biradical. For this purpose, nutation measurements were carried out at various microwave field amplitudes. Two frequencies were observed in the Fourier spectra of nutation. The dependences of the difference between these frequencies on the amplitude of the microwave field were obtained. Comparison of experimental and model nutation spectra made it possible to estimate the value of the exchange interaction in the biradical.

## Identification of the signal with $g \sim 6.0$ in the X-band EPR spectra of human blood serum at 5-40 K

**M.I. Ibragimova<sup>1</sup>, A.I. Chushnikov<sup>1</sup>, I.V.Yatsyk<sup>1</sup>, D.Kh.Khaibullina<sup>2</sup>,  
G.G.Gumarov<sup>1</sup>**

<sup>1</sup>Zavoisky Physical-Technical Institute, FRC Kazan Scientific Center of RAS, Kazan, Russia

<sup>2</sup>Kazan State Medical Academy, Kazan, Russia

Previously [1], we showed that at helium temperatures 5-40 K in X-band EPR spectrum of blood serum one more asymmetric single absorption line with an effective  $g$ -factor of  $\sim 6.0$  is observed. We identified this line as a signal from  $\text{Fe}^{3+}$  associated with the second conformation of the N-lobe of transferrin ( $\text{Tf-Fe}^{\text{N}}$ ) with  $E/D \sim 0$ . This conclusion is quite unexpected, since there are quite a lot of X-band EPR studies for both specially prepared transferrin samples and whole blood and its serum, where  $E/D \sim 0.2 - 0.3$  and  $g \sim 4.3$ . A signal with a  $g$ -factor of  $\sim 6.0$  is recorded in the spectra of *whole blood*, and it is clearly identified as the absorption line caused by the ferric heme in the high spin ( $S=5/2$ ) state. Significant contributions to the study of Tf features were made by G. Mathies *et al.* [2] and M. Azarkh *et al.* [3], who used J-band EPR to study this protein. The works [2,3] established the presence of the second conformation of the iron for  $\text{Fe}^{\text{N}}$  with practically axial electronic structure that differs significantly from its main conformation. X-band EPR studies of Tf were carried out mainly at liquid nitrogen temperatures or were limited to temperatures above 40 K, since the signal with  $g \sim 6.0$  appearing in the spectra could not be identified. In our X-band EPR studies of blood serum, the question remains: how pure were the samples prepared, or is the signal we record the result of contamination of the serum samples with hemoglobin?

As part of this work, three groups of samples were prepared. The first group included whole blood samples; the second group included blood sera obtained using standard clinical gel technologies, and the third group included so-called “contaminated” serum samples to which whole blood was specially added. EPR spectra were recorded at 5 K and 80 K from blood serum samples of equal volume (0.3 ml) on a Bruker EMX Plus spectrometer at a frequency of  $\sim 9.38$  GHz with a modulation frequency of 100 kHz and modulation amplitude of 5 G.

The temperature dependence EPR spectra of human blood are shown in Fig.1. The intense absorption line with  $g \sim 6$  in Fig. 1 is the absorption line caused by the ferric heme in the high spin state and this is consistent with the data given, in particular, in [4]. In Fig.2 shows an enlarged (from Fig.1) blood spectrum recorded at 80 K, as well as spectra of blood serum of the same sample, recorded at 5 and 80 K. From Fig.2 it is clearly seen that the shape and width the lines with  $g' \sim 6.0$  is different in spectra recorded at 5 K (in serum) and 80 K (in blood). Moreover, special “contamination” of the samples with whole blood showed no change in signal intensity with  $g' \sim 6.0$  in the EPR spectra recorded at a temperature of 5 K.

The results obtained confirm that the absorption line with  $g' \sim 6.0$  recorded in the spectra of blood serum in the temperature range 5 - 40 K is indeed a signal from iron associated with the second conformation of the iron site of the N-lobe of transferrin with  $E/D \sim 0$ .

1. Ibragimova M.I. *et al.*: Abtr. of Inter.Conf. “Modern development of magnetic resonance” and “Spin physics, spin chemistry, and spin technology”, 129-130 (2022)
2. Azarkh M. *et al.*: Phys.Chem.Chem.Phys. **21**, 16937-16948 (2019)
3. Mathies G. *et al.*: Biol Inorg Chem. **20**, 487-496 (2015)
4. Svistunenko D A.: J Biomed Res **35**, 294-300 (2021)

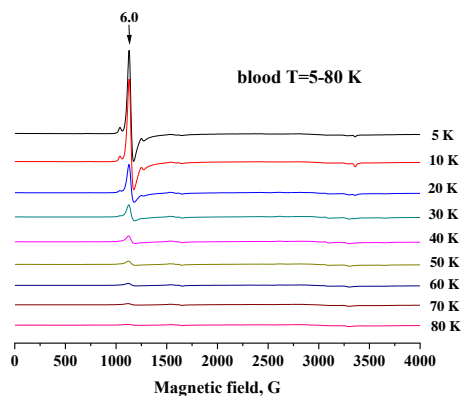


**Fig. 1.** X-band EPR spectra of human blood recorded in a temperature range of 5–80 K

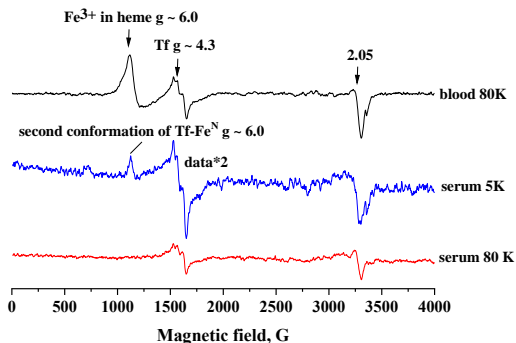


**Fig.2.** X-band EPR spectra of human blood and serum

## TRANSLATIONAL DIFFUSION FEATURES OF AN INTRINSICALLY DISORDERED PROTEIN

**D.L. Melnikova<sup>1</sup>, I.V. Nesmelova<sup>2</sup>, V.D. Skirda<sup>1</sup>**

<sup>1</sup> Institute of Physics, Kazan Federal University, Kazan, Russia

<sup>2</sup> Department of Physics and Optical Sciences, University of North Carolina, Charlotte, USA

Today, a huge amount of experimental data on the translational dynamics of linear flexible-chain macromolecules has been acquired [1], making it possible to form unambiguous ideas about the regularities of macromolecule behavior in a wide range of molecular masses and concentrations. The area of globular proteins can be considered relatively well studied (theoretically and practically) [2, 3]. Now it is fundamental to obtain information on the peculiarities of the behavior of proteins with intrinsically disordered structure in solutions in a wide range of concentrations and, first of all, in the area of concentrated solutions. That is, in conditions when effects due to protein-protein interactions can be expected. Such information can be obtained using the unique capabilities of the NMR method with a pulsed magnetic field gradient in the spectrally resolved mode.

Hypothetically, one can assume that for proteins with internal disorder, as well as for linear polymers, globular proteins, and dendrimers, the possibility of existence of a generalized concentration dependence of self-diffusion coefficients in solutions is not excluded. It is not clear only to what extent such a generalized dependence will be specific for them? And will it be close to the generalized concentration dependence of self-diffusion coefficients of linear flexible-chain macromolecules? In any case, the search for an answer to the formulated questions is of interest and is one of the goals of the study presented in this paper.

This work was funded by the subsidy allocated to Kazan Federal University for the state assignment in the sphere of scientific activities number FZSM-2023-0016.

1. Maklakov A.I., Skirda V.D., Fatkullin N.F.: Self-Diffusion in Polymer Solutions and Melts. Kazan University Press: Kazan, Russia (1987), 224 p. (In Russian)

2. Nesmelova I.V., Skirda V.D., Fedotov V.D.: Generalized concentration dependence of globular protein self-diffusion coefficients in aqueous solutions. *Biopolymers* **63**, 132–140 (2002)

3. Wüthrich K., Wagner G., Richarz R., Braun W.: Correlations between internal mobility and stability of globular proteins. *Biophysical journal*, **32**, 549–560 (1980)



## EPR INVESTIGATIONS OF COMPOSITE MATERIALS BASED ON BIOCOMPATIBLE POLYMERS WITH CALCIUM PHOSPHATES

**A.A. Petrova<sup>1</sup>, G.V. Mamin, F.F<sup>1</sup>. Murzakhanov<sup>1</sup>, I.V. Fadeeva<sup>2</sup>, A.A. Forysenkova<sup>2</sup>, M.R. Gafurov<sup>1</sup>**

<sup>1</sup> Institute of Physics, Kazan Federal University, Kazan, 420029, Russian Federation, e-mail  
Petrovaalinakfu@gmail.com

<sup>2</sup> A.A. Baikov Institute of Metallurgy and Material Science, Russian Academy of Sciences, Leninsky  
Avenue 49, 119334 Moscow, Russia; fadeeva\_inna@mail.ru

Since calcium phosphates (CP) constitute the primary mineral component of bone, composite materials containing CP are taken into consideration when treating bone tissue [1]. Materials with the required mechanical and biological qualities can be produced by combining the features of CP (hemostatic and antibacterial) with those of polymers (hydrophilicity, solubility, swelling). It's critical to comprehend the mechanism underlying the interaction between the polymer and calcium phosphates while developing composite materials.

To make composites, a variety of polymers, both synthetic and natural, can be used, including synthetic polyvinylpyrrolidone (PVP) and natural polysaccharide alginate (ALG) [2-4]. In this work we investigate composites containing synthetic CP hydroxyapatite (HA,  $\text{Ca}_{10}(\text{PO}_4)_6(\text{OH})_2$ ) and mentioned polymers prepared by freeze-drying of the gel by using photoinduced pulsed X- and W-band EPR spectroscopy.

In the temperature range of 100–300 K, no EPR signals were detected since the materials do not contain paramagnetic impurities at least within the sensitivity of the spectrometer. Under laser radiation, stable paramagnetic centers can be created (Figure 1) which disappear after several hours after switching off the laser.

Signal from PVP is mainly due to the isotropic hyperfine interaction of carbon-centered defects ( $g_{\text{PVP}} = 2.0040$ ) with the polymer  $^{14}\text{N}$  nuclei (Table 1). The EPR spectra of the irradiated HA and of the PVP-HA composite are mainly defined by the presence of the impurity of nitrates. The extracted EPR parameters correspond to  $\text{NO}_3^{2-}$  in B position (i.e., phosphate site) in the HA structure (Table 1).

Mixing HA with PVP-Alg somewhat changed the hyperfine interaction constants  $A_{\perp}$  and  $A_{\parallel}$  upwards, and also increased the distribution of the constants  $\Delta A_{\perp}$  and  $\Delta A_{\parallel}$  (Table 1). Analysis of changes in  $A_{\perp}$  and  $A_{\parallel}$  showed that the isotropic part of the hyperfine interaction increased by 3.7 MHz, which corresponds to an increase in the electron density at the nitrogen nucleus in the HA  $\text{NO}_3^{2-}$  complex by 2%. It can be assumed that, when HA is added ex situ, PVP-Alg molecules form a positively charged layer around the HA particles with the formation of a chemical bond, which increases the electron density in its near-surface layer. Due to electrical neutrality, the charge on the outer surface of the PVP-Alg shell will be negative.

Table 1. EPR parameters (axial components of  $g$ -factors, hyperfine values  $A$  and their distribution  $\Delta A$ ).

Sample	$g_{\perp}$	$g_{\parallel}$	$A_{\perp}$ MHz	$A_{\parallel}$ MHz	$\Delta A_{\perp}$ MHz	$\Delta A_{\parallel}$ MHz
PVP	2.0040	2.0040	2.75	2.75		
PVP-Alg	2.0022 (2)	2.0026(2)	$38 \pm 8$	$106 \pm 10$	-	-
HA	2.0011(1)	2.0052(1)	$92.4 \pm 0.5$	$186 \pm 1$	$7 \pm 1$	$12 \pm 1$
PVP-Alg-HA	2.0011(1)	2.0052(1)	$93.6 \pm 0.5$	$191 \pm 1$	$13 \pm 1$	$18 \pm 1$

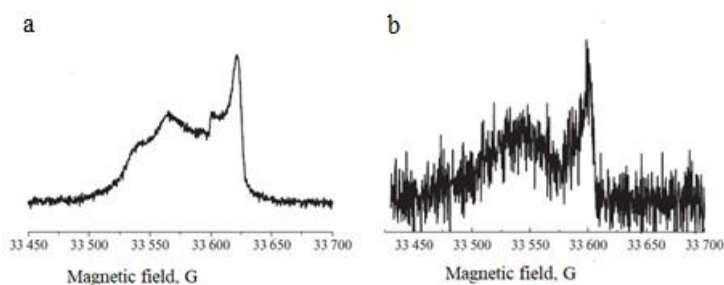
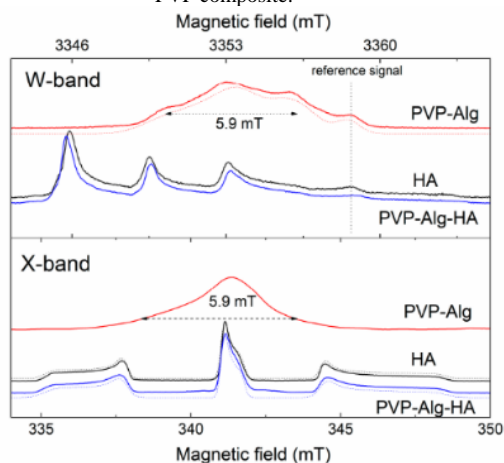
Fig.1. W-band EPR spectra at  $T = 200$  K under irradiation with light of 355 nm: a - PVP; b — HA–PVP composite.

Fig.2. Pulse EPR spectra for PVP-ALG (red lines), HA (black lines), and PVP-ALG-HA (blue lines) after X-ray irradiation (W-band at the top; X-band below). Dashed lines are the fits with the parameters given in Table 1.

The work is supported financially by Russian Science Foundation Grant No. 23-23-00640

1. Barinov S. M. Ceramic and composite materials based on calcium phosphates for medicine // *Advances in chemistry*. – 2010. – T.79(1). – P.15-32.
2. Furko, M.; Balázs, K.; Balázs, C. Calcium Phosphate Loaded Biopolymer Composites—A Comprehensive Review on the Most Recent Progress and Promising Trends. *Coatings* **2023**, *13*, 360.
3. Fadeeva, I.V. et al. Composite Polyvinylpyrrolidone—Sodium Alginate—Hydroxyapatite Hydrogel Films for Bone Repair and Wound Dressings Applications. *Polymers* **2021**, *13*, 3989.
4. Forsyenkova AA, et al. Polyvinylpyrrolidone—Alginate—Carbonate Hydroxyapatite Porous Composites for Dental Applications. *Materials*. 2023; 16(12):4478. <https://doi.org/10.3390/ma16124478>

## Study of hydroxyapatite doped with rare earth ions by various EPR spectroscopy techniques

**M.A. Sadovnikova<sup>1</sup>, G.V. Mamin<sup>1</sup>, F.F. Murzakhanov<sup>1</sup>, M.A. Goldberg<sup>2</sup>,  
N.V. Petrakova<sup>2</sup>, V.S. Komlev<sup>2</sup>, M.R. Gafurov<sup>1</sup>**

<sup>1</sup> Kazan Federal University, Kazan, Russia

<sup>2</sup> A.A. Baikov Institute of Metallurgy and Material Science, Russian Academy of Sciences, Moscow, Russia

Nowadays, in order to fully restore bone tissue functionality, biocompatible materials based on hydroxyapatite (HAp) with the chemical formula  $\text{Ca}_{10}(\text{PO}_4)_6(\text{OH})_2$  are widely used in medical applications [1]. An important feature of HAp is that its structure allows it to include a wide range of impurity ions, which, even at low concentrations can modify its biological and physicochemical properties. In recent years, various rare earth (RE) ions doped HAp materials have attracted special attention in biomedical imaging [2, 3]. RE dopants have long fluorescence lifetime, photostability, low toxicity, and other unique luminous advantages. These properties allow them to be used in a wide range of applications in biomarkers, detection, and imaging. The detection and imaging features play a key part in complex biological interactions, such as monitoring the real-time distribution of drugs, revealing in vivo distribution and osteointegration of the implanted materials and distinction from the bone apatite, and so on. Early studies showed that RE elements are found in extremely low concentrations in inorganic salt components of solid tissues of the human body, which play an important role in regulating the functions of cells and tissues [4]. Thus, the introduction of a certain amount of RE elements (Gd, Ce, Nd, Er) into the crystal lattice of HAp can improve the biomedical properties of the material and will make it possible to use the biomatrix for diagnostic imaging. In this regard, questions arise regarding analytical control (qualitative and quantitative) of the introduction of RE elements and other impurities into HAp.

The present study focuses on the characterization of synthetic HAp (ceramics and powders) doped with rare earth ions (Gd, Ce, Nd, Er) using electron paramagnetic resonance (EPR) spectroscopy. EPR spectra in continuous wave and pulsed modes were detected using the Bruker Elexsys E580 spectrometer (Bruker, Karlsruhe, Germany), microwave frequency  $\nu_{\text{MW}} = 9.6$  GHz (X-band) at a temperature  $T = 10$  K. Electron-nuclear interactions exhibited in ESE decay modulation were analyzed using the Electron Spin Echo Envelope Modulation (ESEEM) experiment.

Thus, the structural features of the RE-HAp spin systems in the form of powders were studied using EPR spectroscopy methods. The use of pulsed non-destructive EPR methods, highly sensitive to the presence of paramagnetic defects, made it possible to analyze electron-nuclear hyperfine interactions to identify nuclei near a paramagnetic ion, as well as to estimate the distance between the nuclear and electronic subsystems. Based on the results obtained, it is shown that EPR spectroscopy is an effective experimental tool for studying cationic RE doping.

The research was funded by the Russian Science Foundation, grant number 23- 63-10056

1. Q. R. T. Lim, X. Y. Cheng, C. Y. Wee, *Advanced Mater Sci Technol.*, 5 (2) (2023).
2. V. Balaram, *Geosci. Front.*, 10 (4), 1285-1303 (2019).
3. N. Iyad, M. S. Ahmad, S. G. Alkhatib, M. Hjouj, *Eur. J. Radiol. Open*, 11, 100503 (2023).
4. K. Saranya, S. Bhuvaneshwari, S. Chatterjee, N. Rajendran, *J. Mater. Sci.*, 55 (25), 11582-11596 (2020).

## Determination of water content in crude oil by nuclear magnetic resonance: problems and possible solutions

**E.I. Shamsiyarova<sup>1</sup>, D.L. Melnikova<sup>1</sup>, D.S. Ivanov<sup>1</sup>, M.M. Doroginizky<sup>1</sup>,  
V.D. Skirda<sup>1</sup>**

<sup>1</sup> Institute of Physics, Kazan Federal University, Kazan, Russia

Today petroleum and the products obtained after its technological processing are the main raw materials not only in Russia, but also all over the world. However, nowadays more and more difficulties arise in the production of well fluid, as mainly heavy hydrocarbons are extracted from petroleum reservoirs. This type of crude oil is characterized by high viscosity in connection with which special enhanced oil recovery [1] measures are applied at injection wells, which lead to the fact that there is an increase in the water cut of crude oil. Thus, in addition to hydrocarbons, well fluid always contains water, rock particles, dissolved salts and gases. All these "harmful" impurities lead to corrosion of equipment, besides, water present in the composition of oil fluid at almost every stage of its production is the so-called ballast, which requires additional costs for transportation and disposal. Based on the above mentioned, the problem of operational control of the composition of fluid flowing through the pipes in order to improve oil recovery and subsequent resource saving is still topical.

The work is devoted to the study of crude oil samples and model samples of emulsions based on oil and petroleum by nuclear magnetic resonance. The problems of emulsion formation process during well fluid production are highlighted. The possibilities of using NMR spectroscopy and relaxometry [2] to obtain quantitative information on water content of emulsions are demonstrated.

Using special software, the original spin-spin and spin-lattice relaxation data were converted into spectra of  $T_2$  and  $T_1$  times, respectively. Figure 1 shows the  $T_2$  relaxation spectra of the emulsion sample.

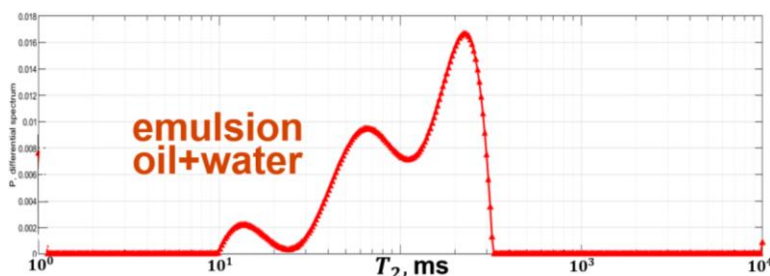


**Fig. 1.** Typical spin-spin relaxation spectra of model samples of water-oil emulsions

This work was funded by the subsidy allocated to Kazan Federal University for the state assignment in the sphere of scientific activities number FZSM-2023-0016.

1. Zadymova N.M., Skvortsova Z.N., Traskin V.Y., Yampol'skaya G.P., Mironova M.V., Frenkin E.I., Kulichikhin V.G., Malkin A.Ya.: *Colloid journal* **78**, 735–746 (2016).
2. Liu J., Feng X., Wang D.: *Petroleum Science and Technology* **37**, 1123–1135 (2019).

## EFFECT of COUNTERION on MAGNETIC PROPERTIES of the NEW Fe(III) COMPLEXES WITH a N2O TRIDENTATE LIGAND

**A.R. Sharipova<sup>1</sup>, E.N. Frolova<sup>1</sup>, O.A. Turanova<sup>1</sup>, L.V. Bazan<sup>1</sup>,  
A.T. Gubaidullin<sup>2</sup>, A.N. Turanov<sup>1</sup>**

<sup>1</sup> Zavoisky Physical-Technical Institute, FRC Kazan Scientific Center of RAS, Kazan, Russia

<sup>2</sup> Arbuzov Institute of Organic and Physical Chemistry, FRC Kazan Scientific Center of RAS, Kazan, Russia

The magnetic properties of metal complexes depend not only on the nature of the ligands forming them, but, in some cases, can be determined by the properties of external counterions or solvates. In this work, the influence of fluorine-containing counterions on the magnetic properties of new spin-crossover Fe(III) complexes was studied using EPR and UV spectroscopy.

A new series of spin-crossover Fe (III) complexes,  $[\text{FeL}_2]\text{Y}$  ( $\text{L} = 1\text{-phenyl-3-(quinolin-8-ylamino)prop-2-en-1-onato}$ , and  $\text{Y} = \text{BF}_4, \text{PF}_6, \text{SbF}_6$ ), were synthesized. The Fe (III) ion has an octahedral coordination geometry with N2O donor atoms of the tridentate ligand.

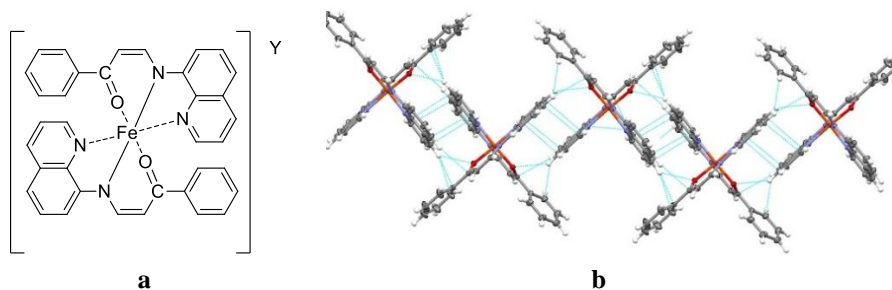


Fig. 1. **a.** Scheme of Fe(III) complex. **b.** Intermolecular  $\pi \dots \pi$  and C-H  $\dots \pi$  interactions (shown in blue dotted line) in a  $[\text{FeL}_2]\text{SbF}_6$  complex single crystal according to X-ray diffraction data

The complexes were all synthesized by layered diffusion of  $\text{FeY}_3$  prepared in situ in MeOH on top of a solution of HL and  $\text{NEt}_3$  in  $\text{CH}_2\text{Cl}_2$ . A composition and structure of all obtained compounds were characterized by elemental analysis and UV spectroscopy. X-ray crystallography has also characterized some products. Magnetic properties were studied using EPR and UV-Vis (in solution) spectroscopy. UV-Vis spectroscopy data show that in acetonitrile solution at room temperature, the molecules of the complexes under study are simultaneously present in both low-spin ( $S = 1/2$ ) and high-spin ( $S = 5/2$ ) states.

EPR studies revealed that polycrystalline samples of the compounds have an incomplete smooth spin-crossover, ( $S = 1/2 \leftrightarrow S = 5/2$ ) in the temperature range of 4-340 K. Thus, the spin-crossover occurs at room temperature also. The type of counteranion affects the parameters of the spin-crossover.

## Study of trans/cis isomerization of molecules of two 2-hydroxy-5-phenylazobenzaldehyde derivatives by NMR and UV spectroscopy

**A. R. Sharipova, M. Yu. Volkov, O. A. Turanova**

<sup>1</sup> Zavoisky Physical-Technical Institute, FRC Kazan Scientific Center of RAS, Kazan, Russia

Azo dyes are of interest for their photoactive properties, good chemical stability and high solubility. Availability, low cost and wide color palette leads to use of azo compounds in all technical areas. They are used in textiles, printing, as medicines. Azo dyes, in particular azobenzene, can be useful in creating photoswitchable catalysts and in creating polymers which can store solar thermal energy.

In the present work, two derivatives of 2-hydroxy-5-phenylazobenzaldehyde were studied: 2-hydroxy-5-(4-nitrophenylazo)benzaldehyde and 2-hydroxy-5-(4-chlorophenylazo)benzaldehyde. Molecules of these substances can exist in an azo form, in a hydrazone form and in a quinonoid form. The azo form is most often observed in non-polar solvents and acidic media, while the hydrazone form is most often observed in polar solvents and alkaline media. The quinonoid form is sometimes observed in polar solvents in the presence of strong electron-attracting substituents such as the nitro group, the hydroxy group, etc.

In these dyes a reversible trans-cis isomerization can occur under UV irradiation. The study of trans-cis photoisomerization process is of both scientific and practical interest. Experimental studies devoted to the trans-cis isomerization of azobenzene derivatives are constantly being published. The features of mechanisms of the trans-cis isomerization process of azobenzene and its derivatives, the change in the energy of the molecule during this process are still being studied by theorists. The trans-cis photoisomerization of molecules is usually carried out experimentally by NMR, UV-vis spectroscopy and others methods. Because the trans-cis photoisomerization of molecules of these azobenzene derivatives has not yet been studied, this work is devoted to studying these processes.

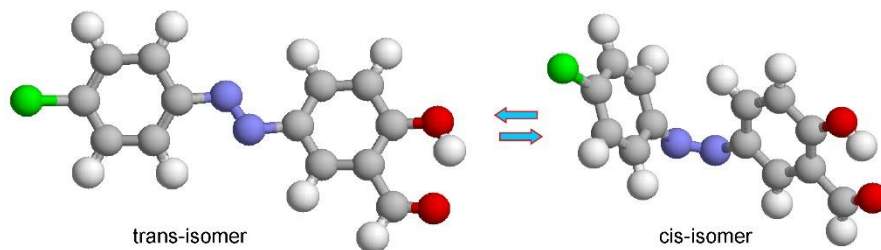


**Fig. 1.** 3D view of the trans- and cis-isomers of 2-hydroxy-5-(4-chlorophenylazo)benzaldehyde.

The two above-mentioned compounds were dissolved in carbon tetrachloride, hexane, acetone, acetonitrile and then were irradiated with 365 nm UV light. It has been established by NMR and UV-vis spectroscopy that reversible trans/cis isomerization of the molecules of these substances (Fig. 1) occurs in the non-polar solvents and is not observed in the polar solvents. This phenomenon was explained by the fact that molecules of polar and non-polar solvents interact differently with the molecules of the studied substances.

## **$^1\text{H}$ NMR ANALYSIS of ACETONITRILE INTERCALATED into the INTERPLANE SPACE of GRAPHITE OXIDE**

**Yu. Slesareva<sup>1</sup>, M. Volkov<sup>1</sup>, E. Vavilova<sup>1</sup>, D.A. Astvatsaturov<sup>2,3</sup>,  
N. Chumakova<sup>2,3</sup>**

<sup>1</sup> Zavoisky Physical-Technical Institute, FRC Kazan Scientific Center of RAS, Kazan, Russia

<sup>2</sup> N. N. Semenov Federal Research Center for Chemical Physics, Russian Academy of Science, Kosygin St. 4, Moscow, 119991, Russia

<sup>3</sup> M.V. Lomonosov Moscow State University, Chemistry Department, Leninskiye Gory, 1/3, Moscow 119991, Russia

Graphite oxide (GO) is a layered material consisting of graphene planes with attached oxygen groups. There is significant interest in GO and GO-based materials due to their promising practical applications, with a major focus on developing robust and cost-effective GO membranes for liquid and gas purification and separation. The molecular mobility of substances in between the oxidized graphene layers that is a key to mechanism of the membranes permeability is currently unclear.

Several graphite oxide samples with acetonitrile intercalated between the layers were studied using  $^1\text{H}$  nuclear magnetic resonance (NMR) spectroscopy. By examining the temperature-dependent  $^1\text{H}$  NMR spectra of samples with varying levels of intercalated acetonitrile, we determined the activation energy of the acetonitrile molecules. Also, it was shown that with increasing temperature, the spectral lines narrow, and side signals can be clearly visible. Experiments performed in magnetic fields of different strengths showed no change in the splitting value, suggesting that the side signals might arise from dipole-dipole interactions rather than the presence of different signals. The impact of the graphite oxidation method on proton formation on the surface of graphite oxide layers was examined.

Nuclear magnetic resonance measurements were performed with the financial support from the government assignment for FRC Kazan Scientific Center of RAS.

## Studying of paramagnetic effect of Dy<sup>3+</sup> ion on the complex of cyclosporin C (CsC) and DPC micelle in aqueous solution determined by NMR spectroscopy

**A. S. Tarasov, S. V. Efimov, V. V. Klochkov**

Kazan Federal University, Kazan, Russia

The study of the influence of metal ions on biologically active molecules and cell membrane is relevant, as the interaction of metal ions with organic compounds leads to various biological effects. Cyclosporins are natural or synthetic organic biologically active compounds consisting of 11 amino acids. The cyclosporin family is quite diverse and includes more than 20 different molecules. Cyclosporin C (CsC) (Fig. 1) was used in this study because it has different permeability and showed a different biological action on organic objects compared to another cyclosporins. The Dodecylphosphocholine (DPC) micelle was used to dissolve CsC in deuterated water (D<sub>2</sub>O) and imitate cell membrane. Micelle based on DPC is a spherical aggregate of molecules in which hydrophilic heads are on the surface and in contact with water, and the hydrophobic tails of the fatty acids of these molecules are inside the sphere and only contact with each other or with hydrophobic compounds co-dissolved with the lipid. Usually, it is used as a simplified membrane model.

The spectral characteristics of CsC complex with Dy<sup>3+</sup> ions incorporated into a DPC micelle in D<sub>2</sub>O were investigated by high-resolution NMR spectroscopy. The study focused to finding the interaction between CsC and Dy<sup>3+</sup> ions within DPC micelle. By employing a combination of one-dimensional (<sup>1</sup>H, <sup>13</sup>C) and two-dimensional (<sup>1</sup>H-<sup>1</sup>H TOCSY, <sup>1</sup>H-<sup>13</sup>C HSQC) NMR techniques, we were able to provide information on the spectral features and possible interactions in the CsC–DPC–Dy<sup>3+</sup> complex.

NMR measurements were carried out on a Bruker Avance III HD 700 spectrometer (700 MHz for <sup>1</sup>H, 175 MHz for <sup>13</sup>C). All samples were prepared in standard 5-mm NMR tubes. The solution volume was 0.6 ml. Solution was prepared in D<sub>2</sub>O, the sample concentration of CsC was 1.5 mM, concentration of DPC was 46.6 mM. Two-dimensional spectra (<sup>1</sup>H-<sup>1</sup>H TOCSY, <sup>1</sup>H-<sup>13</sup>C HSQC) were recorded at the temperature of 298 K. TOCSY mixing time was 0.35 s. The spectral window was 12 ppm. A series of one-dimensional <sup>1</sup>H and two-dimensional <sup>1</sup>H-<sup>13</sup>C HSQC NMR spectra was acquired with 2 sets of Dy(NO<sub>3</sub>)<sub>3</sub> salt concentration in probe (1.0 mM, and 2.0 mM).

Total signal assignment was obtained for <sup>1</sup>H-<sup>13</sup>C HSQC spectra CsC with different concentrations (1 mM, 2 mM) of Dy(NO<sub>3</sub>)<sub>3</sub> in micellar solution in D<sub>2</sub>O (Fig. 1). By adding Dy<sup>3+</sup> ions in the CsC – DPC – D<sub>2</sub>O system, it was revealed that CsC and DPC micelle were affected by surrounding Dy<sup>3+</sup> ions. This influence can be described by shifts (or displacements) of certain peaks in the HSQC spectrum and additional line broadening for both CsC and DPC. An attempt to characterize the effect of Dy<sup>3+</sup> ion based on measuring the autoscaled signal volume  $V_i^{p,d}$  in HSQC spectrum was made for CsC fragments and also was calculated paramagnetic attenuation values  $A_i$  for different CsC fragments (Fig. 1). In this research we may predict that system CsC – DPC has possible site of interaction with Dy<sup>3+</sup> ion. From analysis was revealed that Dy<sup>3+</sup> ion interacts with hydrophilic part of DPC with some fragments of CsC amino



acid residues such as MeLeu<sub>4</sub> (NCH<sub>3</sub> group), Val<sub>5</sub>, MeLeu<sub>6</sub>, Ala<sub>7</sub>, D-Ala<sub>8</sub> (CH<sub>α</sub> groups). Interaction between ion and CsC-DPC may lead to conformation changes in system.

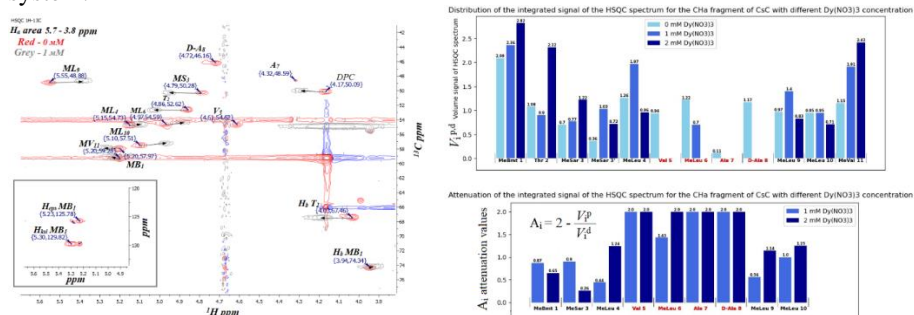


Figure 1. Fragment of <sup>1</sup>H-<sup>13</sup>C HSQC NMR spectrum of CsC – DPC with different concentrations of Dy(NO<sub>3</sub>)<sub>3</sub> (red, 0 mM Dy<sup>3+</sup>; grey, 1 mM Dy<sup>3+</sup>) in D<sub>2</sub>O (700 MHz, 298 K)(left). Autoscaled volume signals  $V_i^{p,d}$  distribution of HSQC spectrum for CH<sub>α</sub> groups of CsC, where light blue color bars – absence of Dy<sup>3+</sup> ( $V_i^d$  values), blue color bars – presence of 1mM Dy<sup>3+</sup> ( $V_i^p$  values), dark blue color bars – presence of 2mM Dy<sup>3+</sup> ( $V_i^p$  values) (upper right). Attenuation coefficients  $A_i$  distribution for CH<sub>α</sub> groups of CsC, where blue color bars – presence of 1mM Dy<sup>3+</sup>, dark blue color bars – presence of 2mM Dy<sup>3+</sup> also here located formula for finding  $A_i$  values(lower right). Red colors correspond to CH<sub>α</sub> groups of CsC that located near to Dy<sup>3+</sup> ion.

The work was supported by the Russian Science Foundation (project no. 24-23-00427). V.V. Klochkov also acknowledges the support from the Kazan Federal University Strategic Academic Leadership Program (PRIORITY-2030).

## Structure of the amyloidogenic peptide SEM2(49-107) by NMR spectroscopy

**Anastasia A. Troshkina, Dmitriy S. Blokhin, Vladimir V. Klochkov**

Kazan Federal University, Kazan, Russia

The human immunodeficiency virus (HIV) was first identified more than 30 years ago. Human seminal fluid is considered as the main factor in increasing HIV activity [1]. Describing the interaction of the HIV virion and human target cells, they are considered as negatively charged particles that will have an electrostatic repulsion [2]. Studies have shown [3] that certain fragments of seminal fluid are capable of forming amyloid fibrils. It has been found that the surface of amyloid fibrils has a positive charge, which increases the likelihood of infection by reducing the electrostatic repulsion between the negatively charged HIV virus and human cells. A class of the two homologous amyloids has been found to be formed from peptide fragments of semenogelin 1 (SEM1) and semenogelin 2 (SEM2) proteins [4]. In our study, we investigate the amyloidogenic peptide SEM2(49-107). This peptide is produced by the cleavage of the protein spermogelin 2 (SEM 2), which is expressed in the seminal vesicles and is cleaved by internal proteases after ejaculation.

The SEM2 (49-107) peptide fragment is composed of 59 amino acids MFGQKDQQQHTKSKKGSFSIQHTYHVDINDHDWTRKSQQQQYDLNALHK ATKSKQHLGGSQQLLEHHHHHHH corresponding to 49-107 residues of human semenogelin 2 protein including 6 histidine residues ( $6 \times$  His tag) at the C-terminus of the peptide. The molecular weight of the peptide SEM2(49-107)  $M=6.85$  with isoelectric point (pI)=9.46. NMR measurements were carried out on a Bruker Avance III HD 700 spectrometer (700 MHz for  $^1\text{H}$ , 175 MHz for  $^{13}\text{C}$ , 70,9 MHz for  $^{15}\text{N}$ ). The solution volume was 220  $\mu\text{l}$ . Solution was prepared in  $\text{D}_2\text{O}$ , the sample concentration of SEM2(49-107) was 0,469 mM, concentration of SDS was 4 mM/L. In this work, 1D ( $^1\text{H}$ ), 2D ( $^1\text{H}$ - $^{15}\text{N}$ ) и 3D ( $^1\text{H}$ - $^{13}\text{C}$ - $^{15}\text{N}$ ) NMR spectra of SEM2 (49-107) peptide were recorded at a temperature of  $T=293\text{K}$ . The obtained spectra were processed using TOPSPIN software (version 3.6). The analysis and correlation of the signals were carried out in the CCPNMR V2 Analysis program [5].

In this study, 2D ( $^1\text{H}$ - $^{15}\text{N}$ ) and 3D ( $^1\text{H}$ - $^{13}\text{C}$ - $^{15}\text{N}$ ) NMR spectra were recorded to assign chemical shifts of the peptide SEM2(49-107). It was possible to identify 48 of the 59 amino acids residues (86%). The values of chemical shifts are deposited in an international database BMRB ID 52356 [6]. In the CCPNMR program the secondary structure of the SEM2(49-107) peptide was predicted based on ( $^1\text{H}$ - $^{13}\text{C}$ - $^{15}\text{N}$ ) chemical shifts using CSI (Chemical Shift Index). It has been shown that the SEM2(49-107) peptide contains helical fragments at the C-terminus. This was confirmed by the data from TALOS-N experiments and relaxation NMR experiments on  $R_1$ ,  $R_2$  and (heteronuclear Overhauser effect (hetNOE)).

This work is supported by the Russian Science Foundation (project no. 20-73-10034). The NMR study was financially supported by the subsidy allocated to Kazan Federal University for the state assignment in the sphere of scientific activities (project FZSM-2023-0012).

1. Simon, V. HIV/AIDS epidemiology, pathogenesis, prevention, and treatment / V. Simon, D. D. Ho, Q. A. Karim // *The Lancet*. – 2006. – V. 368(9534). – P. 489 – 504. [https://doi.org/10.1016/S0140-6736\(06\)69157-5](https://doi.org/10.1016/S0140-6736(06)69157-5)
2. Westermark, P. Aspects on human amyloid forms and their fibril polypeptides / P. Westermark // *The FEBS journal*. – 2005. – V. 272(23). – P.5942–5949. <https://doi.org/10.1111/j.1742-4658.2005.05024.x>
3. Blokhin, D.S. Extent of N-Terminus Folding of Semenogelin 1 Cleavage Product Determines Tendency to Amyloid Formation / D.S. Blokhin, D.A. Osetrina, A.M. Kusova, A.G. Bikmullin, E.A. Klochkova, A.R. Yulmetov, E.A. Semenova, T.A. Mukhametzyanov, K.S. Usachev, V.V. Klochkov // *International journal of molecular sciences*. – 2023. – V. 24(10). – P. 8949. <https://doi.org/10.3390/ijms24108949>
4. Blokhin, D.S. Spatial structure of the fibril-forming SEM1(86–107) peptide in a complex with dodecylphosphocholine micelles / D.S. Blokhin, V.V. Klochkov, D.A. Sanchugova // *Russ Chem Bull*. – 2021. – V. 70. – P. 2422-2426.
5. Vranken, W. F. The CCPN data model for NMR spectroscopy: development of a software pipeline. / W. F. Vranken, W. Boucher, T. J. Stevens, et al. // *Proteins*. – 2005. – V. 59. – P. 687-696
6. Troshkina, A.A. <sup>1</sup>H, <sup>13</sup>C, and <sup>15</sup>N Chemical Shift Assignments for amyloidogenic SEM2(49-107) peptide / A.A. Troshkina, D.S. Blokhin, V.V. Klochkov // *BMRB*. – 2024. doi:10.13018/BMRB5235

## Features of nuclear magnetic relaxation in aqueous solutions of saccharides

**D.A. Tsukhlova, D.L. Melnikova, V.D. Skirda**

Department of Molecular Physics, Institute of Physics, Kazan Federal University, Kazan, Russia

Along with proteins and lipids, saccharides are the main biological compounds found everywhere in nature. It is known that saccharides are mainly found in the form of aqueous solutions. Due to their unique properties, aqueous solutions of saccharides are used in various fields such as medicine [1], pharmaceuticals [2], chemical and food industries [3]. In order to reveal the possibilities of using saccharides in the designated areas and to search for new applications, it is necessary to study the mechanisms of interaction of water molecules and saccharides in solutions. Currently, the mechanisms of interaction of water molecules and saccharides remain poorly studied [4].

The purpose of current work was to study the features of the interaction of water molecules and saccharides in aqueous solutions using nuclear magnetic resonance method. The objects of the study were monosaccharides D-mannose and d-xylose, disaccharides sucrose and maltose, and the oligosaccharide raffinose. The concentration dependences of relaxation times and the coefficient of self-diffusion of water in aqueous solutions were studied. It was found that the spin-spin relaxation of water molecule protons is characterized by an anomalously strong concentration dependence for both studied saccharide solutions. A correlation between the number of hydroxyl groups in the saccharide composition and the time of transverse relaxation of water in solutions was found.

This work was carried out on the equipment of the Federal Center of Shared Facilities for physical and chemical research of substances and materials (FCSF) KFU Bruker AVANCE 400 MHz spectrometer optimized for microtomography, solid state and self-diffusion.

1. Yu W., Zhang N., Li C.: *Curr. Pharm. Des.* **15**, 3826-3836 (2009)
2. Pooresmaeil, M., Namazi H.: *Eur. Polym. J.* **148**, 110356 (2021)
3. Kaneko Y., Kadokawa J. I.: *Biomater. Sci., Polym. Ed.* **17**, 1269-1284 (2006)
4. Heugen U., Schwaab G., Bründermann E., Havenith M.: *PNAS.* **103**, 12301-12306 (2006)

## INVESTIGATION of Mn VALENCE STATE in $\text{Sr}_2\text{Ti}_{1-x}\text{Mn}_x\text{O}_4$ COMPOSITION COMPOUNDS by EPR METHOD

**A.M. Uporova<sup>1</sup>, U.A. Deeva<sup>1</sup>, T.I. Chupakhina<sup>1</sup>, R.M. Eremina<sup>2</sup>,  
I.V. Yatsyk<sup>2</sup>**

<sup>1</sup> Institute of Solid State Chemistry of the Russian Academy of Sciences (UB), Yekaterinburg, Russia

<sup>2</sup> Zavoisky Physical-Technical Institute, FRC Kazan Scientific Center of RAS, Kazan, Russia

Strontium titanates are wide-gap semiconductors and are used in various fields of electronic engineering, such as electro-optical devices, multilayer capacitors, and thermistors [1]. Strontium titanates were found to be advanced materials for use in photosystems [2, 3].

The synthesis of the  $\text{Sr}_2\text{Ti}_{1-x}\text{Mn}_x\text{O}_4$  composition compounds (where  $x = 0; 0.01; 0.025; 0.05; 0.1$ ) was carried out using the formate method. Stoichiometric portions of previously obtained strontium and manganese formates were dissolved in concentrated formic acid without heating. Titanium butoxide was added to the resulting mixture with constant stirring, which immediately forms a complex precipitate. The resulting suspension is evaporated at 25–40°C to a dry residue. The resulting precursors were annealed at 1050°C for 24 hours until the phase formation process was completed.

A Bruker EMXplus spectrometer was used to record ESR spectra in the X range at a frequency of  $\sim 9.3$  GHz in the temperature range of 5–300 K. The measured ESR spectrum  $d\chi''/dH$  for  $\text{Sr}_2\text{Ti}_{1-x}\text{Mn}_x\text{O}_4$  (Fig. 1 (a, insert)) consists of several lines, each of which was described as fine structure ESR lines for which the crystal field parameter  $E$  is greater than  $D$ .

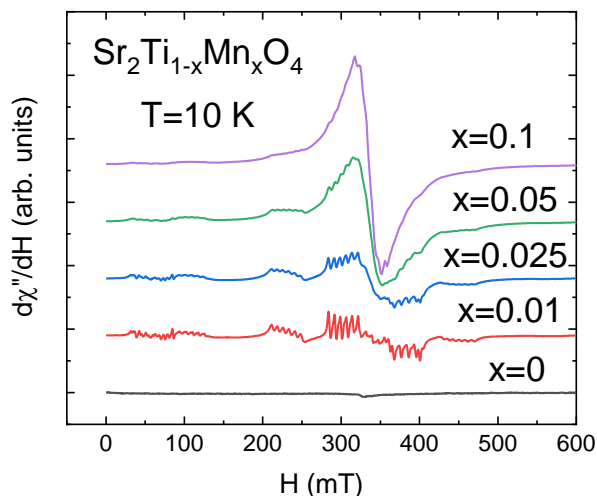


**Fig. 1.** ESR spectra in  $\text{Sr}_2\text{Ti}_{1-x}\text{Mn}_x\text{O}_4$  ( $x = 0, 0.05, 0.025, 0.01, 0.1$ ) samples

ESR lines of hyperfine structure are superimposed on lines of fine structure. With an increase in the concentration of manganese, an exchange narrowed line is additionally observed in ESR spectra. The EPR spectrum is symmetric, well described

by the Lorentz function. The parameters of the Lorentz curve are: resonance field  $H_{res} \approx 3379.9$  Oe, line width  $\Delta H \approx 173.2$  Oe, g-factor is 1.99, which corresponds to the  $Mn^{4+}$  ion.

The crystal field and hyperfine structure parameters are established.

The work was supported by the Russian Science Foundation, project No. 24-23-20123.

1. B. Liu, L. Li, X. Q. Liu, X. M. Chen, *JACerS*, **100**(2), 496-500 (2017).
2. L. W. Lu, M. L. Lv, D. Wang, G. Liu, X. X. Xu, *Appl. Catal. B: Environ.*, **200**, 412-419 (2017).
3. L. W. Lu, M. L. Lv, G. Liu, X. X. Xu, *Appl. Surf. Sci.*, **391**, 535-541 (2017),

## Magnetic and EPR properties of the second generation dendrimeric $\text{Fe}^{3+}$ complexes with fluorescent environment

**Valerya E. Vorobeva<sup>1</sup>, Denis V. Starichenko<sup>2</sup>, Matvey S. Gruzdev<sup>3</sup>,  
Ulyana V. Chervonova<sup>3</sup>, Ivan V. Yatsyk<sup>1</sup>**

<sup>1</sup>Zavoisky Kazan Physical-Technical Institute, Russian Academy of Science, 420029 Kazan, Russia

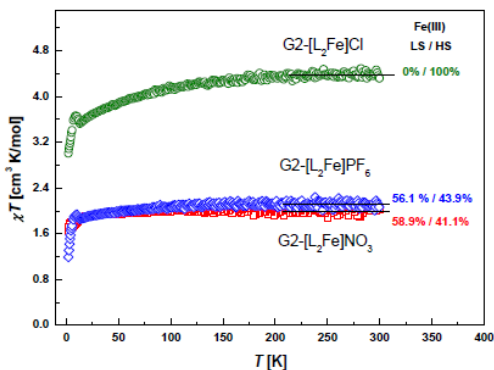
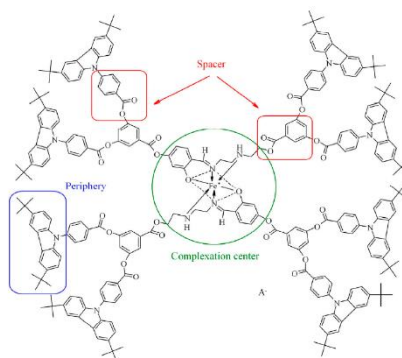
<sup>2</sup>M.N. Mikheev Institute of Metal Physics of the Ural Branch of the Russian Academy of Sciences, 620108 Ekaterinburg, Russia

<sup>3</sup>G.A. Krestov Institute of Solution Chemistry of Russian Academy of Sciences, 153045 Ivanovo, Russia

The metal-containing second-generation dendrimeric complexes of Schiff bases, named  $\text{G2-}[\text{L}_2\text{Fe}]^+\text{A}^-$  ( $\text{A}^-$  is  $\text{NO}_3^-$ ,  $\text{Cl}^-$ ,  $\text{PF}_6^-$ ), were synthesized (Fig. 1). The magnetic and resonance properties of the  $\text{G2-}[\text{L}_2\text{Fe}]^+\text{A}^-$  complexes were studied using SQUID magnetometry and EPR spectroscopy. Magnetic measurements showed that  $\text{G2-}[\text{L}_2\text{Fe}]\text{NO}_3$  and  $\text{G2-}[\text{L}_2\text{Fe}]\text{PF}_6$  at high temperatures were in mixed low-spin (LS,  $S = 1/2$ ) and high-spin (HS,  $S = 5/2$ ) states (Fig. 2). In the range of 200-300 K the  $\text{G2-}[\text{L}_2\text{Fe}]\text{NO}_3$  contained 58.9% LS and 41.1% HS; and the  $\text{G2-}[\text{L}_2\text{Fe}]\text{PF}_6$  contained 56.1% LS and 43.9% HS  $\text{Fe}^{3+}$  ions.

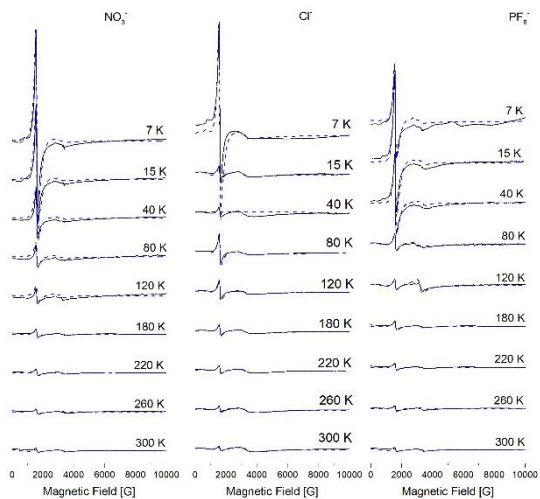
Complex  $\text{G2-}[\text{L}_2\text{Fe}]\text{Cl}$  was in a single-phase HS state. No SCO transitions were detected over the entire temperature range. All  $\text{G2-}[\text{L}_2\text{Fe}]^+\text{A}^-$  complexes were characterized by antiferromagnetic exchange interactions between neighboring  $\text{Fe}^{3+}$  ions, which probably arose due to the  $\pi$ -stacking of benzene rings. Analysis of the ground spin state at 2.0 K showed that it was characterized by the Brillouin contribution from non-interacting LS and a proportion of the HS  $\text{Fe}^{3+}$  ions not participating in AFM interactions. For  $\text{G2-}[\text{L}_2\text{Fe}]\text{Cl}$ , this proportion was 57%; for  $\text{G2-}[\text{L}_2\text{Fe}]\text{NO}_3$  and  $\text{G2-}[\text{L}_2\text{Fe}]\text{PF}_6$  it was 18% and 16%, respectively.

EPR measurements confirmed the presence of magnetically active HS and LS  $\text{Fe}^{3+}$  ions states and made it possible to distinguish two HS types: I-type with strong low symmetry and II-type with weak, distorted octahedral environments (Fig. 3). It was shown that  $\text{G2-}[\text{L}_2\text{Fe}]^+\text{A}^-$  complexes are magnetically inhomogeneous and consist of



two magnetic sub-lattices. The I-type HS  $\text{Fe}^{3+}$  centers probably form AFM-correlated chains in layers. The LS and II-type HS  $\text{Fe}^{3+}$  centers are in a fluctuating short-range AFM ordered state which is not detectable by static magnetic susceptibility and is likely located between the layers.

This work was supported by the Russian Science Foundation (Project number no. 23-13-00015)





## MAGNETIC PROPERTIES OF PEROVSKITE TYPE HIGH ENTROPY OXIDES

J.D. Reyes<sup>1</sup>, I.V. Yatsyk<sup>2</sup>, R.M. Eremina<sup>2</sup>, R.G. Batulin<sup>1</sup>, Maiti T.<sup>3</sup>

<sup>1</sup>Kazan (Volga Region) Federal University, Kremlevskaya st., 18, 420008 Kazan, Russia

<sup>2</sup>Zavoisky Physical-Technical Institute, FRC Kazan Scientific Center of RAS, Kazan, Russia

<sup>3</sup>Department of Materials Science and Engineering, Indian Institute of Technology, Kanpur, 208016, India

Lanthanum cobalt perovskite is promising for solid oxide fuel cell and is an attractive material due to its good oxidation ability, thermal stability, superconductivity and exceptional catalytic activity [1, 2].

EPR measurements were performed using a Bruker EMXPlus (Xband) spectrometer, equipped with continuous-flow He and N<sub>2</sub> cryostats. In these measurements we used the X-band with a frequency of 9.4 GHz, a temperature range of 5–340 K, and a magnetic-field range of 0–1.4 T. The ESR spectra are shown in Fig. 1.

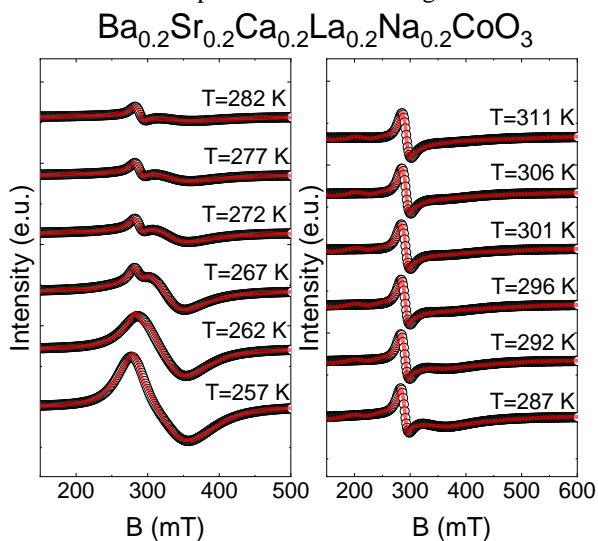


**Fig. 1.** Evolution of electron spin resonance spectra with temperature (from 176 to 320 K) for  $\text{Ba}_{0.2}\text{Sr}_{0.2}\text{Ca}_{0.2}\text{La}_{0.2}\text{Na}_{0.2}\text{CoO}_3$ . Circles – experimental data, solid line – approximation

It can be seen that the shape of the magnetic resonance line from 176 K to 275 K changes greatly, which indicates a change in the magnetic phase. The phase transition temperature is 254 K.

This research was supported by the Russian Science Foundation (Project No. 22-42-02014)

1. Shikha Dhakar, Sanchayita Mukhopadhyay, Musthafa Ottakam Thotiyl, Sudhanshu Shar-ma Structural, Methanol assisted water electrooxidation on noble metal free perovskite: RRDE insight into the catalyst's behaviour // *Journal of Colloid and Interface Science.* – 2024. – V. 654. – Part A. – Pp. 688-697.

2. A.N. Petrov; O.F. Kononchuk; A.V. Andreev; V.A. Cherepanov; P. Kofstad. Crystal structure, electrical and magnetic properties of  $\text{La}_{1-x}\text{Sr}_x\text{CoO}_{3-y}$  // *Solid State Ionics.* – 1995. – V. . – Iss. 3–4. – Pp. 189-199

## Effect of motor activity restriction on copper content in rat liver

**R.I. Zaripova<sup>1</sup>, G.G. Yafarova<sup>1,2</sup>, V.V. Andrianov<sup>1,2</sup>, M.I. Sungatullina<sup>1</sup>,  
N.I. Ziyatdinova<sup>1</sup>, Kh.L. Gainutdinov<sup>1,2</sup>, T.L. Zefirov<sup>1</sup>**

<sup>1</sup> Institute of Fundamental Medicine and Biology of Kazan Federal University, Kazan 420008, Russian Federation;

<sup>2</sup> Zavoisky Physical-Technical Institute, FRC Kazan Scientific Center of RAS, Kazan 420029, Russian Federation

[ratno1992@mail.ru](mailto:ratno1992@mail.ru)

One of the most important trace elements for the normal functioning of the human body is copper. Copper is involved in cellular respiration, iron metabolism, neurotransmitter production, pigment formation, connective tissue biosynthesis, hormonal regulation, and immune disorders. Copper is a constituent of many essential enzymes such as ceruloplasmin, cytochrome oxidase, tyrosinase, ascorbinase, amine oxidase [1, 2]. Copper is involved in the body's antioxidant defense system, being a cofactor of the enzyme superoxide dismutase (SOD) [2-6]. SOD is an essential component of the antioxidant system. Modern living conditions lead to a decrease in the share of physical activity at work and at home. Limitation of motor activity is caused by automation and mechanization of work, professional activity, long bed rest, lifestyle. Physical activity and motor activity constitute a biological necessity for human life and health. The problem of changes in physiological functions and mechanisms of their development of the growing organism in conditions of reduced motor activity has acquired great relevance. Given the vital role of copper in organisms, accurate regulation of copper content is critical to maintaining homeostasis in living organisms. In connection with a significant decrease in physical activity, especially in school-age children, it is relevant to study the effect of restriction of motor activity on the growing organism. The aim of the study was to investigate the intensity of copper formation in liver tissues of growing rats after restriction of motor activity. Electron paramagnetic resonance (EPR) spectroscopy was used to detect and quantify copper in liver samples. The copper content in the liver of rats after 30-day restriction of motor activity was studied by EPR spectroscopy. To simulate increasing restriction of motor activity, rats were kept in individual pen cages for 30 days starting at 21 days of age; the details of this method have been described by us previously [7]. The copper content in rat organs was determined by a technique developed at the Institute of Chemical Physics of the Russian Academy of Sciences by Prof. A.F. Vanin and coworkers, which uses the spin capture method. The details of the experiment and methodology have been described by us previously [8, 9]. Components of the spin trap were administered to anesthetized animals. As anesthesia we used 25% urethane solution at the rate of 800 mg/kg of animal weight, which was administered intraperitoneally. All drugs used by us were diluted in physiological solution. Measurements of the spectra of a complex of biological samples  $\text{Cu}^{2+}\text{-(DETC)}_2$  was performed on a Bruker X-band spectrometer (9.5320 GHz) EMX/plus. The amount of Cu was estimated by the intensity of the characteristic EPR signal belonging to the  $\text{Cu}^{2+}\text{-(DETC)}_2$  complex. It was found that after restriction of motor activity for 30 days there is an average 3-fold increase in copper content in liver tissues ( $p < 0.05$ ). The increase of copper content at restriction of motor activity allows us to conclude that

there is a close relationship between the level of copper in the body and the mode of motor activity.

- [1] Banci L. et al.: *Nature*, 465, 645-648 (2010).
- [2] Festa R.A. et al.: *Current Biol.*, 21 (21), 877-883 (2011).
- [3] A.F. Müller.: *FEBS Lett.*, 586, 585-595 (2012).
- [4] Sheng Y. et al.: *Chem. Rev.*, 114, 3854–3918 (2014).
- [5] Fukai T., M. Ushio-Fukai: *Antioxid Redox Signal*, 15 (6), 1583-606 (2011).
- [6] Sheng Y. et al.: *J Am Soc Mass Spectrom.*, 30 (2), 218-226 (2019).
- [7] Zaripova R.I. et al.: *Zhurnal tekhnicheskoy fiziki* 92(7), 999-1003 (2022)
- [8] Gainutdinov Kh.L. et al.: *Applied Magnetic Resonance*, 40(3), 267-278 (2011).
- [9] Zaripova R.I. et al.: *Biophysics (Russian Federation)*, 66(3), 572-576 (2021).

## IMPLEMENTATION OF QUANTUM LOGIC BY PHASE SHIFT PULSES AND HIGH-SPIN IONS

**M.R. Arifullin<sup>1</sup>, V.L. Berdinskiy<sup>1</sup>**

<sup>1</sup> Orenburg State University, Orenburg, Russia

In order to build scalable quantum computers it is essential to properly design and develop physical qubits [1]. The use of high-spin ions embedded in crystal matrices as a new qubit platform would avoid the technical difficulties associated with other qubit platforms, such as high vacuum, strong magnetic fields, and laser radiation. This would simplify the management of qubits and scale systems, increasing the stability and reliability of their operation.

The use of multi-spin paramagnetic ions and phase modulated microwave pulses allow to manipulate individual qubits, for example, a high-spin paramagnetic center with spin  $S = 2$  in a zero magnetic field. One of the unique advantages of this approach based on microwave manipulation of high-spin ions in zero magnetic field. To describe the implementation of quantum logic algorithms, it is necessary to have a consistent theory of pulsed spin evolution for high-spin ion systems.

The vast majority of modern magnetic resonance theories focus on describing spin dynamics and relaxation in strong magnetic fields. In order to construct pulse sequences for implementing quantum logic by high-spin systems in zero magnetic fields, we need a rigorous and consistent theory for their spin evolution.

As a first step in studying the possibilities of high-spin ions, it is necessary to study the spin dynamics of particles whose state is described by the zero-field splitting Hamiltonian without taking anisotropy terms into account. The spin states of paramagnetic ions in zero magnetic fields do not produce the observed magnetization; they correspond to states that are described in optical spectroscopy by the term "alignment". Such states are entangled ones similar to  $\{|T_+\rangle + |T_-\rangle\}$  and  $\{|T_+\rangle - |T_-\rangle\}$ . Therefore, the proposed theory should describe microwave control of the ion spin "alignment". Resonant microwave pulses are also capable of creating magnetization of high-spin metal ions, even in the absence of an external magnetic field. This transformation of the spin states is similar to the alignment-orientation transition in atomic spectroscopy [2], which allows to observe the results of induced spin manipulations. The phase shift of the microwave pulses is equivalent to a change in the direction of the vector of the effective magnetic field in a rotating frame. Such pulses are shown to produce different spin evolutions of the high spin ions similar to quantum logic operations [3-6].

1. Sevilla J., Riedel C. J. Forecasting timelines of quantum computing. arXiv:2009.05045 (2020)
2. Chaika M.P.: Interferentsiya vyrozhdennykh atomnykh sostoyaniy. Leningrad: Leningrad Univ. Pub. (1975), 192 p. (In Russian)
3. Arifullin M.R., Berdinskii V.L. Phys. Solid State 62, Iss 3, 440 - 444 (2020)
4. Arifullin M.R., Berdinskiy V.L.: Russ. Phys. J. 63, 888–893 (2020)
5. Arifullin M. R., Berdinskiy V. L.: Russ. Phys. Bull 88, № 7 (2024)
6. Arifullin M. R., Berdinskiy V. L. AIP Conference Proceedings 2241, 1–8 (2020)

## The SILICON SURFACE MICROSTRUCTURES INITIATED by a POWERFUL LIGHT PULSE for INCREASE The EFFECTIENCY OF a SOLAR CELLS

**B.F. Farrakhov<sup>1</sup>, Ya.V. Fattakhov<sup>1</sup>, A.L. Stepanov<sup>1</sup>, R.I. Batalov<sup>1</sup>,  
V.V. Bazarov<sup>1,3</sup>**

<sup>1</sup> Zavoisky Physical-Technical Institute, FRC Kazan Scientific Center of RAS, Kazan, Russia

The aim of the work was to modify the near-surface silicon layer before and after ion implantation, followed by pulsed light annealing, to structurize the surface of the substrates to increase the efficiency of their use in solar energy converters [1,2].

Single-crystal polished silicon samples with surface orientation (100) were selected for the study. Implantation was carried out with Mn ions with an energy of 40 keV and a dose of  $3 \times 10^{16} \text{ cm}^{-2}$ , and one sample was also alternately implanted with In and As ions with an energy of 30 keV and a dose of  $2 \times 10^{16} \text{ cm}^{-2}$  for both ion types.

Pulsed light treatment of non-implanted samples was performed by the influence of powerful light pulses of millisecond duration from xenon lamps on the UOL.P.-1 setup. In the second case, pulsed light annealing of ion-implanted samples was carried out using radiation from halogen incandescent lamps on the Impulse-6 setup.

The resulting microstructures (fig.1) made it possible to increase the absorption capacity by up to 7-8 percent for several wavelengths of light.

1. Lima Monteiro D., Honorato F., Oliveira Costa R. and Salles L.: International Journal of Photoenergy. **2012**, Art. ID 743608 (2012).

2. Macdonald D., Cuevas A., Kerr M. et al.: In Solar World Congress (Adelaide, Australia, 2001).

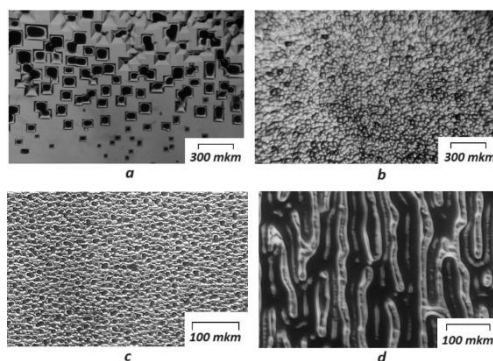


**Fig. 1.** Photographs of non-implanted silicon (100) after pulsed light annealing on UOL.P-1 with a power density of  $1200 \text{ W cm}^{-2}$  and durations of 70 ms (a) and 90 ms (b) (in fig (b) the surface was sanded before annealing). Photographs of the surface of ion implanted silicon (100) (c- by Mn ions, d- by In and As ions) after pulsed light annealing on the Impulse-6 setup with a power density of  $20 \text{ W} \times \text{cm}^{-2}$  and a duration 6 s, respectively.

## DEVELOPMENT OF A PHASE-ADJUSTED RADIO-FREQUENCY SOLENOID SENSOR FOR MEDIUM-FIELD MAGNETIC RESONANCE IMAGING SYSTEM

A.A. Bayazitov, Ya.V. Fattakhov, V.L. Odivanov

Zavoisky Physical-Technical Institute, FRC Kazan Scientific Center of RAS, Kazan, Russia

In recent years, there has been an increasing interest in low- and medium-field magnetic resonance imaging in the world. This is due to the fact that new technical and software solutions have made it possible to bring the technical and diagnostic capabilities of such devices closer to the characteristics of high-field MRI [1-3].

The paper will focus on the radio-frequency receiving sensors for medium-field MRI. In particular, the operating frequency of reception is 17.5 MHz. The design of the phase coil is investigated using the example of a cylindrical sensor. The phase coil includes six consecutive inductors (tape of equal length) and capacitors. The sequential switching on of the capacitors compensates for the total inductance and allows you to adjust the circuit to the operating frequency. To balance the voltage at the ends of the coil, the sensor cable is connected via capacitors.

The contour modeling is carried out in the work. The amplitude-frequency and phase-frequency characteristics are considered.

The receiving circuit is located inside the transmitting circuit. The parameters of the capacitors are selected taking into account the amplitude-frequency and phase characteristics of the circuit at the operating frequency. Capacitors must compensate for the phase shift at the source points (the beginning of the inductive turn) of each for two adjacent turns. At these points, the phase shift in voltage should be zero in the frequency range in the near of resonance. The characteristics of the contour outside and inside the magnet are investigated.

1. Bayazitov A. A., Fattakhov Ya. V., Fakhrutdinov A. R., Shagalov V. A.: *J. Instruments and Experimental Techniques*, vol. 63, no. 6, 875-879 (2020)
2. V.A. Arhangel'skij, V.V. Churayanc, Sh.Sh. Shotemor, E.A. Knorin, S.M. Gorbunov, V.V. Lykov, A.M. Smirnov, V.I. Sporysh *Perspektivy razvitiya nizkopolevoj tomografii*. M: Biomedpribor (2000).
3. Marusina M.Ya. Kaznacheeva A.O. *Sovremenyte vidy tomografii: Uchebnoe posobie*. SPb.: SPbGU ITMO, (2006), 152 p.

## Study of the interaction of lovastatin with a transition group metal - gadolinium in solution using NMR spectroscopy

**T.R. Islamov<sup>1</sup>, O.V. Aganova<sup>1</sup>, A.R. Julmetov<sup>1</sup>, V.V. Klochkov<sup>1</sup>**

<sup>1</sup>Institute of Physics, Kazan Federal University, 420008, 18 Kremlevskaya st., Kazan, RF  
E-mail: relifer2000@mail.ru

Modification of biologically active compounds through the use of metal complexes is one of the promising directions in the development of drugs that must have certain previously known properties. Statins, being the most effective way to relieve atherosclerosis, have a wide range of side effects, such as myositis, increased production of liver enzymes. Studying the interaction of statins with transition group metals will help clarify ways to create a stable metal complex and subsequent studies on changes in pharmacokinetics.

The statin group is represented by a wide variety of molecules that differ in medical activity, solubility, etc. Lovastatin is the first approved HMG-CoA reductase inhibitor, clinical trials of which have provided evidence of the ability of drugs in this class to reduce morbidity and mortality associated with cardiovascular diseases [2]. Its structure with the numbering of carbon atoms is presented in Figure 1 a.

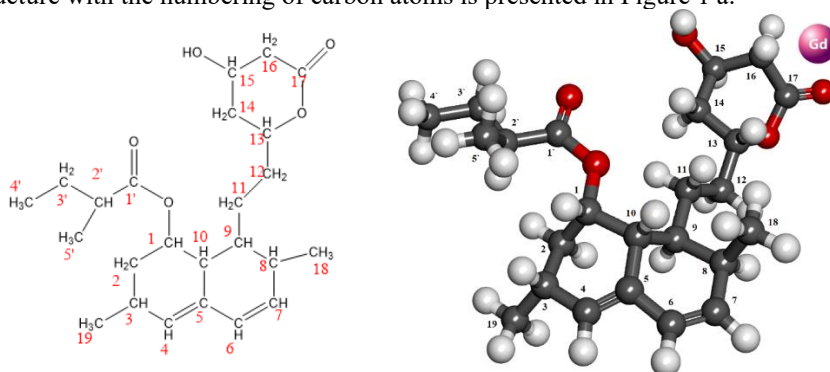


Figure 1 – The chemical structure of lovastatin (a) and schematic representation of the gadolinium ( $Gd^{+2}$ ) – lovastatin complex (b).

The main requirement for a ligand is low toxicity of the ion. Transition group metals, such as gadolinium, are widely used as a contrast agent for MRI and are a low-toxic element.

$^1H$  (700 MHz),  $^{13}C$  (175 MHz),  $^1H$ - $^{13}C$  HMBC NMR spectra of lovastatin in deuterated acetone at various concentrations of gadolinium chloride  $GdCl_2$  (gadolinium/lovastatin: 1/5, 1/10) at temperature of 308 K were recorded using Bruker “Avance -700 III TM” spectrometer.  $^1H$  NMR spectrum was recorded using  $90^\circ$  pulse, delay between pulses 2 with spectral width 10 ppm. The correlation of one-dimensional spectra was performed using TopSpin software.

The study of complex formation in the gadolinium ( $Gd^{+2}$ ) – lovastatin system was carried out using two-dimensional  $^1H$ - $^{13}C$  HMBC NMR spectroscopy within the framework of the approach discussed in our previous works [3,4].

Figure 2 shows heteronuclear experiment  $^1\text{H}$ - $^{13}\text{C}$  HMBC spectra of lovastatin with gadolinium ion  $\text{Gd}^{2+}$  in deuterated acetone ( $\text{C}_3\text{H}_6\text{O}$ ) with different solution concentrations.

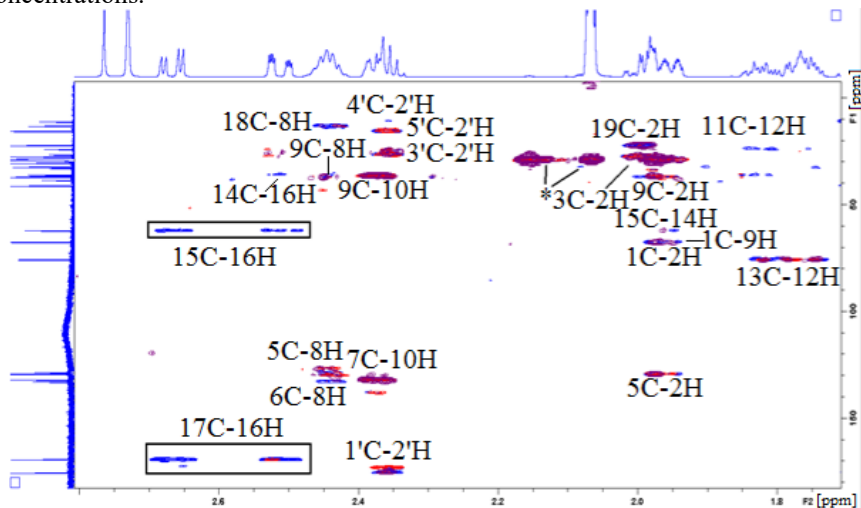


Figure 2 – Fragment of the  $^1\text{H}$ - $^{13}\text{C}$  HMBC NMR spectra ( $^1\text{H}$ , 700 MHz) of lovastatin in a solution of acetone ( $\text{C}_3\text{H}_6\text{O}$ ) with gadolinium (blue – pure lovastatin, red – lovastatin with gadolinium ion in a molar ratio of 1/75 ion/statin, purple – lovastatin with ion gadolinium in a molar ratio of 1/50 ion/statin, \* - solvent signal)

When comparing  $^1\text{H}$ - $^{13}\text{C}$  HMBC NMR spectra, the following differences can be identified: signals from 15C-16H, 17C-16H, 14C-16H are present only in “pure lovastatin”, while they are not observed in other samples. The signal from 15C-14H is also not observed when gadolinium ion  $\text{Gd}^{2+}$  is added. The signals of the remaining peaks change slightly. Thus, it can be assumed that the localization of the gadolinium ion will be located in the environment of C-14, C-15 and C-16 atoms (figure 1b).

1. Kuranova N. N. et al. Complexation of Gold (III) with Pyridoxal 5'-Phosphate-Derived Hydrazones in Aqueous Solution // *Molecules*. – 2022. – V. 27. – №. 21. – P. 7346.
2. Hamelin B.A., Turgeon J. Hydrophilicity/lipophilicity: relevance for the pharmacology and clinical effects of HMG-CoA reductase inhibitors. // *Trends Pharmacol. Sci. England*, 1998. Vol. 19, № 1. P. 26–37.
3. Abdrakhmanov, Rustam, Modeling the  $\text{Co}^{2+}$  Binding to Amyloid Peptide A $\beta$ 13-23 in Water Environment by NMR Spectroscopy / Rustam Abdrakhmanov, Dmitriy Blokhin, Konstantin Usachev, Vladimir Klochkov // *BioNanoScience*. – 2018. - V. 8, Issue 1.- P. 423-427.
4. Tarasov, A.S. The effect of gadolinium ion on micelles and reverse micelles by NMR spectroscopy / A.S. Tarasov, I.Z. Rakhmatullin, G.S. Shurshalova, A.V. Klochkov, K.A. Il'yasov, V.V. Klochkov // *BioNanoScience*. - 2021. - V.11, Issue1. - P.136-141.



## HOME-BUILT SET-UP FOR NMR/DNP IN STRAY FIELD OF SUPERCONDUCTING MAGNET

**V.V. Kuzmin<sup>1</sup>, G.A. Dolgorukov<sup>1</sup>, A.S. Makarchenko<sup>1</sup>**

<sup>1</sup> Kazan Federal University, Kazan, Russia

Nanodiamonds and other nontoxic nanoparticles are widely used as a biomedical platform for drug-delivery, imaging, and subcellular tracking. Recently it was shown that paramagnetic centers on the surface of nanodiamonds could be used for dynamic nuclear polarization of the surrounding water solution and MRI enhancement at ultra-low fields and room temperature [1].

We plan to verify and extend the applicability of such method not only to nanodiamonds but also to other nanoparticles that contain surface defects. To explore the maximum achievable Overhauser DNP enhancements and underlying physical mechanisms we intend to study magnetic field dependence of the DNP effect. To achieve this goal the experimental set-up that can operate in the broad range of magnetic fields was assembled.

Here the tests of this home-built set-up for ultra-low field DNP in water solutions in the range 1-20mT are described and presented. The magnetic field is achieved in stray field of the unshielded superconducting NMR magnet (4.7 T). This set-up consists of active shim coils, NMR coil and loop-gap EPR resonator, low-frequency NMR preamplifier, passive switch to direct microwave and radiofrequency power from single broadband amplifier (Rohde Schwartz, BBA100, 500W continuous wave, 9kHz-250MHz) to resonator and NMR coil. The NMR receive/excitation system of our home-build broadband NMR spectrometer is described elsewhere [2].

The stray field gradient is measured to be 3%/cm in the radial direction on the distance of ~0.5m from the magnet center where average magnetic field was measured to be 14mT. Shim coils allow to generate linear gradients in three directions (0.5mT/cm/A) for most critical direction) to increase magnetic field homogeneity in the sample of diameter up to 40mm. The gradient coils dimensions and geometry were optimized in terms of linearity using Python script and Magpylib library for magnetic field calculations. The gradient coil holders (external dimensions of ~17cm) are 3D-printed using PETG plastic.

The preamplifier was assembled using low-cost INA-02186 MMIC amplifier (1.8db noise figure and 31db gain) and AD797 operational amplifier with total gain of 68db, 0.05-1.2MHz bandwidth and 180 $\mu$ s dead time.

Successful DNP enhancement of 155 was achieved in the test sample containing 0.6mL water solution with TEMPOL (1mmole/L) at microwave power 20Watts at the magnetic fields of 14 and 4.1mT.

This work was financially supported by the Russian Science Foundation (project no. 24-22-00336).

1. Waddington A. et al.: Nature Communications. **8**, 15118 (2017)

2. Kuzmin V.V. et al.: Magnetic Resonance in Solids. **21**, Is.1, 19104 (2019)

## Targeting interface for MR imaging

**V.Odivanov, Y.Fattakhov, A.Fakhrutdinov, V.Shagalov, A.Bayazitov**

Laboratory of medical physics, Zavoisky Physical-Technical Institute,  
FRC Kazan Scientific Center of RAS, Kazan 420029, Russia  
odivanov@mail.ru, yfattakhov@yandex.ru

When performing examinations using magnetic resonance imaging, an important aspect is obtaining images of the examined organs sections in given positions and at given angles. In this regard, when generating gradient actions, a superposition of the amplitudes of the main gradient influences is performed - selective, frequency-encoding and phase-encoding, taking into account the orientation angles of the target image planes. The approach to generating these control signals is based on using Euler angles to set the angular position of the layers. When specifying orthogonal target projections, 24 variants for the orientation of the image axes are possible, from which 3 main ones are selected, the orientation of which is generally accepted for MRI images: Sagittal, Transaxial and Coronal. In addition, in most cases it is necessary to obtain images of inclined layers close to the main orientations. For correct aiming, it is necessary to obtain a certain reference image in one of the main projections, relative to which the position, thickness, number, pitch and angle of inclination of the target layers are selected. The angle of rotation of the layers relative to the reference one is also specified by Euler angles. Multiplying the reference image matrix and the rotation matrix gives the target image matrix and its corresponding Euler angles. 2 of the 3 Euler angles of the target images follow the angles of the main projections, and the third one reflects the tilt of the layers. If we use the resulting images as reference for new aiming, then the target angles will vary in 2 out of 3 parameters. Thus, in the general case, orientation angles can be arbitrary, but close to one of the main projection.

In the Laboratory of Medical Physics of the Zavoisky Physical-Technical Institute, an MRI installation based on a permanent magnet with an induction of 0.4 Tesla has been developed and is used. In the previously used spectrometer block, the formation of the resulting gradient signals was carried out by means of multiplying digital-to-analog converters, the signals of the main gradient influences were supplied to the reference voltage input, and the rotation of the direction was carried out by specifying codes proportional to the sine and cosine of the rotation angle. This approach ensured the accuracy of the phase-encoding gradient step with a limited bit capacity of gradient DACs (12 bits). The disadvantage of this approach is the difficulty of compensating for gradient shifts when using shimming, as well as the impossibility of targeting inclined layers. Currently, a new microcontroller-based radio spectrometer block has been developed, which, in particular, controls gradient signals with a resolution of 16 bits, which allows the use of software control of layer orientation. The MRIScan v.5.1 computer application provides interaction with the radio spectrometer during examinations, saving and analyzing the resulting images. The targeting control user interface allows scanning targeting to set the field of view, thickness, number, position, pitch and tilt of layers, both based on the main projections and relative to the tilted layers. Control of the position, pitch and inclination of layers can be carried out both

by the controls of the aiming window, and by directly controlling the image of the layer's projections on the aiming image using the mouse. The scanning technique development library includes functions and macros for calculating gradient pulse amplitudes based on the main actions using a rotation matrix. The spectrometer controller firmware provides for both direct control of gradients using codes in the pulse program, and control using codes from special control arrays loaded along with the program. This allows you to directly set constant parameters of influences in the cycle and obtain variable parameters with changes in the phase-coding gradient from control arrays. This approach is used to save their volume.

General view of the MRI Scan application window with aiming dialog open is shown on Fig. 1.

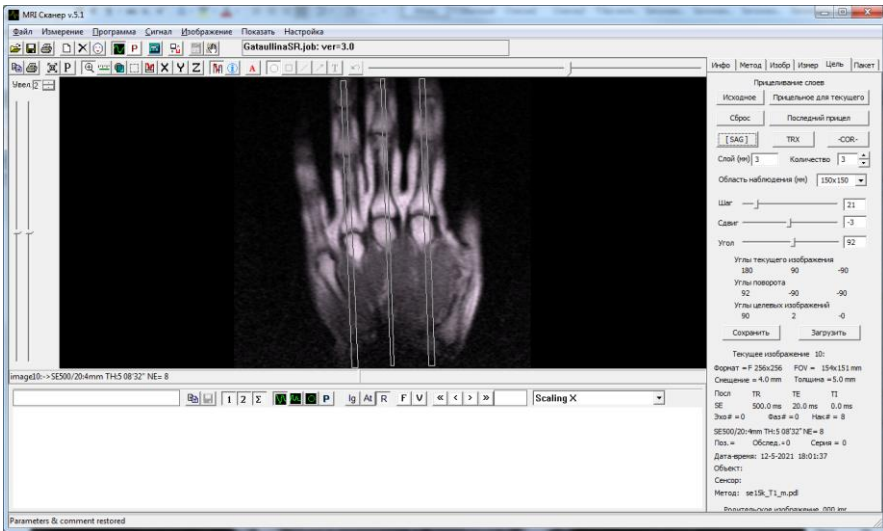


Fig. 1. General view of the MRI Scan application window with aiming dialog open

## **Investigation of NO and copper content in different segments of spinal cord 24 hours and 7 days after combined brain and spinal cord injury in rat with using the method EPR Spectroscopy**

**D. I. Silantyeva<sup>1,2</sup>, V. V. Andrianov<sup>1,2</sup>, G. G. Yafarova<sup>2</sup>, L. V. Bazan<sup>1,2</sup>,  
T. K. Bogodvid<sup>2,3</sup>, A. I. Arslanov<sup>1</sup>, I. B. Deryabina<sup>2</sup>, L. N. Muranova<sup>2</sup>,  
S. G. Pashkevich<sup>4</sup>, T. A. Filipovich<sup>4</sup>, V. A. Kulchitsky<sup>4</sup>, Kh. L. Gainutdinov<sup>1,2</sup>**

<sup>1</sup> Zavoisky Physical-Technical Institute, FRC Kazan Scientific Center of RAS, Kazan 420029, Russian Federation;

<sup>2</sup> Institute of Fundamental Medicine and Biology of Kazan Federal University, Kazan 420008, Russian Federation;

<sup>3</sup> Volga Region State University of Physical Culture, Sport and Tourism, Kazan 420010, Russian Federation;

<sup>4</sup> Institute of Physiology of Nat. Acad. of Sci. of Belarus, Minsk 220072, Belarus  
silantyevad@gmail.ru

Discovery of the ability of mammalian cell to produce nitric oxide (NO) is incentive to study the role of NO in all areas of biology and medicine [1, 2]. It was found that NO is a key signaling molecule which participated in regulation of physiological function, such as vasodilatation, neurotransmission, immunity and metabolism [1, 5]. Additionally in the brain NO acts as a neuromodulator which control behavioral activity, influence memory formation, and enhance responses to painful stimuli [3]. Moreover in present time the attention of scientists is drawn to the participation of NO not only in physiological processes, but also in the mechanisms of development of various pathological conditions of the body. The NO is involved in the mechanisms of secondary spinal cord injury [6, 7], which characterized by appearance of reactive oxygen and nitrogen species and development of secondary injury processes [1]. However there is now proven hypothesis about role of endogenous NO in nervous system as information from different research groups is contradictory and require proven methods of evaluation of NO content [8].

The chemical properties of NO guide the efforts of developing sensitive and selective procedures for its measurements in biological samples. The free radical nature of NO complicates its studying by shortening its half-life in biological systems. There are several methods of NO measurements in biological tissue, such as chemiluminescent detection or fluorometry but accurately measuring both the constant concentration of NO and the rate of NO production in biological systems is challenging due to its short half-life. More than several decades, electron paramagnetic resonance was proved as one of the most effective methods for the detection and quantification of nitric oxide in biological tissues [9]. Therefore the aim of the present research was to study NO and copper content in different segments of spinal cord 24 hours and 7 days after combined brain and spinal cord injury in rat with using the method EPR spectroscopy. The intensity of NO formation 24 hours and 7 days after combined brain and spinal cord was measured by EPR spectroscopy using the spin trap method [8, 9]. This method is based on the reaction of a radical (in this case NO) with a spin trap. Complex of Fe<sup>2+</sup> with diethyldithiocarbamate (DETC) was used to capture NO and form a stable ternary complex (DETC)<sub>2</sub>-Fe<sup>2+</sup>-NO in animal tissues. These complexes have EPR spectra with triplet hyperfine structure and value of  $g=2,035 - 2,040$  [2, 9]. The

measurements were made were made using a Bruker X-band (9.5320 GHz) EMX/plus spectrometer.

It was found that intensity of NO production in spinal cord was significantly reduced by 60% ( $p < 0.05$ ) in rostral segments, which situated above the injury whereas intensity of NO production in injured segments and caudal segments (situated lower injured segments) did not change 7 days after combined injury of brain and spinal cord. The intensity of NO production in similar segments of the spinal cord in intact animals remained unchanged. Content of NO in spinal cord reduced in caudal segments 1 day after injury. The copper content did not change both 1 day and a week after the combined injury.

The work was supported by the Russian Scientific Fund No. 23-45-10004 and Belarusian Republican Foundation for Basic Research (grant M23RNF-067).

- [1] Lundberg J.O.; Weitzberg E.: *Cell* **185**, 2853-2878 (2022)
- [2] Vanin A.F.: *Nitric Oxide* **54**, 15-29 (2016)
- [3] Steinert J.R. et al.: *Neuroscientist* **16** 435-452 (2010)
- [4] Zariyova R.I. et al.: *Zhurnal tekhnicheskoy fiziki* **92**(7), 999-1003 (2022)
- [5] Ignarro L.J. et al.: *J Cardiovasc Pharmacol.* **34**(6), 879-886 (1999)
- [6] Jia Z. et al.: *Spinal Cord* **50**, 264–274 (2012)
- [7] Yafarova G.G. et al.: *Bull Exper Biol Med.* **162**(9), 295-299 (2016)
- [8] Wierónska J.M. et al.: *Biomolecules* **11**, 1097 (2021)
- [9] Mikoyan V.D., Kubrina L.N. et al.: *Biochim. Biophys. Acta*, **1336**, No 2, 225-234 (1997)

## EMR signals in rat spinal cord 7 days after its traumatic injury

**S.V. Yurtaeva<sup>1</sup>, G.G. Yafarova<sup>1,2</sup>, I. V. Yatsyk<sup>1</sup>, A.A. Rodionov<sup>3</sup>,  
Kh.L. Gainutdinov<sup>1,2</sup>,**

<sup>1</sup>Zavoisky Physical-Technical Institute, FRC Kazan Scientific Center of RAS, Kazan, Russia

<sup>2</sup>Institute of Fundamental Medicine and Biology Kazan Federal University, Kazan, Russia

<sup>3</sup>Institute of Physics, Kazan Federal University, Kazan, Russia

Recently, the study of molecular mechanisms of nerve tissue damage, and the search for ways to recover from the resulting disorder, have been carried out very intensively. One of the metabolites actively involved in the development of post-traumatic conditions when nerve tissue is damaged is iron. It is known that spinal cord (SC) injury is accompanied by cell death and bleeding, which cause an increase of free iron pool. In this case, it is possible an increase of the processes of iron biomineralization in tissues, which results in the formation of crystalline iron oxides. The EPR technique makes it possible to detect such crystals.

To date, it is known about the observation of electron magnetic resonance (EMR) signals in injured nerve tissues depending on magnetic field orientation, but their nature is insufficiently explored. The aim of the work was to study the emerging EMR signals in the tissue of injured rat SC and compare them with signals in healthy tissues. SC tissues were studied: control (n=3) and with an experimental model of spinal cord injury (SCI) for 7 days (n=6). Two types of EMR signals were detected in SC tissues, corresponding to crystalline iron oxides formed as a result of biomineralization. Their temperature and angular characteristics have been studied. The first type, characterized by the dependence of  $H_{res}$  on orientation of the magnetic field, is attributed to nanocrystalline magnetite. The second type, characterized by superparamagnetic temperature behavior, is evidently attributed to the crystalline core of ferritin, ferrihydrite.

A noticeable increase in the EMR signal in the area of SC injury was found compared with neighboring areas of the SC, as well as compared with similar non-injured SC tissues of control rats, on average more than twice, indicating the accumulation of crystalline iron in the injured tissue. In rat, with the maximum effect, the signal in the area of SC injury increased 10 times.

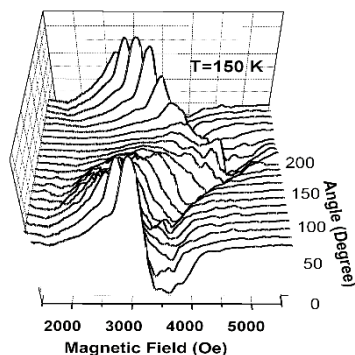


**Fig. 1.** An example of the EMR signal in injured spin cord and its angular dependence.

## FIRST PRINCIPLES CALCULATIONS of MAGNETIC ORDER of Fe-Al BASED TERNARY ALLOYS

A.F. Abdullin, E.V. Voronina

Kazan Federal University, Kazan, Russia

The authors [1] demonstrated the possibility spin-spiral magnetic structure in the  $\text{Fe}_9\text{Al}_7$  structure in [001] and [111] directions using first principles calculations. Later [2] neutron diffraction discovered a spin density wave in the Fe-Al alloy with a 40% aluminum concentration at 1.7 K. Today the origin for the breakdown of the ferromagnetic order, as a result of the phase transition to a spin-density state, is unclear and requires further theoretical research.

This work presents quantum mechanical calculations of various non-collinear spin structures in the WIENncm software package [3]. Fig. 1 demonstrates the dependence of the energy difference between the ferromagnetic ( $E_{\text{FM}}$ ) and spin-spiral ( $E_{\text{SS}}$ ) states on the average magnetic moment per Fe atom. The magnetic moment varies with changing lattice parameter. Clearly seen (Fig. 1a) for the  $\text{Fe}_9\text{Al}_7$  structure the spin-spiral state is preferable to other Fe-Al systems. In turn, the realization of a spin-spiral state depends on the value of the magnetic moment.

Fig. 1b shows a similar dependence for ternary  $\text{Fe}_9\text{Al}_6\text{B}$  and  $\text{Fe}_9\text{Al}_6\text{Ga}$  systems. It can be seen that the spin-spiral state is most advantageous compared to the ferromagnetic state (absolute maximum on the graph) with the value of the average magnetic moment approximately equal to  $1 \mu_{\text{B}}/\text{atom}$  for all structures. It should be noted that when a certain threshold value of magnetic moment is exceeded, the spin-spiral structure breaks down and passes into a ferromagnetic, which confirms the dependence on the value of the magnetic moment. The results of the presented calculations are consistent with the Mossbauer measurement data of binary and Fe-Al based ternary alloys.

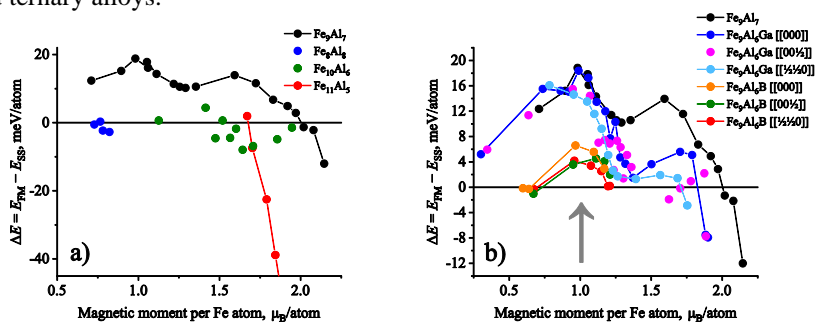


**Fig. 1.** The dependence of the energy difference ( $\Delta E$ ) of the ferromagnetic ( $E_{\text{FM}}$ ) and spin-spiral ( $E_{\text{SS}}$ ) states on the total magnetic moment of the unit cell divided by the number of Fe atoms. a) Binary Fe-Al systems with different Al concentration. b) Based on Fe-Al ternary systems with impurities B and Ga in different positions (double square brackets) of the unit cell.

1. Bogner J. et al.: Phys. Rev. B **58**(22), 14922-14933 (1998)
2. Laskowski R., Blaha P.: Phys. Rev. B **69**, 140408 (2004)
3. Noakes D. R. et. al.: Phys. Rev. Lett. **91**(21), 217201-1 (2003)

## MÖSSBAUER STUDY OF THE MINERALS FORMED DURING SYNTHESIZED FERRIHYDRITE REDUCTION BY REPRESENTATIVES OF THE *MELIORIBACTERACEAE* FAMILY

**N.I. Chistyakova<sup>1</sup>, V.A. Pikhtereva<sup>2</sup>, D.I. Komleva<sup>1</sup>, M.V. Lesnaya<sup>1</sup>,  
A.V. Semeno<sup>1</sup>, O.A. Podosokorskaya<sup>2</sup>, D.G. Zavarzina<sup>2</sup>,  
V.S. Rusakov<sup>1</sup>**

<sup>1</sup>Department of Physics, M.V. Lomonosov Moscow State University, Moscow, Russia

<sup>2</sup>Winogradsky Institute of Microbiology, FRC Biotechnology, Russian Academy of Sciences, Moscow, Russia

Dissimilatory Fe(III)-reduction is the widespread and ancient metabolic process by which anaerobic prokaryotes transform Fe(III)-containing minerals into Fe(II)-containing ones to obtain energy for life. This process plays significant role in the subsurface environment, where microorganisms have occupied the cracks in the rocks using Fe(III)-containing minerals as the electron acceptors. The aim of the present work was to study minerals formed during the reduction of synthesized ferrihydrite (SF) by members of the *Melioribacteraceae* family, which are typical of the subsurface microflora [1, 2].

Fe(II)-containing minerals produced by six strains of the *Melioribacteraceae* family were studied. Anaerobic media with three different content of the SF, (10, 50 and 100 mM of Fe(III)) and organic electron donors were used for the experiments. During the experiments, cells were counted and Fe(II) production was measured.

All samples were examined using <sup>57</sup>Fe Mössbauer spectroscopy at room temperature. Mössbauer phase analysis was performed by use of SpectrRelax software [3]. The relative intensities of subspectra which corresponded to Fe<sup>2+</sup> and Fe<sup>3+</sup> atoms were found.

The work supported by the RNF project №24-64-00023.

1. Podosokorskaya O.A., Kadnikov V.V., Gavrilov S.N., Mardanov A.V., Merel A.Y., Karnachuk O.V., Ravin N.V., Bonch-Osmolovskaya E.A., Kublanov I.V. *Environ Microbiol* **15**:1759-1771 (2013).

2. Podosokorskaya O.A., Elcheninov A.G., Gavrilov S.N., Petrova N.F., Klyukina A.A., *et al. Water* **15**:3451 (2023).

3. Matsnev M.E., Rusakov V.S.: AIP Conf. Proc.:1489, 178–185 (2012).

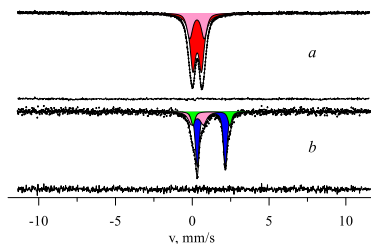


**Fig. 1.** Mössbauer spectra of initial SF (a) and mineral obtained during the reduction of SF by member of the *Melioribacteraceae* family. The spectra corresponding to the new formed phases are marked in green and blue.



## MÖSSBAUER SPECTROSCOPY BASED ON FAST STREAMING ANALOG TO DIGITAL CONVERTORS

**E.N. Dulov<sup>1</sup>, M.T.R. Zaitov<sup>1</sup>**

<sup>1</sup> Kazan (Volga region) Federal University, Kazan, Russia

The rapid growth of microelectronics in last decades opens new possibilities in obtaining Mössbauer data. For example simultaneous registration of spectra for many different discrete amplitude of pulses from a detector is very useful in depth-selective conversion-electron Mössbauer spectroscopy (DCEMS) [1]. Besides, this technique allows skipping selection of discrimination levels stage before an experiment. The selection can be performed after experiment with much better accuracy and for more than one range of amplitudes [1, 2].

This work offers generalized approach based on digital signal processing of multiple signals of different types that can be used in Mössbauer spectroscopy. Our implementation of this approach is based on general purpose four-channel digital oscilloscope Picoscope™ 4424 (USB 2.0 interface) with streaming data acquisition mode. The streaming mode is a key feature because sampled data must be uninterrupted during an experiment.

The implementation includes fixed function for each of the input channels of the oscilloscope. First two channels are inputs for pulses from detectors of particles and are coupled with software digital pulse processor modules with trapezoidal shapers that are typical for high-resolution gamma- and X-ray spectroscopy. The modules can determine time-of-arrival for registration events with precision that at least equals to sampling time of 250 ns. These two channels can work in time-delayed coincidence mode. Third input channel is intended for signal from the velocity transducer and followed by original finite-impulse response filter providing accurate synchronization of counting rate with Doppler's velocity of the source. Fourth channel is general purpose input allowing registration of Mössbauer spectra depending on external signal which can be temperature, pressure, magnetic field strength or any other physical value that can be turned into electrical signal with some probes. Note that bandwidth of the signal is limited only by the oscilloscope's bandwidth, which equals to 20 MHz in our implementation and provides an ability to register rapid processes.

The solution presented covers and unifies many specific experimental techniques, and it is applicable to upgrade functionality of any existing Mössbauer spectrometer, which can provide at least two signals in analog form: pulses from detector and Doppler velocity of the source.

1. Ivoilov N.G. et al.: Multilevel Mössbauer spectroscopy. Bull. of RAS, Phys. series. **65**, 1068–1072 (2001). (In Russian)

2. Pawlak J. et al.: 2D data processing with MIMOS. Hyp.Int., **244:20**, (2023).

## MÖSSBAUER SPECTROSCOPY of Fe ORGANIC-DERIVED COMPOSITE FISCHER-TROPSCH CATALYSTS OBTAINED by the HYDROTHERMAL SYNTHESIS

**K.V. Frolov<sup>1</sup>, O.A. Anosova<sup>1</sup>, M.V. Kulikova<sup>2</sup>, M.I. Ivantsov<sup>2</sup>,  
A.Yu. Krylova<sup>2</sup>, A.E. Kuzmin<sup>2</sup>**

<sup>1</sup> Shubnikov Institute of Crystallography, KCC&Ph NRC Kurchatov Institute, Moscow, Russia

<sup>2</sup>A.V. Topchiev Institute of Petrochemical Synthesis RAS, Moscow, Russia

Synthesis gas is a valuable feedstock that allows to obtain a wide variety of organic products such as hydrocarbons, alcohols, aldehydes, ethers, esters, etc [1]. Fischer–Tropsch synthesis (conversion of synthesis gas into hydrocarbons) is the commercially used second stage of processing of fossil fuels (coals, shale oil, peat, etc.) into liquid hydrocarbons mainly for fuel purposes over Fe- (>90 wt %) and Co-based catalysts (10–30 wt %) [2–4]. Concerning biomass as a primary feedstock, this method makes it possible to convert cheap CO<sub>2</sub>-neutral raws into valuable liquid chemical products (hydrocarbons of different fractions and homologous series) as well as CO<sub>2</sub>-neutral fuel fractions.

Four samples of the Fe-based composite catalysts for the high-temperature Fischer–Tropsch synthesis were obtained by hydro-thermal treatment of an aqueous solution of precursors: Fe nitrate and an organic compound (PVA, starch, glucose) – 24% wt. Fe on polyvinyl alcohol, synthesis at 230 °C; 35% wt. Fe on polyvinyl alcohol, synthesis at 270 °C; 25% wt. Fe on glucose, synthesis at 270 °C; 24% wt. Fe on starch, synthesis at 270 °C. The coexistence of different nanoscale Fe oxides and carbonates particles encapsulated within a carbon-containing composite matrix in fresh catalysts was revealed and studied by Elemental Analysis, Scanning and Transmission Electron Microscopies, Inductively Coupled Plasma Atomic Absorption Spectroscopy, Fourier Transform Infrared Spectroscopy, X-ray photoelectron spectroscopy, X-ray diffraction, and <sup>57</sup>Fe Mössbauer absorption spectroscopy.

The Mössbauer measurements were performed within the framework of the state assignment of NRC “Kurchatov Institute”.

1. Martinelli M., Gnanamani M.K., LeViness S. et al.: *Appl. Catal. A* **608**, e117740 (2020)
2. Mahmoudi H., Mahmoudi M., Doustdar O. et al.: *Biofuels Eng.* **2**, 11–31 (2017)
3. Suo Y., Yao Y., Zhang Y. et al.: *J. Ind. Eng. Chem.* **115**, 92–119 (2022)
4. Ma W., Jacobs G., Sparks D.E. et. Al.: *Catal. Today* **343**, 125–136 (2020)

## The WEATHERING RATE of ATACAMA METEORITES STUDIED by MOSSBAUER SPECTROSCOPY

**D. M. Kuzina<sup>1</sup>, A.V. Pyataev<sup>1</sup>, J. Gattacceca<sup>2</sup>, C. Sadaka<sup>2</sup>**

<sup>1</sup> Kazan Federal University, Kazan, Russia

<sup>2</sup> CNRS, Aix Marseille Univ, IRD, INRAE, CEREGE, Aix-en-Provence, France

Meteorites are unique objects whose study can shed light on questions related to the origins and evolution of the Solar system, and ultimately the formation of the Earth.

Among the interesting questions that can be addressed by studying meteorites is the intensity of their flux to the Earth and its possible evolution with time. For meteorite collections assembled in deserts, this requires determining the terrestrial age (i.e., the age of the fall) of the recovered meteorites.

Classically, the terrestrial age of meteorites is obtained from the study of cosmogenic nuclide  $^{14}\text{C}$  or  $^{36}\text{Cl}$ , depending of the age range. However, this requires complex chemical preparation of samples, and the use of an accelerator mass spectrometer. On the other hand, the weathering of meteorites during their stay on Earth may be a good proxy to their terrestrial age. In particular, the transformation of primary metallic minerals (mainly kamacite and taenite) [1, 2] into paramagnetic and ferromagnetic oxides and oxyhydroxides that are resistant to terrestrial conditions may be used as a proxy to the terrestrial age. Mössbauer spectroscopy is a powerful technique to explore complex assemblages of iron oxides oxyhydroxides, and has been already used to assess the weathering of meteorites in terrestrial conditions [3].

In order to test whether the weathering state of meteorite could be used as a proxy of their terrestrial, we present the study by Mössbauer spectroscopy of meteorites for which a terrestrial age is available.

The Atacama Desert (Chile) is a choice place for thus study because it has a high density of meteorite finds and a wide range of terrestrial ages (for instance the average terrestrial age of meteorites is 710 ka for the El Medano dense collection area [4], allowing studying weathering over longer time scale compared comparison with other hot deserts.

Mössbauer spectroscopy was performed on ordinary chondrites with the different terrestrial ages. The ages were estimated by measuring their content in cosmogenic nuclide  $^{36}\text{Cl}$  at ASTER accelerator mass spectrometer in CEREGE (Aix en Provence, France). The  $^{57}\text{Fe}$  Mössbauer spectra of seventy powdered samples were obtained on a standard MS-1104Em spectrometer at room temperature.

According to Mössbauer spectroscopy, the main products of weathering in the studied ordinary chondrites are hematite, magnetite, goethite, maghemite. For all studied samples, the relative content of weathering products of initial minerals was determined. We will discuss if the abundance and paragenesis of these weathering mineral depend on the terrestrial age of meteorites. If such, Mössbauer spectroscopy could be used as an alternative technique to estimate the terrestrial age, providing proper calibration of the method.

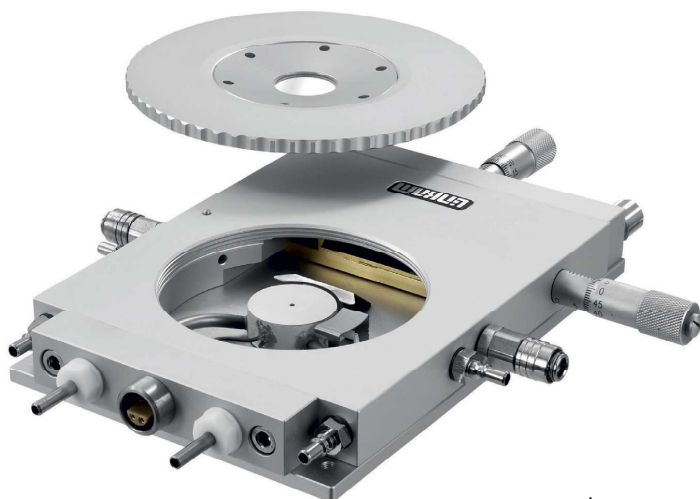
The study was supported by the Russian Science Foundation (project no. 24-27-00388, <https://rscf.ru/project/24-27-00388/>).

1. Oshtrakh M. I., Petrova E. V., Grokhovsky V. I. and Semionkin V.A.: *Meteoritics and Planetary Science*. **43**, 941-958 (2008).
2. Uehara M., Gattacceca J., Rochette P., Demory F., Valenzuela E. M.: *Phys. Earth Planetary Interiors*, **200-201**, 113-123 (2012).
3. Munayco P., Munayco J., De Avillez R. R., Valenzuela M., Rochette P., Gattacceca J., Scorzelli R. B. : *Meteoritics and Planetary Science*, **48**, 457-473 (2013).
4. Drouard A., Gattacceca J., Hutzler A., Rochette P., Braucher R., Bourlès D., ASTER Team, Gounelle M., Morbidelli A., Debaille V., Van Ginneken M., Valenzuela M., Quesnel Y., Martinez R.: *Geology*. **47** (7), 673–676 (2019).

# SPONSORS

# УНИВЕРСАЛЬНАЯ СИСТЕМА НАГРЕВА И ОХЛАЖДЕНИЯ THMS600

**LINKAM**



## НАГРЕВ И ОХЛАЖДЕНИЕ

Диапазон температур  
от  $-195^{\circ}\text{C}$  до  $600^{\circ}\text{C}$

## ОПТИЧЕСКИЕ МЕТОДЫ

Поддержка конфокальной,  
рамановской, световой  
микроскопии,  
рентгенографии и др.

## ПЕРЕМЕННАЯ СКОРОСТЬ НАГРЕВА

Точный контроль  
от  $0,01^{\circ}\text{C}$  до  $150^{\circ}\text{C}$  / мин

# "НАУКА"

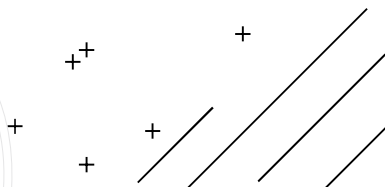
ЦЕНТР ТЕХНИЧЕСКОГО СОПРОВОЖДЕНИЯ

Адрес: 129626, Россия, Москва,  
ул. Маломосковская, 22, стр. 1, «Технопарк»  
Телефон: +7 (499) 322 06 62  
E-mail: info@nauka-shop.ru  
[www.nauka-shop.ru](http://www.nauka-shop.ru)

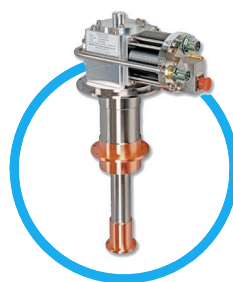
# "НАУКА"

ЦЕНТР ТЕХНИЧЕСКОГО СОПРОВОЖДЕНИЯ

Адрес: 129626, Россия, Москва,  
ул. Маломосковская, 22, стр. 1, «Технопарк»  
Телефон: +7 (499) 322 06 62  
Моб.: +7 926 422 93 04  
E-mail: info@nauka-shop.ru



## КРИОГЕННЫЕ РЕФРИЖЕРАТОРЫ SHI CRYOGENICS СЕРИИ RDK



Компания «ЦТС Наука» предлагает приобрести криогенные рефрижераторы производства компании SHI Cryogenics:

- + рефрижераторы Гиффорда-МакМагона,
- + рефрижераторы с импульсной трубкой
- + рефрижераторы Гиффорда-МакМагона/Джоуля-Томпсона, с диапазонами температур от 4 К до 77+ К.
- + Криогенные рефрижераторы SHI Cryogenics изготавливаются на производственных объектах мирового класса с использованием современных производственных и технологических возможностей в соответствии с концепцией «шести сигм». В результате получается продукция, отличающаяся высокой надежностью, удобством использования, поддерживаемая международными торговыми и обслуживающими сетями.
- + Криогенные рефрижераторы Гиффорда-МакМагона на 4К от SHI Cryogenics Group — надежные и универсальные системы. Они гораздо выгоднее экономически, чем системы с незамкнутым циклом на основе жидкого гелия. Криогенные рефрижераторы RDK характеризуются высокой холодопроизводительностью, компактной конструкцией и универсальностью, признаны стандартными для МРТ. Рефрижераторы SHI применяют для охлаждения широкого спектра устройств в экспериментах и аналитических исследованиях.

**SHI**  
Cryogenics Group

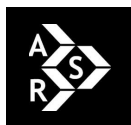
ЛАБОРАТОРНОЕ ОБОРУДОВАНИЕ | РАСХОДНЫЕ МАТЕРИАЛЫ | СЕРВИС



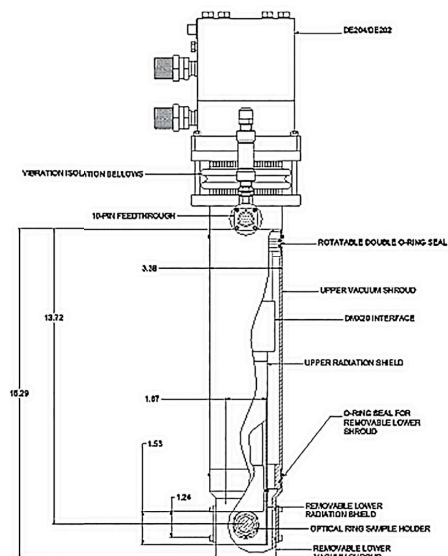
# КРИСТАТЫ ЗАМКНУТОГО ЦИКЛА С ИЗМЕНЯЕМОЙ ТЕМПЕРАТУРОЙ С НИЗКИМ УРОВНЕМ ВИБРАЦИЙ И ПРИМЕНЕНИЕМ РЕЗИНОВОГО СИЛЬФОНА

+

+



+



## ПРИНЦИП РАБОТЫ

+ Этот инновационный криостат, изготовленный Cryo Industries, работающий по схеме «Образец в вакууме», имеет крайне низкий уровень вибраций благодаря конструкции с гибким резиновым сильфоном и теплопередаче через газ. **Результатом является сверхнизкий уровень вибраций образца!**

+ Охлаждение для долгой работы при низких температурах обеспечивается рефрижератором замкнутого цикла, работающим на пульсирующих трубках или по принципу Гиффорда-МакМагона. **Жидкий хладагент не требуется!**

+ Стандартная комплектация может быть с различными криостатами: трубчатым, оптическим со сверхвысоким вакуумом и с узким зазором. **Доступные диапазоны рабочих температур вплоть до 3 К.**

- + Доступные диапазоны рабочих температур вплоть до 3 К.
- + Доступны системы с охлаждающими головками на 10К, 6,5 К и 4 К с различной мощностью охлаждения
- + Системы со сверхнизкой вибрацией доступны с четырьмя стационарными опорами и/или мобильной опорой с регулируемым креплением и подъёмным рычагом.

++



+

+

# "НАУКА"

ЦЕНТР ТЕХНИЧЕСКОГО СОПРОВОЖДЕНИЯ



Адрес: 129626, Россия, Москва,  
ул. Маломосковская, 22, стр. 1, «Технопарк»  
Телефон: +7 (499) 322 06 62  
E-mail: info@nauka-shop.ru  
[www.nauka-shop.ru](http://www.nauka-shop.ru)



# "НАУКА"

ЦЕНТР ТЕХНИЧЕСКОГО СОПРОВОЖДЕНИЯ

Адрес: 129626, Россия, Москва,  
ул. Маломосковская, 22, стр. 1, «Технопарк»  
Телефон: +7 (499) 322 06 62  
Моб.: +7 926 422 93 04  
E-mail: info@nauka-shop.ru

## ПОЛНОСТЬЮ АВТОМАТИЗИРОВАННАЯ ИЗМЕРИТЕЛЬНАЯ СИСТЕМА

### Диапазон температур

- + 1,6 К–400 К в стандартной версии
- + Минимальная температура 300 мк в версии с вставкой реконденсации He-3:
- + Минимальная температура 50 мК
- + Вставки для высоких температур: 700 / 1000 К
- + Стабильность температуры — мК во всем диапазоне магнитного поля
- + До 9 Т версии mini-CEMIS
- + До 18 Т в версии CFMS с сильным полем
- + Опция низких полей — для измерения полей в области практически нулевого поля

## СУХИЕ КРИОГЕННЫЕ ИЗМЕРИТЕЛЬНЫЕ СИСТЕМЫ (CFMS)

### ПРЕИМУЩЕСТВА БЕЗЖИДКОСТНОЙ ИЗМЕРИТЕЛЬНОЙ СИСТЕМЫ (CFMS)

#### Объекты общего пользования — для всех пользователей

- + Полное отсутствие криогенных жидкостей
- + Не требуется специальный опыт
- + Большие интервалы обслуживания

#### Высокий уровень безопасности и удобства

- + Отсутствие перекачивания криогенных жидкостей
- + Отсутствие опасности из-за испаряющихся газов
- + Полная защита при отключении электроэнергии
- + Быстрая замена образца

#### Модульная архитектура

- + Совместимость с любыми измерительными модулями
- + быстрая взаимозаменяемость модулей

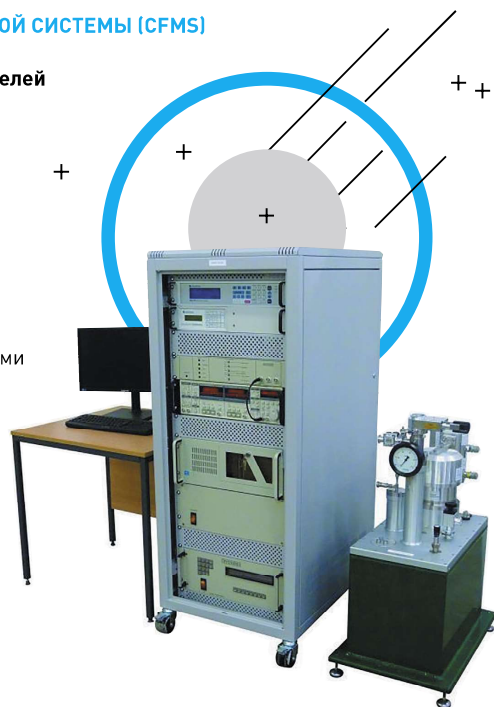
#### Автоматическое управление

- + Стабильные эксплуатационные характеристики поля и температуры.
- + Работа в автоматическом режиме (не требует присутствия)
- + Обеспечение возможности проведения сложных и длительных экспериментов

#### Поддержка в течение всего срока службы

- + Прямая поддержка со стороны производителя
- + Удаленная поддержка системы через Интернет
- + Международная команда обслуживания
- + Бесплатные обновления программного обеспечения

## CRYOGENIC



ООО «Криотрейд инжиниринг» – это торгово-производственная компания, выполняющая поставки научного оборудования для лабораторий и промышленности на протяжении 15 лет. Основное направление деятельности – производство криостатов для научных исследований. Также выполняется гарантийное и постгарантийное сервисное обслуживание криостатов и криогенных систем, а также их модернизация под новые задачи. Наши высококвалифицированные технические специалисты всегда готовы помочь с подбором оборудования, максимально соответствующего требованиям заказчика.



### *Собственное оборудование:*



- Компактные заливные азотные криостаты моделей LN-120 и LN-121-SPECTR (диапазон температур – от 77 до 500K);

- Азотные и гелиевые криостаты проточного и замкнутого типа – как стандартные, так под задачи пользователя;
- Гелиевые криостаты замкнутого типа со

сниженными вибрациями для оптических экспериментов;

- Сверхпроводящие магниты любой конфигурации;
- Криостаты с базовой температурой 0.3 и 0.8K;



- Переливные устройства для  $LN_2$  и  $LHe$  с ЭВТИ, а также системы выдачи азота (азотные питатели);
- Криовакуумные камеры и холодные экраны, а также температурные столы для



вакуумных камер;

- Генераторы жидкого азота производительностью от 20 до 300 л/сутки.

**Поставляемое криогенное, холодильное и вакуумное оборудование:**

- Гелиевые ожижители и реконденсаторы производительностью от 20 до 200 л/сутки;
- Термостатируемые столики с диапазоном температур  $-190...+1200$  °С, подходящие в том числе для микроскопии;
- Любое сопутствующее криогенное оборудование – криогенные провода, температурные датчики, мониторы и контроллеры температур, источники тока сверхпроводящих магнитов, сосуды Дьюара др.;



- Турбомолекулярные откачные посты, вакуумные датчики, насосы, а также сопутствующие товары и арматура;
- Криогенные рефрижераторы, в том числе компактные
- Оборудование для вакуумных систем – сверхвысоковакуумные переносные камеры, системы линейного перемещения (от 1 до 5 осей), высокотемпературные испарители, затворы и многое другое;
- LN<sub>2</sub> генераторы смесового типа производительностью от 1 до 50 л/ч.



Кроме того, мы занимаемся **выполнением обслуживания криогенных и вакуумных систем**. Наша производственная база имеет все необходимые инструменты, оборудование и ЗИП. Основные выполняемые работы: плановые ТО, диагностика неисправностей, вакуумирование объемов и проверка на течи, обслуживание криорефрижераторов и компрессоров, модернизация оборудования.

### Лабораторное и измерительное оборудование:

- Электромагниты, в том числе векторные, катушки Гельмгольца, а также установки на их основе (VSM, системы измерения эффекта Холла, Керра, установки размагничивания и другие);
- Гаусс-метры и флюксометры, а также зонды для них, в том числе криогенные;



- Электрическое измерительное оборудование (мультиметры, источники тока/напряжения, LCR-метры, источники-измерители, импедансные анализаторы, тестеры проводов и батарей и т.п.);



- Синхронные усилители с частотным диапазоном до 60 МГц (с конца 2023 года доступны модели с частотой до 300 МГц);

- Лабораторные планетарные шаровые мельницы;



- Системы перемещения (линейное, вращение, качание) с пьезоприводами, в том числе криогенные пьезосканеры и пьезоступени;



- Оборудование для СВЧ-измерений, в том числе для криогенных: детекторы, циркуляторы, изоляторы, коаксиальные провода, малошумящие усилители, фазовращатели, зонды, фильтры и другое;

- Оборудование для квантовых компьютеров;
- Возможна поставка любого оборудования под заказ и оснащение лабораторий «под ключ».



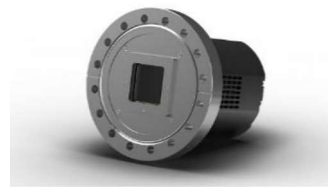
### Оптическое оборудование и фотоника:

- Узкополосные одночастотные лазеры с длиной волны от 185 до 2 371 нм и мощностью от 1 мВт до 18 Вт;
- Квантово-каскадные ИК-лазеры с длиной волны от 760 до 14 000 нм и мощностью от 1 мВт до 9 Вт;
- Импульсные твердотельные лазеры с длиной волны от 236 до 1 342 нм;
- Терагерцовые источники излучения от 1.3 до 4.7 ТГц мощностью от 0.1 до 5.0 мВт;
- Широкополосные источники излучения мощностью до 1 кВт;
- Волоконные оптические усилители;
- Лазерные диоды;
- Кремниевые фотоумножители;



- Электро- и акустооптические модуляторы;
- Микроскопы, в том числе стерео-микроскопы, конфокальные, сканирующие, биологические, металлургические и т.п.;

- Спектрометры комбинационного рассеяния;
- TCSPC системы, FLIM, конфокальные системы;
- Научные и промышленные камеры в таких спектральных диапазонах, как рентген, видимый, ближний и дальний ИК, с возможностью интеграции в систему заказчика;
- виброизоляционные столы и аксессуары к ним;
- оптические компоненты, полупроводниковые подложки (Si, GaAs, GaSb, InSb, Ge и многие другие), сцинтилляционные кристаллы и массивы, кристаллы для лазеров, окна прозрачности.



### Чиллеры и термостабилизаторы:

**Компания Coolingstyle** специализируется на проектировании, разработке и производстве высокоточных устройств контроля температуры широкого спектра применения, включая промышленные чиллеры, системы охлаждения корпусов, микрокомпрессоров, и др.

Продукция отличается высокой надёжностью, эффективностью энергоиспользования и компактными размерами. Точность контроля температуры оставляет  $\pm 0.1$  °C, что позволяет их активно применять для поддержания температуры лазеров, где незначительно изменение температуры может привести к сдвигу частоты.

#### Основные преимущества:

- Компактная конструкция позволяет существенно экономить пространство в лаборатории. Имеет возможность размещения как в стандартной стойке, так и просто на любой горизонтальной поверхности;
- При низких нагрузках скорость вращения вентилятора охлаждения существенно снижается, что позволяет снизить шум;
- Несмотря на компактные размеры, чиллеры укомплектованы мощными насосами, позволяющими обеспечить высоту водяного столба до 50 м.
- Диапазон мощностей охлаждения – от 480 до 2700 Вт (измеряется при уставке 25 °C и окружающей температуре 25 °C).
- Имеется возможность установки интерфейса для связи с ПК.
- Практически всегда имеются чиллеры в наличии на складе РФ.



**Термостабилизаторы серии НТИ** могут широко применяться в лабораториях и на производствах при необходимости выполнять охлаждение оборудования с выделяемой тепловой мощностью от 3 до 100+ кВт.

Особенности конструкции термостабилизаторов НТИ

Система охлаждения:

- В термостабилизаторах НТИ применяется экологически чистый хладагент R-407c;
- Используется популярный и надежный спиральный компрессор Japan Panasonic;
- Конденсатор с алюминиевым оребрением и медной трубкой легко поддается чистке;
- Мощный вентилятор обеспечивают достаточный объем охлаждающего воздуха
- В конструкции используется пластинчатый теплообменник из нержавеющей стали SS304;
- Система управления обеспечивает стабилизацию температуры в пределах  $\pm 1-2$  °C (опционально доступная версия со стабильностью  $\pm 0.1$  °C в случае низкопроизводительных моделей и  $\pm 0.5$  °C для высокопроизводительных)
- Предохранительные устройства обеспечивают стабильную и безопасную работу чиллера.

Встроенные модули защиты:

- Перегрузка двигателя,
- Высокое и низкое давление,
- Перегрев охлаждающей воды,
- Уровень воды в баке,
- Фазовая защита, защита от замерзания, переключатель потока





## КВАНТОВЫЙ NV-МАГНИТОМЕТР на базе АСМ (QNMV)



Прибор для получения магнитных изображений, который совмещает в себе две технологии: магнитометрия с использованием NV-центров в алмазе и сканирование изображений методом атомно-силовой микроскопии (АСМ)

QNMV

## КВАНТОВЫЙ NV-МИКРОСКОП (QDM)

Уникальное оборудование, где сенсором магнитного поля выступает центр окраски, NV-центр. В отличие от QNMV позволяет получать магнитные изображения одновременно на большой площади



QDM

Компания «ЭЛЕМЕНТ» более 20 лет на рынке аналитического оборудования



Подбор оборудования под задачи пользователя



Запуск оборудования в эксплуатацию, обучение пользователей



Прямые поставки оборудования от производителей



Гарантийное и постгарантийное обслуживание, ремонт

Аналитическое оборудование по запросу пользователя



8 (800) 250-34-64  
www.element-msc.ru  
info@element-msc.ru

 ZHONGTAI





## СПЕКТРОМЕТРЫ ЭЛЕКТРОННОГО ПАРАМАГНИТНОГО РЕЗОНАНСА



**ZT60W**  
W-Band высокочастотный  
ЭПР спектрометр

**ZT6500**  
Настольный  
ЭПР спектрометр

**ZT15C**  
X-Band  
CW-ЭПР спектрометр

**ZT15P**  
X-Band импульсный  
CW-ЭПР спектрометр

Линейка ЭПР спектрометров ZHONGTAI включает в себя компактную настольную модель ZT6500, две модели ЭПР X-диапазона для работы в CW – ZT15C или в импульсном + CW режиме – ZT15P (обе модели можно дооснастить для работы в Q-диапазона с магнитом 1,8T) и высокочастотный ЭПР спектрометр W-диапазона ZT60W



Больше информации о технических характеристиках ЭПР спектрометров ZHONGTAI и программному обеспечению для настройки экспериментов, сбора и обработки данных вы можете найти на нашем сайте [element-msc.ru](http://element-msc.ru)

Компания «ЭЛЕМЕНТ» - официальный представитель ZHONGTAI в России

# CMS8400 Neo



## ЭПР СПЕКТРОМЕТР

настольный

ПРИБОР ДЛЯ ИЗУЧЕНИЯ ПАРАМАГНИТНЫХ КОМПЛЕКСОВ ИОНОВ ПЕРЕХОДНЫХ МЕТАЛЛОВ, И ДЛЯ ДЕТЕКТИРОВАНИЯ СВОБОДНЫХ РАДИКАЛОВ В ЖИДКОСТЯХ И ТВЁРДЫХ ОБРАЗЦАХ



- Компактный дизайн электромагнита и СВЧ тракта
- Высокая чувствительность и разрешающая способность
- Автоматический расчет g-фактора
- Оптимизированные параметры магнитного поля: высокая точность задания поля, стабильность
- Автоматическая настройка при смене образца
- Встроенный частотомер, датчики магнитного поля и температуры

ООО «АДАНИ РУС»  
190005, Российская Федерация, г. Санкт-Петербург,  
Набережная Обводного канала 118А, литер X, помещение 7-Н, офис 7  
+7 (812) 389-23-88



ISO 9001:2015  
ISO 13485:2016

# POWDIX 600



## РЕНТГЕНОВСКИЙ ДИФРАКТОМЕТР

настольный

КАЧЕСТВЕННЫЙ И КОЛИЧЕСТВЕННЫЙ  
РЕНТГЕНОФАЗОВЫЙ АНАЛИЗ

- Компактный дизайн
- Тета/Тета геометрия
- Быстродействующий линейный детектор
- Высокое отношение сигнал/шум
- Продолжительные сроки эксплуатации рентгеновской трубки и детектора
- Не требуется внешнее водяное охлаждение
- Гарантированная безопасность
- Аналитическое ПО с интегрированной базой данных
- Лучшее соотношение цена/качество

ООО «АДАНИ РУС»  
190005, Российская Федерация, г. Санкт-Петербург,  
Набережная Обводного канала 118А, литер X, помещение 7-Н, офис 7  
+7 (812) 389-23-88



ISO 9001:2015  
ISO 13485:2016